EXPLORING THE USE OF THE MICROFLOWN

Ron Raangs

This research project, TWO.5154, was supported by the Dutch Technology Foundation (STW).

De promotiecommissie is als volgt samengesteld:

Voorzitter en secretaris:

Prof.dr.ir. A.J. Mouthaan	Universiteit Twente

Promotor:

Prof.dr.ir. W.F. Druyvesteyn	Universiteit Twente

Leden:

Prof.dr.ir. H. Tijdeman	Universiteit Twente
Prof.dr.ir. C.H. Slump	Universiteit Twente
Prof.dr.ir. A. Gisolf	TU Delft
Prof.dr.ir. N.B. Roozen	TU Eindhoven
Dr.ir. H-E. de Bree	Hogeschool Arnhem Nijmegen
Dr.ir. J.G.A.M. van Heck	DAF Trucks N.V.

Print: PrintPartners Ipskamp, Enschede

Typesetting: Microsoft Word 2002

On the cover: A SEM photograph of a microflown

ISBN 90-365-2285-4

EXPLORING THE USE OF THE MICROFLOWN

PROEFSCHRIFT

ter verkrijging van
de graad van doctor aan de Universiteit Twente,
op gezag van de rector magnificus,
prof. dr. W.H.M. Zijm,
volgens besluit van het College voor Promoties
in het openbaar te verdedigen
op vrijdag 9 december 2005 om 16.45 uur

door

Raang Raangs

geboren op 30 juli 1968

te Lochem

Dit proefschrift is goedgekeurd door de promotor:

Prof.dr.ir. W.F. Druyvesteyn

Samenvatting

Het meten van geluid wordt vandaag met de dag steeds belangrijker. De bevolkingsdichtheid neemt toe en door economische groei neemt ook het gebruik van machinale apparatuur steeds meer toe. Geluidshinder neemt hierdoor eveneens toe. Het beheersen van geluid, en het bewaken van geluidsnormen wordt daarom steeds belangrijker. Ook klanten en afnemers van allerlei apparatuur stellen een aangenaam geluidsniveau op prijs, denk hierbij bijvoorbeeld aan het geluidsniveau binnen in een autocabine. In dit proefschrift worden verschillende meettechnische toepassingen van een relatief nieuwe akoestische meetsensor, de microflown, onderzocht.

Geluid wordt over het algemeen beschouwd als kleine variaties in de druk die zich door lucht, of een ander medium, in de verschillende richtingen voortplanten. Het geluid plant zich hierbij voort doordat ook de deeltjes in de lucht bewegen met zeer kleine amplitude ten gevolge van kleine drukvariaties. De snelheid van deze beweging van de deeltjes in de lucht, dit is niet de geluidssnelheid, bevat ook zeer veel informatie over het uitgestraalde geluid. Een belangrijk aspect van deze snelheid is de richting waarin het geluid zich verplaatst, de richting waarin het geluid zich verplaatst is namelijk dezelfde als de richting waarin de kleine deeltjes in de lucht heen en weer bewegen.

In dit proefschrift wordt het gebruik van een nieuwe kleine akoestische deeltjessnelheid opnemer beschreven. In de wereld van akoestiek wordt vooral gedacht in termen van geluidsdruk en zijn veel natuurkundige wetten en gestandaardiseerde meetmethoden vooral op de geluidsdruk en deeltjessnelheid gebaseerd. Dit komt vooral omdat de drukmicrofoon al circa 100 jaar bestaat en gedurende deze tijd doorontwikkeld is. Deeltjessnelheid sensoren zijn echter relatief nieuw. De gebruikte deeltjessnelheid opnemer, de microflown, is uitgevonden in 1994. In dit proefschrift beschrijven we toepassingen waarin de eigenschappen van druk en van de deeltjessnelheid van elkaar verschillen of elkaar zeer goed aanvullen.

Voor bijna iedere meting geldt dat de meting niet beter zal zijn dan de kalibratie van de gebruikte opnemer. In Hoofdstuk 2 van dit proefschrift beschrijven we uitvoerig de kalibratie van deze microflown. Hierbij hebben we vooral gebruik gemaakt van een staande golf buis. Een dergelijke staande golf buis is relatief

klein, terwijl de relatie tussen druk en deeltjessnelheid toch goed bekend is. Daarnaast hebben we de samen met de Universiteit van Edinburgh de microflown vergeleken met een optische methode. Deze vergelijking geeft duidelijk aan dat de microflown de deeltjessnelheid meet en niet de geluidsdruk.

In hoofdstuk 3 hebben we het gedrag van de kruiscorrelatie van twee microflown signalen onderzocht. De kruiscorrelatie geeft aan hoe, en op welke manier, de twee signalen op elkaar lijken. We laten zien dat we de kruiscorrelatie kunnen gebruiken om signalen te meten die zich in de ruis van één sensor bevindt. Door lang te middelen kunnen we zo effectief de ruis in de meting met 30 dB, een factor 30, verminderen.

In paragraaf 3.4 van dit proefschrift passen we de kruiscorrelatie toe op de signalen van twee microflowns die op dezelfde positie in de ruimte meten in richtingen die loodrecht op elkaar staan. Voor een zeer galmende kamer tonen we aan dat we de invloed van de galm en het geluid van de bron zelf van elkaar kunnen scheiden. Hierdoor kunnen we de deeltjessnelheid bepalen als of de bron in een ruimte zonder galm zou staan.

In hoofdstuk 4 beschrijven we de geluidsintensiteit. Geluidsintensiteit is het akoestische vermogen per oppervlak. Op dit moment wordt vaak dure apparatuur toegepast waarbij met twee zeer gelijke microfoons deze geluidsintensiteit wordt bepaald. Omdat deze geluidsintensiteit gedefinieerd is als het product van de deeltjessnelheid en de geluidsdruk, is het logisch om de nieuwe deeltjessensor hiervoor in te zetten. In dit hoofdstuk vergelijken we deze nieuwe sensor (p-u probe) met een traditionele p-p sensor. Daarnaast beschrijven we een zeer kleine driedimensionale geluidsintensiteitprobe opgebouwd uit drie kleine microflowns geplaatst rond een kleine drukmicrofoon.

In hoofdstuk 5 behandelen we de effecten die optreden in metingen dicht bij een bron. Zulke metingen in bijvoorbeeld een meetvlak bij een geluidsbron worden vaak gebruikt voor het terug rekenen naar de vibraties op de geluidsbron zelf. In dit hoofdstuk laten we situaties zien waarin druk en deeltjessnelheid (keer de karakteristieke impedantie voor lucht voor vlakke golven) ongelijk aan elkaar worden. Voor veel situaties wordt de deeltjessnelheid relatief zelfs veel groter dan de druk als we dit vergelijken met de situatie voor vlakke golven. Dit gebeurt

vooral bij lage frequenties bij kleine geluidsbronnen en een kleine afstand tot de bron.

Voor het geval er meerdere kleine ongecorreleerde bronnen aanwezig zijn kunnen we, door gebruik te maken van de richtingsgevoeligheid van de microflown en meerdere microflowns, signalen af leiden die direct gerelateerd zijn aan het afgestraalde geluid. Hierdoor kunnen we uit de totale druk in dit geluidsveld de contributie in de druk bepalen per geluidsbron. Hetzelfde geldt ook voor de deeltjessnelheid uiteraard.

In paragraaf 5.8 van dit proefschrift wordt het gebruik van de microflown in het very near field, of ook wel bekend als het hydrodynamic near field, beschreven. Dit zeer nabije veld heeft zeer interessante eigenschappen, zeker als de structurele snelheid wordt vergeleken met de deeltjessnelheid vlak boven het oppervlak. In het zeer nabije veld wordt de deeltjessnelheid vrijwel gelijk aan de snelheid op het oppervlak van het vibrerende object.

Geconcludeerd kan worden dat dit proefschrift een beschrijving en toepassingen van een zeer interessante akoestische sensor bevat. Het proefschrift bevat een omschrijving van de kalibratie van deze sensor evenals een aantal voorbeelden waarbij deze sensor duidelijk voordelen biedt tegenover een conventionele drukopnemer.

Summary

Noise pollution has become more important over the last decades for several reasons. This increase is caused by the increase in human population combined with economical growth that makes sound radiating equipment and their use affordable for an increasing group of the population. The effects of noise in urban areas can affect human health and well-being in a number of ways, which is why governments take the responsibility in order to minimise all forms of noise pollution. This responsibility is often met in the form of noise pollution acts including standardised measurement methods. Also customers are often interested in the decrease of sound levels or increase in sound quality. This thesis discussed several acoustical measurement techniques based on the application of a relatively new acoustical particle velocity sensor.

Sound is generally described as an auditory sensation often caused by small pressure variations, which propagate through the air, or another elastic medium. The sound waves propagate through the air by pressure, but also by the oscillatory movements of air particles. The velocity of the movement of these particles is known as the particle velocity. The particle velocity is along with the sound pressure an important aspect of a sound wave. An important feature of the particle velocity is the fact that it includes information of the direction. In the direction of propagation of the sound wave, the particle will often be in the direction in which the particle velocity shows a maximum.

In this thesis, we describe the use and some applications of a relative new, and small, particle velocity sensor. In the world of acoustics, properties of sound waves are generally described in terms of sound pressure. This is caused by the fact that the microphone sensitive for pressure was invented about a century ago and has developed in an accurate and robust acoustical measurement device. True particle velocity sensors are rather new. The particle velocity sensor applied in the measurement described in this thesis was invented in the year 1994. In this thesis, we describe applications in which the properties of sound pressure, and the particle velocity, differ from each other or situations for which the combination of pressure and particle velocity measurements has a benefit.

Generally, a measurement will never be more accurate than the calibration, or the accuracy of the calibration, of the sensor used. In chapter 2 of this thesis, we

describe several calibration techniques of the microflown. In this chapter, the use of the standing wave for calibration is described. Such a standing wave tube is relatively small, and the relation between pressure and particle velocity is well known. Together with Dr. Ted Schlicke of the University of Edinburgh, we compared the measurements using the microflown in a standing wave tube with measurements obtained using a photon correlation laser doppler technique. This comparison clearly showed that the microflown is sensitive for particle velocity and not for pressure variations.

In chapter 3, we discuss the behaviour of the cross-correlation of two particle velocity signals. If two microflowns measure the particle velocity in the same direction, the cross-correlation almost equals the autocorrelation. We show that for long averaging times, the noise in the cross-correlation diminishes as compared with the autocorrelation of one sensor because uncorrelated noise is averaged out. We showed that the difference can be up to 30 decibels for an averaging time of two minutes.

In paragraph 3.4 of this thesis, we apply the cross-correlation on signals derived from two microflowns who measure in two directions perpendicular with reference to each other. In a reverberant room, we can retrieve information of the reverberant and of the free-field particle velocity, using the cross- and auto-correlations.

In chapter 4, we describe the phenomenon of sound intensity. The sound intensity is the acoustical power per unit area. At the moment the sound intensity can only be measured with expensive and specialised instruments. Since the sound intensity is per definition the product of sound pressure, and sound particle velocity, it is logical to use a microflown in combination with a pressure sensor for such a measurement. In this chapter, we compare this new sensor (p-u probe) with a commercially available p-p probe. Measurements are performed in an ordinary room, between two loudspeakers, radiating uncorrelated sound waves, and in front of one loudspeaker. The both measurement methods were shown to be in good agreement with each other. In this chapter, we also describe a small three-dimensional p-u probe, which can be used for measuring the three-dimensional sound intensity vector.

In chapter 5, we treat the effects at close range of a sound source. Measurements in such a near region are often used as input for inverse techniques, so that out of

measurements in the sound field, the surface velocity, or pressures at the surfaces, can be computed. In this chapter, we show situations in which particle velocity times the characteristic impedance or air is much larger than the pressure at these positions. This usually occurs at low frequencies, small structural sound sources, and short distances from the sound source. This chapter also includes some situations for which the structural information of the sound source is more clearly visible in the particle velocity than in pressure measurements. In pressure measurements, the information smears out, and the reconstruction of the surface velocity out of the measured pressure data can be more difficult than the reconstruction using particle velocity data.

In case of multiple small sound sources, the use of the directivity of the microflown can be used to obtain a signal that is only related with one of the sources. This signal can then be used to obtain the sound field only caused by this sound source. Theoretically, this information can be used for reconstructing the structural surface velocity and pressure due to this single sound source.

In close range of the sound source, we defined a “Very Near Field” which is also known as the “hydrodynamic near field”. This very near field is the part of the near field at such a close range so that the sound particle velocity almost equals the surface velocity. The chapter includes a practical situation that shows that the difference between the pressure level and the particle velocity level is about 20 decibel at a frequency of 50 hertz in close vicinity of a low frequency loudspeaker, a piston in a baffle, with a diameter of 19 centimetres.

In conclusion, this thesis describes an interesting acoustical sensor and some applications. The thesis includes a description of calibration techniques, and some practical applications for the use of this interesting sensor, the microflown. In some examples, the use of the microflown clearly shows advantages if compared with the application of pressure microphones. In general, the combination of both sensors, a microphone and a microflown, shows to be a very powerful combination for acoustical measurements.

Table of Contents

Chapter 1
Introduction

1.1 General Introduction

Sound can be defined as the auditory sensation produced by transient or oscillatory pressures acting on the ear, or by mechanical vibration of the cranial bones at audio frequencies (Morfey, 2001). More generally, sound can refer to any type of mechanical wave motion that propagates through the action of elastic stresses and that involves local compression and expansion of the medium. Often, sound is mainly described by the pressure fluctuations, relative to atmospheric pressure, the sound pressure, but in this thesis, the particle velocity is treated as having the same, or more importance as the sound pressure.

The work presented in this thesis is part of the STW project TWO.5154 "Efficient acoustic calculation and measurement techniques". In this interdisciplinary project three groups worked in parallel. It concerned a combination of acoustic measurement and calculation techniques and involved; (1) The development and validation of a new method for acoustic source identification based on a so-called Boundary Element Method (Visser, 2004). An essential element was the extension of the method to the use of particle velocities. (2) The development of an advanced mathematical method to perform the required computations in a very efficient way (Hernández-Ramírez, 2005). (3) The thorough exploration of the Microflown, a new type of sensor, in which particle velocities are measured instead of pressures (the subject of the present PhD thesis).

1.2 Properties of Sound

Sound is produced by a source and travels through the air with a certain velocity (which is about 340 m/s or 1225 km/h) and can be reflected by walls or the floor. An ear or microphone detects it. After perceiving the sound one can distinguish its origin. Besides that, it can be said to be loud and perhaps to be an annoying experience.

This annoying experience, or the quantification "loud", is a subjective interpretation of sound. If large amounts of people are annoyed by a certain

distress factor, regulations will follow. In this case sound measurements to quantify the amount of noise should be performed.

The human ear can hear very loud sound, and very quiet sounds in terms of sound pressure. Therefore, the sound (pressure) level is expressed in a decibel scale (dB) which is a logarithmic scale. Often a frequency dependent filter is applied so that the sound level behaves more or less like the human ear and the obtained sound levels do reflect the perception more accurately.

Often, a periodicity will occur in sounds. This periodicity is known as the frequency of the sound.

The human ear is very sensitive for small pressure variations in the air. Not all frequencies are perceived similar. The human ear is most sensitive for pressure variations of about 3 kHz. For frequencies of 30 Hz the ear is about 200 times less sensitive. The static air pressure is about hundred thousand Pascal (Pa), a pressure variation of one Pascal is perceived as very loud at 1 kHz, but as a soft tone at 20 Hz.

Sound can be understood as variations of the static air pressure and of the velocity of air particles: particle velocity (Beranek, 1954). Pressure, p, is defined as force per unit area. This force is influenced by the amount of air particles at a certain position within a certain volume. So variations in the (sound) pressure are influenced by variations in the number of air particles. If the number of particles in a certain volume changes during time, there must be a particle motion towards that volume and backwards. The velocity of the movement of these air particles is called particle velocity, u, or sometimes referred to as fluid velocity (Pierce, 1989). Therefore, sound consists always of two parts: the sound pressure and the particle velocity. Note that the particle velocity is not the actual velocity of air molecules, but a mass-weighted local average velocity (Pierce, 1989). For complete quantification of a sound field, both sound pressure as particle velocity should be measured.

In an electrical analogy, sound pressure corresponds to an electric voltage and particle velocity to an electric current. The amount of acoustical power is quantified in Watts. Multiplications of voltage and current results in electrical power and analogously, sound pressure times particle velocity is associated with sound power per unit area in the acoustical domain.

The ratio between the sound pressure and particle velocity, $z_s = p/u$, is known as the specific acoustic impedance. For plane progressive waves this ratio equals $\rho_0 c$, and is the characteristic impedance of air.

We can distinguish different types of sound fields. Depending on distance from the source, we can distinguish the far field, and the near field. In the far field, the pressure diminishes with distance and the particle velocity and pressure are in-phase with each other, and $p = u\rho_0 c$. The near field is the region surrounding a sound source in which these far field conditions do not apply (Morfey, 2001). Since in this near field, pressure and particle behave differently, and acoustical measurements are often performed in this near field, this is an interesting region for measuring the particle velocity.

Another special sound field is the diffuse sound field. In the diffuse sound field, the sound waves arrive from all directions are uncorrelated. In this sound field, a pressure sensor behaves very different from a particle velocity sensor.

A more thorough description can be found in literature, see for example (Beranek, 1954;Bree de, 2005;Kinsler et al., 2000).

1.3 Primary Techniques for Measurement of Sound Pressure and Particle Velocity

In acoustics, there has been a lack of a reliable sensor that accurately measures the true acoustic particle velocity. Several attempts were made, starting with the Rayleigh disc (König, 1891), and velocity microphones (Olson, 1932). The Rayleigh disc (König, 1891) was a very good attempt to measure particle velocity. In fact, the Rayleigh disc has been applied for calibrating pressure microphones (West, 1949). Actually, the Rayleigh disc did not measure particle velocity, but was sensitive for the squared particle velocity and had a $\cos^2\theta$ directional characteristic (Wood, 1935). Until the invention of the microflown in 1994 (Bree de et al., 1995), no robust and applicable acoustic particle velocity sensor has been available. The science of acoustics therefore had to be and was mainly based on pressure and pressure measurements.

In the meantime, sound was often described mainly in terms of sound pressure. The condenser microphone is today the accepted standard acoustic transducer for all sound and noise measurements. Even sound intensity measurements, where

sound intensity is by definition the time integral of the product between pressure and particle velocity, is standardized using two spatially separated pressure microphones.

1.4 Short Introduction to Microphones

Since there are several types of sound fields, and applications in which one would like to obtain the sound pressure, several types of measurement microphones are available. Microphones are meant to convert pressure fluctuations in electrical signals. There are several types of measurement microphones (Brüel&Kjær, 2005):

- free field
- pressure
- random incidence.

Free field microphones are typically used where the sound mainly comes from one direction, and typical applications are in outdoor measurements and indoor measurements with very few- or no reflections. Pressure microphones are mainly used in cavities and for measurements where they can be mounted with its diaphragm flushed with the surrounding surface (Acoustics & Vibration Technologies, 2005). The random incidence microphone is mainly used in situations where sound waves arrive simultaneous from all angles. These situations are found in reverberation chambers, but also in many indoor situations.

Other types of microphones, such as for example pressure gradient microphones, are mainly used for music and speech applications and are not discussed in this thesis.

For reasons of physics (capsule dimensions), the omni-directional pattern can be maintained in its ideal form only up through the midrange frequencies. At higher frequencies, sound waves arriving on axis are progressively emphasized by the interaction of the capsule housing with the shorter wavelengths. The larger the diameter of the housing, the greater the difference in high-frequency response between on-axis and off-axis sound It is the reason for their differing frequency response in the direct versus the diffuse sound field (Schoeps, 2005).

Note that the different types of microphones are meant for different types of sound fields and thus the selection of the correct microphone is not an easy task by definition. Furthermore, although pressure is a scalar quantity of the sound field,

pressure microphones tend not to be omni-directional for midrange and higher frequencies.

1.5 Introduction to the microflown particle velocity sensor

The microflown, see Figure 1-1, was invented in 1994 at the University of Twente, the Netherlands (Bree de et al., 1995;Bree de et al., 1996b). The transducer is a micromachined hot wire anemometer, but based on two heated extremely thin wires and not one as in the classical anemometer. A particle velocity signal in a direction perpendicular to the wires and in the plane of the wires changes the temperature distribution instantaneously, because the upstream wire is cooled more than the downstream wire by the acoustic airflow. The resulting resistance difference provides a broad band (0 Hz up to at least 20 kHz) linear signal with a figure of eight directivity that is proportional to the particle velocity up to sound levels of 135 dB. Between 100 Hz and 10 kHz the lower (noise) level is in the order of -10 dB (i.e. 20 10^{-9} m s^{-1}) in 1 Hz bandwidth which is comparable to the performance of high quality pressure microphones (see Figure 1-10).

Between 100 Hz and 1 kHz the frequency response is relatively flat. Between 1 kHz and 10 kHz there is a roll off of 6 dB per octave, caused by diffusion effect related with the distance between the two wires. Above 10 kHz the sensitivity decreases an additional 6 dB per octave because of the thermal heat capacity of the wires.

In the year 2000, Svetovoy and Winter (Svetovoy and Winter, 2000) developed a mathematical model of the operation principle of the microflown that predicted the two high frequency corner frequencies. This mathematical model was based on two boundary layers. In 2001 a similar model was developed at the University of Twente without any boundary layers (Honschoten et al., 2001;Honschoten, 2004). Enhanced calibration measurements proved another corner frequency at low frequencies (in the year 2004). At low frequencies, the sensitivity of this particle velocity transducer increases 6 dB per octave (Bree de, 2005). Since this first corner frequency is out of the range of frequencies as described in this thesis, this corner frequency is not used in the model used for the sensitivity we applied.

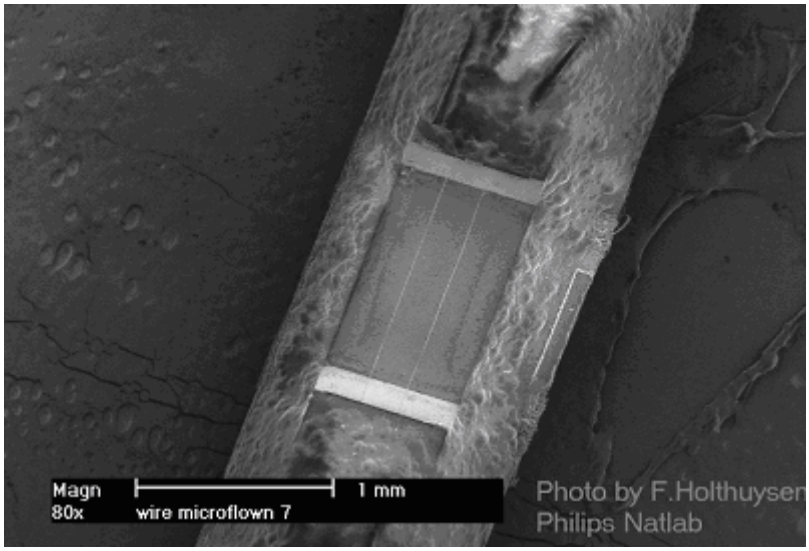

Figure 1-1: SEM photograph of a microflown sensor.

The working principle is described in more detail in literature (Bree de, 1997;Bree de, 2003b;Bree de, 2003a;Bree de, 2005;Honschoten, 2004).

1.6 Applications of microflowns

Applications of the microflown particle velocity sensor can be found in every field in acoustics where particle velocity times $\rho_0 c$ differs from the sound pressure. This difference will usually add to the knowledge of the sound field and/or sound source that is topic of research. Differences will especially be found nearby a sound source, or in sound fields where the directivity is concerned. Due to the working principle of the microflown, the used medium should preferably be electrically non-conducting and preferably a gas such as air.

Of course, it was clear from the beginning that with the use of a microflown sound intensity can be measured but it was not clear what the exact benefits for the industry could be. Why would this sensor be more interesting than already existing sensors? The answer is that the microflown method could operate in sound fields where the traditional probe has problems and its small size allows measurements on places where the traditional probe cannot reach and it allows high-resolution measurements on very small objects. See further Chapter 4: Sound Intensity.

One of the results of near field holography research was that it became clear that the particle velocity close to a vibrating object coincides with the vibrating of the object itself. Until that moment there were a few methods to determine the vibration of a structure, such as for example a laser and an accelerometer. The first

one is very expensive, large and therefore difficult to use and the accelerometer is small and low cost but have to be attached to the vibrating object and this alters the structure and it is much work. The microflown is an alternative to these methods. It is small, a non-contact method and easy to use. See further Chapter 5: Mapping of the Sound Field in different types of sound fields.

Furthermore, there will be many applications of the microflown, which are not discussed in this thesis. Other applications are measurement of acoustical impedance, in situ reflection coefficient measurements, and reciprocal methods. For an overview of these applications of the microflown see (Bree de, 2001;Bree de, 2005) and the website of Microflown Technologies BV. (Microflown Technologies, 2004).

1.7 Properties of microflowns

The microflown particle velocity sensor has many interesting acoustical properties. The most important properties are: (1) the microflown is sensitive for acoustical particle velocity, and not for pressure, (2) the small size, (3) the directional pattern is a purely figure of eight response, for all frequencies, (4) there are no moving parts involved at all, (5) the microflown is sensitive for low frequencies down to zero hertz.

1.7.1 Polar pattern

A polar pattern (or directivity) expresses the sensitivity to the angle of incidence of the sound field. A sound pressure microphone should be omni-directional which implies a constant sensitivity for any angle of incidence of the sound field. A microflown however only measures the particle velocity in the direction for which it is sensitive. The directivity of a microflown is therefore a purely figure of eight pattern, see Figure 1-2, which can be expressed by (Bree de, 2001):

$$\frac{\text{output}}{\text{particle velocity}} = \text{Sensitivity} \cdot \cos(\theta) \tag{1.1}$$

where θ is the angle of incidence.

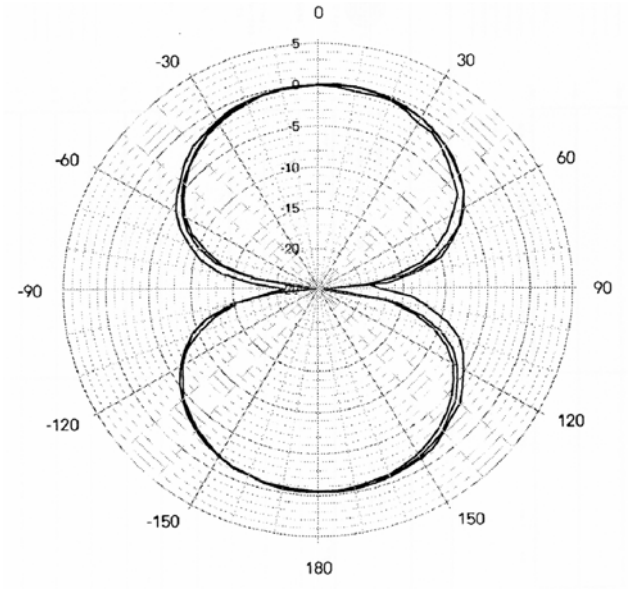

Figure 1-2: Directional characteristics of a microflown measured at 150 Hz, 2 kHz, and 4 kHz (Bree de, 2005).

1.7.2 Sensitivity vector

The sensitivity vector is defined as a vector of magnitude S_u, and direction $\vec{\mu}$, which is the direction in which the microflown measures. The polar pattern is thus explained since the microflown only measures in the direction $\vec{\mu}$ and thus measures only the projection of the true particle velocity on $\vec{\mu}$. The electrical output of the microflown is given by the scalar product:

$$\text{output} = S_\mu \left(\vec{\mu} \cdot \vec{u} \right) \tag{1.2}$$

with S_μ the sensitivity of the microflown in volts per metre per second.

1.7.3 Package Gain

Apart from protection of microflown's fragile sensors, packaging has also acoustic

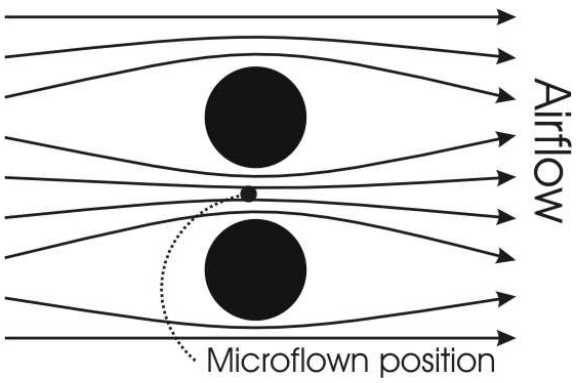

Figure 1-3: By forcing the flow through two bars, the sensitivity of the microflown is effectively increased. This effect is known as the package gain.

effects. When the 0.5 inch packaging is applied, see Figure 1-3, the particle velocity level rises considerably (about 10 dB) at the position of the microflown, and the phase response alters slightly. The increase of particle velocity level inside the package (the so-called package gain) is mainly caused by a channelling effect: the particle flow is "forced" through the package causing an increase in level.

In Figure 1-4 a finite element simulation shows the increase in level due to the packaging (Honschoten, 2005). Obviously due to the frequency response of the 0.5 inch package, the overall frequency response of the microflown alters. Figure 1-5 shows the amplitude response of the 0.5 inch package. The amplitude response is obtained out of the microflown sensitivity with, and without the added package. The phase response is altered between zero and minus ten degrees (Microflown Technologies, 2004).

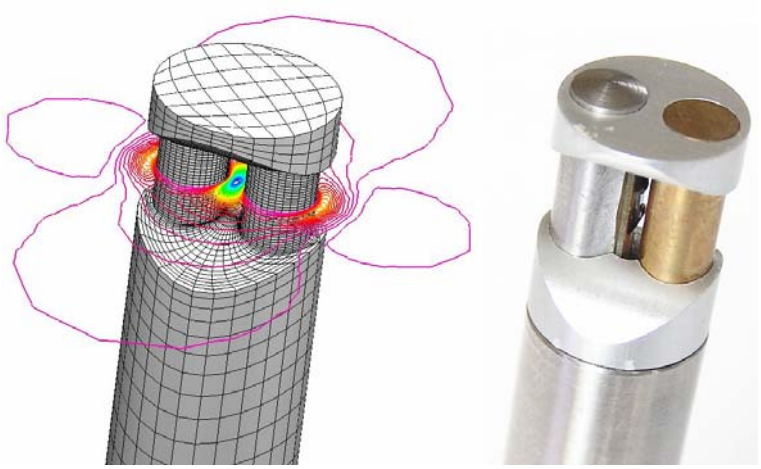

Figure 1-4: A well-chosen package will result in a particle velocity gain, left the finite element simulation with the iso-velocity results and right the realisation of the half inch package.

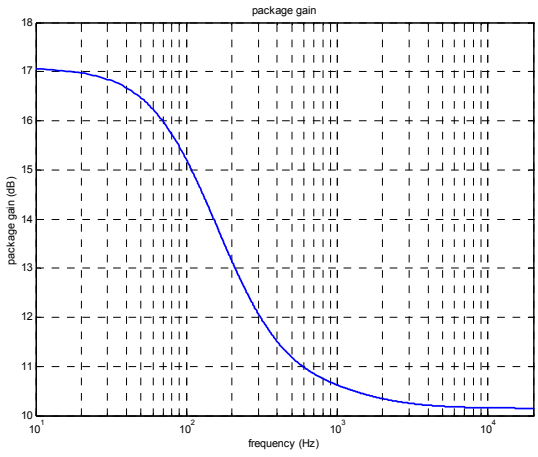

Figure 1-5: Package gain of a 0.5 inch ICP packaged.

1.7.4 Description of the different type of microflowns

Over time, we have used various versions of microflown sensors for the experiments described in this thesis. Some of them were in a prototype stage, while others where custom build for us. Since we do refer to the commercial names in the text, as used by Microflown Technologies BV (Microflown Technologies, 2004), an overview of the various sensors is given in this section.

For pressure measurements, there are different types of microphones depending on the sound field in which they are used; free field microphones, pressure microphones, and random incidence microphones, see section 1.4. The difference between the particle velocity microflowns however is not dictated by the sound field in which they are used. The differences are merely the addition of a package (size), the electronics (equivalent self-noise, dynamic range), and the addition of multiple sensors combined in one sensor (three-dimensional p-u probe).

Figure 1-6: Different types of 0.5-inch packaged microflowns. At the left, an ICP® powered microflown is visible, in the middle and right, microflowns with LEMO® connectors are shown.

1.7.4.1 ICP microflown:

With the ICP type microflown, Figure 1-6(left), the first commercial type of microflowns is meant. The microflowns were fitted in a 0.5 inch stainless steel package, and were powered by ICP. The abbreviation ICP® means “Integrated Circuit Piezoelectric”. ICP is a two-wire standard that supplies power to the electronics by the 4.0 mA current, while the signal is contained in the output voltage. For various reasons Microflown Technologies BV integrated the power supply regulator in the cables, and the ICP microflowns have become obsolete.

1.7.4.2 0.5 inch p-u probe

The half-inch p-u probe is basically a half inch packaged microflown (such as the ICP microflown probe) whereas a small microflown has been built in the package itself. This sensor has been used and described in a conference- and a journal-paper (Raangs et al., 2001a;Raangs et al., 2003). This sensor has shown to be a fully functional sound intensity probe. This microflown is nowadays also known as the PU probe (Microflown Technologies, 2004).

Figure 1-7: photograph of a half inch p-u probe (courtesy Microflown Technologies BV.).

1.7.4.3 USP microflown:

USP is an abbreviation of “Ultimate Sound Probe”. The name was chosen since it was, and still is the state of the art in terms of microflowns concerned. It is a miniature three-dimensional sound probe that is capable of measuring broad banded sound pressure and particle velocity in three orthogonal directions. The USP is a compact and fully integrated sound probe that combines three orthogonally positioned particle velocity sensors and a miniature pressure

microphone. The actual sensor configuration without its protective cap is less than 5×5×5mm³, see Figure 1-8. In this thesis, we also refer to this microflown and its predecessors as the three-dimensional p-u probe. Note that the microflowns are aligned differently on the latest USP probes in order to minimize errors in alignment.

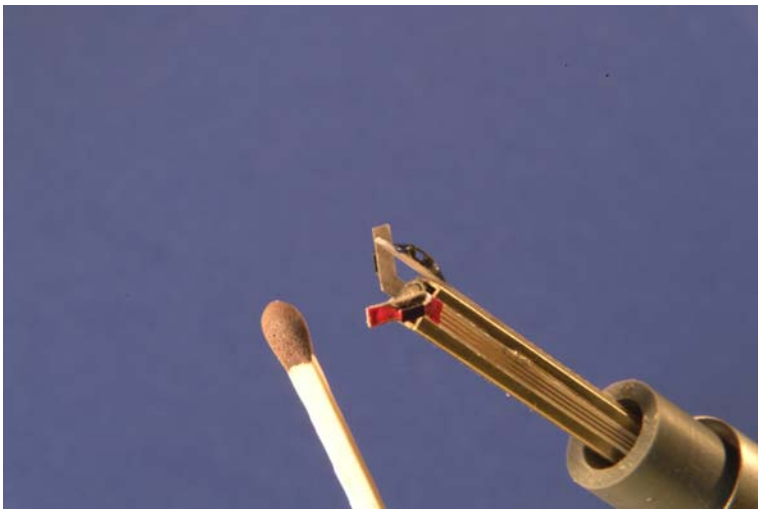

Figure 1-8: Photograph of a half-inch three-dimensional p-u probe (Microflown Technologies, 2004).

1.7.4.4 Scanning Probe

The name "scanning probe" is used for very small microflowns. The scanning probe is designed in such a way that is possible to measure close to a surface. It consists of the small micro-machined sensor itself glued on a small piece of printed circuit board (PCB). These microflowns are very small and influence the sound field as least as possible. The sensor wires of the microflown are protected by a little cap. This way of packaging does not increase the particle velocity at the element so there is no package gain. The self-noise therefore is 10 dB higher as the

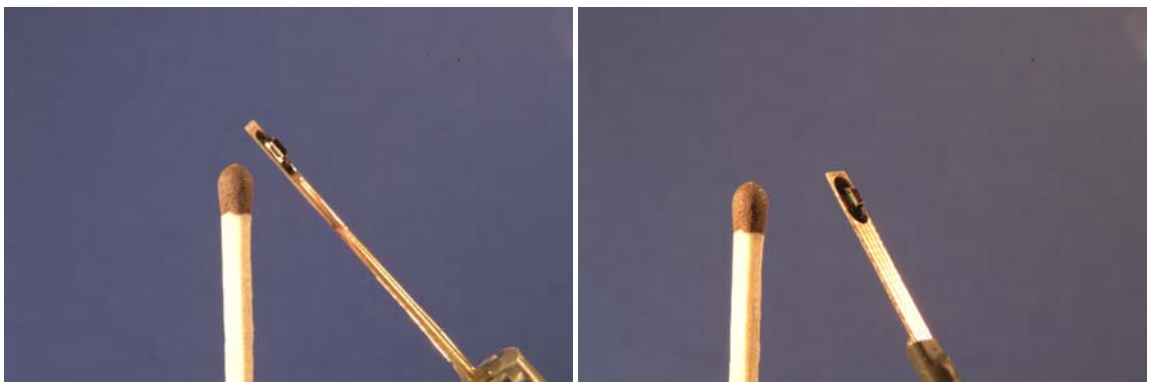

Figure 1-9: Photograph of a scanning probe (courtesy Microflown Technologies BV.). Left: old two-wire sensor, Right, the new microflown sensor.

0.5 inch probe and the upper usable sound level is also 10 dB higher. Figure 1-9 shows two examples of scanning probes.

1.7.4.5 Other microflowns

There are many other types of standard and specialised microflowns. For example the PU-match, which is a small p-u probe. The PU-match is basically a scanning probe, with attached a miniature microphone so that a true p-u measurement is feasible with a minimum of distortion of the sound field itself.

Furthermore, Microflown Technologies is also specialised in arrays of microflowns of various size.

1.7.5 Noise Properties

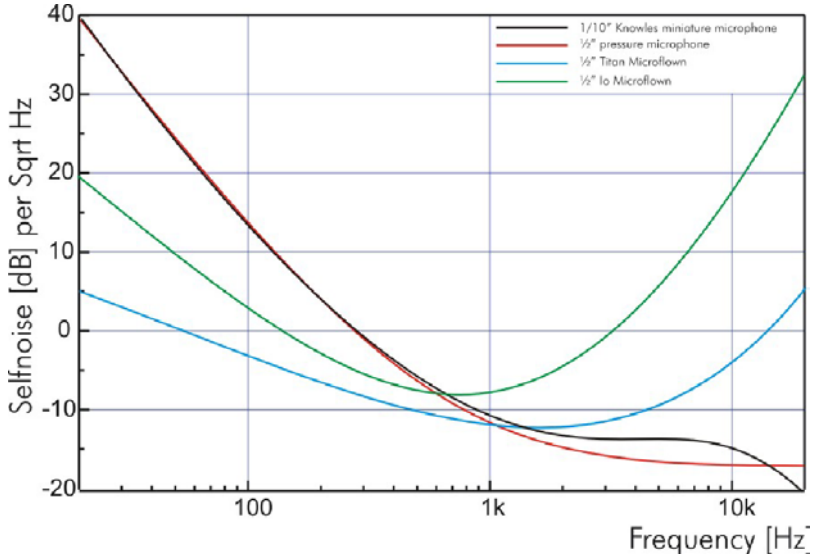

Figure 1-10: Self-noise of the Titan and Io microflown packaged in a 0.5 inch package in 1 Hz bands compared with the noise the particle velocity measured with a 40AC GRAS pressure microphone and a 1/10-inch FG Knowles microphone (courtesy Microflown Technologies).

The microflown has a somewhat different noise spectrum as compared with that of pressure microphones. Figure 1-10 shows a few noise spectra of several types of microflowns. In section 2.8 of this thesis, the equivalent self-noise is discussed more thoroughly. This equivalent self-noise makes a comparison possible between the noise properties of particle velocity and sound pressure sensors. For comparison the self-noise spectrum of a 0.5 inch condenser microphone and of a small miniature microphone is also shown in the figure.

In Figure 1-10 the general shape can be seen. For low frequencies, the self-noise increases (for decreasing frequency) due to $1/f^{\alpha}$ noise (Honschoten, 2004) but in general the self-noise is lower than that of microphones. For midrange frequencies, modern microflowns show fairly well equivalent self-noise values. For high frequencies, the self-noise increases again due to the decrease in sensitivity.

1.8 Acoustical quantities and measures

1.8.1 Sound Pressure Level

The sound pressure level (L_p), abbreviated as SPL, is a convenient measure in acoustics. The sound pressure level is defined as (Morfey, 2001):

$$\mathrm{SPL} = 10\log\left(\left(\frac{p_{\mathrm{rms}}}{p_{\mathrm{ref}}}\right)^2\right) = 20\log\left(\frac{p_{\mathrm{rms}}}{p_{\mathrm{ref}}}\right) \tag{1.3}$$

where the reference pressure p_{ref} is chosen as 20 μPa.

Notice that the sound pressure level is only defined at a given point (Morfey, 2001). The term average sound pressure level refers to a spatial average over a finite region.

The sound pressure level is only a measure of the rms-value of the pressure. The spectrum pressure level, the level of the autospectral density of the pressure, is therefore a more convenient measure if frequencies are taken into account, in case of time-stationary random signals. The standard bandwidth is 1 Hz, but levels can also be defined for given frequency bands.

1.8.2 Particle Velocity Level

The particle velocity level (L_v), also abbreviated as PVL, is a convenient measure of the particle velocity.

$$\mathrm{PVL} = 20\log\left(\frac{u_{\mathrm{rms}}}{u_{\mathrm{ref}}}\right) \tag{1.4}$$

where u_{ref} can be chosen as 5 10^{-8} m s^{-1} (which equals $p_{\mathrm{ref}}/400$), as $p_{\mathrm{ref}}/415$, or as p_{ref}/Z_s where Z_s is the actual measured or estimated specific acoustical impedance of a plane wave in air.

1.8.3 Sound Intensity Level, Sound Intensity and Sound Power

1.8.3.1 History of sound intensity

Often the history starts with the patent of Harry Olson in 1931 (Olson, 1932). He describes a tool for measuring sound intensity, including particle velocity sensor, filters, and etcetera. It did not seem very practical. In 1943 Bolt and Pretrauskas (Bolt and Petrauskas, 1943) measured acoustical impedance of materials using two spaced microphones. Schultz (Schultz, 1958) used that idea in order to measure sound intensity using two spaced microphones. In 1974, Van Zyl (Zyl and Anderson, 1975) presented a prototype of an analog sound intensity measurement. The year 1977 was an important year, two commercial products were introduced and Fahy (Fahy, 1977) and Chung presented a method of using FFT analyzers in a smart way.

In 1994, the microflown, a micromachined sensor, was invented (Bree de et al., 1995) which was a true particle velocity sensor. Although first, de Bree showed that an “apparent pressure” could be measured using two microflowns (Bree de et al., 1996a). Later Druyvesteyn and de Bree showed that combining the microflown with a pressure microphone resulted in a sound intensity measuring system (Druyvesteyn and Bree de, 2000). In 2001, a half-inch p-u probe was realised by including a small microflown into a half-inch microflown (Raangs et al., 2001a). Due to improvements on the microflown sensor itself, three-dimensional p-u probes could be realised (Bree de, 2003a).

The Sound Intensity Level (L_I), abbreviated in this thesis as SIL, is defined as:

$$\mathrm{SIL} = 10\log\left(\frac{I}{I_{\mathrm{ref}}}\right) \tag{1.5}$$

where the reference sound intensity I_{ref} is defined as 10^{-12} Wm^{-2}. See for example references such as (Gameiro da Silva, 2002).

1.8.3.2 Sound Power

Sound power is the rate of acoustic energy flow across a specified surface, or emitted by a specified sound source (source power). Sound intensity can be used in order to measure the sound power radiated by a device since the summation of all powers of areas surrounding the sound source equals the source power.

The Power level (PWL) is the level of sound power, expressed in decibels relative to a stated reference value, 1 pW. The sound power is not treated further in this thesis but in general, the measurement of sound power is often the main purpose of sound intensity measurements. The sound power can also be obtained using pressure measurements in a reverberating room with well-known properties.

1.8.4 Characteristic Specific Acoustic Impedance of air

The characteristic specific acoustic impedance or characteristic impedance is the complex ratio, in a single-frequency sound field, between the acoustic pressure p and the particle velocity u at the same point (Morfey, 2001). The real part is known as the specific acoustic resistance and the imaginary part is the specific reactance.

$$Z = \frac{P}{U} \tag{1.6}$$

The calculation of the specific impedance of air, Z, out of environmental qualities such as atmospherical pressure, relative humidity, and temperature can be found in Appendix C.

A microflown particle velocity sensor can be calibrated against a reference microphone, meaning that the sensitivity is than calibrated in terms of V Pa^{*-1} where Pa^{*} is the particle velocity in m s^{-1} which is connected with a plane sound field of 1 Pa. The sensitivity is thus known except for a factor $Z_{air} = \rho_0 c$.

The particle velocity at the same position as the microflown particle velocity sensor can also be measured with other methods, for example an LDA technique such as photon correlation. Taken that the same particle velocity is being measured with the LDA technique and the microflown particle velocity sensor, the specific impedance of the medium can be measured, taken the calibrated microflown is calibrated against a pressure sensor. Combining such a measurement with an independent measurement of the particle velocity such as LDA gives the specific impedance of the medium as is shown in Figure 1-11. The specific impedance was calculated to be 407.5 Pa s m^{-1} using the measured atmospherical conditions.

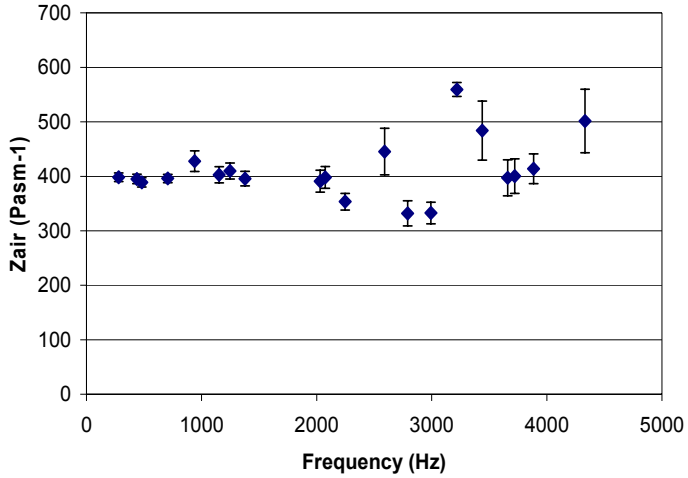

Figure 1-11: The specific impedance of air as measured using the microflown (calibrated using a reference pressure sensor) and the particle velocity as measured using the LDA photon correlation method. Frequencies greater than 4kHz cannot be produced in the standing wave tube used in the experiments due to its physical dimensions.

1.8.5 Surface velocity

Another field of application of the microflown is the direct measurement of the structural surface velocity. In case the structural size and the wavelength are large compared to the measurement distance, it can be shown that the particle velocity almost equals the surface velocity (Bree de et al., 2004;Bree de et al., 2005). These conditions often occur, for example in vehicle interiors where noise is more and more often the focus of acoustical investigations. Applications of microflowns have already shown to improve acquisition time and showed excellent results on the whole frequency range (Rondeau et al., 2005;Wolff and Sottek, 2004;Wolff and Sottek, 2005). In section 5.8 of this thesis numerical and experimental results are discussed for a piston in a baffle.

1.9 Outline of the Thesis

The present chapter covers an introduction to sound, sound pressure, sound particle velocity, acoustic impedance, and a short introduction in the microflown particle velocity. This chapter also includes a discussion of applications of the particle velocity sensor.

Chapter 2 discusses properties of the microflown particle velocity sensor such as a model of the sensitivity curve which is used for calibration and measurements. Further several calibration techniques of the microflown are discussed, such as the

standing wave tube, a photon correlation laser doppler technique, and a near field technique. Additionally, noise properties of the microflown and measurement techniques for measuring self-noise are shortly discussed.

Chapter 3 discusses the application of cross- and autocorrelations. Applications are (i) noise reduction in auto-spectra/autocorrelation using two microflowns, and (ii) reverberant free measurements and source localization in the far field in a reverberant environment. The first application is based on the utilisation of cross-correlation spectra instead of auto-correlation spectra of two of these sensors. The reverberant free measurements are shortly compared with the sound intensity obtained by the same sensor but a different technique, namely the p-u method.

Chapter 4 discusses properties, applications, and measurement techniques of sound intensity. Discussed will be the history of sound intensity, the various techniques available, and specifically the application of the so-called PU probe. Combined with our MATLAB® software using a good quality sound card (A/D converter) sound intensity measurements are made easily. Results are compared with a commercial p-p type sound intensity probe and the obtained sound intensities were found to be in good agreement with measurements obtained using the commercially available sound intensity probe.

Chapter 5 will discuss properties of pressure and particle velocity sensors measurements meant for inverse acoustics such as NAH, PNAH, IBEM, IFRF, STSF, and so on. For of few sound sources, it will be shown that particle velocity times the characteristic impedance of air is higher than the sound pressure in the near field. For such cases, application of a particle velocity sensor will enhance the results since the measured surface scan is or can be of higher quality and a higher signal to noise ratio can be obtained.

Another interesting aspect of sound particle velocity is the fact that reference signals for multiple (small) sound sources can be obtained in the measured particle velocity data. In section 5.7 we show that in case of multiple small sound sources, the use of the directivity of the microflown can be used to obtain a signal that is only related with the sound radiated by one of the sound sources. This signal can then be used to obtain the sound field only caused by this sound source. Theoretically, this information can be used for backward propagation so that the

structural surface velocity and pressure due to this single sound source can be computed.

Very close to a relative large structure, we defined a very near field. In this part of the near field, the relation between particle velocity and structural velocity becomes almost linear. In Chapter 5 we show some experimental and numerical experiments for a piston in a baffle. It was shown that the measured particle velocities and pressure were in good agreement with the analytically predicted values, but most important, the particle velocity becomes closely related and almost the same as the surface velocity as measured using a laser vibrometer.

Chapter 6 contains the conclusions.

Some sections are copied out of published journal papers. The formatting of equation numbers, figure captions and references has been changed in order to comply with the formatting of the rest of the thesis. In these sections a slightly smaller letter and line spacing is applied such as the current paragraph.

Chapter 2
Calibration of microflown Particle Velocity Sensors

2.1 Introduction

Calibrating a particle velocity probe is not as obvious as in case of a pressure microphone. For the microphone several methods are available (Wong and Embleton, 1994), with the piston phone as a simple to use example. For the microflown particle velocity probe, no such standardized procedures are available yet. The sensitivity of a microflown, the electrical output for a given particle velocity in the sound field, depends on the frequency. For convenience, a model is used for the absolute sensitivity and phase as function of frequency. This model is presented in section 2.2.

In this chapter, several techniques are described. The first technique we use most often, described in section 2.3, is the standing wave tube. By comparing the microflown signals with the signal from a calibrated (pressure) microphone, the sensitivity and the phase can be estimated using a model of the standing wave tube. A few models are described with difference in complexity and accuracy. In section 2.3.5 a three-dimensional calibration technique using the standing wave tube is presented. By rotating the probe around two axes in the standing wave, the sensitivity can be retrieved for the three orthogonal directions. In Chapter 3 and Chapter 4, the three-dimensional calibration will be applied in measurements. For, and with Microflown Technologies BV, we designed a portable small standing wave tube. The small, short, standing wave tube was needed since other standing wave tubes were considered to large. The functioning of this portable calibration method was examined, and the results are shown in section 2.3.6.

The most straightforward method is the use of a free-field calibration as presented in section 2.4. In the free field, no reflections occur and the ratio between pressure and particle velocity in the far field simply equals $\rho_0 c$. A disadvantage of this method is the fact that such a free-field environment is not always available and is not easy to create. A crude approximation is the open window. For high frequencies, a small anechoic chamber can be used.

In section 2.5, a so-called reverberant room calibration technique is described. If the acoustical field in a room is totally diffuse, meaning that reverberant sound is radiated in the same extent from all directions, we can derive the free field portion in the particle velocity and pressure by straightforward signal processing techniques.

Another known method for measuring particle velocity in air is the use of a laser. The use of the photon-correlation Laser Doppler technique is described in section 2.6. This section is based on a journal paper (Raangs et al., 2005). The major advantage of the LDA photon-correlation technique is the fact that the measured particle velocity is an absolute, and non-intrusive, calibration technique meaning that the technique only requires measuring length, force, voltage, and so on (Kinsler et al., 2000). This calibration technique is therefore fully independent of another acoustical measurement. We compared the results of the absolute LDA technique and the relative technique using the standing wave tube and a reference pressure sensor

The technique described in section 2.7 uses a well-defined acoustical sound source. In case of the rigid piston, an analytical solution exists (Beissner, 1982) on the axis of rotation. This analytical equation can be used for calibrating the microflown particle velocity sensor.

Although self-noise technically is not part of a calibration method, the self-noise is an important technical specification. The self-noise spectrum, or better, the equivalent noise levels, clearly show which sound fields/levels can be measured using a certain sensor. In section 2.8 a few examples of self-noise spectra are shown for modern microflowns.

2.2 Sensitivity and frequency response curve of the microflown

For an acoustical sensor, or in fact any sensor used in physical measurements, it is essential that the relation between the physical quantity measured and the output is known well. This relation between the output of a linear sensor and the physical input is known as the sensitivity of the device (Morfey, 2001). Note that the sensitivity is only defined for linear sensors. For very loud sounds, almost all acoustical sensors will start to behave non-linear and/or linear acoustics will not be applicable any more.

In general, the output of a measuring device can be everything, from the height of the mercury column in a mercury thermometer or barometer, a capacitance in a condenser microphone, each tipping of a tipping bucket electric rain gauge, et cetera. For convenience, the output of a sensor is often an electrical voltage given in volt or millivolt. Furthermore, it is desirable that the measuring device is only sensitive for a single physical quantity. The sensitivity is therefore defined as

$$S = \frac{\text{output[volts]}}{\text{input[xxx]}} \tag{2.1}$$

where for a particle velocity sensor the input is given in m s^{-1} and for a pressure sensor in pascal. The sensitivity is then given in volt or millivolt per m s^{-1} (or millivolt per pascal for a pressure sensor):

$$S_u = \frac{\text{output}}{\text{input}}\left[\text{V m}^{-1}\text{ s}\right] \quad S_p = \frac{\text{output}}{\text{input}}\left[\text{V Pa}^{-1}\right] \tag{2.2}$$

In practice, the sensitivity of acoustical sensors is a function of frequency. The sensitivity of measurement microphones are often almost flat over a broad frequency range.

At higher frequencies, the sensitivity of the microflown is decreasing. This high-frequency roll-off is caused by diffusion effects (to which the time it takes heat to travel from one wire to the other is related). The effect can be estimated by a first order low pass frequency response that has a (diffusion) corner frequency (f_d) in the order of 500 Hz – 2 kHz (depending on geometry and operating temperature) (Honschoten, 2004). The second high frequency roll-off is caused by the heat capacity (thermal mass) and shows an exact first order low pass behaviour that has a heat capacity corner frequency ($f_{heatcap}$) in the order of 2 kHz to 15 kHz for microflowns (depending on geometry and operating temperature). These effects are explained in more detail in (Honschoten et al., 2001) and (Svetovoy and Winter, 2000).

A good approximation of the frequency dependent sensitivity of a microflown can be described with (Bree de, 2003a)

$$\text{output} = \frac{\text{LFS}}{\sqrt{1+f^2/f_{heatcap}^2}\sqrt{1+f^2/f_d^2}}. \tag{2.3}$$

where LFS being the low frequency sensitivity, the output signal at frequencies below f_d, the thermal diffusion corner frequency.

Note that, although the sensor acts as a low-pass filter, the sensor is still linear and equation (2.1) is still applicable although the sensitivity S becomes a function of frequency $S(f)$. The same low-pass behaviour of the microflown particle velocity sensor causes the phase of the electrical output signal to be shifted with reference to the acoustical particle velocity. If the phase is important in the measurement, then the phase should also be calibrated. The measured phase response can be fitted by (Bree de, 2003a):

$$\text{Phase} = -A \quad \arctan\left(\frac{f}{f_{ph}}\right) \tag{2.4}$$

A and f_{ph} being arbitrary constants that can be found by fitting the calibration data.

2.3 Standing Wave Tube (SWT)

The calibration of the microflown in a standing wave tube is our favourite calibration method because the acoustical impedance in this tube is well understood and this calibration yields both the sensitivities of the pressure and the particle velocity sensor against a known (calibrated) pressure microphone with little effort. It is possible to fit the sensitivity on the maxima in the calibration curves, or we can compare the measurement against a model of the standing wave tube including the effects of viscosity. The latter method also yields the phase of the pressure and velocity sensors. The phase however can also be derived from the mean of two measurements whereas the probe is rotated by 180 degrees in the tube. The latter method is allowed in case the total time average intensity is zero in the tube.

A standing wave tube can be used for calibration the microflown and has the advantage of its small size and is therefore easy to use. Another advantage is the fact that the sound field is purely one-dimensional. The disadvantage of the use of an SWT is the fact that the sound field is not as simple as in case of an ideal anechoic room. The comparison with a model is quite complex because many parameters are involved (distance between the p and u sensors, diameter, viscosity, shear, etc.) and is hard to automate by a software system. For a three-dimensional p-u probe the problem is even more complex since for this probe we are not only

interested in the frequency response (sensitivity and phase) of the 3 (or more) microflowns and the microphone, but also in directivity function of the microflowns with reference to a known direction and to each other.

Figure 2-1: Standing Wave Tube available for three-dimensional calibration of multi-microflown sensors (source: Microflown Technologies). Notice the extra 0.5 inch opening needed for the three-dimensional calibration technique (see section 2.3.5) or microflowns placed under 45 degrees.

There are basically three techniques we can use for post-processing the standing wave tube measurement:

The simplest method is to find the maxima in the transfer function $G_{\mathrm{p_{ref}u}}(f)$. Since this is the simplest method to implement, it is a good method for at least obtaining well starting values for the other models, taken that a minimization of a cost function is used and a good starting values for the constants (see equation (2.3)). In section 2.3.2 this method is described in more detail.

Somewhat more difficult is to use a more accurate model of the standing wave tube including viscothermal losses (Honschoten et al., 2000). Although this is theoretically a good approach, practically it would require a very well designed standing wave tube since only viscothermal effects are taken into account. For completeness, this model is described in this section below.

The third method uses an estimate (using for example technique nr.1 based on the maxima in the transferfunction $G_{\mathrm{p_{ref}u}}(f)$) which is then used to accurately describe the standing wave tube. With use of only three parameters an accurate model of the used standing wave tube can be fitted which is then used to retrieve a more accurate sensitivity (and phase) curve of the microflown. This approach is described in section 2.3.1.

The disadvantage of the standing wave tube is the fact that it functions only between a lower and upper frequency. Because of the physical size of our 0.5 inch package, we are not able to use a standing wave tube that functions above ~4 kHz

because of its diameter. The lowest frequency depends on the length of the standing wave tube so two tubes should be used if low frequencies (< 100 Hz) should be implemented correctly.

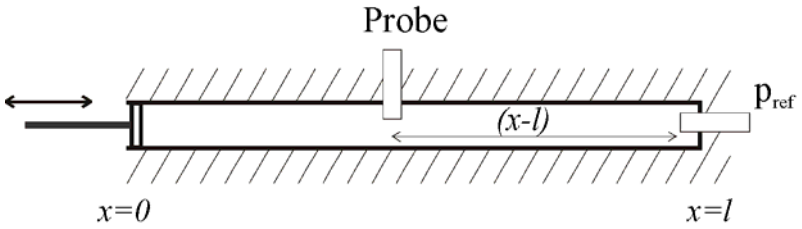

Figure 2-2: A tube that is rigidly terminated at $x = l$ and in which the fluid is driven by a vibrating loudspeaker at $x = 0$.

Above the cut-off frequency, the standing waves are no longer one-dimensional. The set-up will then be very difficult to use since the acoustic impedance is not a real and constant any more. For a tube, this cut-off frequency is given by (Rienstra and Hirschberg, 2002):

$$f_c = \frac{c}{1.71 \cdot d} \tag{2.5}$$

where d represents the diameter of the tube, and c the speed of sound (approximately 343 m s^{-1}). In a standing wave tube, the sound field is one-dimensional, and in case the tube is rigidly terminated with rigged sidewalls, all sound will be reflected at the end of the tube.

The specific acoustic impedance inside the SWT can be calculated by solving the wave equation. The fluid is excited by a loudspeaker with velocity amplitude U at the left-hand end and is terminated by a rigid boundary at the right-hand end, see figure 2-2. The sound pressure and particle velocity at any place in the tube is given by:

$$p(x) = -\mathrm{i}\rho_0 cU \frac{\cos(k(l-x))}{\sin(kl)} \quad u(x) = U \frac{\sin(k(l-x))}{\sin(kl)} \tag{2.6}$$

A good place to put a reference microphone is at the end of the tube since the sound pressure is at its maximum at that place; so $p_{\mathrm{ref.}}(x=l) = p_{\mathrm{ref.}}(l) \equiv p_{\mathrm{ref}}$

If a p-u sound intensity probe is put at a certain position x in the tube the relation between the pressure microphone of the p-u sound intensity probe and the reference (pressure) microphone at the end of the tube is given by: ($p_{\mathrm{probe}} = p_{\mathrm{probe}}(l)$).

$$\frac{p_{\text{probe}}}{p_{\text{ref.}}} = \cos(k(l-x)) \tag{2.7}$$

The relation turns out to be a simple cosine function. The distance (*l*-*x*) can easily be obtained by measuring two minima of the cosine function.

Analogously, almost the same applies for the particle velocity ($u_{\text{probe}} = u(x)$):

$$\frac{u_{\text{probe}}}{p_{\text{ref.}}} = \frac{\mathrm{i}}{\rho_0 c}\sin(k(l-x)) \tag{2.8}$$

The relation of the particle velocity and sound pressure at the end of the tube turns out to be a simple sine function. The phase shift between them equals plus or minus 90 degrees.

It shows that for calibrating the p-u probe for obtaining the sound intensity only the phase mismatch (φ_p-φ_u) should be determined and individual phase mismatch of both probes does not have to be determined. The p-u probe phase mismatch (φ_{p}-φ_{u}) can be determined by measuring the ratio of the particle velocity and the sound pressure in the tube. The equation of the ratio is given by:

$$\frac{u_{\text{probe}}}{p_{\text{probe}}} = \frac{\mathrm{i}}{\rho_0 c}\tan(k(l-x)) \rightarrow Arg\left\{\frac{u(x)}{p(x)}\right\} = \pm 90^{\circ} \tag{2.9}$$

This relation shows that in a standing wave tube particle velocity and sound pressure are 90 degrees out of phase. In this way the p-u probe is phase calibrated in the arrangement as it is used: the pressure microphone is positioned face-to-face to the microflown.

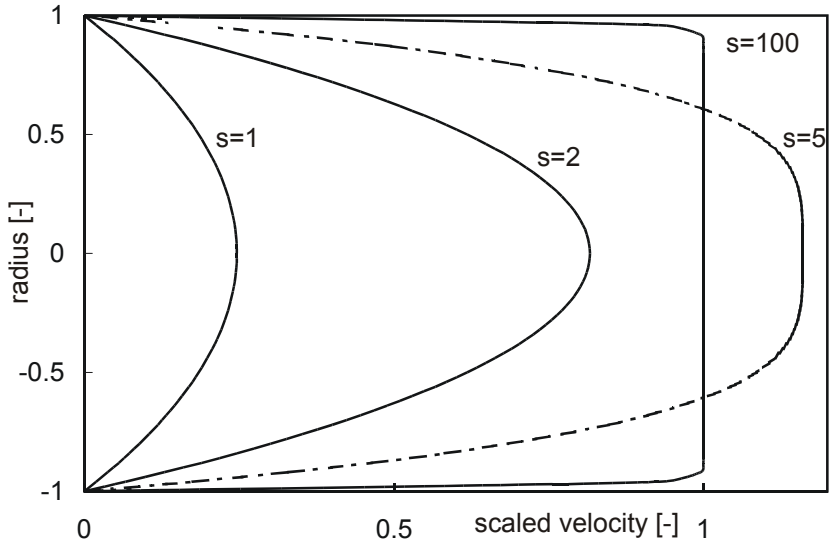

Figure 2-3: Particle velocity profile in a tube as a function of the shear wave number *s*.

In practice, the sound in the tube is slightly damped. Two effects cause this. The particle velocity is zero at boundaries of the tube. In the middle of the tube the sound wave propagate as a plane wave as is shown in Figure 2-3. The friction in the air between zero velocity and plane wave causes damping. This effect is noticed most at low frequencies. At high frequencies, the damping of the air itself will be noticeable. For an exact solution, see (Tijdeman, 1975).

If thermal viscous effects (damping) are considered, equation (2.8) will alter in to (Honschoten et al., 2000):

$$\frac{u_{\text{probe}}}{p_{\text{ref}}} = \frac{1}{\rho_0 c}\left(\frac{\cosh\Gamma(k(x-l))}{\gamma\zeta} + \frac{\mathrm{i}\sinh\Gamma(k(x-l))}{\Gamma}\right) \tag{2.10}$$

Using Γ as the viscothermal wave propagation coefficient which is given by:

$$\Gamma = \mathrm{i} + \frac{1+\mathrm{i}}{\sqrt{2}}\left(\frac{\gamma - 1 + \sigma}{s\sigma}\right) \tag{2.11}$$

Using γ= 1.4 as the ratio of specific heats of air, σ = 0.845 square root of the Prandtl number and s as the shear wave number:

$$s = \frac{d\sqrt{\omega}}{2}\sqrt{\frac{\rho_0}{\mu}} = 346d\sqrt{f} \tag{2.12}$$

Using $\mu = 17.1\cdot10^{-6}$ [Pa s] as the dynamic viscosity and ρ_0 = 1.3 [kg m^{-3}] as the density. To use this model the shear wave number must be much larger than unity, which is in practical cases true. The viscothermal wave propagation coefficient can be simplified to:

$$\Gamma = \mathrm{i} + \frac{1+\mathrm{i}}{332d\sqrt{f}} \tag{2.13}$$

As can be seen, for higher frequencies or large diameters, Γ will reach i and the simple model may be used.

One should dimension the diameter and the tube's length in such way the factor $332d\sqrt{f}$ is as large as possible. For low frequencies we use a tube of 16 cm in diameter and 8 metres in length. In this case, at 20 Hz the effect of damping is not noticeable. The tube can be used up to 1 kHz due to the corner frequency of the tube. For higher frequencies we use a tube that is 5 cm in diameter and 75 cm in length. This tube is used in a 250 Hz - 4 kHz bandwidth. For half-inch probes, it is not possible to use tubes with smaller diameter.

Although the thermal viscous effects are relative small, they are observed mostly clear in the phase response (Honschoten, 2004). In case of an ideal standing wave tube with no losses, the phase response in the tube should be plus or minus 90 degrees. The measured response shows “rounded edges” (see Figure 2-16). This is partly due to these thermal viscous effects.

In practical standing wave tubes, for example 5 cm diameter and 70 cm long, equation (2.10) does not fully explain all losses. In fact, the description of the standing wave tube is much more complicated if the coupling between the loudspeaker driving the open end, and the standing wave tube is considered (Kinsler et al., 2000).

2.3.1 Standing wave Tube (SWT Model fitting)

In this section, an empirical function has been applied which models various losses inside the standing wave tube (MacGillivray, 2002). From the measured signals, properties of the standing wave tube and the sound field inside are obtained. These properties can be: (i) the position with reference to the closed end, (ii) an overall standing wave ratio (SWR) describing losses and non-idealities in reflection coefficients, and (iii) an angle (θ) describing the non-idealities in reflection coefficients (MacGillivray, 2002). Since the used model of the standing wave tube contains only two extra variables, which can easily be obtained using the thousand frequency points, the presented method is very practical.

A problem of this idealized relationship given in equation (2.8) or even in equation (2.10) between particle velocity and reference pressure is the fact that they do not describe the results well/fully over the whole frequency range from f_l (the lowest usable frequency, about 250 Hz), to f_c (about 4 kHz). The frequencies for which this transfer-function has its minimum cannot be explained by a single distance parameter over this whole frequency domain. Including viscosity losses in the sound field improves the transfer-function $u_{\text{probe}} / p_{\text{ref}}$ but because of the size of the used tube this effect is mainly limited to the phase of the transfer-function itself and can often be neglected (Honschoten et al., 2000).

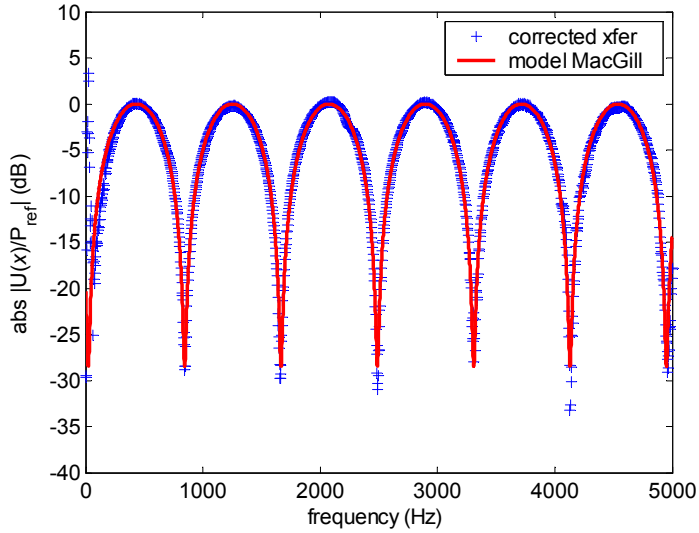

Figure 2-4: Measured transfer function between particle velocity at position *x* and pressure *p* at the closed-end corrected for the sensitivity behaviour of the microflown itself. The line represents the model (see equation (2.14)) which is fitted on the corrected data $U(x)/P_{ref}(l)$.

We can incorporate the non-ideal behaviour of the wave tube by implementing a attenuation in amplitude and a small phase change, θ occurring on the reflection at the closed-end (MacGillivray, 2002): $p_i = Ae^{i(\omega t - kx)}$; $p_r = Be^{i(\omega t + kx + \theta)}$, where p_i and p_r are the initial and the reflected pressures, A and B the amplitudes and θ a small phase change. The ratio of the acoustic particle velocity at x to the pressure at $x = l$ is given by (MacGillivray, 2002)

$$\frac{u(x)}{p(l)} = \frac{1}{\rho_0 c}\left(\frac{1}{\mathrm{SWR}}\cos\left(k(l-x)-\theta/2\right)+\mathrm{i}\sin\left(k(l-x)-\theta/2\right)\right) \qquad (2.14)$$

where the standing wave ratio, SWR, is

$$\mathrm{SWR} = \frac{A+B}{A-B} \qquad (2.15)$$

A first estimate of the microflown sensitivity curve (see equation (2.3)) is obtained by fitting a curve through the maxima in the transferfunction between particle velocity $u(x)$ and $p_{ref}(l)$ since for the maxima, the relation is well known, see also section 2.3.2.

With use of a first estimate of the microflown sensitivity the transfer function between particle velocity $u(x)$ and $p(l)$ can be determined and the model (see equation (2.3)) can be fitted on to this data by minimizing the mean square difference between data and model while adjusting the parameters SWR, the phase θ, and the distance (l-x) (see equation (2.14)). The result of this procedure is

shown in Figure 2-4; for this standing wave tube the parameters were SWR = 26.6, θ = 10.2 degrees, and the distance (l-x) = 0.210 m. Although this model is only empirical, it clearly describes the measured data better than the other models.

The main advantage of using this description of the transfer function, see equation (2.14), is that the SWR, the phase change θ, and the distance (l-x), can be obtained from the data using an un-calibrated particle velocity probe. With this knowledge of the standing wave tube, almost all frequency data can be used to obtain the absolute sensitivity and the phase of the microflown particle velocity sensor. The use of more frequency data will then increase the resolution of the calibration of the sensor. In Figure 2-5 the raw measured data and the measured data corrected for the standing wave tube, see equation (2.14), is presented with a fit of the sensitivity as function of the frequency. Only data with coherence larger than 0.98 are plotted in Figure 2-5. The root mean squared error (RMSE) was estimated as 2.8% (0.24 dB) for the coherent frequency data points between 250 Hz and 4 kHz and the three different sound levels (of respectively 94 dB, 110 dB, and 130 dB). Normally, the uncertainty in the pressure measurement would also be included but since the microphone was recently calibrated by the National Physical Laboratory this error can be assumed to be smaller than other errors.

Note the difference between the data and the fit can be minimized by decreasing the frequency span if the sensitivity needs to be known more accurate for a certain frequency. For example, if a frequency span of 900 Hz is used (800 Hz –

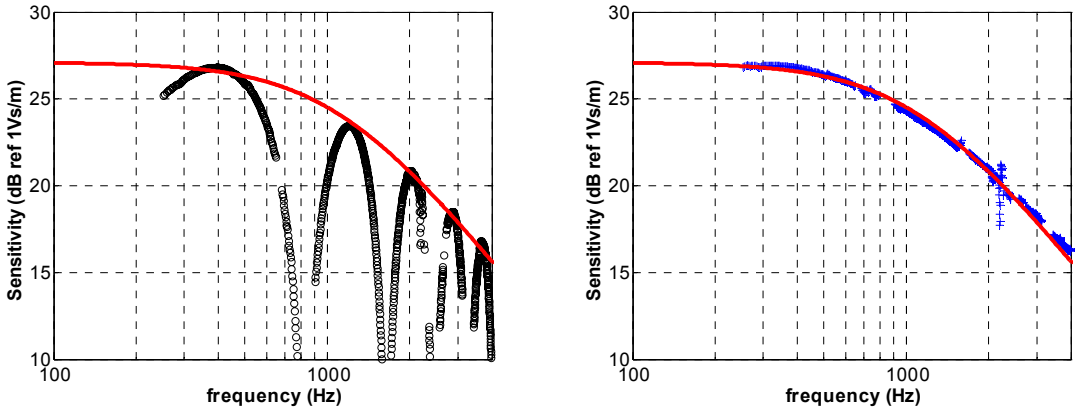

Figure 2-5: Microflown calibration using a standing wave tube and a calibrated microphone. Shown are the measured transfer function ($V_{microflown}/P_{ref}$) as the o-marks (left figure), the + marks (right figure) represent the corrected measurement data using equation (2.14) (see text) and the line (both figures) represents the fit of the sensitivity.

1700 Hz), the RMSE is decreased to 1.3% (0.11 dB).

2.3.2 Standing wave Tube (Finding Maxima in transfer function)

In the previous section, section 2.3.1, a procedure is described in which a model for the standing wave tube has been used in order to optimise the parameters for the microflown sensitivity curve, as given in equation (2.3). In this section a faster, though less accurate method is given which uses the maximum in the transferfunction between the particle velocity signal $u(x)*S_u$ [V] and the pressure signal $p_{ref}(l)*S_p$ [V] at the closed end. Since the frequencies for which the maxima occur almost equals the frequency at which the maximum in the transferfunction between the particle velocity and pressure, the sensitivity curve can be fitted using these frequencies since the relationship between pressure and particle velocity equals $\left|u_{probe}/p_{ref.}\right| = \left(\rho_0 c\right)^{-1}$ as is given in equation (2.8).

Procedure used for finding the maxima:

- Read the measurements to workspace
- Estimate frequencies of the maxima in the transfer between the microflown and reference microphone
- Fit a function for the absolute transfer function (in dB scale) around these maxima (e.q. ± 100 Hz for the long-distance and ± 200 Hz for the short distance microflown-microphone), this way we use more data points than only selecting one frequency.
- Find the maxima of this fit.
- Fit a function through these maxima, either a polynomial or a second order low pass function, or another function.

The frequencies are estimated using the simple wave equation, using no viscosity effects.

$$f_{maxest}=1/l_x*(1/4 + [0:n_{max}]/2)\ c \tag{2.16}$$

with n_{max} is the number of the maxima from 0 to 4 kHz (f_{max}).

$$n_{max}=\text{fix}(2*l_x*f_{max} / c - 0.5) \tag{2.17}$$

Note that in case the driver (loudspeaker) is coupled to the standing wave tube, the frequencies for the maxima in the transfer function can be shifted (downwards) severely, especially for a light, flexible driver (Kinsler et al., 2000) and might not

yield good starting values for finding the correct maxima in the measured transfer function.

The fit in dB scale has the advantage that the error in smaller values is weighted similarly, in practice this are the levels for higher frequencies (> 1 kHz). In Figure 2-6 an example of the transfer function is shown.

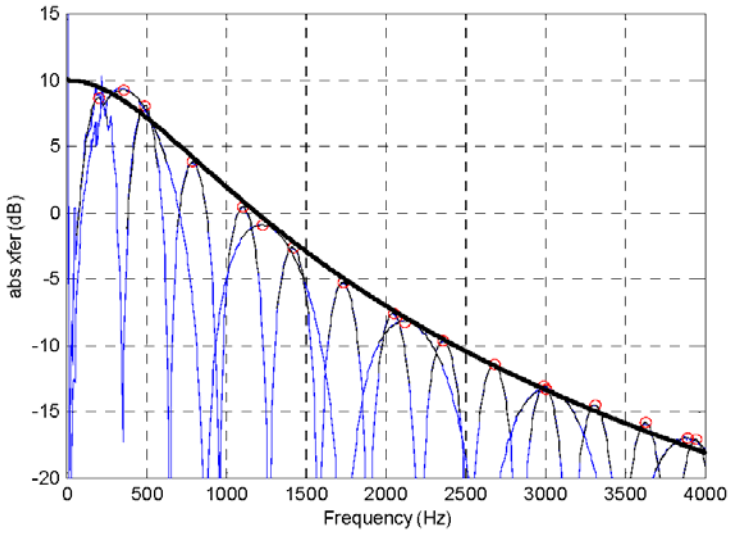

Figure 2-6 Microflown placed in the Standing Wave Tube (perpendicular) and measuring along the centre axis of the SWT. The red circles are the fitted maxima and the black line is the fitted second order low pas function.

Note the second order low pass filter fit underestimates the transfer for 400 Hz (about 1 dB) for the given example in Figure 2-6. From 1000 to 1800 Hz the fit overestimates the measurements slightly by 0.5 dB, and for higher frequencies the fit underestimates (0.5 dB at 4 kHz). The accuracy can therefore be estimated as being 0.5 dB. The standard deviation between fitted point and measurement point as shown in Figure 2-6 yields an estimated accuracy of 0.6 dB.

The maxima in the transfer function between particle velocity at position x and the pressure at the closed-end do not always represent the correct frequencies (maximal particle velocities) and thus a small error is induced due to this mismatch. However, the advantage is that we use measurement data and this method is therefore less sensitive for the first estimation of the acoustical length between microflown and reference microphone. By using the inverse sensitivity curve on the measured transfer function, we achieve almost the true transfer function between the particle velocity and reference pressure. The maxima in this

transfer-function are positioned at the correct frequencies and this frequency data can be used to improve the sensitivity curve.

2.3.3 A numerical simulation

In order to give an overview of the methods used, we have prepared a numerical simulation of a measurement based on the MacGillivray model (MacGillivray, 2002). "Measured" data are prepared by using a model for the standing wave tube as given in equation (2.14). This hypothetical sound field is the measured using a hypothetical microflown which measures this sound field in the standing wave tube. The sensitivity of the microflown is given by equation (2.3).

We have chosen to use the following constants for the model of the standing wave: distance (l-x) = 0.2 m, the standing wave ratio SWR = 25, the angle θ= 10 degrees. The parameters are based on actual measurements. The particle velocity in such a standing wave tube, with reference to the pressure at the closed-end is given in Figure 2-7. For the microflown sensitivity we have chosen a low frequency sensitivity LFS = 22 V s m^{-1}, and two corner frequencies at 1 kHz and at 3 kHz. Such a sensitivity curve is given in Figure 2-8.

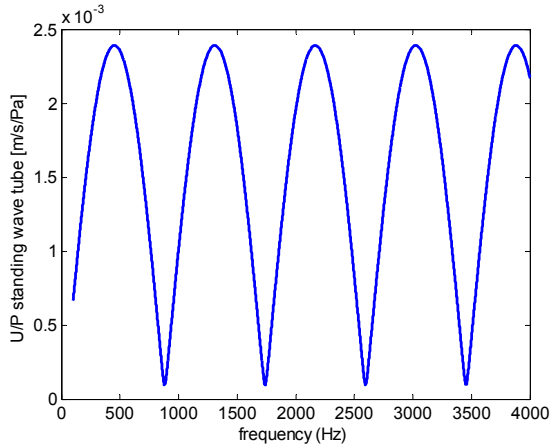

Figure 2-7: The particle velocity in a standing wave tube with reference to the pressure at the closed-end.

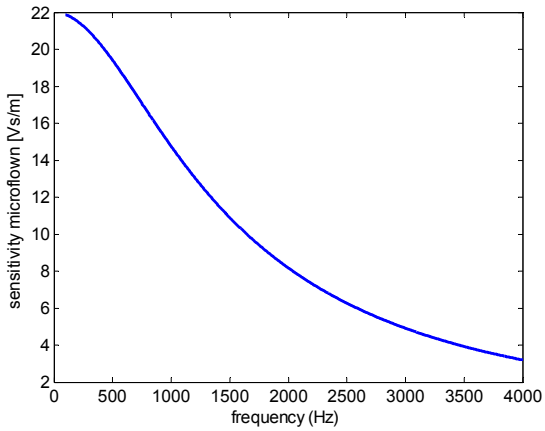

Figure 2-8: Microflown Sensitivity of a hypothetical microflown.

Using the sound field (Figure 2-7) and the sensitivity curve (Figure 2-8), "measured data" can be simulated for such a situation. Additionally some white noise has been added such that the signal to noise ratio of the "measured data" was 76 dB.

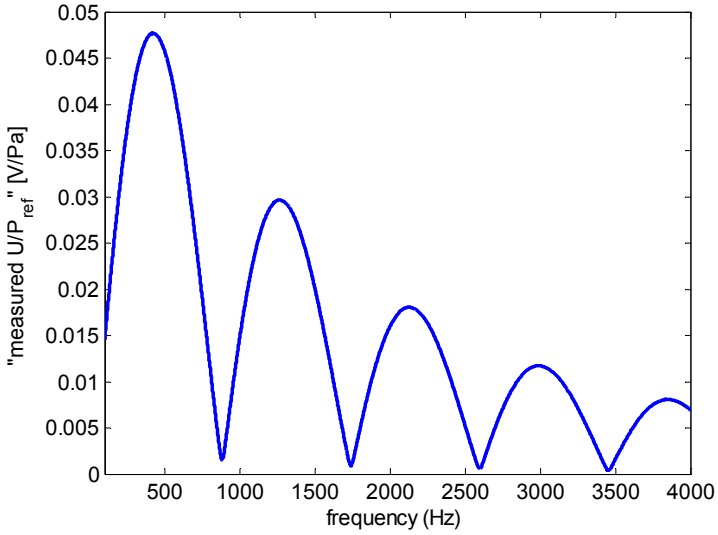

Figure 2-9: Simulated measurement data in the described sound field (see Figure 2-7), measured with microflown (see Figure 2-8), and added noise of 76 dB SNR.

The simplest method to post-process this data is to find the maxima in this curve. This can performed by fitting a polynomial around the estimated frequencies found by using equation (2.16) as is shown in Figure 2-10. These maxima can then be used since for the maxima in the transfer-function of $u(x\text{-}l)$ and $p_{\text{ref.}}$ (see Figure 2-7) are already free-field values as can be seen in equation (2.8). The fitted sensitivity curve is also shown in Figure 2-10 and in Figure 2-13 (first fitted function). The disadvantage of this procedure is the fact that the maxima of the measured transfer-function (see Figure 2-9) are not the correct maxima as in Figure 2-7. Due to the low-pass behaviour of the microflown, a small error is

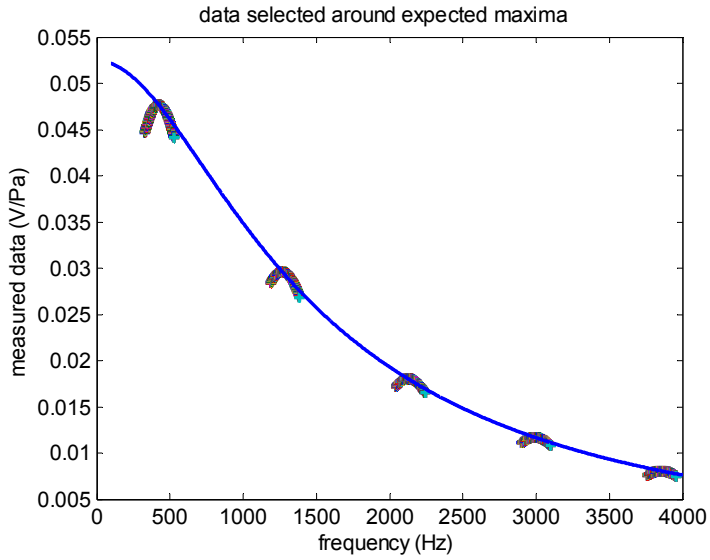

Figure 2-10: The data near expected maxima can easily be used to find the microflowns sensitivity.

introduced.

The first improvement we can make is to use this first estimated microflown's sensitivity so that we can measure the particle velocity in terms of m s^{-1}. For convenience, the "measured" transfer-function between particle velocity and pressure is multiplied by $\rho_0 c$ in Figure 2-11. Unlike the positions of the maxima in Figure 2-10, the maxima in Figure 2-11 coincide with the desired frequencies.

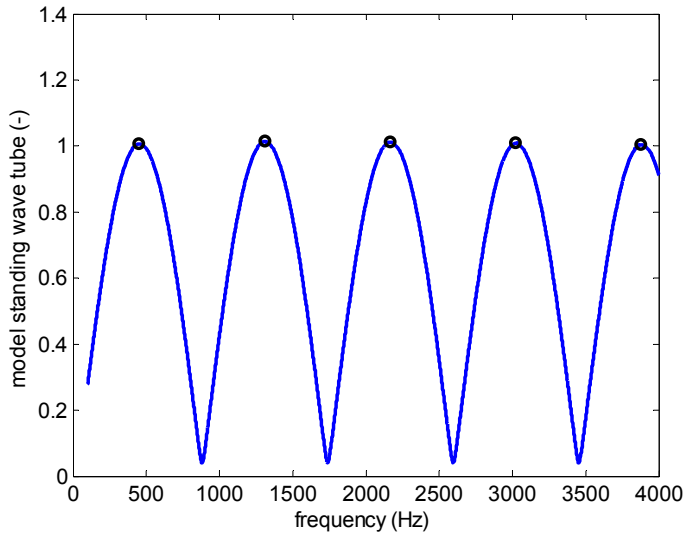

Figure 2-11: "measured" model of the standing wave tube.

The "measured" data (see Figure 2-9) at these frequencies are then used for fitting a sensitivity curve using a direct search method. In Figure 2-13 (second fitted function) the fitted sensitivity curve is shown.

Although the previous result is already quite good, a next step in accuracy can be made. Figure 2-11 already resembles the given behaviour of the standing wave tube. Therefore, out of the measured data (see Figure 2-9), by using the earlier steps, the "measured" model of the standing wave tube can be used. With a simplex search method (Nelder and Mead, 1965), the parameters (l-x), SWR, and θ in equation (2.14) can be found. Using these parameters, the "measured data" (Figure 2-9) then can be used to fit the sensitivity curve of the microflown as given by equation (2.3). In Figure 2-12 the fitted curve, equation (2.3) times equation (2.14), is shown. In Figure 2-13 (third fitted function) the fitted sensitivity curve is shown.

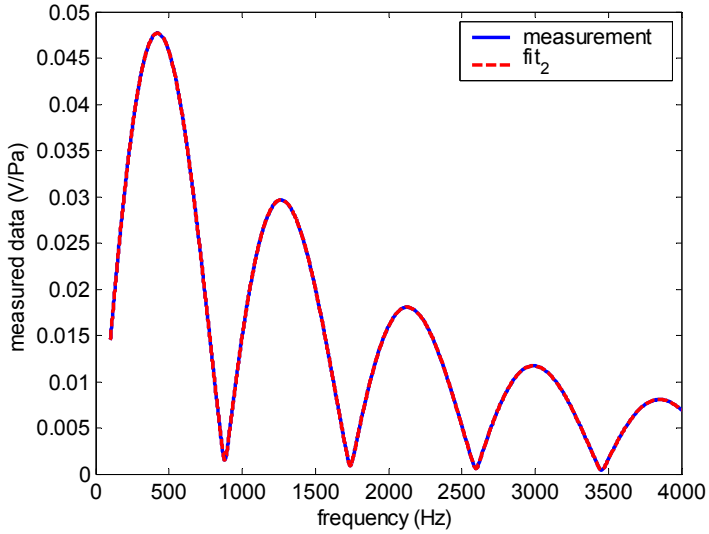

Figure 2-12: The simulated "measured" data (---line) and the fitted curve (- - line).

The result of the three sensitivity curves are shown in Figure 2-13.

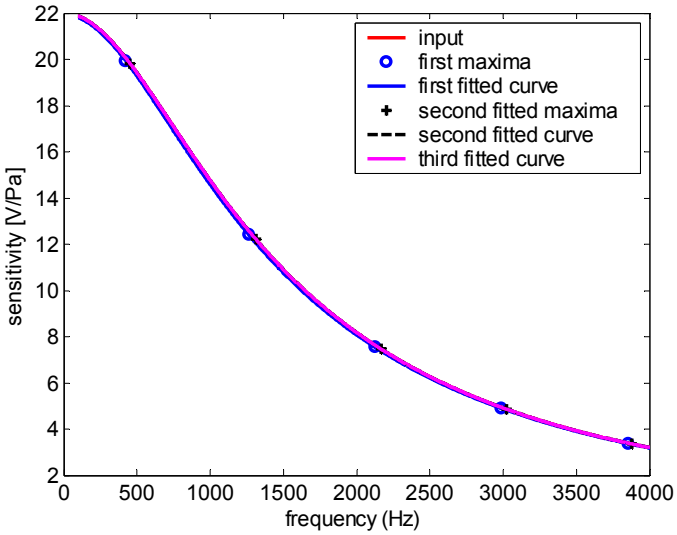

Figure 2-13: The results of the three different calibration methods.

In Figure 2-14 the difference between the obtained sensitivity curves and the correct sensitivity curve (the sensitivity we started with).

For the given simulation it can be seen that the first estimate is the worst one. The error in this first estimation is mainly caused by the fact that the maxima are not at the desired frequencies as has been discussed above. This error can be reduced by increasing the distance between microflown and microphone at the closed end. On the other hand, increasing the distance will increase the effect of viscosity losses in the tube (Rienstra and Hirschberg, 2002).

If we use the maxima for the corrected data (using the first estimate), the error is already very small. This second estimation is already much improved compared with the first estimate. The error in this situation is mainly caused by the fact that only five data-points are being used for fitting the sensitivity curve of the microflown.

For this situation, the error can be decreased by using a fitted model of the standing wave tube (dash-dot line in Figure 2-14). The advantage is that more data-points are used in order to fit the sensitivity curve of the microflown. A disadvantage is the computational effort and this method is somewhat sensitive for noise in the measured data.

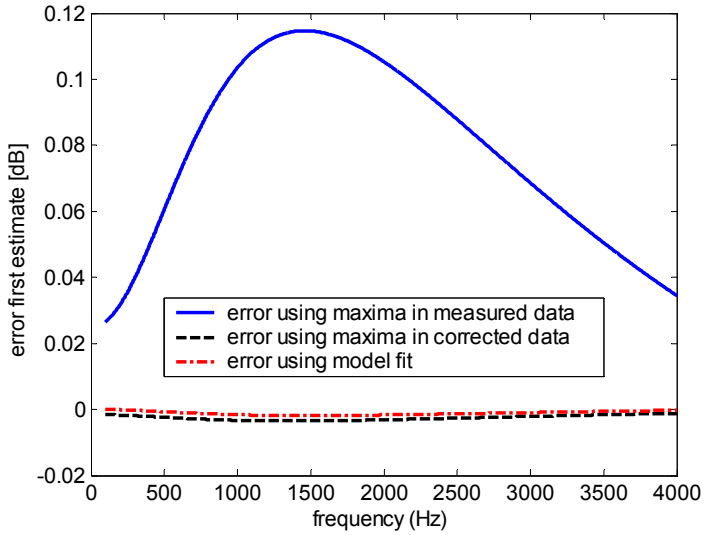

Figure 2-14: Difference (in decibels) between the correct sensitivity and the obtained sensitivity using the three methods.

It can be concluded that the proposed methods will yield a good estimate of the sensitivity curve of the microflown. Although a more thorough analysis of the errors introduced is required.

2.3.4 Phase Calibration

The phase of the microflown is simply measured by taking the phase around the frequencies with maxima in $u(x)/p_{\text{ref}}$ as is shown in Figure 2-15.

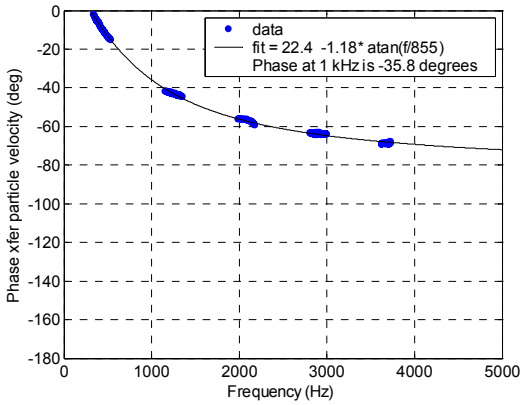

Figure 2-15: The phase of the microflown around frequencies with maxima in $u(x)/p_{ref.}$.corrected for the plus or minus 90 degrees due to the standing wave tube (see equation (2.8)). Only data with coherence > 0.98 is used.

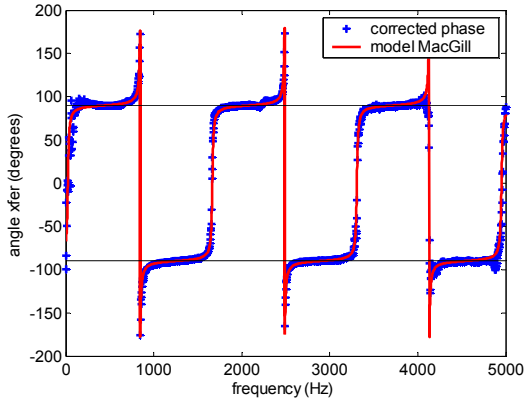

Figure 2-16: The phase between particle velocity $u(x)$ and pressure $p_{ref.}$. The + marks represent the measured data corrected for the fitted phase. The line represents the phase of the model as presented in equation (2.14). The two horizontal lines represent the phase of plus and minus 90 degrees, which is the ideal phase inside the standing wave tube.

The phase of the model of the standing wave tube (section 2.3.1) and the phase of the corrected microflown data using the microflown calibration is shown in Figure 2-16. Although the parameters of SWR and θ in equation (2.14) are only estimated based on the amplitude (see Figure 2-4), the model describes the phase of the particle velocity inside the standing wave tube almost perfectly.

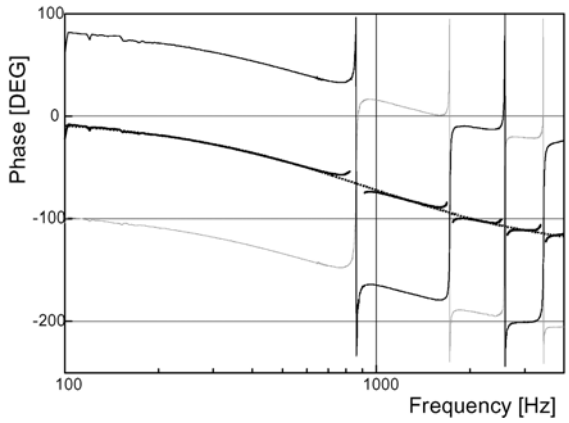

Figure 2-17: Calibration measurement of microflown phase with reference to the pressure sensor in the backplate. ── phase response in the standing wave tube for two microflown orientations; ── (bold) average phase response; ··· model.

Figure 2-17 shows the phase for another microflown than shown in Figure 2-15. Two measurements were made where the microflown was rotated by 180 degrees so the mean phases of the two sound fields in the standing-wave tube equals almost zero (see Figure 2-17). The phase was fitted by

$$\arg\{H_u\} = -1.52 \ \arctan\left(\frac{f}{914}\right) \tag{2.18}$$

Although this seems a crude technique, the advantage is that it is robust against the two various positions, meaning that one does not need to know in which direction the two measurements were performed since the mean phase angle will be equal.

The phase for a pressure sensor, for example build in a p-u probe, the same standing wave tube can be used. Note the phase is 180 and 0 degrees for the pressure inside the standing wave tube, with reference to the pressure at the closed-end, as is shown in Figure 2-18 and equation (2.7). We use a constant value of -177 degrees as a model for the phase response of the miniature microphone (see Figure 2-18).

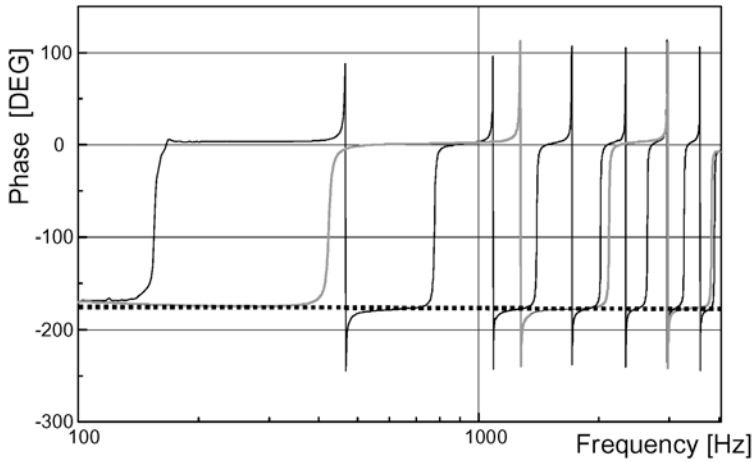

Figure 2-18: Calibration measurement of miniature microphone phase in a standing wave tube; ··· model. Shown are two measurements for two different positions in the standing wave tube.

2.3.5 Three-dimensional Calibration Techniques

One of the most important aspects of the microflown particle velocity sensor is the fact that it truly measures one component of the three-dimensional particle velocity. In this section we describe a three-dimensional calibration technique which not only returns the (absolute) sensitivity of the microflowns, as described in sections 2.3.1 and 2.3.2, but additionally returns the direction in which the microflown measures the particle velocity.

The three-dimensional p-u probe, which has later evolved into the ultimate sound probe (USP) build by Microflown technologies (Microflown Technologies,

2004), as shown in Figure 2-20, has the disadvantages that we cannot calibrate it easily in the SWT (Standing Wave Tube) like the 0.5 inch probes because this would not result in correct magnitudes for the sensitivities and would not give the direction. With use of several calibration measurements while rotation around two axes in the standing wave tube, a three-dimensional calibration has been achieved.

2.3.5.1 Theoretical Description

In the calibration techniques we described in sections 2.3.1 and 2.3.2, the microflown has to be positioned in the direction in which it measures most sensitive. In fact, the sensitivity returned was only the "measured sensitivity" S'_{u} in a certain direction, namely in the direction of the centre axis of the standing wave tube, see also section 1.7.2. This situation is shown in Figure 2-19.

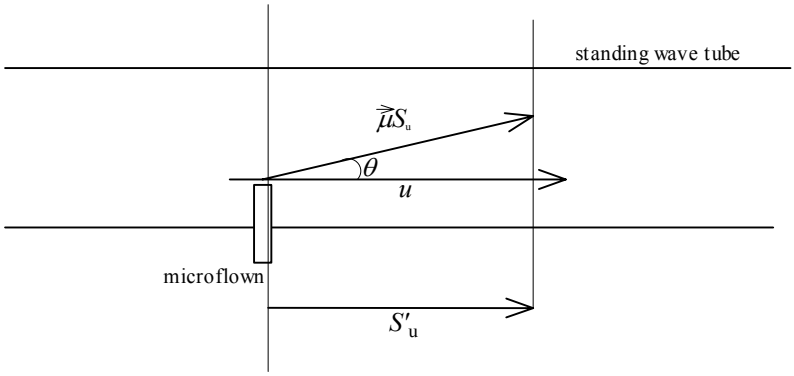

Figure 2-19: Schematically view of microflown in the standing wave tube.

In certain situations however we would like to obtain more information on the sensitivity such as the direction (referred to as $\vec{\mu}$) and absolute sensitivity (S_{u}). The vector with direction $\vec{\mu}$ and length S_{u} is defined as the sensitivity vector $\vec{S}_{\mathrm{u}} = S_{\mathrm{u}}\vec{\mu}_p$, see also section 1.7.2. For example in case of multiple microflowns sensors are positioned on a single probe (such as the three-dimensional p-u probe). For this calibration procedure the microflown sensors can be oriented in an arbitrary direction and is not limited to the angles of 45 and 90 degrees as was used in this section (see Figure 2-20). In general, we can define the direction in which the sensor measures as:

$$\vec{\mu}_1 = \left[\mu_{1x}, \mu_{1y}, \mu_{1z}\right] \tag{2.19}$$

where the reference system *x*-, *y*- , and *z*-direction are best connected to the whole probe since they are physically connected (glued), see for example Figure 2-20.

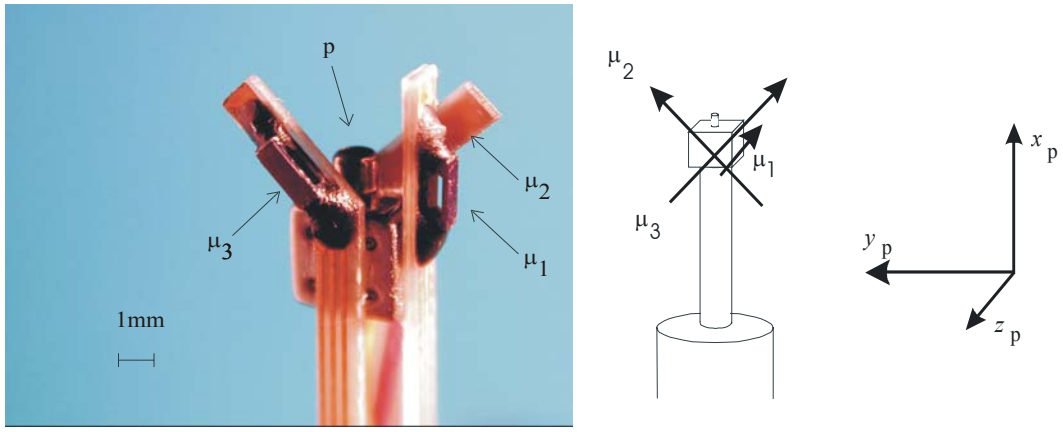

Figure 2-20: A three-dimensional pressure and particle velocity sensor (Microflown Technologies BV.) In the middle we see the pressure sensor, and around the so-called microflowns. Right: a schematic view and the reference axis.

The method of three-dimensional calibration is based on the two important properties. Firstly, the microflown has a perfect figure of eight directivity (cosine θ) in all three-dimensions (Bree de, 2001). This directivity does not depend on frequency except for the absolute value, however for each frequency a sensitivity vector will be returned. Secondly, we use the fact that the sound field in the standing wave tube is one-dimensional. We have chosen to define the centre-axis of the standing wave tube as y_{tube} (see also Figure 2-22) so that the particle velocity is in the direction:

$$\vec{u} = |u|\vec{e}_{y_{\text{tube}}} \tag{2.20}$$

The "measured" sensitivity is thus the "sensitivity" in the direction of the centre-axis of the standing wave tube (y_{tube}):

$$S'_{\text{u}} = S_{\text{u}}\left(\vec{\mu}\cdot\vec{u}\right) = S_{\text{u}}\mu_{y_{\text{tube}}} \tag{2.21}$$

By rotating the probe in the standing wave tube, the measured sensitivity S'_{u} will change depending on the orientation of the microflown on the probe itself. We have chosen to rotate the 0.5-inch microflown around its own axis since this rotation is well guided by the guiding tube and this axis is always well defined with reference to the probe. We have defined this centre axis of the probe as x_{probe}, see Figure 2-20.

Rotating around this axis with the original standing wave tube (see Figure 2-2) only results in two-dimensional information, for example, $\mu_{x_{\text{probe}}}$ will never be measured. We have therefore added another guiding tube on the standing wave tube which is not oriented under 90 degrees (see Figure 2-21).

For this situation, the measured sensitivity S'_{u} as function of angles α and β is given by:

$$S'_{\mathrm{u}}(\alpha,\beta) = S_{\mathrm{u}}\vec{\mu}_p \cdot \vec{u}_{y_{\mathrm{tube}}} = \cos\beta\, S_{\mathrm{u}}\mu_{x_{\mathrm{p}}} + \sin\beta\cos\alpha\, S_{\mathrm{u}}\mu_{y_{\mathrm{p}}} + \sin\beta\sin\alpha\, S_{\mathrm{u}}\mu_{z_{\mathrm{p}}} \quad (2.22)$$

By measuring the sensitivity S'_{u} for many angles α and β, the correct sensitivity vector $S_{\mathrm{u}}\vec{\mu}_p$ can be found by using the least squares method. We have chosen to use 2 different angles for β (45 and 90 degrees) and 12 for angle α (30 degrees interval). We therefore have to solve:

$$\arg\min_{\mu_{x_{\mathrm{p}}},\mu_{y_{\mathrm{p}}},\mu_{z_{\mathrm{p}}}} \sum_{\alpha,\beta}\left(S'_{\mathrm{u}}(\alpha,\beta) - \left|\cos\beta\, S_{\mathrm{u}}\mu_{x_{\mathrm{p}}} + \sin\beta\cos\alpha\, S_{\mathrm{u}}\mu_{y_{\mathrm{p}}} + \sin\beta\sin\alpha\, S_{\mathrm{u}}\mu_{z_{\mathrm{p}}}\right|\right)^2 \quad (2.23)$$

Equation (2.23) is solved using the Nelder-Mead simplex (direct search) method (Lagarias et al., 1998;Nelder and Mead, 1965). Note that there are two solutions since $+S_{\mathrm{u}}\vec{\mu}_p$ and $-S_{\mathrm{u}}\vec{\mu}_p$ both result in the same absolute sensitivity in the given direction. We dealt with this issue by entering good approximates for starting values for $S_{\mathrm{u}}\vec{\mu}_p$ in the numerical solver.

The choices of angle β was based on the first prototype of the three-dimensional p-u probe as shown in Figure 2-20. The two guiding tubes can be seen in Figure 2-1. An extra hole (guiding tube) is fitted in the SWT in which the probe can be placed under 45 degrees with reference to the tube. The position of this extra hole is chosen so the probe is placed almost at the same position (distance between closed-end and the probe) in the centre as if the other hole (perpendicular) was to be used. In Figure 2-22 a schematic picture of this standing wave tube is shown,

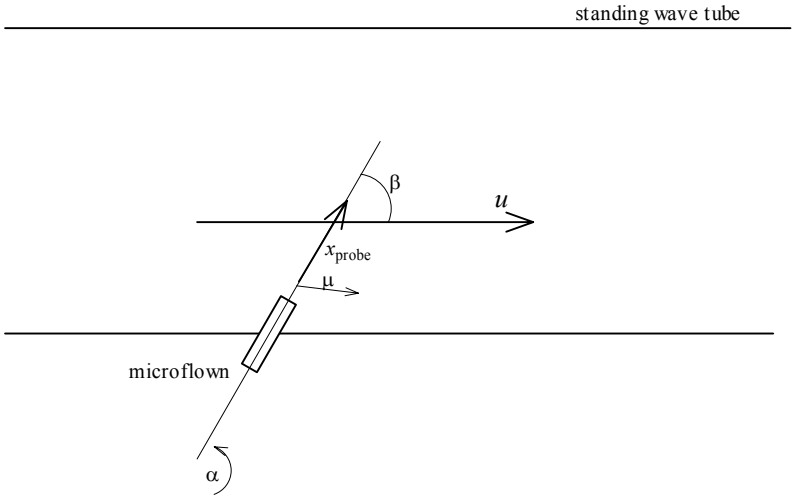

Figure 2-21: Schematic view of a rotation α around a rotation axis that has an angle β with the centre-axis (unequal to 90 degrees).

more detailed photographs are shown in Figure 2-23.

The perpendicular hole (see Figure 2-22) is used for calibrating the sensitivity, phase of sensor 1 (see prototype, equals u_{xp} in Figure 2-20), and the out (perpendicular) of plane (spanned by the two wires) directivity can be measured. Also the sensitivity and the directivity of sensor 2 and 3 (u_{yp} and u_{zp} in Figure 2-20) can be determined directly, however not very accurate because of the 45 degree angle.

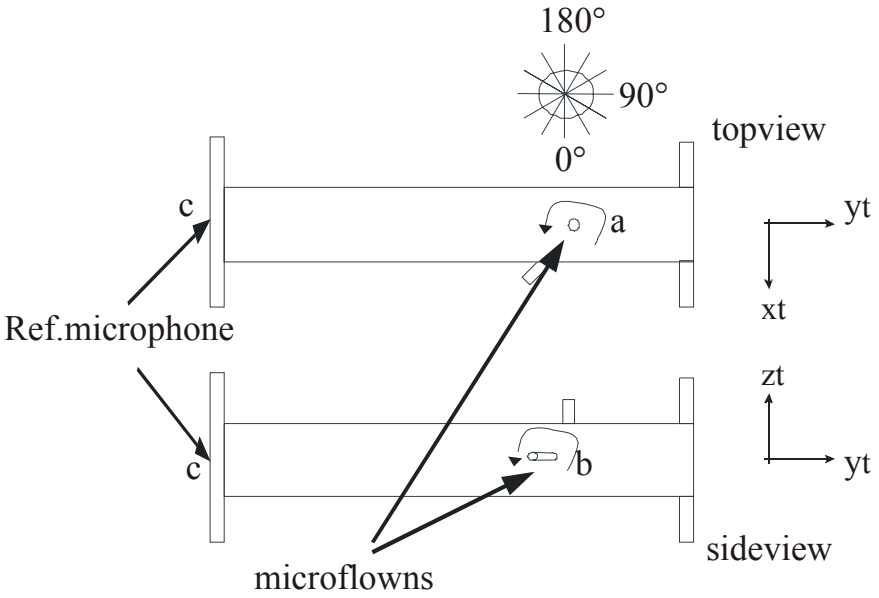

Figure 2-22: Schematic presentation of the Standing Wave tube (a) and (b) are the two mounting positions for the microflown, (c) is the black plate. Top: top view with *x*-vector in the horizontal plane. Bottom: side view, *z*-vector directing upward. Note the perpendicular and 45 degree angle microflown positioning tubes. The reference microphone is positioned in the closed-end of the tube. Both ends can be closed to change the distance between microflown and microphone. Dimensions: length: ~75 cm, width: ~5 cm, distance backplate-microflown ~54 cm

Ideally, the microflowns are placed all at a known angle with reference to the probe itself and building an orthogonal basis.

μ_1:
$$\overrightarrow{\mu_1} = \begin{bmatrix} x_{1p} \\ y_{1p} \\ z_{1p} \end{bmatrix} \approx \pm \begin{bmatrix} 0 \\ 0 \\ -1 \end{bmatrix} |S_1| \tag{2.24}$$

μ_2:
$$\overrightarrow{\mu_2} = \begin{bmatrix} x_{2p} \\ y_{2p} \\ z_{2p} \end{bmatrix} \approx \pm \frac{1}{\sqrt{2}} \begin{bmatrix} 1 \\ 1 \\ 0 \end{bmatrix} |S_2| \tag{2.25}$$

$$\mu_3: \qquad \overrightarrow{\mu_3} = \begin{bmatrix} x_{3p} \\ y_{3p} \\ z_{3p} \end{bmatrix} \approx \pm \frac{1}{\sqrt{2}} \begin{bmatrix} +1 \\ -1 \\ 0 \end{bmatrix} |S_3| \qquad (2.26)$$

In reality, the microflowns are placed at approximately this direction and the real vectors are the ideal vectors rotated over all directions over relative small angles. Note that the direction in which the microflowns measure can easily be changed by 180 degrees (opposite direction) since the positive direction is only determined by the connection of the microflown wires themselves. This 180 degrees difference is denoted by the ± sign in the equation (2.24), (2.25), and (2.26).

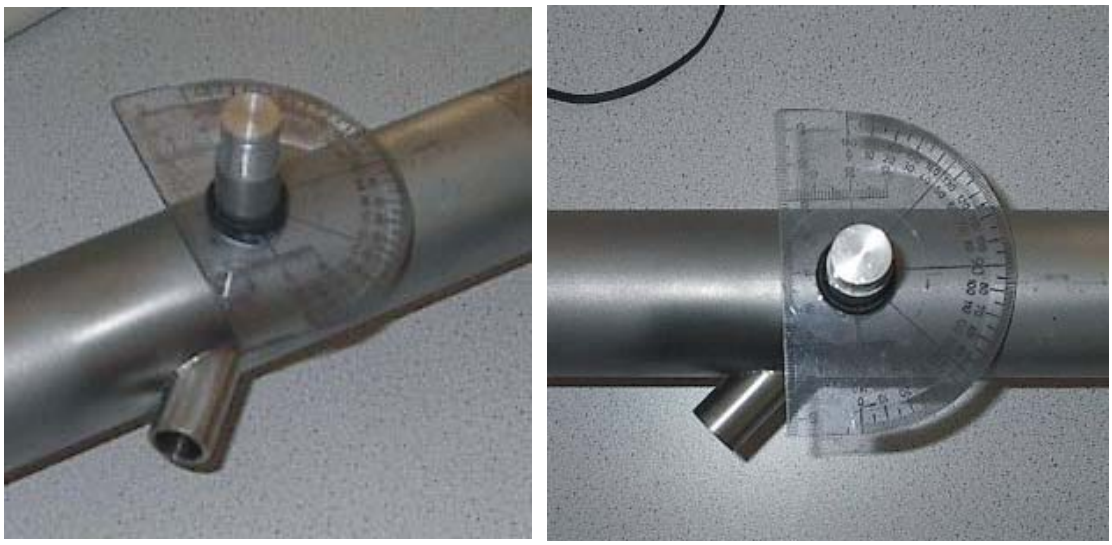

Figure 2-23: Photo of our Standing Wave Tube (see also Figure 2-1). Here the two mounting positions are shown.

2.3.5.2 Measurements and Data processing

Measurements of the transfer functions between the microflowns and the reference microphone are performed for angles α of 0 to 360 degrees with intervals of 30 degrees (plus a –90 degrees measurement). The measurements are repeated for the two distances between microflowns and the backplate in order to obtain more data points. An example of such a measurement for certain angle α and β is shown in Figure 2-24.

Because many measurements have to be processed, it is desired to do this as much as automated as possible. This requirement makes use of a complicated model of the standing wave tube not applicable because most variables needed are not known. For example the distance between microflowns and reference microphone is needed, this distance is, however, not a constant for all

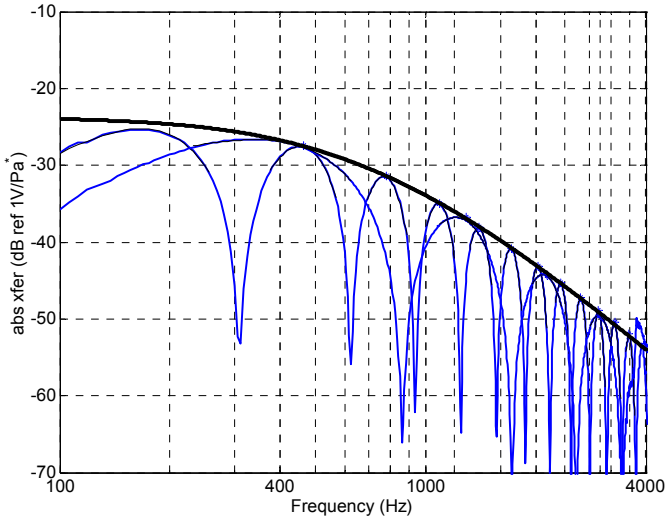

Figure 2-24: The transfer function between a microflown and the reference microphone in the standing wave tube for two distances between the probe and reference microphone for one angle of the probe inside the SWT. The upper curve is the fitted second order low pass function.

measurements but depends on the positions of the microflowns and thus on the angle for the measurement.

For the sake of automation, we chose to use the data for the frequencies of the maximum transfer-function between the particle velocity and pressure at the back-plate. For these frequencies the relation is well-known if we neglect viscosity terms (see section 2.3.2). The disadvantage is that we only gather a few points but by repeating the measurements for another distance between microflown and back-plate we increase the data points. If improved accuracy is required, an improved curve fitting as described in section 2.3.1 can be applied. The upper curve in Figure 2-24 shows the computed sensitivity of the microflown using the measured data.

In Figure 2-25 the measured sensitivities for microflown #1 (see in Figure 2-20), are shown. Since the microflown is almost purely measuring the particle in the *z*-axis (see Figure 2-20), a figure of eight (cosine shaped) sensitivity curve is measured.

2.3.5.3 Results

In Figure 2-26 we see an example for the "measured" sensitivities at various angles of rotation inside the SWT and how both measurements (rotated around the perpendicular axis and the 45° axis) are explained by the three-dimensional fit.

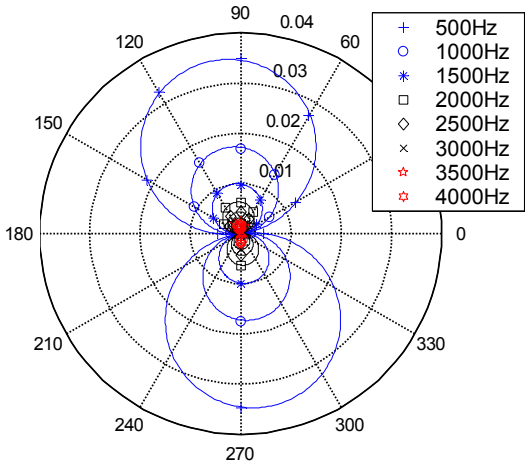

Figure 2-25: The sensitivities measured for the microflown which is positioned orthogonal to the centre-axis of the probe (microflown 1 in Figure 2-20). The probe was rotated around the axis orthogonal to the one-dimensional sound field (mounting a in figure Figure 2-22).

Note the particle velocity probe rotates through a direction for which the "sensitivity" is measured as zero. In Figure 2-26 the "measured" sensitivities for a single microflown sensor are shown for a frequency of 1 kHz.

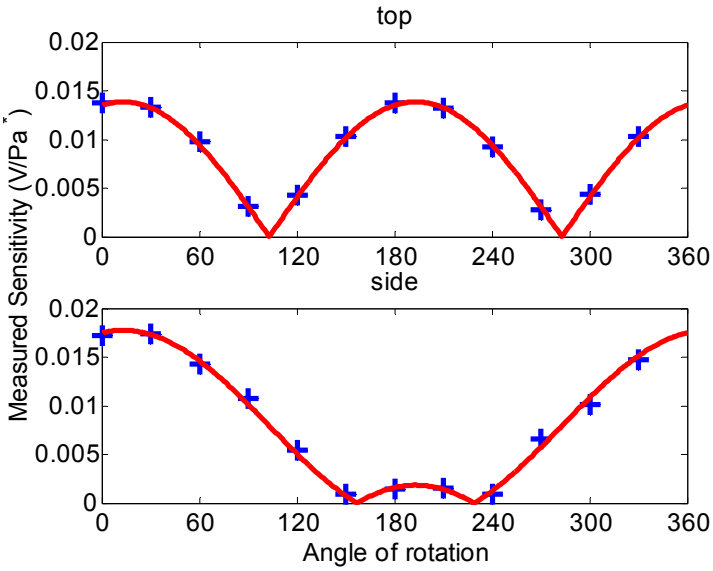

Figure 2-26: The measurements and the fit for microflown #1 (see Figure 2-20). The + signs represent the measurements and the line in both plots represents the three-dimensional fit. Top: the measured sensitivities for the different angles of rotation in the perpendicular mounting. Below: the measured sensitivities for the angles in the 45° mounting on the SWT.

Since the sensitivities of the microflowns are known as function of frequency for all three-dimensional positions (the 24 angles), for each frequency the three-dimensional sensitivity vector can be calibrated. In Figure 2-27(left) the sensitivity

for a single microflown is plotted in three dimensions as function of frequency. Note that for all frequencies the microflown is measuring in the same direction.

In Figure 2-28 the three sensitivity vectors for the three microflowns in our three-dimensional p-u probe are shown for a frequency of 1 kHz.

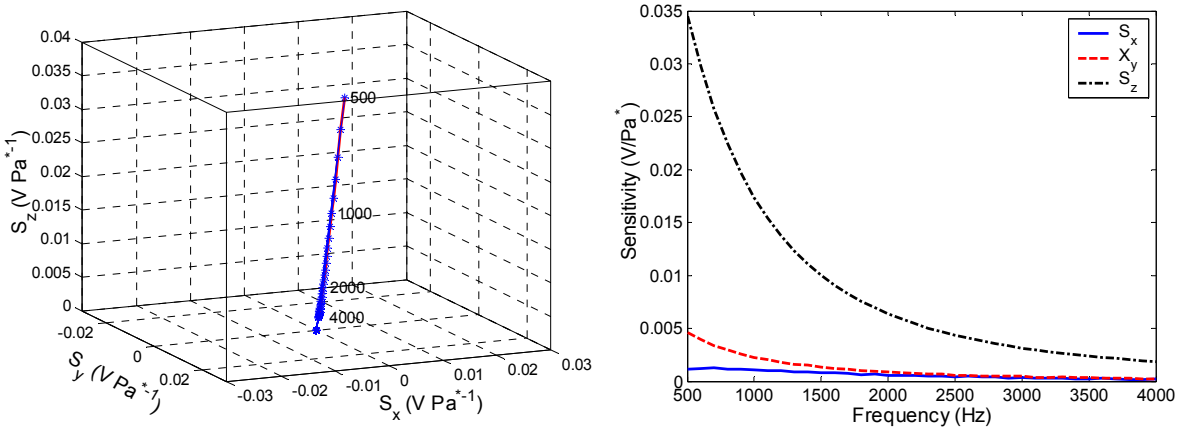

Figure 2-27: The sensitivity vector as calculated. Left: a three-dimensional view of the vector for various frequencies; right: the three components of the vector.

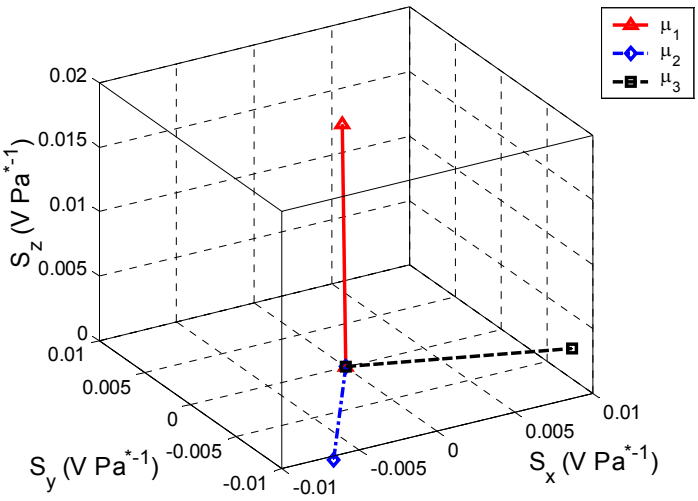

Figure 2-28: The sensitivity vectors for all three microflowns as calculated out of the measurements. The sensitivity axis are given in V Pa^{*-1} at 1000 Hz.

With knowledge of the directions for the three microflowns, the three not orthogonal sound intensity measurements can be combined in a single three-dimensional sound intensity measurement. The dimensionless directivity matrix **A** (Raangs et al., 2002) is given in Table 2-1. For applications of the three-dimensional calibration, see section 4.6.2.

Table 2-1: Dimensionless directivity matrix for the calibrated three-dimensional p-u probe.

	S_x	S_y	S_z
#1	0.065	0.128	0.989
#2	0.612	-0.731	0.299
#3	-0.549	-0.832	0.069

2.3.5.4 Conclusions three-dimensional calibration

Measurements of particle velocity are more useful if the direction in which the particle velocity is measured is known. Especially if we are interested in the particle velocity in a two- or three-dimensional sound field using multiple microflowns the directivity of the microflowns should be known. With the proposed calibration method, we are able to calibrate the sensitivity of a multiple microflown sensor as a vector over a frequency range of about 500 Hz to 4 kHz out of a few simple to perform measurements. In the example given we used 48 measurements, twelve different angles α, two different angles β, and two different distances (l-x). The data processing is largely automated so the sensitivity vectors are obtained without much effort.

2.3.6 Short calibration tube

The conventional standing wave tube is quite large (75 cm length) for portable purposes (see Figure 2-1). With H-E de Bree (Microflown Technologies BV) a short calibration tube has been built. The diameter, length and microflown position are respectively 50 mm, 10 cm, and 4 cm from closed-end. Noticing the dimensions this is strictly speaking not a standing wave tube.

When the tube becomes smaller, less maxima occur (see equation (2.8)) since the distance between the reference pressure sensor and particle velocity probe decreases. Therefore, the models and calibration software like normally used in combination with the standard 75 cm long calibration tube (see sections 2.3.1, 2.3.2, and 2.3.4) cannot be used for the short calibration tube (10 cm length).

A sine function (equation (2.8)) can be used as a model of the standing wave tube where the distance between the closed-end and microflown is used as a fitting parameter along with the microflown properties. This approach gives already a good estimation of the microflown sensitivity. The model including viscothermal

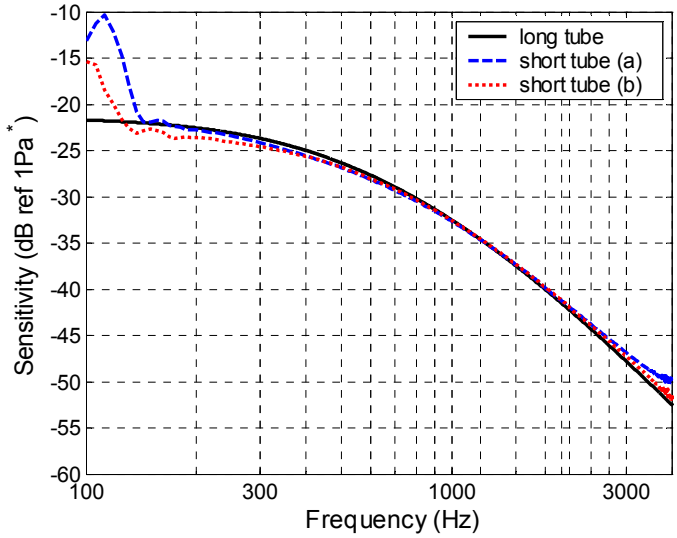

Figure 2-29: Comparison of the calibration using a 75 cm long SWT and a 10 cm long SWT. the — line represents the sensitivity of the microflown particle sensor as determined from a standard calibration (75 cm long) using equation (2.14), the other lines represent the calibration retrieved using the short standing wave tube (10 cm long, 5 cm diameter) using the viscosity model (equation (2.10)).

damping losses (Honschoten et al., 2000) is applied in Figure 2-29 although the influence of the viscothermal losses is small in case the microflown position is close to the rigid end (Rienstra and Hirschberg, 2002). In practice, viscothermal losses can be neglected for the given dimensions (Jacobsen and Bree de, 2005b). In Figure 2-29 the data, corrected for the standing wave tube, is shown and a sensitivity measurement performed in the standard standing wave tube.

In Figure 2-29 two different calibration measurements are shown for the short calibration tube. The difference between the two calibrations (a and b in Figure 2-29) indicate that for intermediate frequencies, the positioning is not very critical. For comparison, the sensitivity curve as obtained using the method as described in section 2.3.1 is shown in Figure 2-29.

Notice the good agreement at intermediate frequencies, ~0.1 dB at 1 kHz. For high and low frequencies the agreement is less accurate (at 300 Hz the deviation is about −1 dB and at 3 kHz approximately 1 dB) and relative sensitive to the positioning inside the small calibration tube.

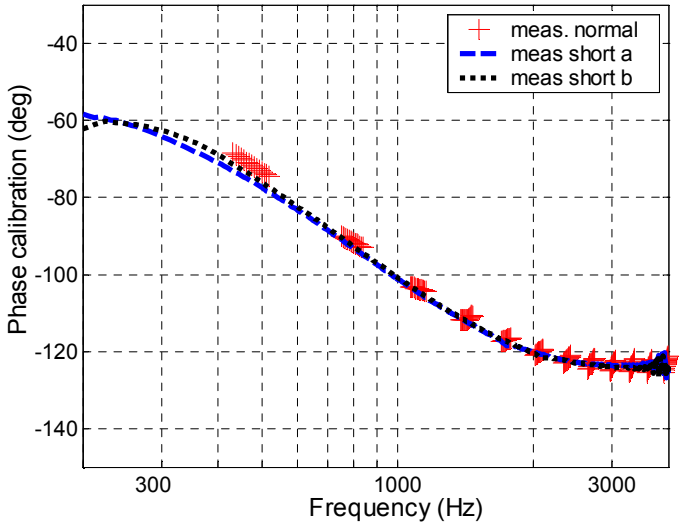

Figure 2-30: The Phase calibration of a microflown sensor. red + marks are the measurements in the normal calibration tube corrected for the phase of the tube itself, the black line is the derived fit; the dotted line represent the phase measured and corrected for the phase of the model (viscosity).

In Figure 2-30 it can be seen that the phase is measured well in the short calibration tube. For intermediate and high frequencies (> 1 kHz) the difference is less than 1 degree. For low frequencies (500 Hz) the error is about 2 degrees.

2.4 Anechoic Calibration

Another method is the calibration in an anechoic environment. For this purpose we use a small $1m^3$ box which is acoustically damped for frequencies above ~1 kHz. Both the standing wave tube and the anechoic measurements can be combined to achieve a useful calibration in the range of 10 Hz up to 12 kHz where this upper frequency mainly relies on the effort done in lining up the sensors in the anechoic cabinet. Also if weather conditions are good, we can use an open window as an anechoic environment with good results.

Measurements of the microflown sensitivity as a function of frequency are shown in Figure 2-31. The model used to estimate the frequency response of the microflown is:

$$|H_u| = \frac{35}{\sqrt{1+f^2/650^2}\sqrt{1+f^2/2500^2}} \quad [\text{mV Pa}^{*-1}] \qquad (2.27)$$

A microflown is sensitive to particle velocity rather than sound pressure, so the sensitivity cannot be given in millivolt per Pascal (mV Pa^{-1}). As a reference we use

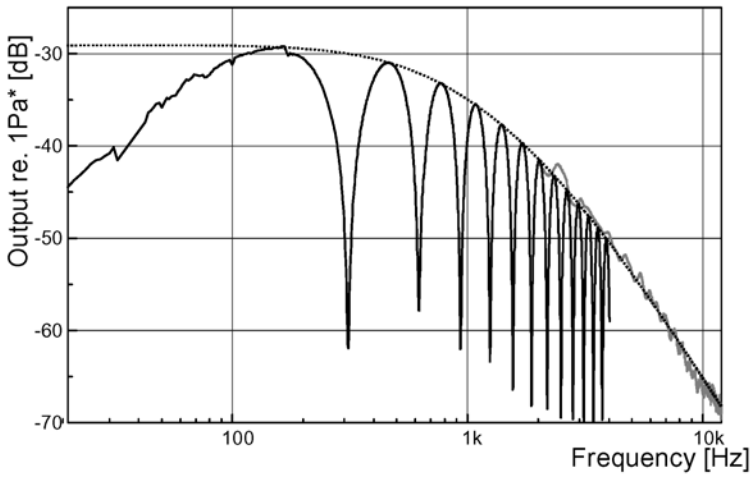

Figure 2-31: Calibration measurement of microflown in standing wave tube and small anechoic room (light gray, above 2 kHz); ··· model (equation (2.27)).

the sensitivity of a microflown in mV Pa^{*-1}, where Pa^{*} presents 1 m s^{-1} divided by the numerical value of $\rho_0 c$ (approximately 415).

Figure 2-31 shows that the anechoic calibration in a 1 m^3 box can be used for mid and high frequencies and is therefore a good addition to the standing wave tube calibration. If the situation is ideal, it has been shown that the anechoic calibration can be used for a broad frequency range (Jacobsen and Bree de, 2004;Jacobsen and Bree de, 2005a).

2.4.1 Open Window method

It seems obvious that a setting without any reflections creates an anechoic environment. So as an alternative for the anechoic room, we carried out

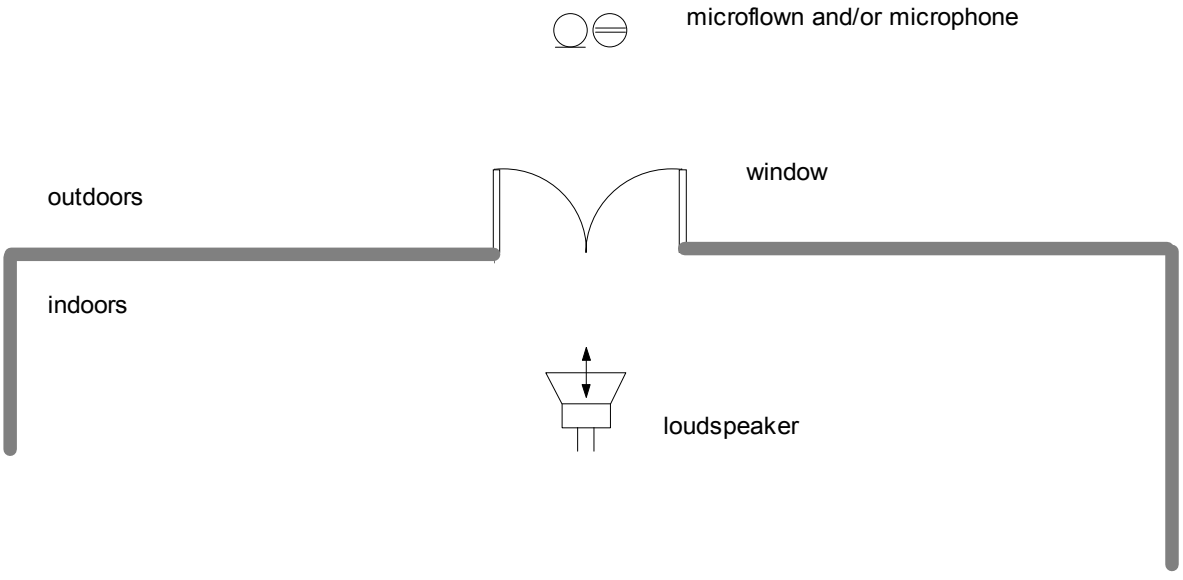

Figure 2-32: Schematic View of the experimental setup of the open window method.

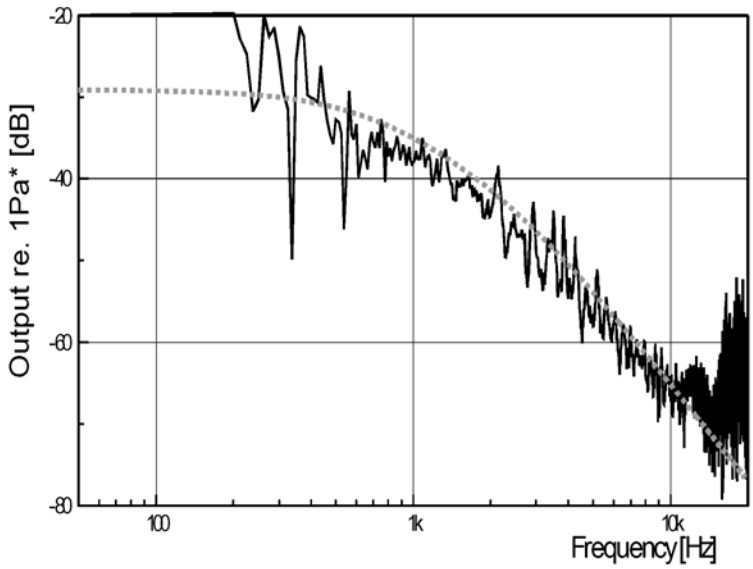

Figure 2-33: Calibration measurement of microflown amplitude response measured with open window method; ··· model (equation (2.27)).

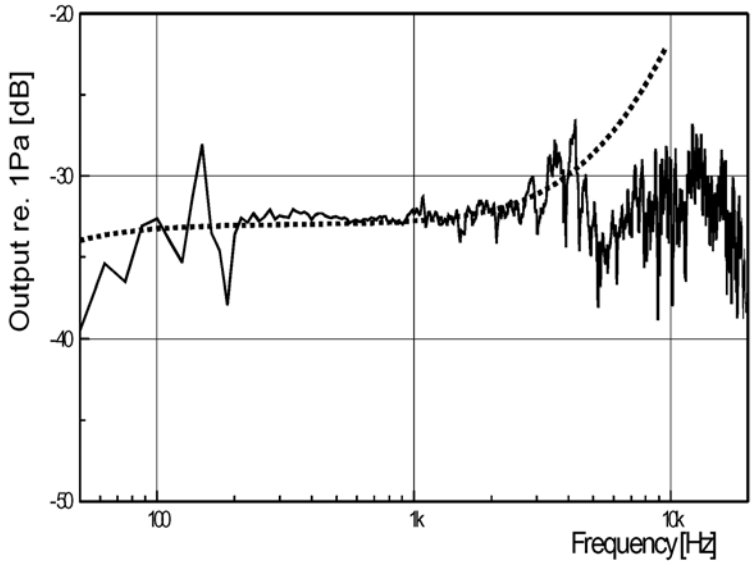

Figure 2-34: Calibration measurement of microphone amplitude response measured with open window method; ··· model fitted using SWT data.

measurements with the sound probes situated outside an open window. The results obtained using the open window method where remarkably consistent with both the standing wave tube and with the small anechoic room measurements.

With the acoustic sensors placed outside an open window we can create an anechoic sound field. The experimental setup is shown in Figure 2-32. Depending on the weather conditions, this can be very effective. While taking the measurements a breeze was present (Figure 2-34, Figure 2-33, and Figure 2-35). This is visible below 100 Hz. The use of windscreens will account for this, but the

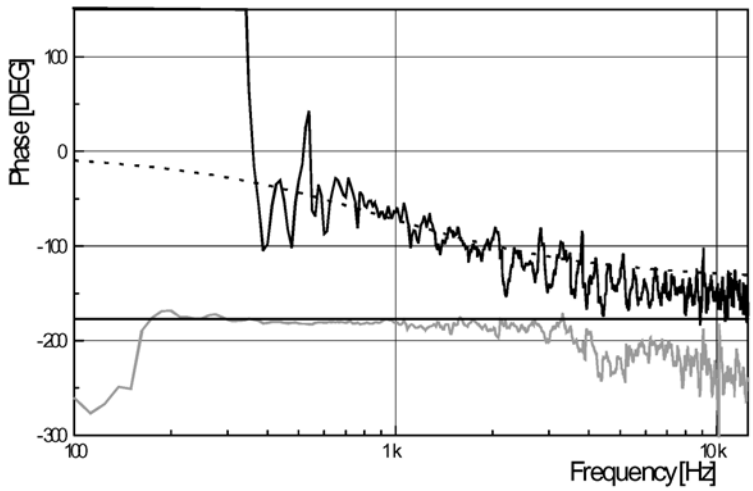

Figure 2-35: Calibration measurement of microflown phase response (top) and miniature microphone (bottom) measured with open window method; ··· model (equation (2.4)).

distance between the p-u probe and the reference microphone should not be that large.

Like the microflown, a microphone sensor has been calibrated using the same techniques as is shown in Figure 2-34.

2.4.2 Comparison Anechoic and Standing Wave Tube

The 0.5 inch sound probe is calibrated in a short standing wave tube and a small 1 m^3 anechoic chamber. The standing-wave tube can be used for frequencies up to 4 kHz, the anechoic chamber for frequencies higher than 1–2 kHz. To estimate the frequency response, a simplified model is used. Figure 2-31 shows the measurements in the standing-wave tube and the anechoic chamber. At 4 kHz the model underestimates by 4 dB, and for frequencies higher than 6 kHz the model overestimates by 3 dB. We think that we can correct for the resulting errors manually later.

2.5 Reverberant Room Calibration Technique

Another interesting technique is the reverberant room calibration. With use of a single sound source in a reverberant room and the p-u probe we are able to find out how much sound is direct and how much belongs to the reverberant sound field (diffuse sound) (Druyvesteyn et al., 1999). See also section 3.4 and Appendix B. From measurements of the particle velocity towards the direct sound wave, combined with measurements of the velocity in the perpendicular direction (only diffuse sound is measured with the particle velocity sensor), we can calculate the

ratio of direct and reverberant sound, knowing that only a third of the power in the diffuse sound field is measured with the particle velocity probe because of the directivity ($\cos(\theta)$) of the microflown.

$$u_{\parallel}^2 = u_{\text{dir}}^2 + \tfrac{1}{3} u_{\text{rev}}^2 \tag{2.28}$$

$$u_{\perp}^2 = \tfrac{1}{3} u_{\text{rev}}^2 \tag{2.29}$$

where $u_{\parallel}^2$ and $u_{\perp}^2$ are the autospectra of the measured particle velocities in the two directions in $(\text{m s}^{-1})^2$, note the units are not important here since ratios are used. We can rewrite this in terms of the ratio of the direct (free field) and reverberant sound as:

$$\left(\frac{u_{\text{dir}}}{u_{\text{rev}}} \right)^2 = \frac{u_{\parallel}^2 - u_{\perp}^2}{3u_{\perp}^2} \tag{2.30}$$

and

$$u_{\text{dir}}^2 = u_{\parallel}^2 - u_{\perp}^2 \tag{2.31}$$

Using a microphone all power in both direct and reverberant field is measured taken the microphone to measure omnidirectional and the reverberant sound field to be uniformly diffuse.

$$p^2 = p_{\text{dir}}^2 + p_{\text{rev}}^2 = p_{\text{dir}}^2 \left(1 + \frac{p_{\text{rev}}^2}{p_{\text{dir}}^2} \right) \tag{2.32}$$

where p^2 is the autospectra of the measured pressure and p_{dir}^2 and p_{rev}^2 of the direct and reverberant pressure.

Taken that the microphone is omnidirectional, we can use this ratio for calculation the pressure on-site of the p-u probe caused by the direct sound. Assuming all sound waves to behave as plane waves, we can derive easily that the ratio between the direct and reverberant particle velocity equals the ratio between the direct and reverberant pressures:

$$\frac{p_{\text{dir}}}{p_{\text{rev}}} = \frac{u_{\text{dir}}}{u_{\text{rev}}} \tag{2.33}$$

Combining the pressure due to the direct sound field and the particle velocity due to the direct sound field yields the sensitivity of the particle velocity sensor.

$$\frac{p_{\mathrm{dir}}^2}{p^2} = \frac{1}{1+\frac{u_{\mathrm{rev}}{}^2}{u_{\mathrm{dir}}{}^2}} \tag{2.34}$$

Since in the far field, and for plane waves, $u_{\mathrm{dir}} = p_{\mathrm{dir}}/\rho_0 c$, the sensitivity of the microflown can be derived. The ratio $u_{\mathrm{dir}}/u_{\mathrm{rev}}$ is obtained out of the measurements and using equation (2.30). The ratio of $p_{\mathrm{dir}}/p_{\mathrm{rev}}$ is obtained using equation (2.34). Combining the pressures and particle velocities of the derived direct sound we are able to calibrate the particle velocity sensor sensitivity S_{u} in terms of [V Pa^{*-1}] or $S_{\mathrm{u}*}$ in [V s m^{-1}]. Denote the measured voltages of the time-averaged autospectra of the p- and u-sensor as V_p, $V_{u_{\|}}$ and $V_{u_{\perp}}$ and the sensitivities (including the amplification factor) of the p- and u-sensor as S_{p} and S_{u}. Assume plane waves, thus $p/(\rho_0 c) = u$, then

$$p_{\mathrm{dir}}^2 + p_{\mathrm{rev}}^2 = (\rho_0 c)^2 \left(u_{\mathrm{dir}}^2 + u_{\mathrm{rev}}^2\right) \tag{2.35}$$

which can be rewritten in to:

$$\frac{V_{\mathrm{p}}^2}{S_{\mathrm{p}}^2} = \frac{(\rho_0 c)^2}{S_{\mathrm{u}}^2}\left(V_{\mathrm{u}_{\|}}^2 + 2V_{\mathrm{u}_{\perp}}^2\right) \tag{2.36}$$

Calibration of the phase between the pressure and particle velocity sensor is more difficult in a reverberant environment because the sound field is generally not known. The method above only yields the autospectra of the free-field pressure and particle velocity (Raangs et al., 2003).

2.5.1 Results Reverberant Room Method

We also applied the so-called reverberant room calibration technique. The two signals of the p-u probe were measured while a reference microphone was positioned as close as possible. The sensitivity of the pressure was calculated using the transfer function between the two microphones and the sensitivity of our reference microphone. The sensitivity of the particle velocity probe was obtained using the calculated autospectra of the free-field pressure and particle velocity, according to the method presented, combined with the sensitivity of the microphone used.

The calculated sensitivities of both the pressure sensor (Figure 2-37) and the particle velocity sensor (Figure 2-36) were consistent with the models obtained

from the standing wave tube and the anechoic measurements. Above 10 kHz the sensitivities calculated from the reverberant measurements were no longer valid (see Figure 2-36) because no acoustic power was available in the sound field since a midrange loudspeaker was used (see also Figure 4-14).

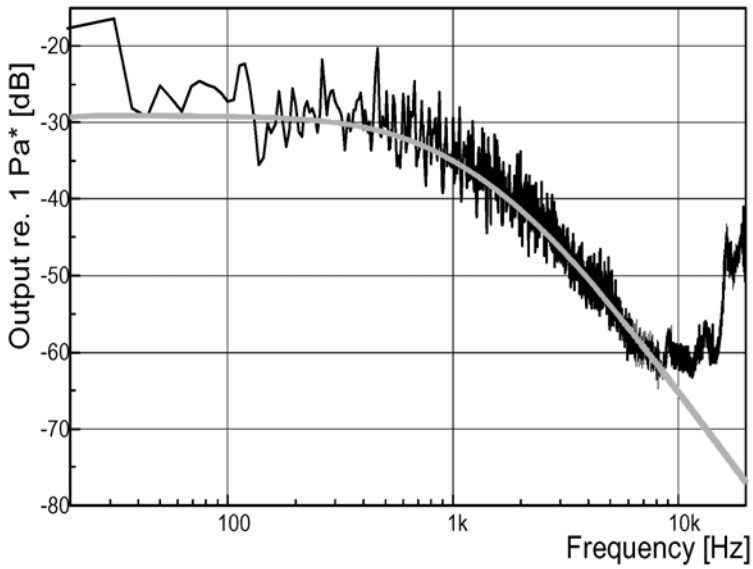

Figure 2-36: Calibration measurement of microflown amplitude response measured with reverberate room method; ── model.

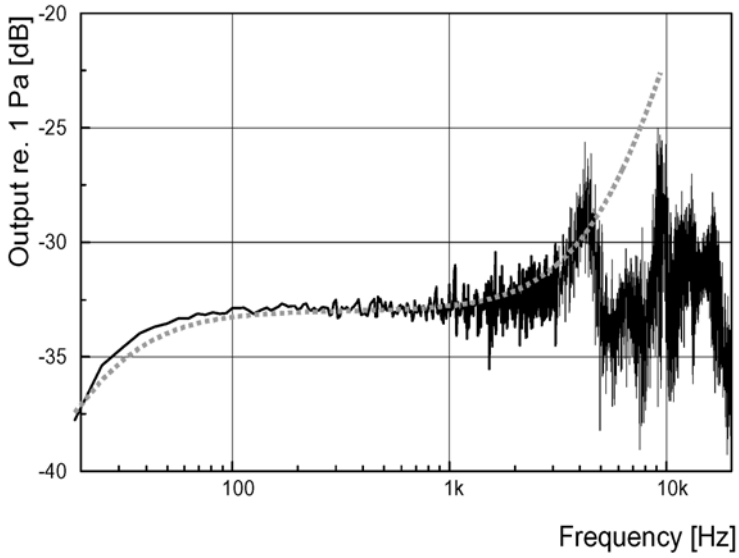

Figure 2-37: Calibration measurement of miniature microphone amplitude response measured with reverberate room method; ··· model fitted using SWT data.

2.6 Laser Doppler Calibration

This section (section 2.6.1 to 2.6.8) is copied from the journal paper (Raangs et al., 2005) we wrote with title "Calibration of a micro-machined particle velocity microphone in a standing wave tube using an LDA photon correlation technique".

References and figure captions have been altered to accord with the rest of this thesis. A photograph of the experimental setup is shown in Figure 2-38. References, figure captions, and equation numbers are updated and consistent with the rest of the thesis.

2.6.1 Abstract

In this paper, a new method of calibrating an acoustic particle velocity sensor using laser Doppler anemometry (LDA) is discussed. The results were compared and were in good agreement with the results obtained by conventional methods, where the sensitivity of the microflown is obtained with the use of a reference microphone and a standing wave tube. The LDA signal generated by the acoustic particle motion was analysed using the photon-correlation method, where the signal is considered to consist of a series of discrete photon events. The photon-correlation system is used to measure particle velocity amplitude next to the microflown particle velocity sensor in a standing wave. Measurements are performed for frequencies between 250 Hz and 4 kHz and velocities between 5 mm s^{-1} and 25 mms^{-1} (root-mean-square (rms) values) which are equivalent to sound fields of 100 and 114 dB SPL in free field. From the output voltage of the probe microflown and the LDA-derived particle velocity in a standing wave, the sensitivity of the microflown is obtained. The two different calibration methods are in good agreement showing a discrepancy of 1 dB for the frequency range of 250 Hz–4 kHz.

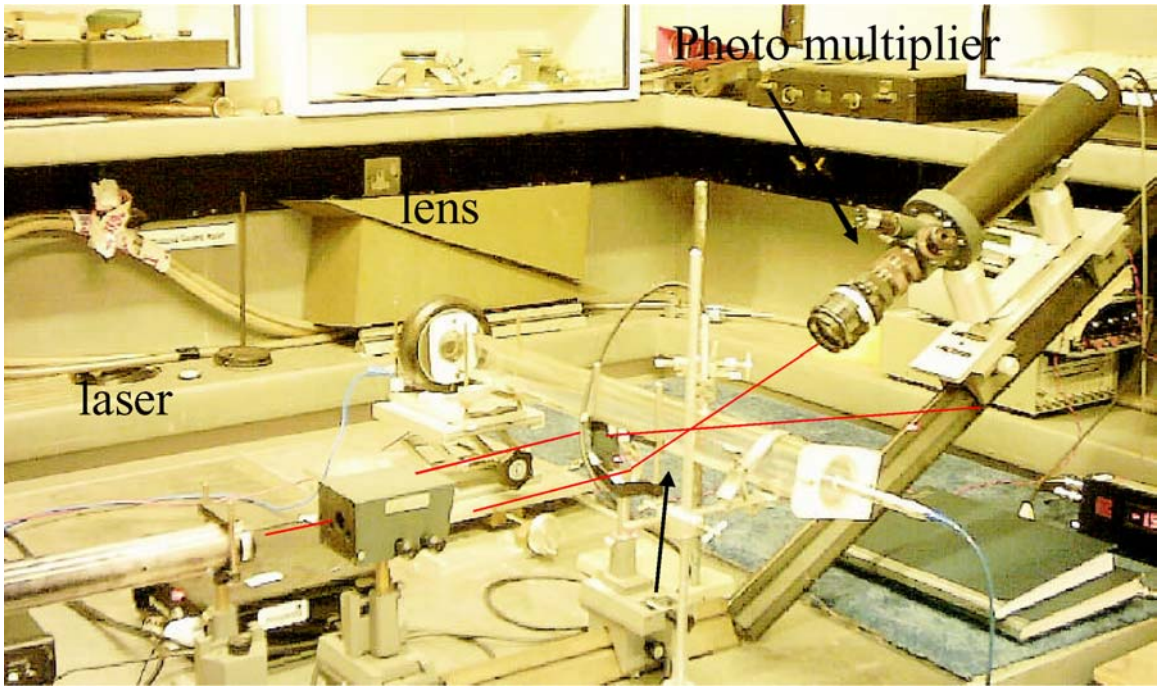

Figure 2-38: Photograph of the experimental setup. From left to right: He-Ne laser, beam splitter, lens, photo multiplier. In the middle the perplex tube is shown with the loudspeaker at one end, and the closed-end including a microphone on the other end. Particle velocity is measured at the position where the two laser beams cross. The microflown was positioned as close as possible to the position where the particle velocity is being measured using the LDA setup.

2.6.2 Introduction

For a measurement to have any technical validity, it must be founded on some physical reference quantity or standard. In acoustics, the fundamental measurement quantities are *sound pressure* measured in pascals and *particle velocity* measured in metres per second. At present, the primary standard for sound pressure in air is based on the measurement of the sensitivity of laboratory standard microphones. Measuring the sensitivity of a microphone, i.e. its calibration, essentially requires the output voltage for a given sound pressure. In the 1960s, reciprocity calibration of microphones was adopted by the International Electrotechnical Commission (IEC) (International Electrotechnical Commission, 1992). For particle velocity sensors, no such reciprocal measurement is possible and no reference particle velocity sensor is available.

Optical techniques provide a direct approach where the acoustic particle velocity is determined using a laser Doppler system. Taylor developed such a system, based on laser Doppler anemometry (LDA) measurements inside a travelling wave tube (Taylor, 1981). Recently, MacGillivray *et al* used LDA in order to calibrate a pressure microphone (MacGillivray et al., 2003). The measured particle velocity is used directly to calibrate the particle velocity sensor and to evaluate the commonly used calibration technique. Recent developments in optical techniques, and particularly LDA, mean that there is potential to improve calibration based on the measurement of acoustic particle velocity and develop measurement standards derived from this.

In this paper, the microflown particle velocity is introduced, along with a calibration method based on a calibrated pressure microphone. The method of LDA is briefly reviewed and its implementation discussed. The microflown and LDA measurements in a standing wave tube (SWT) are combined showing that the LDA measurement can be used in order to calibrate the microflown particle velocity. The advantage of such a method is the fact that it is not subject to other acoustical properties, such as specific impedance, but merely depends on geometrical parameters of the applied laser set-up. The disadvantage is the fact that only single frequency sound fields can be used in case of the LDA measurement, whereas the conventional calibration method yields information about sensitivity (amplitude and phase) within seconds over a practical frequency band (roughly 250-4kHz for the applied standing wave tube).

2.6.3 The microflown

The microflown is a linear acoustic sensor measuring particle velocity instead of sound pressure (Bree de et al., 1996b) which is usually measured by conventional microphones. It is directional, it provides a figure of eight (a cosine-shaped sensitivity directivity) over the full bandwidth and the sign alters when the probe is rotated. The dynamic range and noise properties of the microflown are comparable with pressure microphones. The microflown is not a traditional hot-wire anemometer because it can measure velocity (magnitude and direction) rather than just speed. The microflown can therefore distinguish between positive and negative particle velocity directions. A more detailed

mathematical model of the microflown model is presented in (Svetovoy and Winter, 2000).

The microflown has a number of practical applications due to the importance of particle velocity in acoustics. Its ability to determine particle velocity in a simple reliable manner makes the sensor a powerful tool in sound intensity, acoustic impedance and sound energy measurements, *in situ* impedance determination (Bree de, 2003a), and measurement of structural vibrations (Bree de et al., 2004). Unlike a laser vibrometer, the microflown is capable of: analysing velocities in three dimensions around so-called non-cooperative materials such as damping materials, foam, rubber, other black surfaces, scattering surfaces, airborne sound (Microflown Technologies, 2004). The three dimensional impulse response can easily be measured with the USP but also other properties that relate to the time domain, like reverb time, speech transmission index, echo criteria and so on, see (Microflown Technologies, 2004).

2.6.3.1 Functioning of the microflown sensor

The temperature sensors of the microflown are implemented as two closely spaced thin wires (1500 μm long, 0.4 μm thick and separated by 2.5 μm) of silicon nitride with an electrically conducting platinum pattern as shown in Figure 2-39. Electrical current in the wires dissipates power, thereby heating the wires. The wires therefore act as heater and as temperature sensor. The sensors have a typical operational temperature of about 600 K. When a particle velocity is present, the temperature distribution around the resistors is asymmetrically altered, and a temperature difference between the two wires occurs (Svetovoy and Winter, 2000). Since the resistance of the wires is temperature dependent, this change in temperature profile causes a change of the temperature of the resistors, and thus causes a change of resistance. The difference in resistance of the two sensors quantifies the particle velocity. Due to this differential operation principle, the microflown can distinguish between positive and negative velocity directions.

The sensitivity of the microflown depends on the frequency. In general, the microflown sensitivity decreases as frequency increases. A good approximation of the frequency

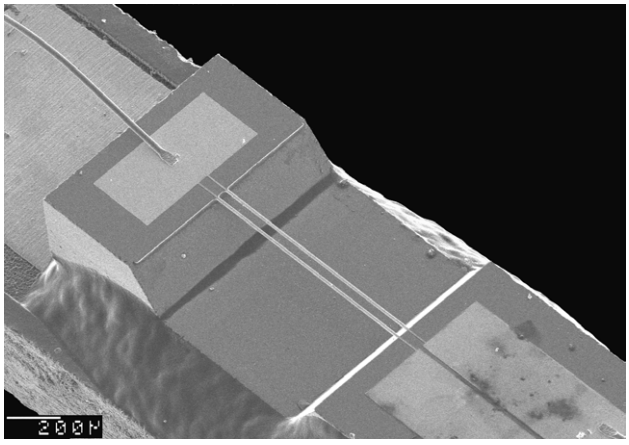

Figure 2-39: SEM photo of a part of a bridge type of microflown. At the top of the sample a wire-bond is visible. Above the gap the two wires are visible which are used to measure the particle velocity out of the temperature difference.

response of a microflown can be described with (Raangs et al., 2003)

$$S_{\text{microflown}} = \frac{\text{LFS}}{\sqrt{1+f^2/f_{\text{heatcap}}^2}\sqrt{1+f^2/f_{\text{d}}^2}} \tag{2.37}$$

where LFS being the low frequency sensitivity, the sensitivity of the microflown sensor at frequencies below f_{d}, the thermal diffusion corner frequency. f_{heatcap} is the second high frequency roll-off caused by the heat capacity (thermal mass). Such typical behaviour is shown in Figure 2-44 (line). The frequency response of a microflown can be described using three parameters: (i) one low-frequency sensitivity, and (ii) two characteristic frequencies. One high-frequency roll-off is caused by diffusion effects. The effect can be estimated by a first order low pass frequency response that has a (diffusion) corner frequency (f_{diff}) in the order of 500 Hz – 2 kHz (depending on geometry and operating temperature). The second high-frequency roll-off is caused by the heat capacity of the wires (thermal mass) and shows an exact first-order low pass behaviour that has a heat capacity corner frequency ($f_{\text{heat cap}}$) between 2 kHz and 15 kHz for modern microflowns, depending on geometry and operating temperature (Honschoten et al., 2001;Svetovoy and Winter, 2000).

The microflown particle velocity sensor is available in various models. Most models use a protective 0.5 inch packaging which also increases the sensitivity (volt per metre per second) by forcing the flow through the package (Bree de et al., 1996b). In these experiments, a so-called “naked” microflown without this packaging was used, as shown in Figure 2-40. This allowed LDA and microflown measurements to be obtained simultaneously and at the same position, with minimal effect on the flow.

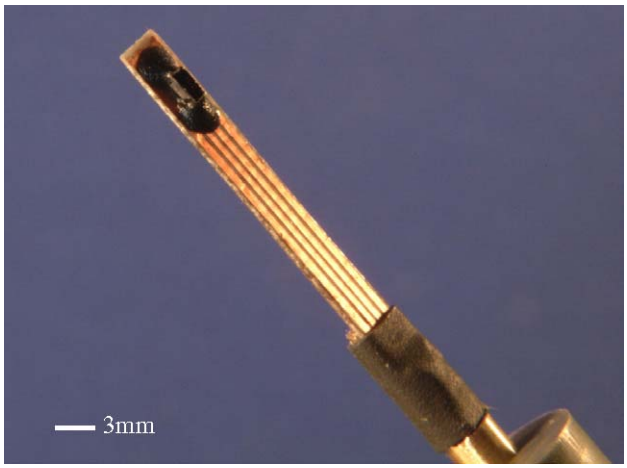

Figure 2-40: The prototype microflown particle velocity sensor used for the present work. The micro-machined sensor is positioned at the tip of the PCB.

More detailed information on the functioning of the microflown can be found in (Bree de, 2003b;Honschoten et al., 2001;Honschoten et al., 2002b;Raangs et al., 2003;Svetovoy and Winter, 2000)

2.6.3.2 Conventional Calibration of a microflown Sensor

Calibration of acoustical sensors in general, and particle velocity sensors in particular, is difficult because the acoustical environment is often not known, and a reference particle velocity sensor is not available. Several acoustical environments can be used such as an anechoic chamber or free field environment (Raangs et al., 2003). If the specific impedance is known, a calibrated pressure microphone can be used as a reference.

An interesting acoustical environment is the standing wave tube; see Figure 2-41, sometimes referred to as Kundt's tube. The specific impedance is well defined in the standing wave tube if the specific impedance of air, $Z_{air} = \rho_0 c$, is known.

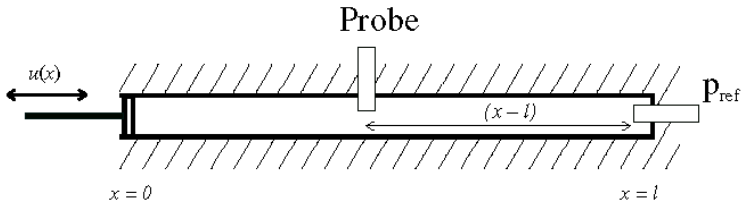

Figure 2-41: A tube that is rigidly terminated at $x = l$ and in which the fluid is driven by a vibrating loudspeaker at $x = 0$.

The specific impedance is the product of the density of air, ρ_0, and the speed of sound in air, c. Both of these depend on the environmental conditions, of which temperature T, atmospheric pressure p_0, and relative humidity RH are most important. Using the relevant equations (Cramer, 1993;Wong, 1995) the density of air, ρ_0, and the speed of sound, c, can be calculated The error in the specific impedance is roughly 1.3%, where 0.8% is caused by the resolution in the measured atmospheric conditions, and 0.5% due to the uncertainty associated with the calculation itself (MacGillivray, 2002).

If the impedance of air is known, a microphone can be used as the reference for the microflown calibration. Additionally, information on certain non-ideal properties of the sound field in the standing wave tube, such as damping and a non-ideal reflection, can be retrieved with use of the uncalibrated microflown. A convenient position for the reference microphone is the closed end where it does not influence the sound field in the tube. A disadvantage of the standing wave tube is the limited frequency range. Due to the diameter of the standing wave tube used (50 mm), the standing wave tube will not function as such above ~4 kHz. The lowest frequency depends on the length of the standing wave tube so a larger tube is required for calibration of a lower frequency range. For a tube the high cut-off frequency is given by (Rienstra and Hirschberg, 2002)

$$f_c = \frac{c}{1.71 \cdot d} \tag{2.38}$$

where d represents the diameter of the tube, and c the speed of sound.

The specific impedance inside the SWT (see Figure 2-41) can be calculated by solving the wave equation. In order to incorporate the non-ideal behaviour of the wave tube, we can implement a degradation in amplitude and a small phase change, θ, occurring on the reflection at the closed end (MacGillivray, 2002): $p_i = Ae^{i(\omega t - kx)}; p_r = Be^{i(\omega t + kx + \theta)}$, where p_i and p_r are the initial and the reflected pressures, A and B the amplitudes and θ a small

phase change. The ratio of the acoustic particle velocity at x to the pressure at $x = l$ is given by (MacGillivray, 2002)

$$\frac{u(x)}{p(l)} = \frac{1}{\rho_0 c}\left(\frac{1}{SWR}\cos\left(k(l-x)-\theta/2\right)+\mathrm{i}\sin\left(k(l-x)-\theta/2\right)\right) \qquad (2.39)$$

where $k = \omega/c$, with k the wave number, x the position in the tube (with $x = l$ the closed end), and i the complex number $\sqrt{-1}$, and the standing wave ratio, SWR, is given by

$$\mathrm{SWR} = \frac{A+B}{A-B} \qquad (2.40)$$

The ratio of the acoustic particle velocity at x to the pressure at $x = l$ can be measured out of the measured signals (in volt) using the sensitivities of both sensors in V Pa^{-1} for a pressure microphone and V m^{-1} s for a particle velocity sensor

$$\frac{U\left[\mathrm{m\,s^{-1}}\right]}{P[\mathrm{Pa}]} = \frac{U[\mathrm{volts}]}{P[\mathrm{volts}]}\cdot\frac{S_\mathrm{p}(f)}{S_\mathrm{microflown}(f)}. \qquad (2.41)$$

The SWR, the phase change θ, and the distance (l-x), can be obtained from the data using an un-calibrated particle velocity sensor by minimizing the absolute difference between the measured transfer function in m s^{-1} Pa^{-1} and the model given in equation (2.39) if the acoustic impedance of air is known, as will be shown in section 2.6.6. This is done by iteratively solving equations. (2.39), (2.37), and (2.41) for the measured transfer function between microflown and pressure sensor over a certain frequency range. For the given standing wave tube, this frequency range is from f_l (the lowest usable frequency, about 250 Hz), up to f_c (about 4 kHz).

If losses in the standing wave tube are neglected, a much simpler approach can be used. In this case the relationship between the particle velocity in the tube at position x, $u(x)$ and the pressure at position l, $p(l)$, is given by ($u_\mathrm{probe} = u(x)$ and $p_\mathrm{ref} = p(l)$)

$$\frac{u_\mathrm{probe}}{p_\mathrm{ref}} = \frac{\mathrm{i}}{\rho_0 c}\sin(k(l-x)) \qquad (2.42)$$

The distance (l-x) can easily be obtained by measuring two minima of the sine function as in equation (2.42) By only using a small frequency data at the maximas of equation (2.42), the sensitivity curve can be fitted (Honschoten et al., 2000;Raangs et al., 2003). This approach is slightly less accurate but yields good starting values for the sensitivity curve of the microflown for the iterative approach.

2.6.4 Laser Doppler Anemometry

Laser Doppler Anemometry (LDA) is a non-intrusive, optical method for measuring fluid velocity at a point (Durrani and Greated, 1977). Since its introduction in the 1960s, it has been used for the measurement of laminar, turbulent and acoustic flows in liquids and gases. The underlying principle of the technique is that the Doppler frequency shift of laser light scattered by seeding particles embedded in the flow is determined. This Doppler shift is directly proportional to the velocity of the moving particles, so by

measuring the shift, the particle velocity is ascertained. If the seeding particles are sufficiently small to follow the fluid motion, the particle velocity is equal to the fluid velocity (Brandt et al., 1937;Hann and Greated, 1993;Taylor, 1976).

In practice, the Doppler shift is minute relative to the laser frequency, and is therefore difficult to measure directly. For this reason, a more complex optical geometry is employed to make an accurate measure of the Doppler frequency shift possible. The LDA experiments described here utilize the dual-beam mode, whereby two coherent laser beams intersect to form a fringe volume, as shown in Figure 2-42. Two parallel beams are obtained by positioning a beam-splitter in front of the laser. These beams pass through a converging lens, and interfere to create a fringe volume at the focal point of the lens. Particles moving through these fringes scatter photons with a probability proportional to the intensity at that point, some of which reach the photomultiplier tube (PMT). The PMT converts the energy from an incoming photon to a current, then outputs a short (5ns) TTL pulse. The PMT signal thus consists of a series of TTL pulses, each of which corresponds to a photon scattered from the fringe volume.

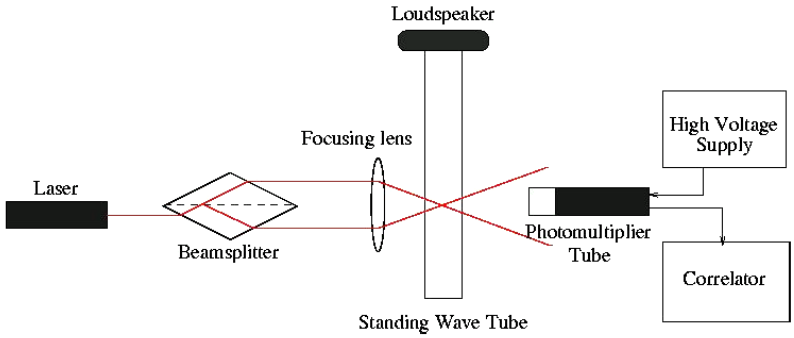

Figure 2-42: Schematic view of the LDA measurement technique. Left: the whole setup showing the laser (left) , right: the two overlapping laser beams create a pattern of fringes through which the particles travel. The acoustic velocity at the intersection of the two beams is measured.

By analysing this signal, the magnitude of the velocity component perpendicular to the fringes can be determined. The LDA signal is directionally ambiguous in that it cannot yield the directional sign of the velocity. This ambiguity can be avoided by frequency shifting one of the beams using, for example, a Bragg cell; this was not done in these experiments as it was the magnitude of the velocity which was of interest (Semenova and Wu, 2004).

If the photon count rate is high, the PMT output can be considered to be continuous, and the signal can either be processed in the time domain by demodulating the Doppler signal, or in the frequency domain by analysing the location and heights of the spectral peaks. In these experiments, the seeding was sufficiently sparse and the photomultiplier was sampled sufficiently quickly that the output signal could be considered to consist of a series of discrete photon events. The signal was then auto-correlated to yield a function whose form is dependent on the flow velocity. This method is known as photon correlation (Durrani and Greated, 1977;Sharpe and Greated, 1987), and is especially

useful in experiments in air, where it can be difficult or undesirable to have a high seeding density in the fringe volume.

Since the mean particle velocity can be neglected (MacGillivray, 2002), the instantaneous velocity of the acoustic flow, $u(t)$, is assumed to have the form

$$u(t) = u_m \sin(\omega t + \varphi) \tag{2.43}$$

where ω is the acoustic angular frequency and φ is a random phase, the autocorrelation function (ACF), $R(t)$, of the PMT output, is given by (MacGillivray, 2002) (see Figure 2-43)

$$R(t) = \exp\left(-2B^2 u_m^{'2}\right)\left(1 + J_0\left(Du_m^{'}\right)\right) \tag{2.44}$$

$B = \cos(\theta)/d$, where θ is the half angle between the laser beams and d is the $1/e^2$ diameter of the beam; $D = 4\pi \sin(\theta)/\lambda$ where λ is the wavelength of the laser light; $u_m^{'} = 2u_m/\omega \sin(\omega t/2)$ where u_m is the acoustic particle velocity amplitude to be determined. If t is small, the ACF has the form of a damped Bessel function of zeroth order. For longer times, the Bessel function J_0 has a sinusoidal argument, resulting in frequency modulation in the correlation function.

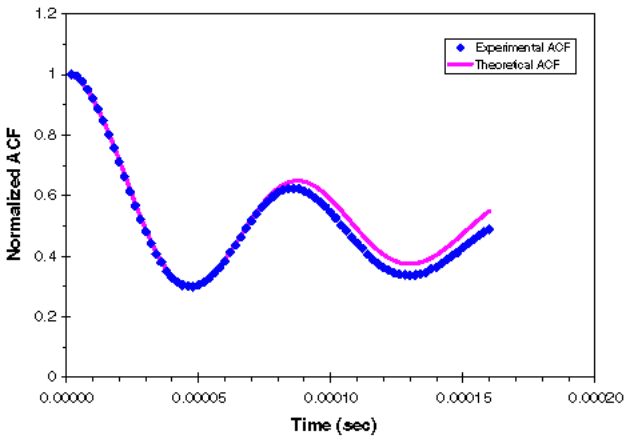

Figure 2-43: Autocorrelation function of the photon multiplier as measured (line, below). The curve above represents the fitted curve, see equation (2.44).

An initial estimate for the acoustic velocity can be obtained by assuming that the damping factor is small and that the small angle sine approximation holds. The Bessel argument, see equation (2.44), is then $Du_m t$. Since the first minimum in the Bessel function occurs when the argument is approximately 3.832, the rms acoustic velocity u_{rms} can be approximated by

$$u_{rms} = \frac{3.832}{\sqrt{2} D \tau_{\min}} \tag{2.45}$$

where $\tau_{\min}$ is the time until the first minimum in the ACF. The factor $\sqrt{1/2}$ is used to convert the peak amplitude to root-mean-square values (rms) since only harmonic signals are used. The value for the acoustic velocity can be refined by minimising the discrepancy between the normalised experimental and theoretical ACFs, using the

method of least-squares. The acoustic particle velocity amplitude can be determined by curve-fitting equation (2.44) to the measured ACF.

2.6.5 Experimental Setup

The experiments were conducted in a Perspex standing wave tube of length 75 cm and internal diameter 50 mm. A B&K type 4133 microphone, recently calibrated using the reciprocity method by NPL, was placed at the closed end. The microphone was connected to the data-acquisition hardware (DSPT, Siglab 40-22) using a preamplifier (GRAS 26 AG) and a Nexus amplifier. The National Physical Laboratory, UK, calibrated the microphone for frequencies between 250 Hz and 4 kHz. A third-order polynomial fit was used to obtain the microphone sensitivity for the various frequencies in between.

A prototype microflown (see Figure 2-40) was positioned 21 cm from the closed end on the central axis of the cylindrical tube in the standing wave tube. At the other end, a loudspeaker was fitted which was driven by the output of the DSPT Siglab signal analyzer at various voltage levels resulting in pressures at the closed end ranging from 1 Pa to 20 Pa. Below 1 Pa (corresponding to a velocity of approximately 2.5 mm s^{-1} at the measurement position), the acoustic velocity was below the lower dynamic limit of the photon correlation method (MacGillivray, 2002).

The specific impedance of air was calculated as described in section 2.6.3.2 (Conventional Calibration of a microflown Sensor). Using these values and the relevant equations (Cramer, 1993;Wong, 1995) the density of air was calculated to be $\rho_0 = 1.184$ kg m^{-3} and the speed of sound $c = 344.14$ m s^{-1}, leading to a value for the specific impedance of 407.5 (± 1.3%) Pa s m^{-1}.

In order to seed the air within the standing wave tube, a burning incense stick was held inside for approximately 1 s. The resulting smoke consists of particles whose diameter is typically 0.5 μm (Cheng et al., 1995;Cullen et al., 1999). Such particles are small compared to the fringe spacing (approximately 3 μm) and follow the acoustic oscillations of the air up to frequencies of 10 kHz (Taylor, 1976). This seeding density is considerably lower than is required for a frequency domain analysis (MacGillivray et al., 2003), and therefore has less effect on the fluid properties of the sound medium. The particle lag can be quantified in terms of the Stokes number,

$$S_t = \frac{\rho D^2}{18 \mu T_c} \tag{2.46}$$

where ρ is the particle density, D is its diameter, μ is the dynamic viscosity of the medium and T_c is a characteristic time scale (acoustic period). The particle lag can be neglected for Stokes numbers less than 0.01 (Dring, 1982). For the seeding used in these experiments, this criterion is valid to an acoustic frequency of approximately 5 kHz.

Photon correlation results from two sets of experiments were obtained in a standing wave within the closed, Perspex tube as shown in Figure 2-42. A Brookhaven BI-9000AT Digital Autocorrelation board was used, which recorded every photon event detected by

the photomultiplier, and performed a time-averaged autocorrelation of the PMT signal. This board had a total of 200 channels, separated in time by Δt, in which values of the discrete ACF were stored. Δt was set to either 2 ms or 5 ms. Simultaneously, and at the same position in the standing wave tube, the signal of a microflown particle velocity sensor was recorded and the LDA measurement was performed. The pressure at the closed end of the standing wave tube was measured using a calibrated pressure microphone (see section 2.6.3.2). The pressure at the closed end was then used as a reference for the microflown calibration. The microflown velocity measurements were then compared to those obtained using the LDA technique.

2.6.6 results

The aim of this section is to describe the measurements performed, and combining the results of these measurements. Examples of a single LDA measurement and a single example of a conventional microflown calibration using the calibrated microphone as a reference sensor are described. Furthermore, LDA and microflown measurements are performed: (i) measuring at a single frequency while changing the sound level and (ii) measuring at different frequencies while keeping the pressure at the closed end constant. The results of these measurements are combined so that: (1) it could be shown that both the LDA and the microflown measurement behaved linearly with sound pressure at the closed end. (2) The measurement using LDA and the microflown (using the conventional calibration) are compared with each other. (3) The measurements using LDA (in m s^{-1}) and the microflown signal (V_{rms}) have been combined in order to present a calibration method which is independent from other acoustical parameters. This calibration is compared with the conventional calibration.

Before and after each measurement scan, the microflown signal and the reference microphone signal were recorded and used to calibrate the microflown at three different sound levels. These sound fields were created by feeding white noise (dc-4 kHz) to the loudspeaker.

2.6.6.1 LDA photon correlation post-processing

Figure 2-43 contains a graph showing the experimental ACF obtained when the acoustic frequency was 1225 Hz and the pressure at the back plate was 10.9 Pa_{rms}, and the best-fit theoretical curve. Until sometime after the first minimum, the agreement between the experimental curve and the theoretical fit is very close; the relative difference at the minimum is less than 0.1%. After this time, it is clear that the theoretical curve predicts a stronger correlation; this discrepancy is due to additional damping not accounted for by the damping term in equation (2.44). The source of the damping is most likely to be imperfections in the LDA optics, most probably a discrepancy in intensity between the two laser beams.

There are a number of sources of error in the estimation of the acoustic velocity. If equation (2.45) is used to calculate *u*, it is clear that the uncertainty depends on *D* and the time taken for the first minimum, $\tau_{\min}$, to be reached. The temporal resolution of the

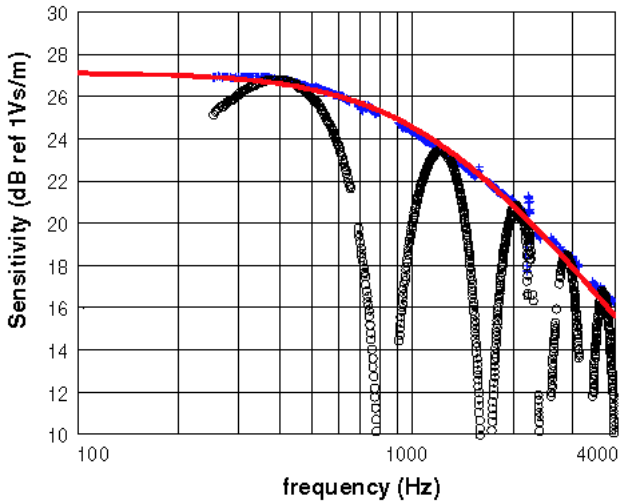

Figure 2-44: microflown calibration using a standing wave tube and a calibrated microphone. Shown are the measured transfer function ($V_{microflown}/P_{ref}$) as the o-marks, the + marks represent the corrected measurement data using equation (2.39) (see text) and the line represents the fit of the sensitivity using equation (2.37).

correlator board was typically 5 μs but the error in τ_{min} can be reduced by using a number of points in the correlation function and interpolating to determine the minimum. The error was reduced further by taking 5 repeats and using the average value. The standard deviation of these repeats was found to be very small compared to the error in D. This in turn was determined by the error in the fringe spacing which was found to be approximately 3%. This was the only error of significance, which resulted in an estimate of 3% for the uncertainty in the velocity measurements. This error is systematic rather than random and could be reduced by measuring the beam separation more accurately.

2.6.6.2 Conventional microflown Calibration

The applied method for calibrating the microflown in the standing wave tube is described in section 2.6.3.2. In Figure 2-44 the raw measured data, and the measured data corrected for the standing wave tube, see equation (2.39), are presented along with a fit of the sensitivity as function of the frequency. Only data with coherence larger than 0.98 are plotted in Figure 2-44. The root mean squared error (RMSE) was estimated as 2.8% (0.24 dB) for the coherent frequency data points between 250 Hz and 4 kHz, and the three different sound levels (of, respectively, 94 dB, 110 dB, and 130 dB). Normally, the uncertainty in the pressure measurement would also be included but since the microphone was recently calibrated by the NPL this error can be assumed to be smaller than other errors.

Note that the difference between the data and the fit can be minimized by decreasing the frequency span if the sensitivity needs to be known more accurate for a certain frequency. For example, if a frequency span of 900 Hz is used (800-1700Hz), the RMSE is decreased to 1.3% (0.11 dB).

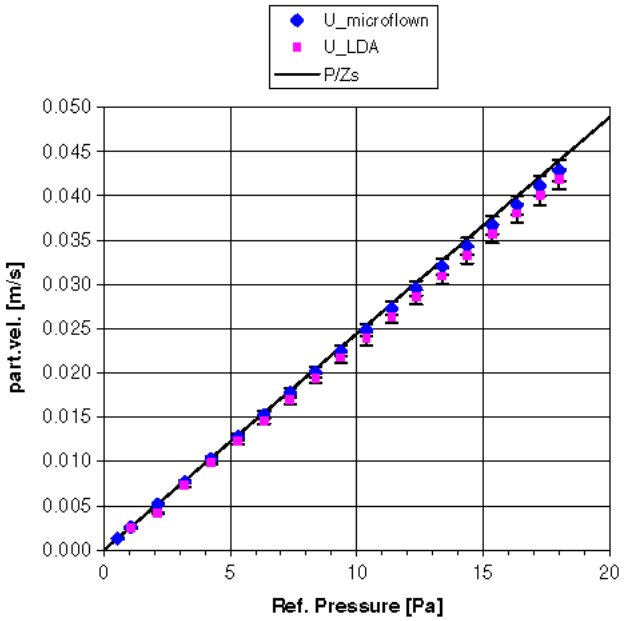

Figure 2-45: Particle velocity measured with a microflown (for calibration see text and Figure 2-44) and measured using the LDA method as function of the pressure at the closed measured at 1247 Hz in the standing wave tube. The plotted line represents the pressure divided by the specific impedance.

2.6.6.3 Particle Velocity measurements at a single frequency

Acoustic velocity measurements were performed inside the standing wave tube at a distance $(l\text{-}x) = 0.21$m from the closed end by means of LDA and the microflown. 1247Hz was chosen as frequency since at this position the ratio of the particle velocity to the pressure at the closed end is a maximum, approximately $\left|u_{\text{probe}} / p_{\text{ref}}\right| \approx 1/\rho_0 c = 1/Z_{\text{air}}$ (see equations (2.42) and (2.39)). Also, the coherence between the reference microphone signal and the microflown signal is optimal for this frequency. Furthermore, the particle velocity does not change significantly with the position along the central axis of the standing wave tube at this frequency since $d\left|u_{\text{probe}}(x)/p_{\text{ref}}\right|/dx$ equals zero at this position and frequency (see Figure 2-47). The sound level was changed while keeping other parameters constant.

The sound level inside the standing wave tube was measured using the calibrated microphone placed at the closed end. The pressure at the closed end was varied from 1 Pa_{rms} to almost 20 Pa_{rms} so that the particle velocity varied between 2.5 mm s^{-1} and 50 mm s^{-1} (rms) which is equivalent to sound (pressure/particle velocity) levels of 94 dB - 120 dB (ref 5×10^{-8}m s^{-1}). It was not possible to measure particle velocities below 2.5 mm s^{-1} at this frequency using the LDA method. This is because the ACF repeats at the acoustic frequency (neglecting damping), so the time to the first minimum in the ACF is now determined by the acoustic frequency rather than the velocity.

In Figure 2-45, the particle velocities measured using the microflown and the LDA method are shown as a function of the pressure at the closed end of the standing wave tube. Figure 2-45 shows that the LDA method and microflown are independently capable of measuring particle velocity both relative to each other and to the theoretical value

$\left|u_{\text{probe}}\right| = \left|p_{\text{ref}}/Z_{\text{air}}\right|$. Both methods show a smaller value than the theoretical value, whereas for the microflown this difference is within the error inherent to the used calibration method itself. The difference between the theoretical value and the measured particle velocity using the LDA method can be explained by the accuracy in the LDA method itself (about 3%) combined with the accuracy in the calculation of the specific impedance (1.3%) and deviations of the flow field from the theoretical model.

In Figure 2-46, the particle velocities measured using the microflown are shown as a function of the velocities measured using the LDA method. The microflown was calibrated before and after the measurement sequence for three different sound levels and the mean sensitivity was used. The specific impedance was calculated to be 409.2 Pa s m^{-1} for this set of measurements. In Figure 2-46, it is shown that the two measurements of the particle velocity do agree with each other. The relative difference between the LDA and microflown measurements is 4%. The error in the LDA measurement is about 3% and the standard deviation in the microflown calibration is estimated at 2.8%. In Figure 2-46, it is shown that these errors explain the discrepancy between the two particle velocity measurements.

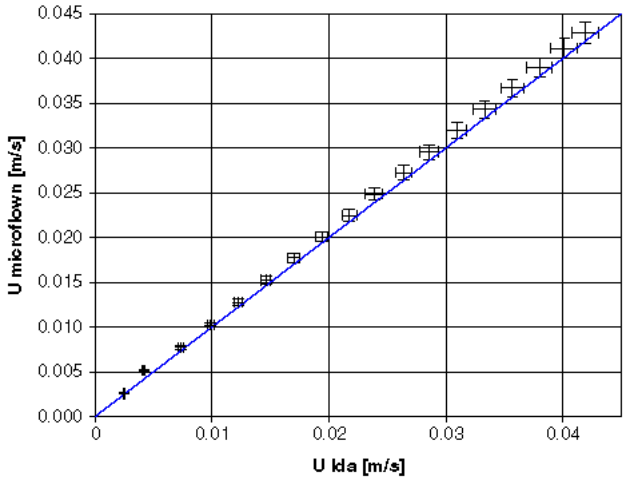

Figure 2-46: Particle velocity measured with a microflown (for calibration see text and Figure 2-44) as function of the particle velocity measured with the non-intrusive LDA method measured at 1247 Hz in the standing wave tube. The line represents $U_{lda} = U_{microflown}$.

2.6.6.4 Particle Velocity measurements versus frequency

Measurements were performed for frequencies from 250 Hz up to 4.5 kHz inside the standing wave tube at position (l-x) = 0.21 m. The frequencies are chosen near resonance frequencies of the standing wave tube. The pressure at the closed end was kept constant at 5.1 Pa_{rms} and was measured using the calibrated 0.5 inch microphone.

Although great care was taken to perform the LDA and microflown measurements at the same position, an additional error will arise from any misalignment. This extra error in particle velocity can be expressed as the derivative of the transfer-function between the particle velocity and the reference pressure against the x-coordinate position. In Figure

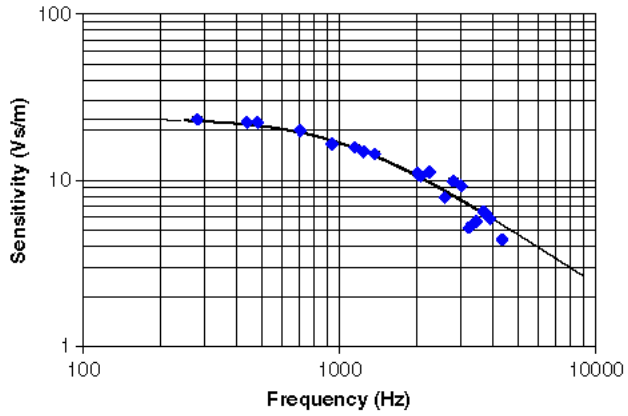

Figure 2-48: Microflown Calibration using the LDA technique in a standing wave tube (diamonds). The — line represents the model fitted using reference microphone positioned in the closed end in the standing wave tube, and the specific impedance. The thick part of the line indicates the frequency region for which the conventional microflown calibration has been optimized (see Figure 2-44).

2-47, it is shown that the difference in particle velocity, given 5 Pa at the closed end and a position differing in position by 1mm, can be as large as 1 mm s^{-1} for certain frequencies.

Using the microflown voltage signal and the particle velocity measured with the LDA method, the sensitivity of the microflown can be measured in V s m^{-1} without the need for a calibrated microphone. In Figure 2-48, this microflown calibration is shown where the data points represent the sensitivity as measured using the LDA method for the various frequencies. The bold line represents the calibration curve obtained using the calibration method using the reference microphone combined with the specific impedance calculated from the atmospheric conditions (see also Figure 2-44). It can be seen from Figure 2-48 that both calibration methods will give the same sensitivity and hence particle velocities.

The particle velocities measured by the microflown and LDA are shown as a function of frequency in Figure 2-49. Note that the particle velocities differ a lot for the several frequencies, whereas the pressure at the closed end was 5 Pa for all frequencies. This behaviour is explained by the fact that we kept the pressure at the closed end constant

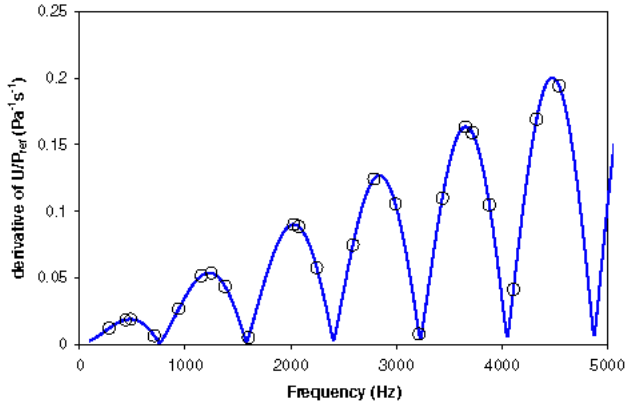

Figure 2-47: The derivative of the transfer-function U/P_{ref} for the measuring position against the position. A large value shows that the particle velocity will strongly vary with position along the standing wave tube. The o- marks represent the frequencies at which the LDA measurements are performed. The line represents the derivative of the fitted model (see equation (2.39)) with regards to the *x*-position.

while the particle velocity is a function of frequency and the pressure at the closed end, expressed in equation (2.42) and (2.39). The solid line in Figure 2-49 corresponds to the theoretical dependence of particle velocity on frequency and pressure at the tube end. The error bar given for the average equals the difference due to an error in positioning of 1 mm. Since the error bars overlap for all but the highest frequency measurements, the velocity values obtained using the microflown agree with those obtained from LDA to within experimental error. There are number of possible contributions to the discrepancy at higher frequencies, including non-linearities in the acoustic flow field or sensor response, and inertial drag of the seeding particles. Further work is required to establish the relative significance of each.

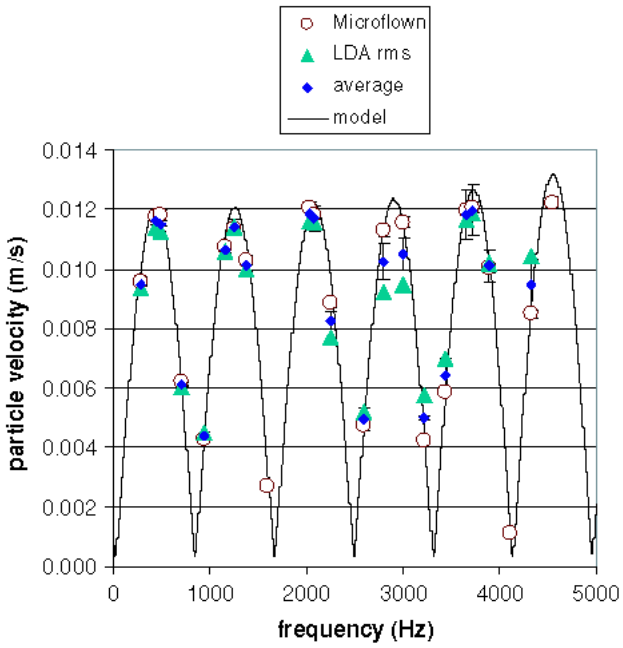

Figure 2-49: A measure of the acoustical particle velocity at different frequencies using the microflown and LDA measurement. The average (the mean of the LDA and microflown measurement for each frequency) including error bars representing an error due to a misalignment of 1mm is added (see Figure 2-47). The line represents a model of the particle velocity given the measured pressure at the closed end. Note that the model does not correspond with the actual values for the different frequencies.

In Figure 2-50, the difference in dB is shown between the microflown and the LDA measurements. This is the same difference as shown in Figure 2-48 and is thus the difference between the conventional calibration and the LDA calibration method applied to the microflown particle velocity probe. The mean difference was 0.0 dB and the standard deviation is 1.1 dB.

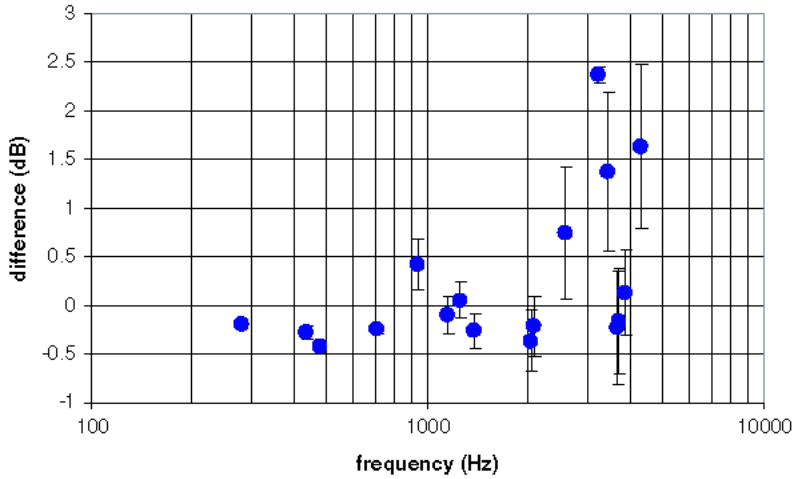

Figure 2-50: Difference between microflown measurement (conventional calibration used) and the LDA photon correlation method. The error bars show the errors in the measurements (difference in position is estimated as 1mm).

LDA measurements performed while the microflown particle velocity sensor has been removed showed that the discrepancies around 3 kHz as shown in Figure 2-47-Figure 2-50 are caused by the presence of the particle velocity sensor itself (see Figure 2-51). By measuring separately, it was possible to calibrate a larger 0.5 inch microflown, although the uncertainty was greater due to errors in alignment.

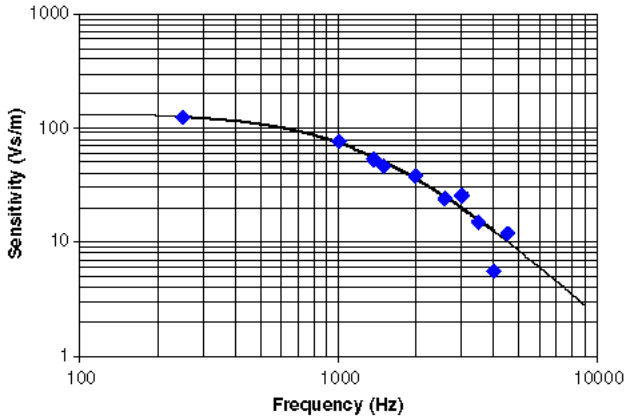

Figure 2-51: Calibration of a half-inch microflown using the LDA technique in a standing wave tube (diamonds). In this experiment the LDA measurement was performed at the same position but while the microflown was taken out the standing wave tube. The — line represents the model fitted using reference microphone positioned in the closed end in the standing wave tube, and the specific impedance.

2.6.7 Conclusions

The microflown was shown to accurately measure particle velocity in sound fields up to 25 mm s^{-1} at 1247 Hz. The difference between the LDA measurements and the microflown measurement are remarkably small using the specific impedance calculated from the pressure, humidity, and temperature values. Furthermore, the difference between LDA and microflown at 1247 Hz is well below the estimated errors of both measurements. The measured particle velocities show good agreement with the particle

velocity calculated using a pressure microphone positioned at the closed end of the standing wave tube combined with the calculated specific impedance.

The LDA photon-correlation method can be used to calibrate the microflown as a particle velocity sensor at various frequencies (between 250 Hz and 4 kHz for the particular standing wave tube used). Errors are introduced due to a difference in the positions of the two measurement techniques; these are frequency and position dependent and for certain frequencies this error is negligible. For certain frequencies around 3 kHz, the discrepancy between the LDA and microflown measurements is somewhat larger than expected. A combination of an LDA measurement and a microflown measurement at the same position, using a reference microphone positioned at the closed end can be used to calculate the specific impedance of the medium.

Remarks can also be made since the LDA photon correlation seems less adequate for particle velocities smaller than 2.5 mm s^{-1} (rms). Also, the standing wave tube with diameter of 50 mm cannot be used for frequencies over 4 kHz.

2.6.8 Acknowledgements

The authors would wish to thank the Dutch Scientific foundation STW and the National Physical Laboratory for their technical and financial support.

end of paper (Raangs et al., 2005).

2.7 Very Near field Calibration Technique

For certain sound sources a relative simple analytical relation between particle velocity in the sound field (and sound pressure) and the sound source exists. Such a sound field is for example a rigid piston in an infinite baffle. In the very near field, the relation between the particle velocity in air and the surface velocity can be even simplified more (Bree de et al., 2004). A more thorough description of the concept of very near field can be found in (Bree de et al., 2004;Microflown Technologies, 2004).

2.7.1 Rigid Piston in an infinite baffle

For a plane rigid circular piston positioned in an infinite baffle the pressure and particle velocity along the axial distance can be described using an analytical solution (Beissner, 1982):

$$\begin{aligned} p &= \rho_0 c u_n e^{\mathrm{i}(\omega t - kx)} \left(1 - e^{-2\mathrm{i}\gamma}\right) \\ u &= u_n e^{\mathrm{i}(\omega t - kx)} \left(1 - \beta e^{-2\mathrm{i}\gamma}\right) \end{aligned} \tag{2.47}$$

with:

$$k = \frac{2\pi f}{c_0},\ \beta = \frac{x}{\sqrt{x^2 + a^2}},\ \text{and}\ \gamma = \frac{k}{2}\left(\sqrt{x^2 + a^2} - x\right) \tag{2.48}$$

There are several reasons why such a piston has advantages for use as source for calibrating the microflown particle velocity sensor. (i)The particle velocity in the sound field near the sound source is approximately the surface velocity. (ii)The influence of the acoustical environment is limited since the distance is much less than the reverberant radius. (iii)The piston will vibrate in a broad frequency range making very low frequency calibration possible.

Figure 2-52: Experimental setup measuring the particle velocity (and pressure) using a 0.5 inch p-u probe as a function of distance and frequency. As a reference a laser vibrometer was used. The sound source is a 2mm thick and 19 cm diameter Aluminium piston.

For the measurements we glued a 19 cm circular aluminium plate on a bass loudspeaker so that a rigid piston was realized as shown in Figure 2-52. The sound field (sound pressure and particle velocity) in front of this piston is simulated and measured as a function of the distance at several frequencies. We used a 0.5 inch p-u probe to measure the sound pressure and the particle velocity.

A disadvantage is the fact that the piston will only behave rigidly well below it's first eigenfrequency. The cylindrical plate will start resonating at a certain eigenfrequency (Powell and Roberts, 1922):

$$f = 0.4745\frac{h \cdot c_1}{a^2} \tag{2.49}$$

where c_1 is the velocity of propagation of extensional waves in an infinite thin plate of the same material and thickness. Given the speed of sound in aluminium is 4877 m s^{-1}, the thickness h is 2 mm, the radius a as 9.5 cm results in a frequency of 514 Hz.

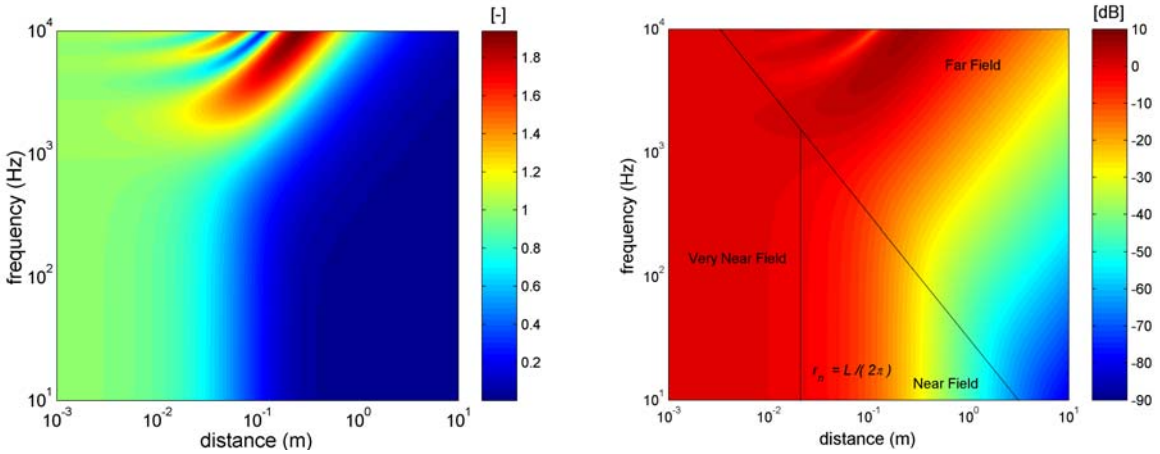

Figure 2-53: Simulated Particle velocity (left: absolute; right: dB scale) for a piston of 9.5 cm radius and 1 mm s^{-1} surface velocity.

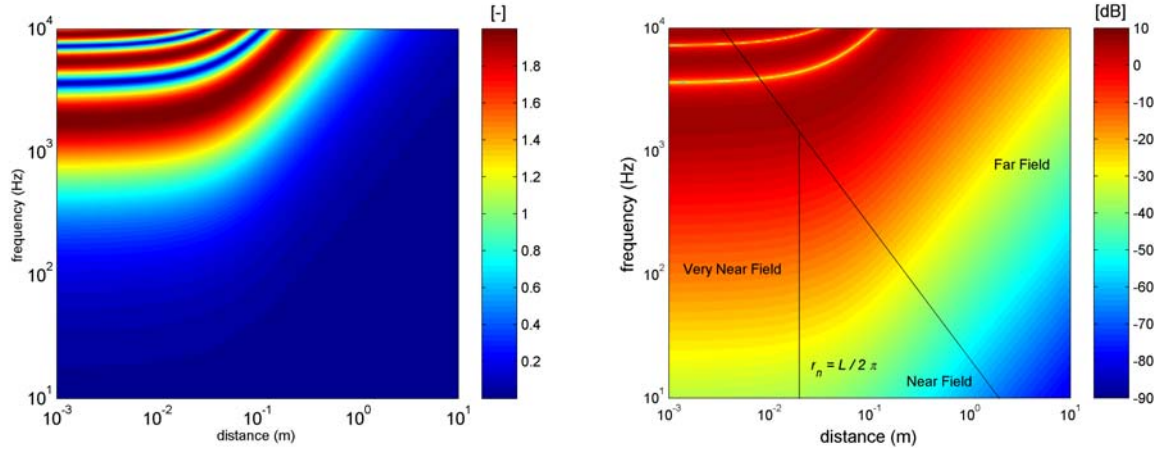

Figure 2-54: Simulated Pressure (left: absolute; right: dB scale) for a piston of 9.5 cm radius and 1 mm s^{-1} surface velocity.

Effectively, a 19 cm diameter piston of 2 mm thickness will be usable in the frequency region from 30 Hz up to approximately 250 Hz.

The computation, using equation (2.47), for the particle velocity and pressure as function of distance and frequency are shown in Figure 2-53 (particle velocity) and Figure 2-54 (pressure). For convenience, the very near field region as defined in (Bree de et al., 2004;Bree de et al., 2005) is illustrated in Figure 2-53(right) and Figure 2-54(right). The plotted particle velocity are relative to the source velocity, and the plotted pressures are relative to the source velocity divided by $\rho_0 c$. In

Figure 2-53 it can be seen that near the rigid piston, the particle velocity almost equals the surface velocity, and, even more important, is independent of the frequency. Figure 2-54(left) clearly shows that the pressure is a more complex function near the surface. For low frequencies, the pressure linear depends on frequency (same surface velocity) but for high frequencies the pressure can be zero due to interference.

In Figure 2-55 the pressure and the particle velocity is measured at the axial axis in front of the piston using a p-u probe which was calibrated in a standing wave tube. Figure 2-55 clearly shows that near the piston, the particle velocity almost equals the particle velocity on the piston itself. Measurements for other frequencies (75 Hz, 125 Hz, and 250 Hz) were presented in (Bree de et al., 2004).

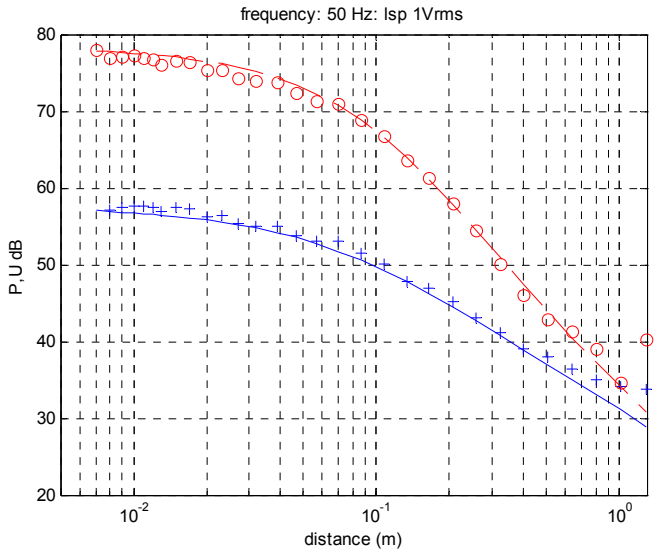

Figure 2-55: Measured pressure (+ marks) and particle velocity (o-marks) along the axial distance for 50Hz. The blue and red lines represent the theoretical pressure and particle velocity (Beissner, 1982) for a surface velocity of 0.42mm/s/(Hz)^{½}.

The values for surface velocity obtained from the measurements of pressure and particle velocity along the axis have been compared with surface velocity measurements obtained with the laser vibrometer. In Table 2-2 the surface velocity fitted out of the measurements of the particle velocity and pressure (see Figure 2-55) using equation (2.47) and (2.48) for different frequencies are given along with the measured surface velocity using a laser vibrometer. Since the difference between the measured and fitted surface velocities is small, it can be concluded that this method can be used for calibrating the microflown for low frequencies.

Note that a single calibration measurement at a known distance of the source will be sufficient if the source is sufficiently rigid so that the relation between particle velocity at the microflown position and the surface velocity can be used according to equation (2.47).

Table 2-2: Comparison between p-u probe measurement and Laser Vibro measurement.

Measurement		**Frequency**			
		50Hz	75Hz	125Hz	250Hz
Fit (see Figure 2-54 **and eq.** (2.47)**)**	mm s^{-1} $Hz^{-0.5}$	0.42	0.27	0.15	0.08
	dB	78.5	74.6	69.5	64.1
Laser vibrometer	mm s^{-1} $Hz^{-0.5}$	0.40	0.27	0.14	0.094
	dB	78.0	74.6	69.0	65.5
difference	mm s^{-1} $Hz^{-0.5}$	0.02	0.00	0.01	-0.014
	dB	0.5	0.0	0.5	-1.4

2.8 Self-noise

Acoustical measurements are limited at lower sound levels by the noise in the measurements themselves. This lower limit is known as noise floor; the measure of the signal created from the sum of all the noise sources and unwanted signals within a measurement system.

The sources of noise in a measurement are (Wong and Embleton, 1994): (1) acoustical background noise, (2) self-noise of the acoustical sensor, and (3) preamplifier. For a given sensor, taken the fact that the preamplifier and data-acquisition path are optimised, the remaining noise in a quiet environment is known as the self-noise. The self-noise is also referred to as equivalent noise level or noise floor although these terms can also refer to the whole measurement chain. Although there are techniques available that enable us to perform measurements below this noise floor in case of certain situations and sound sources, in general an acoustic sensor with a low self-noise is preferable.

2.8.1 Self-noise introduction

Self-noise is the electrical noise, or hiss, an electronic device produces. The self-noise level indicates the sound level that will create the same voltage as the self-noise from the microphone, c.q. microflown, produces The conversion of electrical

noise to equivalent acoustical noise is shown in equation (2.50). The sensitivity of the sensor, see section 2.2, together with its (electrical) noise level leads to the self-noise in Pa/√Hz for pressure sensors, or in m/(s√Hz) for particle velocity sensors. It corresponds to a noise level that can be expressed in an equivalent particle velocity in case of the microflown (Honschoten, 2004), and equivalent pressure in case of a microphone.

In case the sensitivity of the microflown particle velocity is given in terms of equivalent free-field pressure [Pa*], the self-noise can be expressed in Pa*/√Hz. The latter definition inherently has the advantadge that self-noise of a pressure sensor (given in Pa/√Hz) can easilly be compared with the self-noise of a particle velocity sensor (given in Pa*/√Hz).

$$\mathrm{PSD}_{\mathrm{acoustical}} = \frac{1}{\left(S_{\mathrm{microflown}}\right)^2}\mathrm{PSD}_{\mathrm{volts}} \tag{2.50}$$

The self-noise is commonly expressed as a function of frequency, such as a pressure spectral density or power spectrum density (Pa^2 ,or m s^{-1} per 1 Hz bandwidth), see section 3.1.1, or as a single value, such as the squared pressure in a certain bandwidth. Such frequencies are (a) integrated over a broad frequency band (typical 20 Hz to 20 kHz), a ⅓-octave or in octave bands, etc., (b) weighted, (for example A-weighted), or (c) narrow band, for example Δf = 1 Hz.

Equivalent to sound pressure levels (L_p), sound intensity levels (L_I), and particle velocity levels (L_v), it is very convenient to express the self-noise in decibel scales. The reference pressure equals p_{ref} = 2 10^{-5} Pa, and the reference sound intensity equals I_{ref} = 10^{-12} Wm^{-2}. As reference for the particle velocity a value of u_{ref} = 5 10^{-8} m s^{-1} (Finke, 1991b) can be used. Note that these references result in a difference between particle en pressure levels even in case of a plane wave. For example, in case of an atmospheric condition of (p_0 = 1015 hPa, T = 20°C, and RH = 50%), the difference is about 0.3 dB between the particle and pressure levels (in case of a plane wave).

In case the particle velocity is calibrated with reference to a pressure sensor (the sensitivity is then given in V/Pa*) and the specific acoustical impedance, Z_s, is unknown, it is often convenient to use the equivalent p_{ref} as reference for the particle velocity. In case the specific acoustic impedance is known, it is convenient

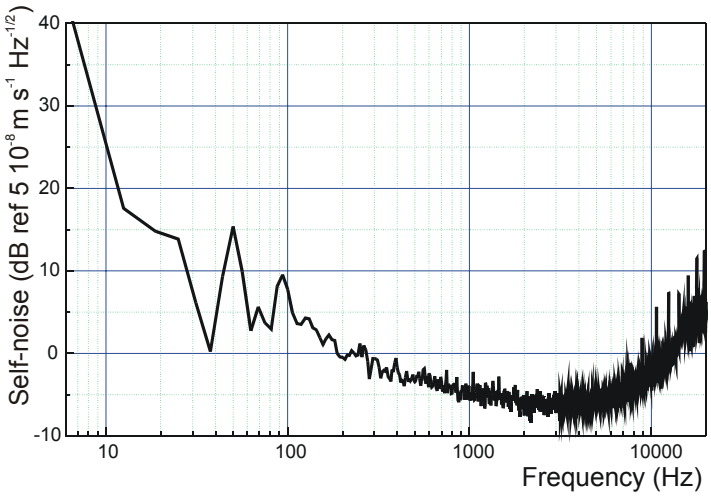

Figure 2-56: Self-noise spectrum of a microflown (2004).

to use $u_{ref} = p_{ref}/Z_s$ as a reference particle velocity. The particle velocity level and pressure levels are then equal for a plane wave.

Figure 2-56 shows the measured self-noise spectrum of a modern three-wire microflown. The probe was placed in a complete silent environment during the measurement.

In case of low frequencies the self-noise of a microflown is equivalent with that of a microphone (Raangs et al., 2001a) and often lower for modern microflowns (Bree de, 2001). A thourough description of low-frequency self-noise can be found in reference (Honschoten, 2004). Due to the working principle of the microflown (Svetovoy and Winter, 2000), the sensitivity decreases for higher frequencies, and therefore the self-noise increases for high frequencies.

Noise of acoustical sensors is less important in the case of sound intensity measurements because in this type of measurements the coherence between the signals of two sensors is involved. The microflown is useful in sound intensity because this quantity equals the cross-spectrum between the particle velocity and the pressure in the frequency domain. The small microflown combined with a miniature microphone can therefore be used to determine sound intensity at a short distance from the surface of a radiating source.

2.8.2 Self-noise spectra of microflowns

In this section, a few examples of self-noise spectra of microflowns and microphones are shown.

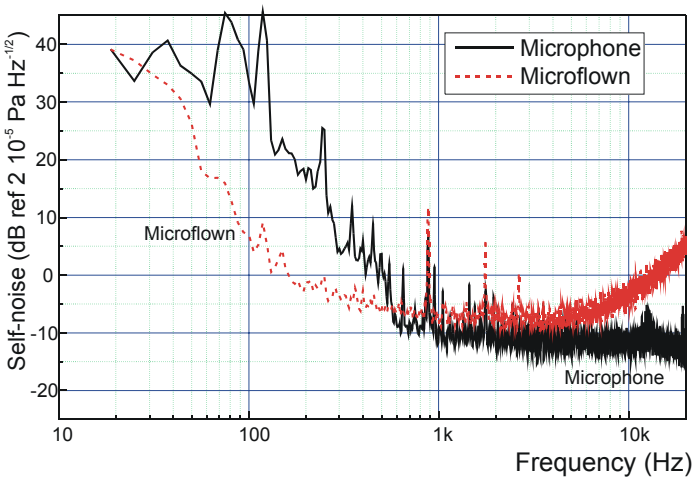

Figure 2-57: Self-noise of the 0.5 inch p-u probe signals given in sound level per √Hz. The self-noise of the microflown (three-wire) is given in dB PVL (re. 50 nm/s) in 1 Hz bandwidth; the self-noise of the 0.1 inch microphone is given in dB SPL (re. 20 µPa) in 1 Hz bandwidth.

Figure 2-57 shows the self-noise spectrum of a regular two-wire microflown whereas the microflown is positioned between two bars, the so-called package, see section 1.7.3, which acoustically amplifies the free-field particle velocity and thus increasing the sensitivity (Bree de, 1997). Since the package acoustically amplifies the flow along the microflown wires, and does not influences the electrical noise, the self-noise of the packaged microflown is lower than that of the same microflown without the packaging. For comparison, the noise spectrum for the 0.1 inch pressure sensor inside the 0.5 inch p-u is also shown in Figure 2-57.

In Figure 2-58, the self-noise of an ultimate sound probe (USP, also known as

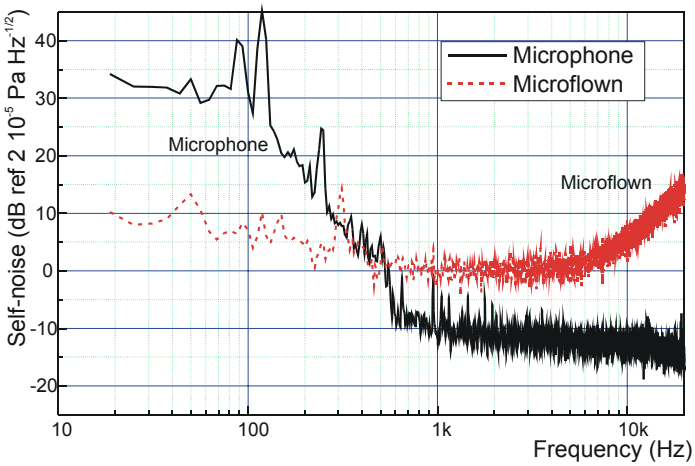

Figure 2-58: Self-noise of the USP probe signals given in sound level per √Hz. The self-noise of the three microflowns are equal and are given in dB PVL (re. 50 nm/s) in 1 Hz bandwidth; the self-noise of the 0.1 inch microphone is given in dB SPL (re. 20 µPa) in 1 Hz bandwidth.

three-dimensional p-u probe (Microflown Technologies, 2004)) is shown. Shown is only the self-noise of one particle velocity sensor in the three-dimensional probe. In Figure 2-58 it can be seen that the self-noise of this probe is somewhat higher than that of a packaged probe, see Figure 2-57, based on the same microflown sensor.

For comparison, the self-noise of a commercial 0.5 inch condenser pressure microphone is shown in Figure 2-59. In general, it can be noted that a large diaphragm microphone has less self-noise than a small diaphragm microphone. This is due to the fact that the self-noise in a microphone is mainly due to Brownian Movements (Wong and Embleton, 1994); i.e. air molecules bombard the diaphragm creating an equivalent noise pressure. Furthermore, the sensitivity of the large and more compliant microphone diaphragm is generally higher than the small and stiff diaphragm.

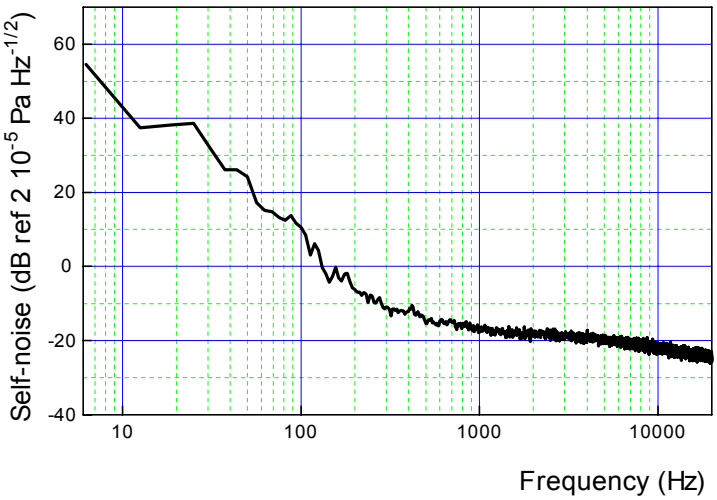

Figure 2-59: Self-noise of a 0.5 inch microphone, GRAS 40AC.

Note that, that sound levels even lower than the self-noise can be measured by using the cross-correlation (Honschoten et al., 2002a;Honschoten et al., 2004). For the same reason, the self-noise in sound intensity using the cross-correlation of two sensors, a pressure and a particle velocity sensors, is lower than the self-noise of the individual sensors, see also Chapter 3 and Chapter 4 and (Raangs et al., 2003). The noise in the particle velocity obtained using a commercial p-p probe is however much higher than the self-noise of a microflown (Bree de, 2005).

2.9 Discussion and Conclusions

Calibration of acoustical sensors in general and particle velocity sensors in particular, is difficult because the acoustical environment is often not known, and a reference particle velocity sensor is not available. Several acoustical environments can be used such as an anechoic chamber or free field environment (Raangs et al., 2003).

In this chapter various methods for calibration are presented, each with their own advantages and disadvantages such as: applicable frequency range, size, sound levels, and so on. A review of the several calibration techniques is given in Table 2-3. Note the shaker, long small SWT, SWT properly closed, and near field: small opening in a baffle is not described in this thesis. Details on these techniques can be found in (Bree de, 1997;Honschoten, 2004;Jacobsen and Bree de, 2005b;Microflown Technologies, 2004;Tijs, 2004)

Table 2-3: Calibration Techniques for the microflown particle velocity sensor.

Technique	Freq. range	processing	size	accuracy
Shaker	~5-200Hz	+	+-	+-
SWT: Long small diameter	100Hz-4kHz	+-	+	+-
SWT: Short small diameter	200Hz-3.5kHz	+-	++	+-
SWT properly closed	40Hz-4kHz			+-
Laser Doppler Anemometry		-	+-	+-
Reverberant room technique	200-4kHz	--	++	--
Open Window		+		--
Near Field: Small opening in baffle	20Hz-20kHz	++	+	+
Very Near Field: Rigid Piston in a baffle	30 Hz-250 Hz	+-	+-	+-

Chapter 3
Applications of Cross-Correlations and Cross-Spectra

3.1 Introduction

In the major part of this thesis and in (acoustical) measurements in general, signal analysis plays an important role. The most common form of signal analysis is the Fourier transformation of a temporal signal into the frequency domain to obtain the frequency spectrum of the signal. For example, often the power in the signal for different frequencies or within a certain frequency band is required. In other situations, the complex relationship between two (or more) signals should be known for different frequencies in order to calculate a transfer function such as an acoustical path, or to retrieve a calibration with reference to a known reference sensor (see Chapter 2).

Applications of auto- and cross-spectral analysis can be found throughout the field of acoustical measurement techniques. In this chapter we will show some extra advantages of cross- and autospectra which are especially very practical in case of a directional sensor such as the microflown.

The time averaged cross-correlation signal of two uncorrelated sources is theoretically zero and this principle is used to decrease the noise of the sensors. Also the influence of reverberation is cancelled in the cross-correlation of two microflown oriented in perpendicular directions orthogonal to each other.

In section 3.2 a method is presented to reduce the noise level of a particle velocity sensor which yields a reduction of the noise of 30 dB. The method is based on utilisation of cross- instead of autocorrelation spectra of two of these sensors. The noise of the sensor becomes even considerably lower than the principle resistance noise level (Johnson noise) of the wires. Since the signal part in the cross-spectrum of two laterally placed microflown signals equals the autospectra, as is shown in section 3.3, the dynamical range is extended accordingly.

The characteristics of an ideal diffuse sound field, a sound field in which sound waves are coming from all directions with random phase and amplitude will

enhance the results obtained by multiple microflowns measuring in different directions as explained in section 3.4. This same principle can also be used for calibration (see Chapter 2) and for measurements which are performed for mapping the sound field (see Chapter 5).

For the theory of auto- and cross-correlation used in this chapter we refer to (Bendat and Piersol, 1986;Bendat and Piersol, 2002;Papoulis, 1991).

3.1.1 Cross-Correlations and Cross-Spectra

In this section, examples are shown such as acoustical power written as cross-correlation between pressure and particle velocity. The use of cross-correlations are shown for active and reactive sound intensity using p-u and p-p methods, et cetera, see (Fahy, 1995;Fahy, 1997;Raangs et al., 2001a)

First the correlation functions and spectra have to be defined. The cross-correlation function of two signals is defined as (Bendat and Piersol, 2002)

$$R_{xy}(\tau) = \lim_{T\to\infty} \frac{1}{T} \int_0^T x(t)\, y(t+\tau)\, dt \tag{3.1}$$

For the special case where $y(t) = x(t)$, $R_{xx}(\tau)$ is called the autocorrelation function. The cross-correlation is always smaller than or equal to the individual autocorrelations according to equation (3.2).

$$\left|R_{xy}(\tau)\right| \le \sqrt{R_{xx}(0) R_{yy}(0)} \tag{3.2}$$

The relationship in equation (3.2) is commonly called the cross-correlation inequality. In the frequency domain, equivalent functions can be defined such as the auto- and cross-spectra. For ergodic signals the cross-spectral density (CSD) function is given by

$$S_{xy}(f) = \int_{-\infty}^{\infty} R_{xy}(\tau) e^{-j2\pi f\tau} d\tau \tag{3.3}$$

For $x = y$, the cross-spectral density function (CSD) is also known as the autospectral density function. Another name is the power spectral density function (PSD). $S_{xy}(f)$ is called the two-sided spectral density function, whereas $G_{xy}(f)$ is called the single sided density function. The single sided density function $G_{xy}(f)$ is defined by:

$$\begin{aligned} G_{xy}(f) &= 2S_{xy}(f) \quad for \quad f>0 \\ &= S_{xy}(f) \quad for \quad f=0 \\ &= 0 \quad for \quad f<0 \end{aligned} \tag{3.4}$$

An important feature of the auto- and cross-correlation function is the fact that its value at $\tau = 0$ can be calculated using:

$$R_{xy}(0) = \int_{-\infty}^{\infty} S_{xy}(f)\,df = \int_{0}^{\infty} G_{xy}(f)\,df \tag{3.5}$$

Similar to the cross-correlation inequality in equation (3.2) in the time domain, equation (3.6) is known as the cross-spectra inequality relation:

$$\left|G_{xy}(f)\right|^2 \le G_{xx}(f)\,G_{yy}(f) \tag{3.6}$$

The auto- and cross-spectral densities can be calculated using the Fourier transforms of the measured time sequences

$$G_{xy}(f) = \lim_{T\to\infty} \frac{2}{T} E\left[X^*(f,T)\,Y(f,T)\right] \tag{3.7}$$

where E is the expectation value of $[\ ]$, and $X(f,T)$ denotes the Fourier transform of $x(t)$ over record length T. Note that, the factor 2 since this is the single sided cross-spectral density function whereas the Fourier transform is also defined for negative frequencies. Further notice the limit for time T goes to infinity, which is rather impossible for measured time history sequences. Also note that the position of the complex conjugate whereas X^* denotes the complex conjugate of X. Which variable is complex conjugated is determined by the previous equations such as equations (3.1) and (3.3). The definition according to equation (3.7) is commonly used (Oppenheim et al., 1989). For the estimation of the auto- and cross-spectra out of the sampled sequences, we used the method of averaged modified periodograms (Welch, 1967).

The major advantage of nowadays signal processing in acoustics is the fact that filtering, which is needed for obtaining for example A-filtered or C-filtered acoustical levels, can now be easily performed in the frequency domain.

Another important feature of the cross-spectra is that for a given linear system with input *x* and output *y*, a complex transfer function can be defined using

$$G_{xy}(f) = H(f)\,G_{xx}(f) \tag{3.8}$$

Equation (3.8) is therefore applied for example in a relative calibration method (as was used in Chapter 2 and Chapter 4).

The average intensity $\int p(t)u(t)dt$ written in terms of cross-correlation.

$$R_{pu}(\tau) = \lim_{T\to\infty} \frac{1}{T} \int_0^T p(t)u^*(t+\tau)dt \tag{3.9}$$

For a plane wave, the sound intensity can be written in terms of pressure as $p^2/\rho_0 c$ or in terms of particle velocity as $u^2\rho_0 c$. By definition, the mean intensity component in the direction of u is $R_{pu}(0)$. The distribution in frequency of the product of the u and u or the p and u components is given by the Fourier transform of the auto- or cross-correlation function:

$$G_{uu}(\omega) = \frac{1}{2\pi} \int_{-\infty}^{\infty} R_{uu}(\tau)e^{-i\omega\tau}d\tau \tag{3.10}$$

and

$$G_{pu}(\omega) = \frac{1}{2\pi} \int_{-\infty}^{\infty} R_{pu}(\tau)e^{-i\omega\tau}d\tau \tag{3.11}$$

and equation (3.11) give the autocorrelation spectrum (the autospectral density) and the cross-correlation spectrum (cross-spectral density) respectively of the signals $u(t)$ and $p(t)$.

3.2 Self-noise reduction using Cross-Correlation and Cross-Correlation

This section is copied from a journal paper "Noise Reduction in Acoustic Measurements with a Particle Velocity Sensor by means of a Cross-Correlation Technique" which was written together with Dr. Joost van Honschoten (Honschoten et al., 2004), also presented earlier (Honschoten et al., 2002a). The authors are J.W. van Honschoten, W.F. Druyvesteyn, H. Kuipers, R. Raangs, and G. J. M. Krijnen. The author of this thesis performed measurements and technical computations. Used electronic equipment was designed and was build by Ing. Henny Kuipers. The summary and the introduction of the included paper is not included since the microflown sensor and its properties have already been introduced in this thesis. The references, equation numbers, symbols, and figure captions are changed and are consistent with the rest of the thesis.

3.2.1 Theoretical Description of the Noise

So far, most of the theoretical descriptions and modelling of the used sensor (Honschoten et al., 2001;Svetovoy and Winter, 2000) has been concentrated on the frequency characteristics and the sensitivity of the sensor. Purpose in the analysis and modelling was, besides understanding the behaviour, the optimisation of the sensitivity. However, a more relevant parameter than the sensitivity only, is the signal-to-noise (S/N) ratio of a particle velocity sensor.

Since a hot-wire particle velocity sensor consists fundamentally of (usually two) electronically heated resistors, an inevitable origin of noise is formed by the so-called resistance noise, which forms therefore a theoretical minimum of the noise from one wire. For a resistance R at absolute temperature T, these voltage variations in a frequency interval Δf are given by (Pathria, 1986); k the Boltzmann-constant):

$$\langle V^2_{\text{noise}} \rangle_{(f, f+\Delta f)} = (4kTR)\Delta f \tag{3.12}$$

It is observed that the noise manifest in the sensor's output signal is, especially for low frequencies, often higher than this Johnson (or Nyquist) noise level.

Several explanations have been considered; the additional noisy signal may have an electronic, thermal, (thermo-)acoustic or mechanical origin or a combination of these. One hypothesis describes the noise as originating from "thermal agitation noise" due to "Brownian motion" (Pathria, 1986;Ziel, 1954) of air molecules or particles of nanometre size present in the air, although calculations on these processes show this thermal agitation noise not to be a significant factor for the particle velocity sensor under investigation. Apart from any acoustic noise or noisy signals related to the gas or flow, the heated wires that are actually thin metal films, show low-frequency $1/f$ or flicker noise. These low-frequency fluctuations in thin films and metals that show power spectra of the form $1/f^{\alpha}$, with $0.5<\alpha<1.5$, cover a wide range of phenomena about which a lot of studies in literature have been published (Dutta and Horn, 1981;Grinstein et al., 1992;Liu, 1977;Scofield et al., 1985). Resistance inhomogeneities or local impurities in the sputtered wire, and the resistivity and corresponding voltage oscillations are likely to play a role in the low-frequency noise of the sensor. It is not the purpose of this paper to give an adequate explanation of the precise origin of the measured noise. Instead, the following method is introduced to reduce significantly the undesirable voltage fluctuations in the output signal of the sensor, see also (Bjor, 1997). The measurement method that will be described here is based on the fact that intrinsic noise sources at two different sensors are mutually uncorrelated. By application of the cross-correlation spectrum of the sensors, this noise power can, for long-time averaging, be eliminated.

The noise occurring in the acoustic measurements manifests itself in the form of small, stochastic voltage fluctuations in the output signal of the sensor. The mean value μ of these voltage fluctuations $v(t)$ is given by

$$\mu = E\{u(t)\} =< u(t) >= 0 \tag{3.13}$$

where $E\{x(t)\} = \lim_{T\to\infty}\int_0^T x(t)\,dt$ represents the expectation value of a stationary stochastic time function $x(t)$. Defining the corresponding autocorrelation function as

$$\begin{aligned} R_{vv}(\tau) &= E\{u(t)u(t+\tau)\} \\ &= \lim_{T\to\infty}\frac{1}{T}\int_{-T/2}^{T/2} u(t)u(t+\tau)\,dt \end{aligned} \tag{3.14}$$

it is seen that the dimension of $R_{uu}(t)$ is V^2, so that it can be interpreted as an averaged power P in a $1\ \Omega$ resistance, in particular (Pathria, 1986) $R_{uu}(0) = E\{u^2(t)\} = P_{\text{average}} = < u^2(t) >$.

The Fourier transform of the autocorrelation function, $\Phi_{uu}(\omega) = F(R_{uu}(\tau))$, represents the power density spectrum and shows how the power of the stochastic signal is distributed over the frequency domain. Furthermore, a cross-correlation function $R_{u_1u_2}(\tau)$ can be defined, which function indicates the mutual correlation between two signals $u_1(t)$ and $u_2(t)$ (Press et al., 1992;Ziel, 1954). If $u_1(t)$ and $u_2(t)$ are two statistically independent variables, and if one of or both of the signals have expectation value zero (i.e. there is no DC-component), then

$$\begin{aligned} R_{u_1u_2}(\tau) &= E\{u_1(t)u_2(t+\tau)\} = E\{u_1(t)\}E\{u_2(t+\tau)\} = \\ &= E\{u_1(t)\}E\{u_2(t)\} = 0 \end{aligned} \tag{3.15}$$

The autocorrelation function of the sum of two signals $u(t) = u_1(t) + u_2(t)$ follows from

$$\begin{aligned} R_{uu}(\tau) &= \lim_{T\to\infty}\int_{-T/2}^{T/2} \{u_1(t)+u_2(t)\}\,\{u_1(t+\tau)+u_2(t+\tau)\}dt = \\ &= R_{u_1u_1}(\tau) + R_{u_1u_2}(\tau) + R_{u_2u_1}(\tau) + R_{u_2u_2}(\tau) \end{aligned} \tag{3.16}$$

If $u_1(t)$ and $u_2(t)$ are statistically independent, $R_{u_1u_2}(\tau) = R_{u_2u_1}(\tau) = 0$, so that $R_{uu}(\tau) = R_{u_1u_1}(\tau) + R_{u_2u_2}(\tau)$, and therefore for the Fourier transforms yields analogously: $S_{uu}(f) = S_{u_1u_1}(f) + S_{u_2u_2}(f)$.

In measurement techniques, the statistical independence of different noise sources in the cross-correlation functions can be applied to reduce the noise [e.g. (Bjor, 1997).

The output signal of the hot-wire particle velocity sensor is proportional to the scalar product $\vec{u}\cdot\vec{n}$, with $\vec{u}$ the local particle velocity and $\vec{n}$ the unit vector in the plane of, and perpendicular to the length of the wires. If now two similar sensors are placed parallel and closely to each other and if the distances between both wires of a sensor and between two different sensors are small compared to the acoustic wavelength, and then both output signals are fully correlated. On the other hand, it seems justified to assume that both intrinsic noise sources of the probes are totally uncorrelated. These noise sources are mainly determined by the resistance noise of the resistors, which are independent. If furthermore both sensors are independently powered, the noise associated with the electrical powering should be uncorrelated as well. Other noise sources that occur in the noise spectrum of a particle velocity sensor, that manifest themselves particularly in the low-frequency region, may, depending on their origin, cause either correlated or

uncorrelated noisy signals. Of course, possible noisy acoustic fluctuations may have correlated influences on both acoustic sensors. Besides, electrical interferences (frequency components of the electrical powering frequency) may cause disturbances.

Assume that a certain particle velocity leads to an output signal $u_1(t)$ of particle velocity sensor 1, that is contaminated by a noise spectrum $n_1(t)$. Sensor 2, located closely to the first sensor, then gives an output signal $u_2(t)$, with additional noise $n_2(t)$. The cross-correlation of $x_1(t) = u_1(t) + n_1(t)$ and $x_2(t) = u_2(t) + n_2(t)$ thus becomes

$$\begin{aligned} R_{x_1x_2}(\tau) &= \lim_{T\to\infty} \int_{-T/2}^{T/2} \{u_1(t)+n_1(t)\}\,\{u_2(t+\tau)+n_2(t+\tau)\}dt = \\ &= R_{u_1u_2}(\tau) + R_{u_1n_2}(\tau) + R_{u_2n_1}(\tau) + R_{n_1n_2}(\tau) = \\ &= R_{u_1u_2}(\tau) \end{aligned} \tag{3.17}$$

The last step in equation (3.17) follows from the fact that the noise of sensor 1 and that of 2 have no mutual correlation (assuming for a moment there are no acoustic but only electrical or thermal noise sources) and are uncorrelated to the signals as well.

Therefore, the power spectrum of the measured output signals $x_1(t)$ and $x_2(t)$, that are contaminated by uncorrelated noise, is found from this cross-correlation;

$$S_{x_1x_2}(f) = S_{u_1u_2}(f) \tag{3.18}$$

and if both sensors have the same sensitivity (i.e. same proportionality between particle velocity and output voltage),

$$\left|S_{x_1x_2}(f)\right| = S_{u_1u_1}(f) \tag{3.19}$$

in which noise is not present anymore.

According to this theory, the approach of the application of cross-spectra leads ideally to a noise spectrum of zero. The two noise sources in the respective signals are assumed to be uncorrelated, so that, the larger the measuring time and therefore the number of data points stored, the more the calculated cross-correlation spectrum of the noise can be reduced (Korn and Korn, 2000).

The mean value of this cross-spectrum is zero, but since the integration time is finite, a more relevant parameter to characterise this quantity is its variance, σ^2. The larger the number of points in the time series of the signals, the smaller this variance. Using the Lindeberg-Lévy Theorem, Central Limit Theorem, (Korn and Korn, 2000), this is illustrated as follows.

Assume that in the calculation of the autocorrelation spectrum and the cross-correlation spectrum, a time signal consisting of a series of N data points is used. To get some insight into the behaviour of the calculated quotient of power in cross-spectrum and power in autospectrum as a function of N, the two time signals are simplified to two uncorrelated arbitrary binary series of N points. They are modelled by two time series of which each data point represents a 1 or a –1 (like throwing a coin).

Define therefore the series as p_i and q_i, consisting only of values 1 and −1. So p_1, p_2, p_3,..=-1, -1, 1,..etc. The total power in the autospectrum of the first signal will therefore be proportional to

$$\sum_{i=1}^{N} p_i^2 = N \tag{3.20}$$

the power in the autospectrum of the other also N, and the power in the cross-spectrum of both will be proportional to

$$\sum_{i=1}^{N} p_i q_i \tag{3.21}$$

Define $p_i q_i \equiv a_i$, so that the expected or mean value (Korn and Korn, 2000) of a_i, $E(a_i)=0$, and its variance σ^2, is $\mathrm{Var}(a_i)=1$. Now the Lindeberg-Lévy Theorem, or Central Limit Theorem states that for a random variable $\overline{a} = \frac{1}{N}(a_1 + a_2 + ... + a_N)$ that converges in probability to $E(a_1)$, (here therefore equal to 0), for which the common variance σ^2 of a_i exist, $\overline{a}$ is asymptotically normal with mean $E(a_i)$ and with a variance σ^2/N. In our calculations we are interested in the ratio (power in cross-spectrum/power in autospectrum), so one should calculate the variance of

$$\frac{\sum_{i=1}^{N} a_i}{\sqrt{\sum_{i=1}^{N} p_i^2 \sum_{i=1}^{N} q_i^2}} = \frac{1}{N}\sum_{i=1}^{N} a_i = \overline{a} \tag{3.22}$$

One sees therefore that the variance of this ratio behaves as σ^2/N; inversely proportional to N.

3.2.2 Experiments

To determine the signal-to-noise ratio of the hot-wire particle velocity sensor, both the sensitivity, i.e. the output response of the sensor to a certain particle velocity, and its noise behaviour had to be measured. For the experiments, use was made of the particle velocity sensor named in the introduction (Bree de et al., 1996b;Honschoten et al., 2001;Microflown Technologies, 2004;Svetovoy and Winter, 2000), consisting of two heated wires. These two closely spaced thin wires of silicon nitride have an electrically conducting platinum pattern of 150 nm on top of them. A SEM photograph of such a sensor is depicted in Figure 1-1. Dimensions of the two wires are 1000 μm ×10 μm x 0.5 μm, their spacing is usually approximately 200 μm. The silicon nitride layer is used as a mechanical carrier for the platinum resistor patterns. The metal pattern can be used as heater *and* as temperature sensor, by using its temperature dependent resistance. The sensors are powered by an electrical current, and heated to an operational temperature between 200ºC and 500ºC.

The sensitivity of the sensor in a bandwidth of about 0-4.0 kHz was determined in a "standing wave tube" (Bree de et al., 1996b;Eerden et al., 1998), by placing the sensor in

the tube with at one side a loudspeaker generating a broad frequency spectrum and at the other side a reference microphone. From the ratio between the output signals of both acoustic sensors, the sensitivity of the particle velocity sensor could be obtained.

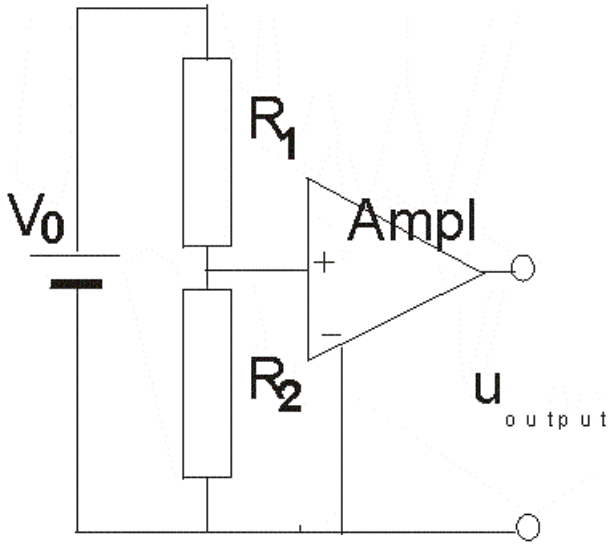

Figure 3-1: Electrical scheme of the set-up to measure the output noise of the hot-wire particle velocity sensor, consisting of resistances R_1 and R_2.

To measure the noise spectrum of one particle velocity sensor, consisting of two (equal) resistances R_1 and R_2, a simple set up as shown in Figure 3-1 was used. R_1 and R_2 were equal to 1.10 kΩ. The DC-powering was obtained from applying a 9 V battery as voltage source. The autospectrum of the noise of one sensor thus measured is plotted in Figure 3-2. Additionally a second set-up, identical to the first (Figure 3-1) with two perfectly similar amplifiers and an identical but independent voltage source, was used for the noise measurement on sensor 2. Both sensors were placed into two different acoustically isolated boxes to reduce acoustic, and correlated, noise. The boxes were attached by

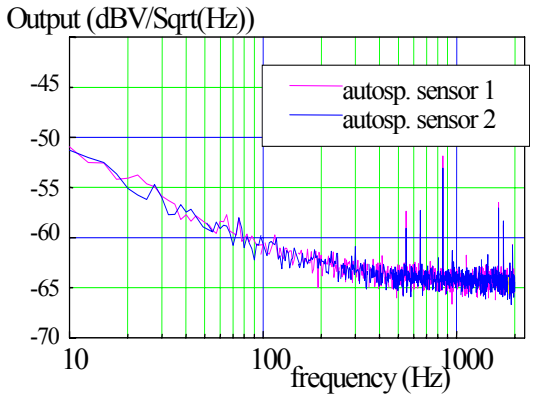

Figure 3-2: Measured autocorrelation spectra of the noise of sensor 1 and 2 (Amplification factor: 100 dB). For frequencies above approx. 600 Hz the spectrum is flat and corresponds to the Nyquist noise level for normal resistances of 1.1kΩ.

elastic bands to reduce possible low-frequency and correlated noisy influences. In these boxes the probes were additionally sheltered in small tins with a transformer in it to balance the output signal. The two signals were led through shielded, balanced XLR cables and then independently amplified, first by a battery powered amplifier with amplification factor 50 dB, then again by a second battery powered amplifier of 50 dB.

The signals were recorded by an analyser: a 20 bits AD-converter (input impedance 30 kΩ, flat frequency response in bandwidth 30 Hz-20 kHz), added to a PC with a 24 bits PCI digital audio card. The sample frequency f_s was $44.1 \cdot 10^3$ Hz.

The noise levels of these autospectra were compared to the Nyquist noise level of resistances of 1.10 kΩ. Analyzing the spectra, it is seen that for frequencies above approximately 600 Hz, the noise spectrum is flat, and the value of -163 dBV/√Hz is only slightly higher than the calculated value according to equation(3.12) with R=1.10 kΩ, -165dBV/√Hz (using the definition dBV= $10 \cdot {}^{10}\log V^2$). See Figure 3-2. The used amplification factor in the experiment was measured to be 100 dB. The amplified (analogue) output signals were thus recorded while the 50 Hz frequency component and its higher harmonics were filtered out.

The two signals were recorded and stored during a total measuring time of 20 minutes.

In the measured autospectra, shown for example in Figure 3-2, it is observed that low frequency noise above the Johnson noise level is present. To investigate the mutual correlation of especially these low frequency noisy influences, we performed a series of different processes to the recorded signals. The recorded signals were subsequently not filtered (a), high-pass filtered above 45 Hz (b), high-pass filtered above 80 Hz (c), and high-pass filtered above 600 Hz (d). For comparison, the method described above to record simultaneously two different sensor signals, was also performed with two normal carbon resistors of 1.10 kΩ in the isolated boxes (e).

A mathematical software program, MATLAB, was used to calculate the cross-

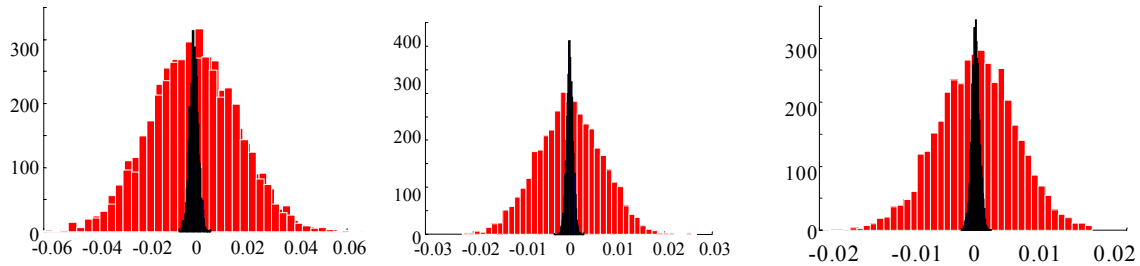

a. b. c.

Figure 3-3a-c: Distributions of the calculated ratios (power in cross-spectrum/power in autospectrum), calculated for N=44.1•103 (measurement time of 1 s); the broad distribution curves, and for N=44.1•105 (measurement time of 100 s); the narrow peaked curves. For N=44.1•105, the variance is approximately 10 times smaller than for N = 44.1•103, in correspondence with the theoretical expectance. a: the cross-spectrum of two sensor signals, high-pass filtered from 45 Hz (i.e. frequencies < 45 Hz are filtered out); b: the two sensor signals, high-pass filtered from 600 Hz; c: the unfiltered cross-spectrum of the signals of two resistors of 1.10 kΩ.

correlation function of these pairs of data files. One time series of 20 minutes consisted of $N = 20*60*44100 \approx 5.29 \cdot 10^7$ data points.

The time signal of 20 minutes was subsequently divided into parts of 240 seconds, parts of 60 seconds and parts of 10 seconds, corresponding to respectively $N = 1.06 \cdot 10^7$; $N = 2.65 \cdot 10^6$ and $N = 4.41 \cdot 10^5$ points. For each N, we calculated the power in the cross-correlation spectrum in the total bandwidth and divided it by the power in the autospectrum. Since we could thus calculate several values for the same N, the variance of this ratio could be calculated. This variance gives a more representative and reliable measure of the ratio for given N than only one result at that N, because we have to do with a stochastically varying variable. It seems justified to assume here that the variable, the power in the cross-correlation spectrum, has a normal distribution. The calculation of the variance for $N = 4.41 \cdot 10^3$ and $N = 4.41 \cdot 10^5$ different values of the variable distributed around its mean value, led to the distributions of the variable as seen in Figure 3-3. Although the curves are not perfectly smooth due to the finite size of the number N, they tend to a Gaussian (normal) distribution. The estimate of the variance σ^2 of the ratio (power in cross-spectrum/power in autospectrum, denoted as x) was determined from

$$\sigma^2 = \frac{\sum_{i=1}^{N}\left(x_i - \frac{1}{N}\sum x_i\right)^2}{N-1} \tag{3.23}$$

The mean value of x, or $E(x)$, in the above expression, should ideally be zero. We might

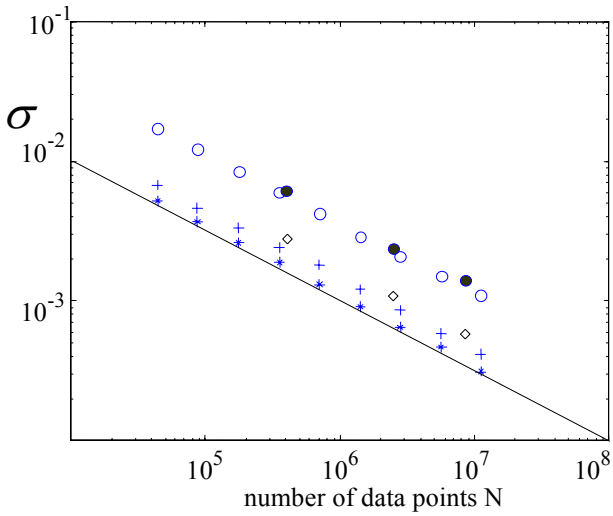

Figure 3-4: Influence of the number of data points N on the variance of the calculated ratio (power in the cross-correlation spectrum in the whole frequency range / the power in the autospectrum). The variance σ^2, equation (3.23), of this value is proportional to N-1; the plotted curve shows $\sigma=1/\sqrt{N}$, (the axes are logarithmically plotted). The variances for different values of N were calculated for the situations a: (•), the unfiltered cross-spectrum of the two sensor signals b: (○) the two sensor signals, high-pass filtered from 45 Hz (i.e. frequencies < 45 Hz are filtered out); c: (◊) the two signals, high-pass filtered from 80 Hz; d: (+) the two sensor signals, high-pass filtered from 600 Hz; e: (*)the unfiltered cross-spectrum of the signals of two resistors of 1.10 kΩ.

expect that due to some possble correlation in the low-frequency region in the unfiltered signals, this $E(x)$ differs slightly from zero. Therefore, in the above expression the value $\frac{1}{N}\sum x_i$ was evaluated for all situations *a*-*e*, and subsequently used in the calculation of the variances (equation(3.23)). The variances as a function of N are plotted in Figure 3-4.

Comparing the experimentally found values in Figure 3-4 to the theoretical variance $\sigma^2 = 1/N$, they behave as expected. For the signals of the resistors (e), the best correspondence to the theoretical dependence of σ^2 on N is seen. Besides it is seen in the figure that the other measured curves, in particular a, b, and c, lie above the theoretical line, although they have the same slope.

The reason for this is that the decrease in the noise of the cross-correlation spectrum, the variance, with N, is most effective for flat, broadband, frequency spectra. In cross-correlation spectra in which a $1/f$-shaped component is present, there is a correlation between subsequent sample points x_i and x_j, while in a flat spectrum there is no correlation between points x_i and x_j ($i \neq j$) in de series of N points. The variance, which is calculated from a summation over all combinations of x_i and x_j, is therefore higher for $1/f$-spectra than for flat curves.

Although the variances of the obtained cross-spectra are somewhat higher than the theoretical value (due to this $1/f$ –component), the deviation of the cross-spectra of the unfiltered output signals (a) with respect to the theoretical $1/N$ is only very limited: a reduction of the noise power in the cross-spectrum with respect to the power in the autospectrum of approximately $1.1 \cdot 10^{-3} \approx$ -30dB is attained, while the theoretically maximum reduction for a measurement time of 240 s equals $1/\sqrt{N} \approx$ -35dB (power reduction).

So, from the figures 3-2, 3-4 and 3-3 it can be concluded that the use of calculating the cross-correlation spectrum can reduce the noise level of the sensors considerably; if for example $N = 1.06\ 10^7$ data points are used, a reduction in noise power of 30 dBV/√Hz compared to the autospectra can be attained. The noise level becomes therefore considerably lower than the Johnson noise for the resistances, $\sqrt{4kTR}$, approx. -165 dBV/√Hz for the present wires (without amplification). This implies that the noise level related to the resistance of the two heated wires is no longer a fundamental limit: although the sensor consists of two resistors R (the wires), its noise can be reduced to below $\sqrt{4kTR}$.

The sensitivity of the used particle velocity sensor was determined in a “standing wave tube” (Bree de et al., 1996b;Eerden et al., 1998;Microflown Technologies, 2004) with a reference microphone in it. The thus obtained sensitivity curve in the frequency range 10 Hz – 4.0 kHz was used to determine the sensitivity S of the sensor as 0.3 mV/Pa at $f = 1$ kHz.

When the sensor is subject to a signal, in principle modulation noise, or signal related noise, may occur. If one would now assume in a first estimation that this signal related noise is negligible and the sensor measures a linear superposition of the acoustic signal and other noise sources, an approximation of the noise floor, (or “self-noise”) in can be

made. Under certain conditions, for example in the "free field" situation, when the specific acoustic impedance $Z \equiv P/U$ (with P and U resp. the complex amplitudes of sound pressure and a vec tor component of particle velocity) is real and equal to $\rho_0 c$, this noise floor can be expressed as an equivalent pressure level in Pa/√Hz. The noise spectrum (in V/√Hz) divided by the sensitivity then gives the equivalent noise "pressure" level in Pa/√Hz. (The noise floor can thus equivalently be defined as the inverse of the signal-to-noise ratio). For a noise power in the cross-correlation spectrum of two identical sensors of $5.0\ 10^{-20}$ V^2/Hz, an integration time of 240 s then yields a noise floor of $7.5\ 10^{-7}$ Pa/√Hz. This noise power is equivalent to -193 dBV/√Hz, a reduction of 30 dBV/√Hz with respect to the resistance noise level of -163 dBV/√Hz.

It should be stated, that in the application of cross-correlation spectra, time averages are involved. Therefore, this method of noise reduction is useful for measurement of stationary signals; stationary sound intensity or particle velocity measurements. However, for instantaneous measurements or applications as sound recording, this method cannot be applied.

3.2.3 Conclusions (self-noise reduction using cross-correlation)

In this section it was shown that a large reduction of the noise of a particle velocity sensor in its application as a sensor for stationary sound measurements could be attained. This is achieved by the simultaneous use of two of these sensors closely spaced to each other and recording the cross-spectrum of the output signals of both. Since in this cross-correlation spectrum the relevant signals add but all the uncorrelated noise sources are eliminated, a significant reduction of the noise can be reached; for an integration time of 240 s this reduction equals 30 dB. The noise level then becomes even lower than the principal resistance noise level of the wire resistors of the sensor. The larger the number of data points used (the larger the measuring time), the larger this reduction becomes. The decrease in noise level as a function of integration time corresponds to theoretically expected values.

End of copy (Honschoten et al., 2004).

3.3 An improvement of the signal to noise ratio

Although we have shown that the cross-correlation method offers the possibility to decrease the noise level, one should actually demonstrate additionally that a measured acoustic signal *S*, does not alter due to this procedure. Only then, a real improvement of the signal to noise ratio is attained.

Therefore we placed two identical microflowns, independently battery powered, very close to each other in a large, acoustically isolated (anechoic) box of about 10 m^3. In the box an active loudspeaker was situated and fed with a harmonic signal of exactly 1000 Hz. The two sensor signals were both independently

amplified (56 dB) and led through short cables to the AD converter (20 bits, sampling frequency 44.1 kHz). The signals were simultaneously recorded during 2 minutes and post processed in the PC. Figure 3-5 and Figure 3-6 shows the result of the measurement of the two autocorrelation spectra of the sensors (denoted as $G_{11}(f)$ and $G_{22}(f)$) and their cross-correlation spectrum ($G_{12}(f)$), for a recording time of 2 minutes. The peak in the spectra at 1000 Hz is well visible; the two autospectra lie approximately on each other due to the fact that the sensors have an equal sensitivity. Figure 3-6 focuses on the region around 1000 Hz to show an equally high signal peak in the cross-correlation spectrum; the difference between the auto- and cross-spectrum at 1 kHz is as small as 0.004 dB. The power reduction in the cross-spectrum, optically about 20 dB, is not as much as could be expected from a measurement time of 2 minutes (N = 2·60·44.1 10^3, so $1/\sqrt{N}$ = $4.35 \cdot 10^{-4}$; or –33 dB). This is caused by the fact that in Figure 3-6 only absolute values are plotted. If the autospectra and cross-spectra are compared over a wide frequency band, the ratio between the measured auto- and cross-spectra decreases accordingly and equals -22.8 dB over a frequency band between 600 Hz and 20 kHz (except for 999 Hz to 1001 Hz). For the frequency band of 950 Hz to 22 kHz the decrease is even more; -32.9 dB, and -33.6dB if only real part of $G_{12}(f)$ is used in the summation, which almost equals the theoretical expected value.

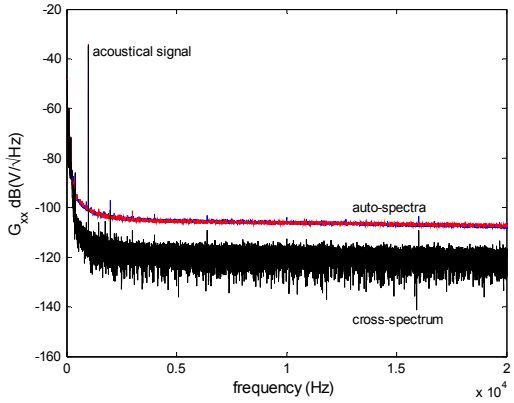

Figure 3-5: Measurement of the autospectra of the two sensors ($G_{11}(f)$ and $G_{22}(f)$) and the absolute values of their cross-correlation spectrum ($G_{12}(f)$) when an acoustic signal of 1000 Hz is applied. The curves of G_{11} and G_{22} lie approximately on each other; the lower curve shows G_{12}.

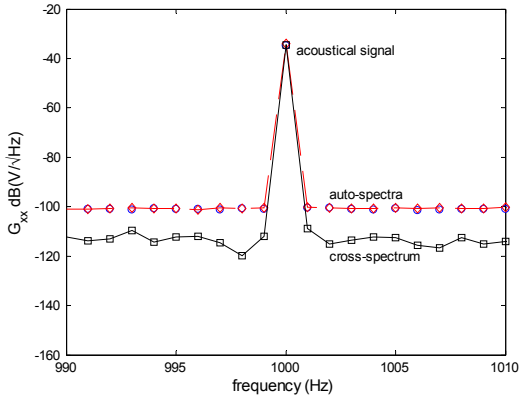

Figure 3-6: Amplification of the left figure around 1kHz. It is seen that the sharp signal peak is for all spectra equally high, the cross-spectrum lies 16.6 dB below the autospectra in the given bandwidth.

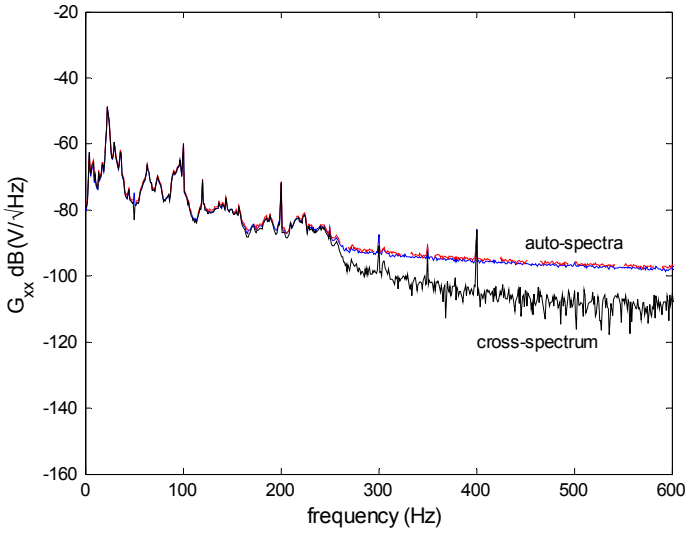

Figure 3-7: Below 250Hz, both signals are correlated very likely due to acoustical noise. Between 250 and 450Hz still electronic noise is visible in the signals in both the auto- and the cross-spectra.

In Figure 3-7 the auto- and the cross-spectra are shown for low frequencies. It can be seen that for low frequencies, below approximately 250 Hz in this experiment, there is no advantage of the cross-correlation. Below 250 Hz, the autospectra equals the cross-spectra which means that both signals are likely to measure the same physical quantity. Also electronic noise, such as harmonics of 50 Hz mains occurs in both the auto- and the cross-spectra between 250 Hz and 450 Hz in this experiment as can be seen Figure 3-7.

A real improvement of the signal to noise ratio is thus achieved. When the sensor is subject to a signal, in principle modulation noise, or signal related noise, may occur. Since we have not observed any difference in noise level with and without an applied acoustic signal, we may conclude that for the investigated sound levels this signal related noise is negligible. The sensor measures a linear superposition of the acoustic signal and other noise sources. This noise floor can be expressed as an equivalent particle velocity level in (m s^{-1})/√Hz. The noise spectrum (in V/√Hz) divided by the sensitivity then gives the self-noise, which is the equivalent noise "particle velocity" level in (m s^{-1})/√Hz. For a more thorough description of self-noise see Chapter 2.

It has to be emphasised that in the application of cross-correlation spectra, time averages are involved. Therefore, this method of noise reduction is useful for measurement of stationary signals; stationary sound intensity or particle velocity

measurements. However, for instantaneous measurements or applications as sound recording, this method cannot be applied.

Note that the same principle is used in case of sound intensity measurements. Sound intensity measurements are always obtained using two different sensors, either two pressure sensors, or a particle velocity combined with a pressure sensor. Practical measurements show that as well as for the p-u and for the p-p measurement technique, the noise in the active sound intensity is lower then the noise in the individual (highest) sensor signal. For details, see Chapter 4 and (Raangs et al., 2003).

3.4 Free-field measurements in a reverberant room

Reverberation is a phenomenon, which plays a major role in every aspect of room acoustics and has therefore been studied widely. Next to reverberation, another significant subject is the diffuse sound field. Both reverberation and diffusion are closely related to each other: the laws of reverberation can be formulated in a general way. Only for sound fields in which sound propagate in all directions and in which every direction contribute equally to the sound field, not only in steady state conditions, but also at each moment in decaying sound fields, at least in the average over time intervals which are short compared with the duration of the whole decaying process. It is clear that in practical situations these stringent conditions are met only approximately. A completely diffuse sound field can be

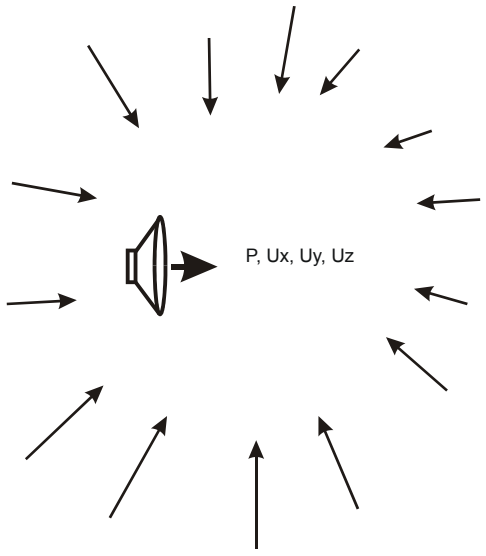

Figure 3-8: Schematic representation of a loudspeaker in a reverberant room.

realised fairly well in certain types of measuring rooms, such as reverberation chambers. A diffuse sound field can also be realised electronically using many loudspeakers positioned in a room (Weikert, 2002). But in other rooms too, the approximation of the actual sound fields by diffuse ones is not to crude an approach (Kuttruff, 1979). In this section, the reverberant sound field will be treated as purely diffuse and no difference is meant between the terms reverberant and diffuse in the rest of this section.

Considering a single sound source in such a reverberant room as shown in Figure 3-8, the sound field realised will differ from a sound field that would be realised using the same sound source positioned in an anechoic room. In the anechoic room, the sound field is only build up by the sound source whereas the reflections at the walls do not contribute to the sound field. In this thesis this sound field directly originated from the sound source is referred to as the "direct" sound field, and the measured pressure, particle velocity therefore equal the direct pressure p_{dir} and direct particle velocity u_{dir}.

In a reverberant room, many reflections do occur and the sound field will differ from the "direct" sound field due to these reflections. Taken the fact that the sound source is not affected by the reflected sound, and since the direct and the diffuse pressures/particle velocities have random phase and amplitude, the sound field can be split up into the "direct" sound field, originating from the sound source itself, and the "reverberant" sound field, originating from all reflected sound waves. The pressure and particle velocity in the diffuse sound field can therefore be written as:

$$\overline{p^2} = \overline{p_{\mathrm{dir}}{}^2} + \overline{p_{\mathrm{rev}}{}^2} \tag{3.24}$$

$$\overline{u^2} = \overline{u_{\mathrm{dir}}{}^2} + \overline{u_{\mathrm{rev}}{}^2} \tag{3.25}$$

The direct sound field will decrease with the distance from the sound source, whereas the diffuse sound field does theoretically not depend on the position in the room (Kuttruff, 1979). In normal rooms or halls the pressure and particle velocity will depend on frequency and position due to mutual cancellation of the various acoustical modes in the room, or do superpose at in-phase conditions (Kuttruff, 1979). By applying uncorrelated noise and averaging over frequency or room position this effect can be overcome in normal rooms.

In a reverberant field there is a certain distance, from a sound source, called the "reverberation distance" or "reverberation radius" r_h. For the distance r_h the direct and reverberant levels are equal. Figure 3-9 shows that for distances $r \gg r_h$ the pressure is mainly caused by the diffuse reverberant sound field, whereas near the source $r \ll r_h$ the direct pressure is higher than the reverberant pressure. The ratio between direct and reverberant sound will depend on the distance from the source and the characteristics, such as the reverberation radius, r_h. In this section it will be shown that using two orthogonally placed microflowns, the ratio between direct and reverberant sound can be retrieved using the diffuse field approximation.

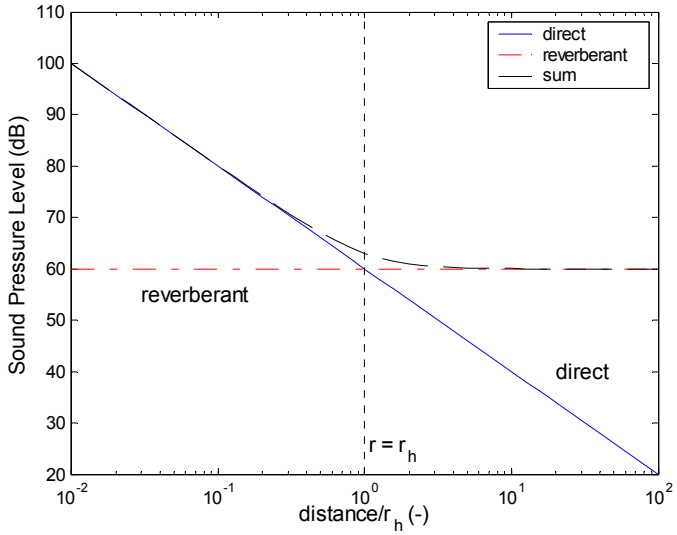

Figure 3-9: The sound pressure as function of the distance from a sound source in a diffuse room. (solid line represents the direct sound, the line -- - --- represents the diffuse sound pressure, the - - line represents the total pressure).

3.4.1 Description of cross-correlation of orthogonal microflown signals

In this section, experimental results are described where in the cross-correlation of two microflowns the contribution of the reverberant field vanishes, which makes it possible to retrieve the free-field properties, although the measurements were done in a reverberant room. As illustration first an experiment is described with two (uncorrelated) sound sources and two orthogonally microflowns. It will be shown that also for this case the contribution of the two sound sources to the cross-correlation of the two microflowns can vanish. The experimental set-up is shown in Figure 3-10.

For the configuration in Figure 3-10 the signal from microflown 1 is proportional to: $x(t)/\sqrt{2} - y(t)/\sqrt{2}$ and for microflown 2: $x(t)/\sqrt{2} + y(t)/\sqrt{2}$. In case the acoustical sensitivities of the loudspeakers and the microflown sensors are not taken into account, the time-averaged cross-correlation is thus

$$R_{12}(0) = \lim_{T\to\infty}\frac{1}{T}\int_0^T\left(\frac{x(t)}{\sqrt{2}}-\frac{y(t)}{\sqrt{2}}\right)\left(\frac{x(t)}{\sqrt{2}}+\frac{y(t)}{\sqrt{2}}\right)dt = \frac{1}{2}\left(x_{\text{rms}}^2 - y_{\text{rms}}^2\right) \qquad (3.26)$$

For $x_{\text{rms}}^2 = y_{\text{rms}}^2$, thus equal power to the two loudspeakers, the cross-correlation vanishes.

In general, the sound sources do not have to be positioned at plus and minus 45 degrees exactly. In the general case, where α is the angle between source 1 and microflown 1 as shown in Figure 3-10, equation (3.26) turns into:

$$\begin{aligned} R_{12}(0) &= \lim_{T\to\infty}\frac{1}{T}\int_0^T\begin{pmatrix}\left(\cos\alpha\, x(t) - \sin(\alpha)\, y(t)\right)\\ \left(\sin(\alpha)\, x(t) + \cos(\alpha)\, y(t)\right)\end{pmatrix}dt \\ &= \begin{pmatrix}\cos\alpha\,\sin\alpha\left(\lim_{T\to\infty}\frac{1}{T}\int_0^T\left(x^2(t)\right)dt - \lim_{T\to\infty}\frac{1}{T}\int_0^T\left(y^2(t)\right)dt\right)\\ +\left(\cos^2\alpha - \sin^2\alpha\right)\lim_{T\to\infty}\frac{1}{T}\int_0^T\left(x(t)\,y(t)\right)dt\end{pmatrix} \end{aligned} \qquad (3.27)$$

where the first cross-term can be written in terms of angle α and the rms-values of

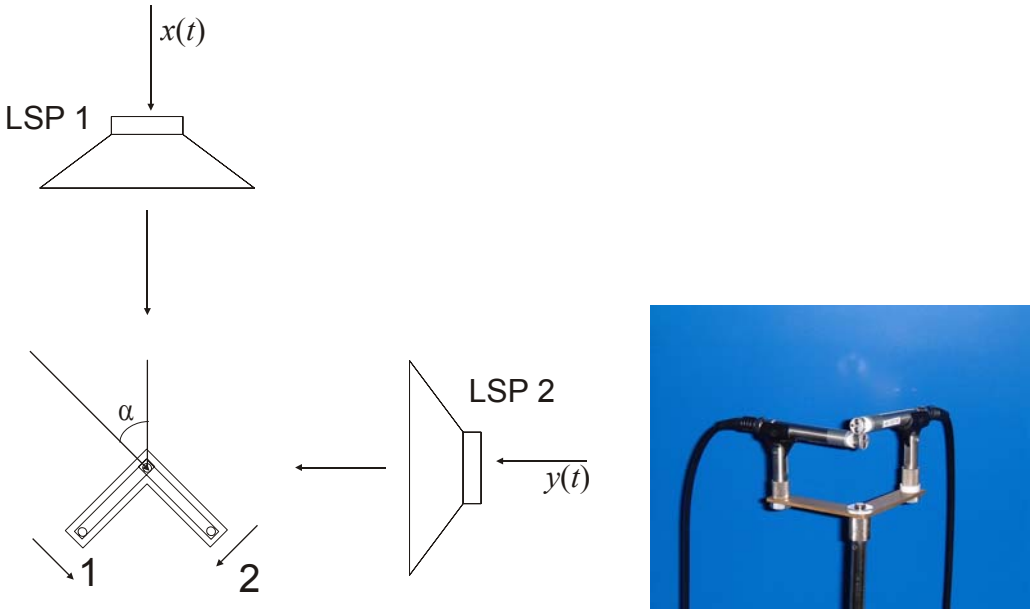

Figure 3-10: Experimental setup. Two orthogonally microflowns positioned in a sound field build up by two loudspeakers positioned orthogonally, which radiate uncorrelated white noise. Right: photograph of the two 0.5 inch microflowns used.

x_{rms}^2 and y_{rms}^2 since $x(t)$ and $y(t)$ are uncorrelated. The second term goes to zero since for the limit of $T \to \infty$, the mean of the product of the uncorrelated signals goes to zero, and equation (3.27) is simplified into:

$$R_{12}(0) = \cos\alpha \sin\alpha \left(x_{\text{rms}}^2 - y_{\text{rms}}^2 \right) \tag{3.28}$$

Figure 3-11 clearly shows that in case the electrical powers of the uncorrelated signals fed to the two loudspeakers are equal, the cross-correlation (the real part) approximates zero. It has been shown that the results were independent on the orientation (rotation) of the microflown pair with reference to the loudspeakers. Further, notice that Figure 3-11 shows the same behaviour as the sound intensity in between of two loudspeakers radiating uncorrelated white noise (see Chapter 4).

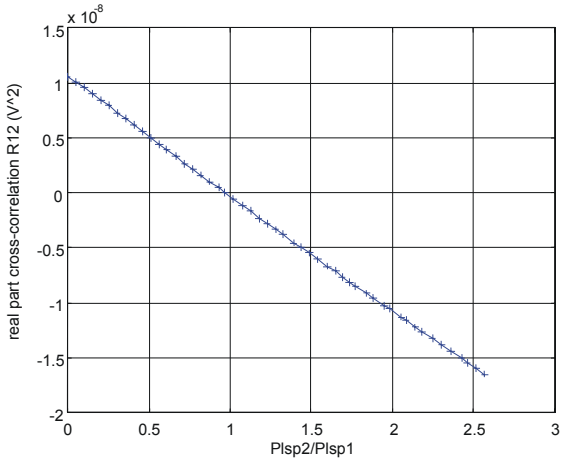

Figure 3-11: Cross-correlation (⅓-octave at 1 kHz) versus the ratio of the powers between loudspeaker 2 and 1 (see Figure 3-10).

In case of $\alpha = \pi/4$, thus for $\cos(\pi/4)\sin(\pi/4) = 0.5$, equation (3.28) turns into equation (3.26). Equation (3.28) furthermore shows that the experiment as described in Figure 3-10, the cross-correlation versus the power ratio, is not sensitive for the angle α, since $\cos\alpha \sin\alpha$ in equation (3.27) can be considered as a constant for a given configuration. If constant $C = \cos\alpha \sin\alpha \left(x_{\text{rms}}^2 \right)$, equation (3.27) can be written as:

$$R_{12}(0) = C\left(1 - \frac{y_{\text{rms}}^2}{x_{\text{rms}}^2} \right) \tag{3.29}$$

where $-C$ is thus the slope as shown in Figure 3-11.

Further, note that the second cross-term $x(t)\,y(t)$ does not vanish because of the signs as equation (3.26) suggests. In the general case, for an arbitrary angle α,

the cross-term vanishes only in case the two signals $x(t)$ and $y(t)$ are uncorrelated as can be seen in equation (3.27).

Notice that this is very different compared with sound pressure. In case of sound pressure, all pressures, from all directions, will add so that no free field measurements can be made using pressure microphones measuring at a single position.

Consider now the case of a pure diffuse reverberant sound field. Next to the fact that the diffuse sound field contains the same power coming from all directions, another important aspect of the diffuse sound field is the fact that the sound waves coming from all different directions are uncorrelated.

Since the particle velocity is a vector quantity, unlike pressure, a measurement of the particle velocity in a certain direction will depend on the direction with reference to the direct sound field. In case the reverberant sound field can be treated as purely diffuse, the magnitude of the particle velocity vector caused by the diffuse part will not depend on the direction (Kuttruff, 1979;Raangs et al., 2001b).

Consider for example the hypothetical situation with many mirror sources equally distributed over a sphere. The arbitrary mirror source, $M(\theta,\varphi)$, on the sphere has a strength u_m^2 per solid angle. The total signal of the hypothetical omnidirectional sensor is proportional to (see Appendix B):

$$u_{\text{rev}}^2 = \int_0^{\pi} \sin(\varphi)\, d\varphi \int_0^{2\pi} u_m^2\, d\theta = 4\pi u_m^2 \tag{3.30}$$

If a true particle velocity, with a figure of eight directivity curve, such as the microflown is positioned in the same diffuse sound field, only part of the reverberant particle velocity will be measured.

Consider two microflowns measuring in arbitrary directions μ_1 and μ_2. The measured cross-correlation measured is then

$$R_{12} = \int_0^{\pi} \sin(\varphi) d\varphi \int_0^{2\pi} (\mu_1 \cdot u_m)(\mu_2 \cdot u_m)\, d\theta = \frac{1}{3} u_{\text{rev}}^2 (\mu_1 \cdot \mu_2) \tag{3.31}$$

In Appendix B, equation (3.31) is described in more detail. In case the two microflowns measure in the same direction, equation (3.31) turns into equation

(3.32). For the special situation of two perpendicular microflowns, the cross-correlation term due to the reverberant sound field equals zero since $(\mu_1 \cdot \mu_2)$ in equation (3.31) then equals zero.

In case the particle velocity in one direction *i* is measured, only ⅓ of the power will be measured:

$$u_{i,\mathrm{rev}}^2 = \frac{1}{3}\left|u_{\mathrm{rev}}\right|^2 \tag{3.32}$$

where the reverberant particle velocity is defined as

$$u_{\mathrm{rev}}^2 = \frac{p_{\mathrm{rev}}^2}{\left(\rho_0 c\right)^2} \tag{3.33}$$

since the diffuse sound field consists of infinitely many uncorrelated plane progressive waves, with their intensity uniformly distributed with respect to direction (Morfey, 2001). The reverberant particle velocity u_{rev} can be measured using an (hypothetical) omnidirectional particle velocity sensor.

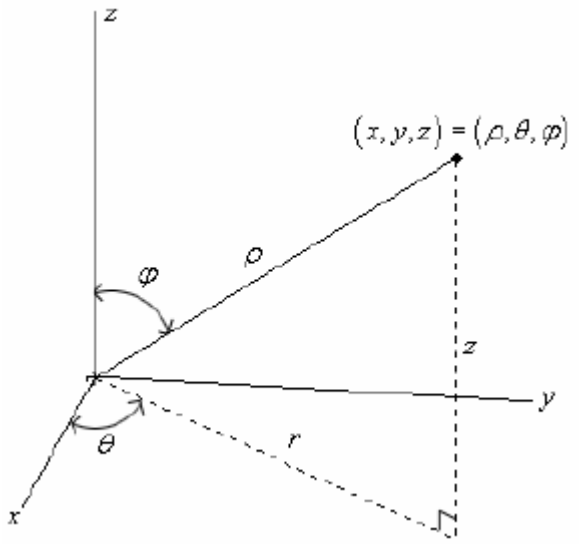

Figure 3-12: Spherical coordinate system.

For the special case that one sensor is an omnidirectional pressure sensor, and the other sensor a microflown, the contribution of the reverberant field to the cross-correlation equals

$$
\begin{aligned}
R_{12} &= \int_0^{\pi} \sin(\varphi) d\varphi \int_0^{2\pi} (p_m)(\mu_1 \cdot u_m) d\theta \\
&= p_m u_m \int_0^{\pi} \sin(\varphi) d\varphi \int_0^{2\pi} \left[\mu_{1x} \sin\varphi\cos\theta + \mu_{1y} \sin\varphi\sin\theta + \mu_{1z} \cos\varphi \right] d\theta \\
&= 2\pi p_m u_m \mu_{1z} \int_0^{\pi} \sin\varphi\cos\varphi d\varphi = 0
\end{aligned}
\tag{3.34}
$$

Since the active sound intensity is equal to the cross-correlation ($\tau = 0$), equation (3.34) shows that the active sound intensity in a purely diffuse sound field equals zero, see also Chapter 4 and (Fahy, 1995). Thus, free-field measurement in a reverberant room can be done via the measurements of the sound intensity.

3.4.2 Sound intensity using cross-correlated orthogonally placed microflowns

The next section describes the three methods denoted as u-u principle 1, 2, and 3. The first method, denoted as u-u principle 1, uses only the autospectra of two perpendicular placed particle velocity sensors. This method can also be used with only one particle velocity sensor measuring in two distinct directions. The second method, u-u principle 2, uses also the cross-correlation in case the angle between the two particle velocity sensors is 90 degrees. The last method, denoted as u-u principle 3, is a generalisation of u-u principle 2, and can be used in case the angles is known and unequal to 90 degrees.

3.4.2.1 Two particle velocity sensors in a reverberant room: autospectra (u-u principle 1)

In a reverberant sound field, containing a single sound source, we can, by measuring the particle velocity in two perpendicular directions, in the direction of the direct sound wave and that in the perpendicular direction, calculate the ratio of direct and reverberant sound. The method presented in this section, named here u-u principle 1, is the most straightforward method since (i) only two directions are used, with, and without a direct contribution of the sound source. Secondly (ii), this method does not use the cross-correlation between the two measurements. Therefore, this method can also be applied if only one microflown is available, or in order to calibrate the microflown (Raangs et al., 2003). See also section 2.5 in this thesis.

Using the fact that due to the directional dependence of the sensitivity of the microflown (the sensor sensitivity in the direction along angle θ is proportional to $\cos\theta$, as can be seen in Chapter 1), only one third of the power of the diffuse field is measured by the sensor, it is seen that

$$\begin{aligned} u_{\parallel}^2 &= u_{\mathrm{dir}}^2 + \frac{1}{3}u_{\mathrm{rev}}^2 \\ u_{\perp}^2 &= \frac{1}{3}u_{\mathrm{rev}}^2 \end{aligned} \tag{3.35}$$

with $u_{\parallel}^2$ and $u_{\perp}^2$ representing the autospectra of the particle velocities measured in the direction of the direct sound wave and in the perpendicular direction, and u_{dir}^2, u_{rev}^2 the autospectra due to the direct sound wave and the diffuse field respectively.

For the ratio of the direct field (the "free-field" sound) and the reverberant sound field thus follows

$$\frac{u_{\mathrm{dir}}}{u_{\mathrm{rev}}} = \sqrt{\frac{u_{\parallel}^2 - u_{\perp}^2}{3u_{\perp}^2}} \tag{3.36}$$

and the direct sound field is calculated as

$$u_{\mathrm{dir}} = \sqrt{u_{\parallel}^2 - u_{\perp}^2} \tag{3.37}$$

Additionally to this u-u measurement, the pressure may be measured using a pressure transducer. (Strictly spoken, the method is not purely an "u-u" measurement anymore when a microphone is added.) Generally the microphone is omnidirectional so that the different pressures related to the direct and the reverberant field are measured equally sensitive (that is, independent of the angle of incidence), and thus $p^2 = p_{\mathrm{dir}}^2 + p_{\mathrm{rev}}^2$.

In the far field, if $u_{\mathrm{dir}} = p_{\mathrm{dir}} / (\rho_0 c)$, we can thus derive the ratio between direct and reverberant pressure

$$\left(\frac{p_{\mathrm{dir}}}{p_{\mathrm{rev}}}\right)^2 = \left(\frac{u_{\mathrm{dir}}}{u_{\mathrm{rev}}}\right)^2 \tag{3.38}$$

The root mean square value of the pressure of the direct sound field p_{dir} can be expressed in the measured total pressure p:

$$p_{\mathrm{dir}} = \sqrt{\frac{p^2}{1+\left(\frac{u_{\mathrm{rev}}}{u_{\mathrm{dir}}}\right)^2}} \tag{3.39}$$

If the "free-field" condition for plane waves is satisfied, so that the specific acoustic impedance is equal to $\rho_0 c$, the (time averaged) sound intensity in a reverberant environment can then be calculated from both the free-field particle velocity u_{dir} ("I_u") and the free-field pressure p_{dir} ("I_p").

This measurement principle, "u-u principle 1", can also be used to calibrate a particle velocity sensor against a reference microphone in a reverberant sound field as is shown in chapter 3. Experimental results are described in (Raangs et al., 2001a).

3.4.2.2 Two perpendicular particle velocity sensors in a reverberant room: u-u principle 2.

A second, somewhat more extensive, method using two perpendicular particle velocity sensors in a reverberant sound field makes it also possible to calculate the angle of incidence in the plane of the sensors of the sound intensity. This measurement, "u-u principle 2" (Raangs et al., 2002), makes use of both the autocorrelation and the cross-correlation spectra of the two particle velocity

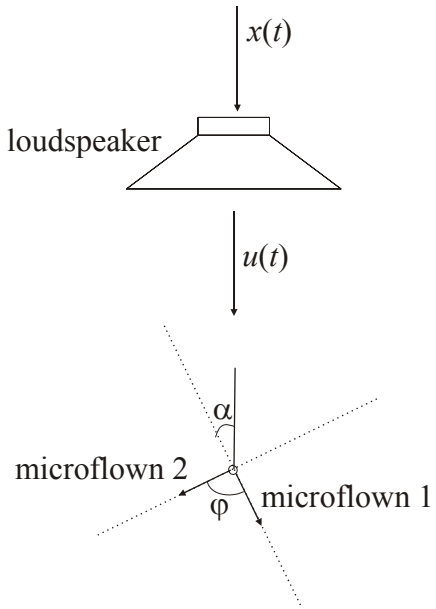

Figure 3-13: The measurement set up, consisting of the two mutually perpendicular particle velocity sensors and a loudspeaker. The orientations of the sensitivities are indicated by the arrows microflown 1 and 2; the angle of incidence α of the sound wave is defined here with respect to the sensitive direction of microflown 1.

sensors.

According to the equations (3.31) and (3.35) the autocorrelation spectra $G_{u_1u_1}$ and $G_{u_2u_2}$ and the cross-correlation spectrum $G_{u_1u_2}$ of the two perpendicular sensors can be constituted, with which the direction α (see Figure 3-13) of the free-field particle velocity (in the plane of the sensors) can be determined. One can write

$$\begin{aligned} G_{u_1u_1} &= u_{\mathrm{dir}}^2 \cos^2\alpha + \frac{1}{3}u_{\mathrm{rev}}^2 \\ G_{u_2u_2} &= u_{\mathrm{dir}}^2 \sin^2\alpha + \frac{1}{3}u_{\mathrm{rev}}^2 \\ G_{u_1u_2} &= u_{\mathrm{dir}}^2 \cos\alpha \sin\alpha \end{aligned} \tag{3.40}$$

which can be solved for u_{dir}:

$$u_{\mathrm{dir}}^2 = \pm\sqrt{\left(G_{u_1u_1} - G_{u_2u_2}\right)^2 + 4G_{u_1u_2}^2} \tag{3.41}$$

where the negative solution cannot exist physically since the power u_{dir}^2 cannot be negative. Solving equation(3.40) for the angle α yields:

$$\alpha = \frac{1}{2}\arctan\left(\frac{2G_{u_1u_2}}{G_{u_1u_1} - G_{u_2u_2}}\right) + n\cdot\frac{\pi}{4} \tag{3.42}$$

On physical arguments α has to be chosen such that $0 < \alpha < \pi/2$. Using the sign of the cross-correlation G_{u1u2} and equation (3.40) the correct solution for angle of incidence α can be determined using the fact that the power in the direct sound field cannot be negative.

Apart from the absolute value of the free-field particle velocity, the particle velocity of the reverberant sound can be determined from these equations, equations (3.40).

If, additionally, this particle velocity measurement is done in a plane perpendicular to the original plane of the sensors, the particle velocity as a full three-dimensional vector can be determined. From the thus found ratio between the values of the direct and the diffuse particle velocity vector, the direct pressure can be determined from the measured total pressure in the sound field (if a pressure transducer is placed in the sound field too) since the ratios of direct and diffuse pressure and of the direct and diffuse particle velocity are equal. For plane waves, when the free-field condition is satisfied, now follows from equation (3.41):

$$I_u = \rho_0 c u_{\text{dir}}^2 = \rho_0 c \sqrt{\left(G_{u_1u_1} - G_{u_2u_2}\right)^2 + 4G_{u_1u_2}^2} \tag{3.43}$$

Measurement principle 2 can be considered as a more general method than principle 1, since the angle of incidence α can also be determined. Determination of the sound field in the plane of the wires is possible if the phase relation between pressure and particle velocity, or the acoustic impedance, is known. However, for both u-u-measurements, principle 1 and principle 2, in general an additional pressure sensor is required to obtain the full sound intensity vector in the plane of the sensors.

3.4.2.3 Two particle velocity sensors in a reverberant room: u-u principle 3.

In section 3.4.2.2 we showed that if we use multiple microflown measuring in different directions, we are able to calculate the free-field particle velocity in a diffuse sound field. In this section this method is referred to as the u-u-method. The method "u-u principle 3" is also applicable in case the two microflowns are not positioned perpendicular, but requires knowledge of the angle between the two microflowns. In case that the microflown pairs are not positioned perpendicular with reference to each other we have to solve the set of equations:

$$\begin{aligned} G_{u_1u_1} &= u_{\text{dir}}^2 \cos^2\alpha + \tfrac{1}{3}u_{\text{rev}}^2 \\ G_{u_2u_2} &= u_{\text{dir}}^2 \cos^2\left(\alpha - \varphi\right) + \tfrac{1}{3}u_{\text{rev}}^2 \\ G_{u_1u_2} &= u_{\text{dir}}^2 \cos\alpha \cos\left(\alpha - \varphi\right) + \tfrac{1}{3}u_{\text{rev}}^2 \cos\varphi \end{aligned} \tag{3.44}$$

where φ is the angle between the microflowns. This set of equations can be solved for the free-field and diffuse particle velocity, and the angle of incidence.

The set of equations (3.44) can be solved by substitution of

$$G_1 = G_{u_1u_1} - G_{u_2u_2} \tag{3.45}$$

and

$$G_2 = \cos\left(\varphi\right) G_{u_1u_1} - G_{u_1u_2} \tag{3.46}$$

The solution for angle of incidence α is then given by

$$\tan\left(2\alpha\right) = \frac{-2\sin\left(\varphi\right)}{\left(\left(\frac{G_1}{G_2}\right) - 2\cos\left(\varphi\right)\right)} \tag{3.47}$$

For the angle of φ = 90 degrees between the two microflowns, as described in section 3.4.2.2, equation (3.46) and (3.47) become:

$$G_2 = -G_{u_1u_2} \tag{3.48}$$

and

$$\tan(2\alpha) = \frac{2G_{u_1u_2}}{G_{u_1u_1} - G_{u_2u_2}} \tag{3.49}$$

The latter equation is equivalent to (3.42) with n = 0.

3.4.2.4 Comparison between two perpendicular microflowns and active sound intensity

If we are able to measure the free-field particle velocity correctly, we can also calculate the active sound intensity as we can calculate this out of the anechoic pressure (taken that density and sound speed is known). With use of our calibrated three-dimensional p-u probe (see section 2.3.5 for calibration) we can measure both the sound intensity (see Chapter 4) using the p-u, and using the cross-correlation method out of only the microflown signals.

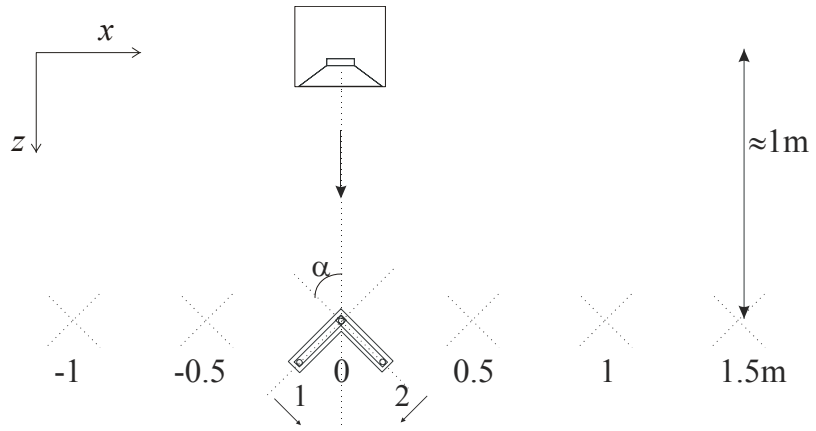

Figure 3-14: Experimental setup. All probe positions and the loudspeaker positions are at the same height in the room.

In the shown experiment, see Figure 3-14, we positioned a loudspeaker in the room. The loudspeaker consists of a 10 cm midrange loudspeaker fitted in a box with dimensions of 12x12x12 cm^3. The microflown signals are measured at various positions in the room along a line at 1 metre distance as shown in Figure 3-14. We positioned the loudspeaker at the same height as the two microflowns and white noise was sent to the loudspeaker in a ⅓-octave frequency band at

1 kHz. As sensor, a three-dimensional p-u probe was used (see Figure 2-20) of which the signals of two microflowns 2 and 3 are used.

The measured signals of the two microflowns are used in order to calculate the direct particle velocity component (see equation (3.44)). In order to check the measured direct particle velocity component a comparison is made with another technique to measure in a reverberant environment the direct sound field: the active sound intensity. In Chapter 4 sound intensity measurements are discussed. A result is that in the far field $I_{\text{active}} = p\,u = p_{\text{dir}}^2/(\rho_0 c) = (\rho_0 c)u_{\text{dir}}^2$, so a direct comparison of u_{dir} can be made using these two measuring techniques.

For comparison, we also defined a reverberant sound intensity I_{rev} as $(\rho_0 c)u_{\text{rev}}^2$ which is shown in Figure 3-15. Note that this I_{rev} is not the sound intensity of the reverberant sound field since the reverberant sound intensity equals zero in a diffuse sound field.

The coincidence between the two curves (I_{pu} and I_{duu2}) in Figure 3-15 shows that an independent measurement of measurement of the direct sound field with two perpendicular oriented microflowns and calculating from that the intensity agrees with a direct measurement of the intensity using the p-u probe. Notice that a pure diffuse reverberant sound field does not contribute to the cross-correlation of two microflowns (section 3.4.1) and not to the active intensity (section 4.6.1).

The agreement between the two sound intensity measurements is remarkable good as can be seen in Figure 3-15. We should notice that the angle between the microflowns in this measurement does influence the outcome so that the calibration is needed since the angles between two microflown in a standard three dimensional p-u probe can be (acoustically) up to 115 degrees. Note that the individual microflown sensors on a modern ultimate sound probes are aligned differently and due to its symmetry the new sensor should behave better. Figure 3-16 shows the result in case the theoretical angle of 90 degrees between the microflowns is used. The difference between Figure 3-15 and Figure 3-16 is only the computation. It is clearly shown that a small error induces a large error in the particle velocity and sound intensity results using the cross-correlation technique.

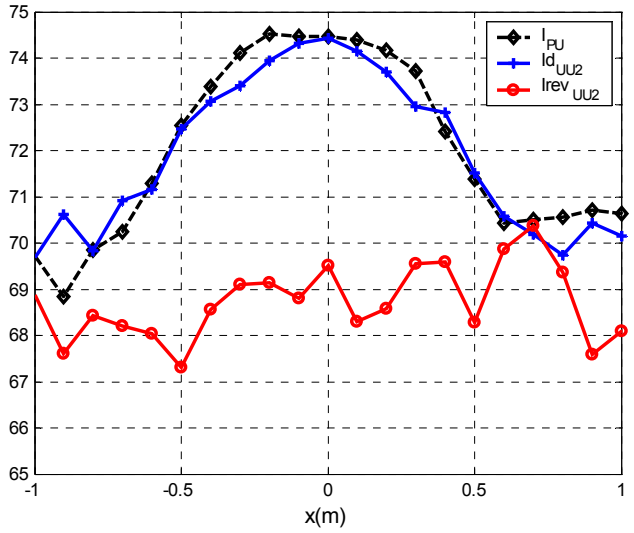

Figure 3-15: Sound intensity measurement in dB (1 kHz ⅓-octave band) using the UU method (using two microflown signals) (blue+) and the p-u method (green). The red o's show the reverberant particle velocity (ref. 2e-5 Pa*), see equation (3.44).

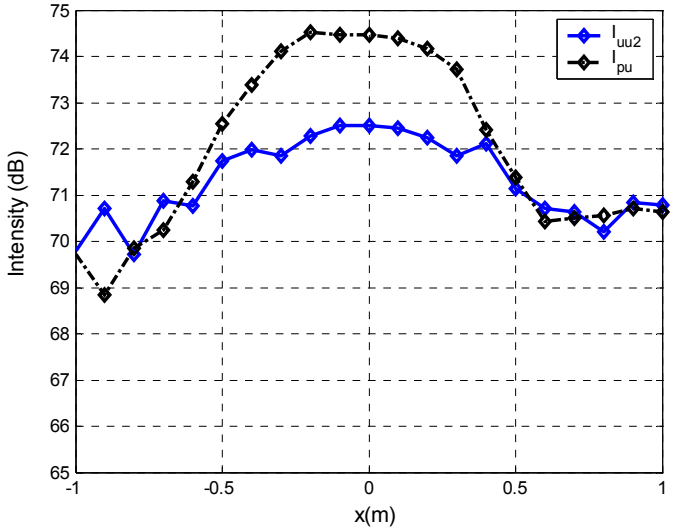

Figure 3-16: Sound intensity measurement (see Figure 3-15) but now computed for the theoretical angle of 90 degrees between the particle velocity sensors (see equation (3.41) in section 3.4.2.2).

It should be noticed however that much more computational power is needed in order to solve equations (3.44) in comparison with equations (3.40) because the cross-correlation due to the diffuse sound field does not approximate zero.

In Figure 3-15 it can be seen that the direct particle velocity (or sound intensity in the far field), is computed quite well. The difference between Figure 3-15 and Figure 3-16 clearly shows that the angle between the two microflowns should be either 90 degrees so that method 2 (equation (3.40)) can be used, or should be

known so that method 3 can be used (equation (3.44)). The error will be quite large if equation (3.40) while the angle between the microflowns is not equal to 90 degrees; in Figure 3-16 the angle was calibrated to be 106 degrees (see calibration in Chapter 2).

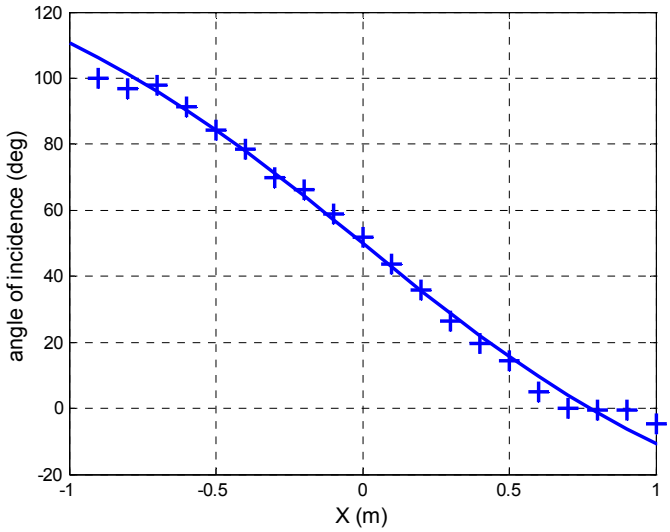

Figure 3-17: Calculated angle of incidence using the u-u method (+), the black line represents a sound source 80 cm away from the line of measurements (see also Figure 3-14 and Figure 3-15).

In Figure 3-17, the solved angle of incidence α is shown (see Figure 3-14 for the experimental setup). The angles shown belong to the solutions for the direct and reverberant sound field as shown in Figure 3-15. The line in Figure 3-17 represents the theoretical curve for the angle of incidence taken a sound source at a distance of 0.8 metres.

Out of the calculated lines (each angle of incidence represents a line on which the sound source is positioned) a sound source position can be reconstructed using a least squares error approach (see Figure 3-18). The reconstructed position is (x,z) = (-0.04, -0.81), while the source was positioned at (x,z) = (0.00, -0.92) in this experiment. Notice that the found position is very similar with the position calculated out of the angle using the arctan function as shown in Figure 3-17).

In Figure 3-19 the results using the three p-u pairs is shown. Using the three p-u pairs available in the three-dimensional probe, see Figure 2-20, the directions of the active sound intensity could be used. Figure 3-19 shows that a source is expected at the position (x,y,z) = (0.00,1.10,0.76) m.

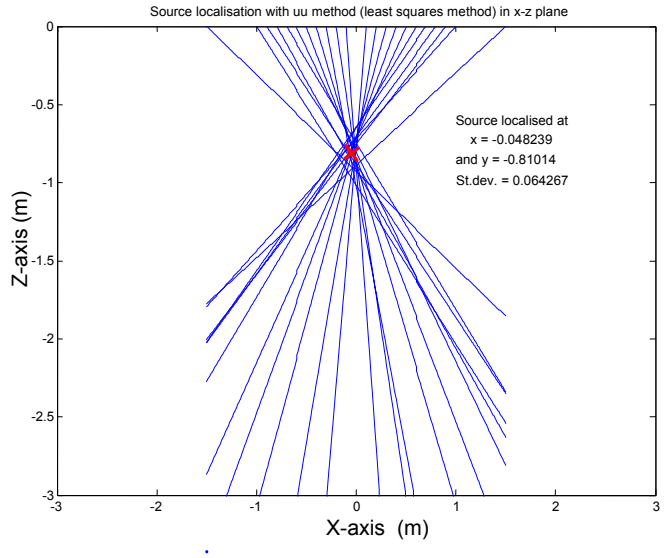

Figure 3-18: Source localization in a (reverberant) room using the UU-method using the two (almost) perpendicular microflowns probe.

The loudspeakers cone was measured to be at a distance of z = 0.92 m, both the u-u method as well as the three-dimensional p-u measurements result in an acoustical source somewhat closer, namely 0.81 m for the u-u method and 0.76 m for the p-u method. The reason for this difference is unknown and was not subject of further research since it was expected that the difference shown could be explained by the non-ideal diffuse field. For example, in acoustical terms, the difference of 10 cm per 1 metre is less than 1 dB, which is in the order of all errors in sensor calibration, computation, reflections, and so on.

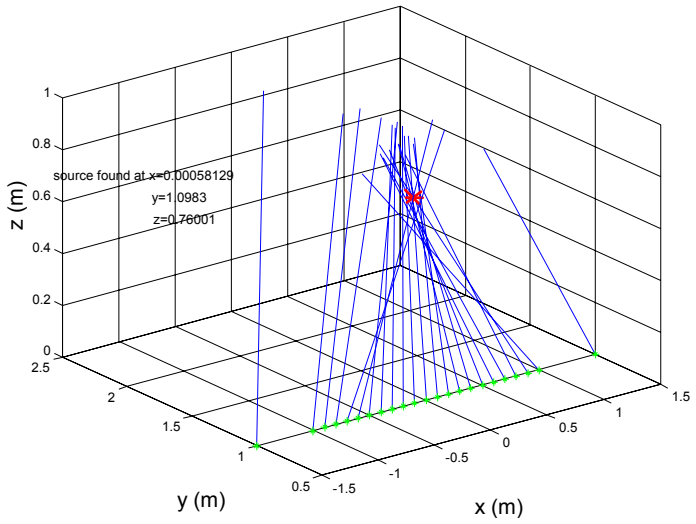

Figure 3-19: Source finding in a reverberant room out of sound intensity using the PU-method measured at several positions. The sound intensity was measured at the positions y = 1 m and z = 0 m (green dots).

The u-u method also calculates the reverberant, c.q. diffuse sound field, and an angle of incidence (± 180 degrees) and delivers therefore much more information about the sound field than a microphone or p-p type intensity measurement. The three-dimensional p-u probe does contain not only the sound intensity in three orthogonal directions (even if the microflown are not positioned orthogonal, see section 2.3.5, and Chapter 4), but also contains information of three perpendicular microflown pairs.

3.5 Discussion and Conclusions

In this chapter, the use of auto- and cross-correlation and spectrum has been demonstrated for acoustical measurements especially using a directive acoustical sensor such as the microflown.

The cross-spectrum is a very powerful tool especially in case where it can be used such as for the measurement of the power in the acoustical particle velocity (PVL). In such a situation the cross-spectrum equals a single auto-spectrum (in case both microflowns measure in the same direction) although signals which are different in the signals of both sensors do not appear in (the real part of) the cross-spectrum. In this chapter, it was therefore shown that a large reduction of the noise of the microflown, and of particle velocity sensors in general, in their applications as sensors for stationary sound measurements can be attained. We achieved this by the simultaneous use of two identical sensors closely spaced to each other and recording the cross-spectrum of the output signals of both. Since in this cross-correlation spectrum the relevant signals add but all the uncorrelated noise sources are eliminated, a significant reduction of the noise can be reached; for an integration time of 240 s this reduction equals 30 dB. The noise level then becomes even lower than the principal resistance noise level of the wire resistors of the sensor. The larger the number of data points used (the larger the measuring time), the larger this reduction becomes. The decrease in noise level as a function of integration time corresponds to theoretically expected values.

In case the sound field in the room is sufficiently diffuse, two orthogonally positioned microflowns can be used in order to retrieve the ratio between the direct (anechoic/free-field) part and the reverberant (diffuse approximation) part of the sound field. In chapter three different methods have been described, all with their

own advantages and disadvantages. It has been shown that method 1 (see section 3.4.2.1) can be used in case of 1 microflown in a stable sound field. Combined with a (reference) pressure microphone this method can be used to calibrate the frequency response of the microflown (see Chapter 2). Methods 2 (section 3.4.2.2) and 3 (section 3.4.2.3) can be used to retrieve the angle of incidence, direct and diffuse particle velocity in case of one sound source in a reverberant room. Since the sound intensity is closely related to the free-field particle velocity in the far field, the sound intensity can be retrieved. It has been shown that the sound intensity using the p-u method (see Chapter 4) is very similar to the sound intensity obtained with two cross-correlated microflowns. Combined with a pressure microphone the direct pressure (rms-values) can be obtained.

Chapter 4
Sound Intensity

4.1 Introduction

This chapter discusses the physical properties of sound intensity and its measurement techniques. The content of this chapter is based on conference papers and journal paper we wrote about sound intensity based on the microflown particle velocity sensor (Raangs et al., 2001a;Raangs et al., 2002;Raangs et al., 2003)

In section 4.1, a short introduction into sound intensity is given. In section 4.2 the different measurement techniques are introduced. The p-p and the p-u techniques are nowadays the most common techniques; these techniques are compared with each other in section 4.2.2.

Section 4.3 treats the design of a 0.5 inch p-u sound intensity probe based on the microflown particle velocity sensor. In addition, a three-dimensional probe is introduced. Since a measuring device needs to be calibrated in order to deliver reliable results, calibration techniques for the p-u sensors are discussed shortly in section 4.4, in Chapter 2 the calibration was treated in more detail.

Software has been written for data acquisition and computation of various acoustical properties, such as the sound intensity, based on the p-u probe. The software is described in section 4.5.

Sound intensity measurements are performed using the 0.5 inch p-u sound intensity probe (see section 4.3.1) with use of a Windows PC and professional sound card and the realised software (see section 4.5). Measurements are performed while using a single loudspeaker as a sound source in a normal (reverberant) room, and between two loudspeakers, independently driven, in the same room. In section 4.6.1 the results of these sound intensity measurements are described and are compared against a commercially available p-p type sound intensity probe. The resulting sound intensities, as measured with the p-u probe and the software realized, are in good agreement with the results obtained by the p-p probe. In section 4.6.2 the results of a few three-dimensional sound intensity measurements are described.

In Chapter 3 we already showed how free-field measurements can be obtained using two microflowns which measure the particle velocity at the same position but in different directions. In the far field, the sound intensity can be calculated out of these free-field particle velocities. In section 4.7 the obtained sound intensities are compared with the results of the p-u probe and were shown to be in good agreement with each other.

The advantage of sound intensity measurement is not just the fact that it delivers free-field results. Additionally, the noise in a sound intensity measurement is often lower than a single pressure or particle velocity measurement. These noise properties are shortly discussed in section 4.8. For a more thorough discussion on cross-correlated noises, see Chapter 3 in this thesis.

4.2 Sound Intensity and its Measuring Techniques

For the determination of sound intensity, the two components of a sound wave, particle velocity and sound pressure, have to be known (Fahy, 1995;Olson, 1932). The measurement of the sound pressure (or particle velocity) only gives the sum of the free and diffuse sound fields. However, the free-field properties (see Chapter 3) are obtained from the (time-averaged) product of the instantaneous pressure $p(t)$ and the corresponding instantaneous particle velocity $\mathbf{u}(t)$ at the same position,

$$\mathbf{I} = \frac{1}{T}\int_0^T p(t)\cdot\mathbf{u}(t)\,dt \tag{4.1}$$

where the intensity $\mathbf{I}$ and the velocity $\mathbf{u}(t)$ are vectors. The measured intensity corresponds in fact to the net flow of acoustic energy at a given position. If the intensity around a sound source is measured at a number of positions, the radiated sound power can be determined. Even in the presence of reverberation or background noise one can determine in this way the (free-field) radiated power of a sound source (Fahy, 1995).

The product of pressure and particle velocity, $\mathbf{I}(t) = p(t)\mathbf{u}(t)$, is called the instantaneous acoustic intensity (Morfey, 2001). Since the sound intensity $\mathbf{I}$ represents the acoustical power travelling through an area, $\mathbf{I}$ is also known as active sound intensity. Often only one direction of the vectors $\mathbf{u}(t)$ or $\mathbf{I}$ are obtained and considered. In this case, the particle velocity and sound intensity are referred to as $u(t)$ and I.

The sound intensity $\mathbf{I}$ in equation (4.1) is only sensitive for the in-phase pressure and particle velocity. In case pressure and particle velocity are out of phase with reference to each other, the sound field is known as reactive, although the term reactive intensity is generally restricted to harmonic sound fields (Morfey, 2001). Jacobsen defines a time-averaged reactive sound intensity as $J = \overline{\hat{p}(t)\mathbf{u}(t)}$ in which $\hat{p}(t)$ is the Hilbert transform of $p(t)$ (Fahy, 1995).

Since the introduction of Fourier transform techniques, it is very convenient to describe the active and reactive sound intensity in terms of the cross-spectrum.

$$I_{\text{active}} = \text{re}\left(G_{\text{pu}}\right) \tag{4.2}$$

$$I_{\text{reactive}} = -\text{im}\left(G_{\text{pu}}\right) \tag{4.3}$$

The reactive sound intensity, in equation (4.3), is also known as $J(\omega)$, and the complex sound intensity as $C(\omega)$, with

$$C(\omega) = I(\omega) + \text{i}\, J(\omega) \tag{4.4}$$

A sound field can be more or less reactive. The "reactivity" is the ratio (of the surface integral) of the reactive intensity to (the surface integral of) the active intensity (Jacobsen and Bree de, 2004;Jacobsen and Bree de, 2005a). The "Reactivity index" is defined in decibels as the difference between active intensity and squared pressure levels: $L_{\text{k}} = L_{\text{I}} - L_{\text{p}}$ (dB) (Finke, 1991b).

Although equation (4.4) might lead to the assumption that vectors can represent both the time-average active and reactive intensities, in fact the average reactive sound intensity must be described by a tensor (Stanzial et al., 1996) because the mean reactive intensity is zero at all frequencies (Fahy, 1995). In this thesis however we used the complex notation as given in equations (4.2) and (4.3) where the imaginary part of $G_{\text{pu}}(\omega)$ represents the magnitude of the reactive intensity (Fahy, 1995).

Since the relationship between pressure and particle velocity is not unique but depends on the sound field, an intensity measurement system should contain transducers to measure both quantities independently. The sound pressure can be measured in a reliable manner using a pressure microphone.

4.2.1 Particle velocity Measurements

The technical difficulties of designing a suitably stable, linear wide-frequency-band transducer for an accurate conversion of the fluid particle velocity into an analogue electric signal make sound intensity measurements difficult (Fahy, 1995). Instead of using transducers for particle velocity and sound pressure in order to measure the sound intensity, it was shown that the sound intensity can also be determined using two nominally identical microphones, see equation (4.5) (Fahy, 1995). This method is referred to as the p-p method.

In the early 1980s the first sound intensity measuring systems became available and consisted of two closely spaced identical microphones, see Figure 4-1. These intensity probes are still commonly used. In this p-p method the particle velocity is calculated by the linearised equation of momentum conservation,

$$u_x(x) = \frac{-1}{\rho_0 \Delta x} \int p(x+\Delta x) - p(x)\, dt \tag{4.5}$$

where ρ_0 is the density, $p(x)$ the instantaneous sound pressure at position x, and Δx the spacing between both microphones. For a p-p type intensity probe, the active sound intensity in direction r can be calculated by combining equations (4.1) and (4.5) (Fahy, 1995):

$$I_r(\omega) = \frac{-1}{\rho_0 \omega \Delta r} \mathrm{Im}\left(G_{p_A p_B}\right) \tag{4.6}$$

A totally different way of sensing the particle velocity is the principle of ultrasonic transduction: two parallel ultrasonic beams are sent in opposite

Figure 4-1: A commercially available p-p type sound intensity meter (Bruel&Kjaer).

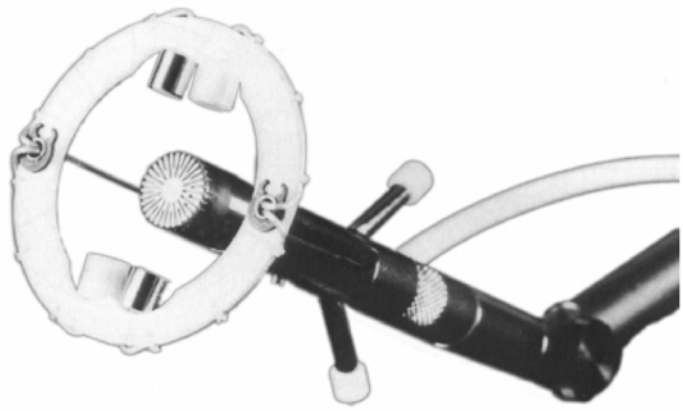

Figure 4-2: Type 216 p-u intensity probe (Norwegian electronics).

directions. The travelling time from the transmitter to the receiver is inversely proportional to the speed of sound in the air. When the air is moving, this movement should be added to the speed. The probe (Figure 4-2) consists of two transmitter–receiver pairs that are positioned in opposite directions. The difference in the travelling times of the ultrasonic sound waves is proportional to the particle velocity.

The length of the ultrasonic path determines the upper frequency response predominantly, which should be no longer than half of a wavelength. The lower frequency is limited only by the electronic circuitry (Finke, 1991a).

The sound intensity probe that is based on this principle is, however, no longer available because of its sensitivity to dc flows (wind). Furthermore, just like the p-p probe, it is a distributed sensor with the problems associated with this type of sensing. (For example, the maximum frequency is limited by the spacing.) Finally, because of its physical dimensions, the probe is difficult to calibrate.

Due to the development of the so-called microflown at the University of Twente in 1994, a novel way of sound intensity measurement became possible (Bree de et al., 1995;Bree de et al., 1996b;Bree de, 1997). Thus, a sound intensity probe is created by the combination of a pressure microphone with this particle velocity sensor.

4.2.2 Comparison p-u and p-p technique

The main difference between the p-u and the p-p method is caused by the sensors itself and the computation of the sound intensity from the measurements.

The well-known p-p method has the advantage of its relatively simple calibration and the fact that it is well described and standardized. A disadvantage of the p-p method is that one must change spacers (and microphones) in order to be able to measure the sound intensity over a broad frequency band. A p-p probe is rather expensive as two identical microphones are used. It should further be noted that the bandwidth of the sound intensity measurements depends on the reactivity of the sound field. (The low end of the bandwidth increases if the reactivity increases.) The high-frequency limit also depends on the reactivity of the sound field and the spacing between the two microphones.

Because the proposed p-u probe is quite different from the p-p probe, the advantages and disadvantages also differ. The main advantage of the p-u probe is that all broadband measurements (for example, 20 Hz to 20 kHz) can be performed using the same probe configuration (and post-processing) without the need to change the spacers, which is needed using the p-p method.

In case of the p-p method, an error occurs due to the phase mismatch between the two microphones. This phase mismatch gives rise to a bias error that can be approximated by (Jacobsen, 1991):

$$\hat{I}_r \simeq I_r - \frac{\varphi_{\mathrm{pe}}}{k\Delta r}\frac{{p_{\mathrm{rms}}}^2}{\rho_0 c} = I_r\left(1 - \frac{\varphi_{\mathrm{pe}}}{k\Delta r}\frac{{p_{\mathrm{rms}}}^2}{I_r\rho_0 c}\right) \tag{4.7}$$

where $\hat{I}_r$ is the estimated intensity, in direction r, and I_r is the true intensity unaffected by the phase mismatch φ_{pe}. Equation (4.7) shows that the effect of a given phase error in the p-p method is inversely proportional to the frequency and the microphone separation distance and is proportional to the ratio of the mean square sound pressure to the sound intensity. If this ratio is large, even small phase errors will result in a significant bias error. The ratio of the phase error can be measured usually in the form of the so-called “residual pressure-intensity index”. The pressure residual intensity index is defined as (Morfey, 2001):

$$\delta_{\mathrm{pI_0}} = L_{\mathrm{p}} - L_{\mathrm{I_0}} \ \mathrm{(dB)} \tag{4.8}$$

where L_{p} and $L_{\mathrm{I_0}}$ are the indicated sound pressure level and intensity level at the measurement position, when the intensity probe is oriented to measure in a null direction (the direction from which no sound power is received).

In case of the p-u method there will also be an error induced by the phase mismatch between the pressure and the particle velocity. This error will however be sensitive to the reactivity rather then the pressure residual intensity and will be of the form (Jacobsen and Bree de, 2004;Jacobsen and Bree de, 2005a):

$$\hat{I}_r \simeq I_r + \varphi_{\mathrm{pe}} J_r \tag{4.9}$$

where J_r is the reactive part of the "real" sound intensity, and φ_{pe} the phase mismatch. Although a small error in phase calibration will result in a significant bias error in case of a reactive sound field, in an active sound field with $J_r \ll I_r$, substantial phase errors can be tolerated. For example, phase mismatches of 35 degrees give a bias error of less than 1 dB under such conditions (Druyvesteyn and Bree de, 1998).

Since the 0.5 inch p-u probes, both one- and the three-dimensional, are relatively small, we can use standard 0.5 inch accessories and take measurements very close to the radiating surfaces. In addition, the sensory is a relatively small acoustical obstacle due to its small size. Disadvantages of the p-u probe are difficulties in calibration and the fact that these calibration data (which is not a constant over frequency) have to be accounted for and the p-u method is not a standardized method.

4.3 Design considerations

4.3.1 One-dimensional 0.5 inch p-u probe

In the beginning, only a specialized 0.5 inch microflown was used to perform the p-u measurements, as shown in Figure 4-3. The combination of this bowed version of a 0.5 inch particle velocity probe, a microflown, and a standard 0.5 inch microphone seemed to be the most cost-effective realization of a one-dimensional p-u intensity probe. Those interested in sound intensity are likely to own a 0.5 inch microphone, so only the 0.5 inch microflown is needed to create an intensity probe. Although this sounds logical, it seemed not to be the right way to go. It was found that the fabrication of a holder to position the microflown and the microphone in a sound field introduced mechanical problems, and standard accessories such as windscreens did not fit.

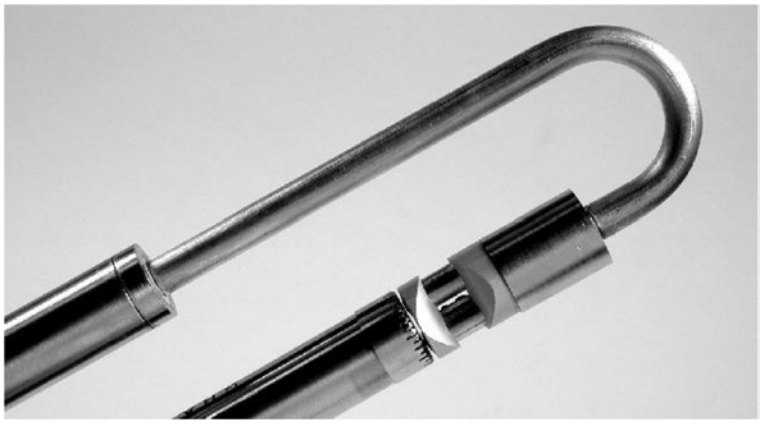

Figure 4-3: Sound intensity probe consisting of 0.5 inch microflown with bowed mounting and 0.5 inch microphone.

Figure 4-4: 0.5 inch p-u sound intensity probe.

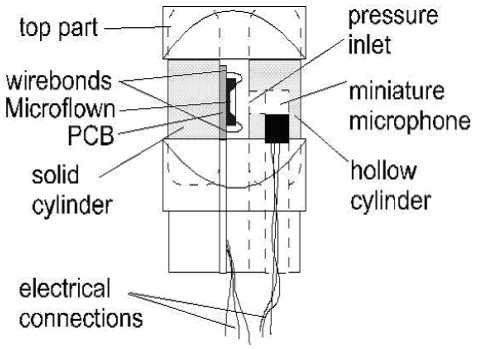

Figure 4-5: Cross-section of 0.5 inch sound intensity probe.

Hence a 0.5 inch probe containing a microflown and a miniature microphone was realized (see Figure 4-4 and Figure 4-5). Although the miniature microphone introduced new costs (it must be fitted into the 0.5 inch microflown) and called for new calibration efforts (now both microflown and miniature microphone need to be calibrated), this realization proved to be most convenient. Standard 0.5 inch accessories can be used, and the miniature microphone can be calibrated at the same time as the microflown. This type of realization will determine sound pressure and particle velocity at the same position.

4.3.2 Three-dimensional p-u probe

Prior to the design of the 0.5 inch p-u probe realisation of three-dimensional sound intensity probes had started based on microflown technologies. At the time, three-dimensional sound intensity probes were all based on three microphone pairs, so that the sensors were all very large. An example of such a realisation is shown in

Figure 4-6. The three-dimensional sound intensity probes were therefore quite large but most of all costly since three carefully matched microphone pairs were needed.

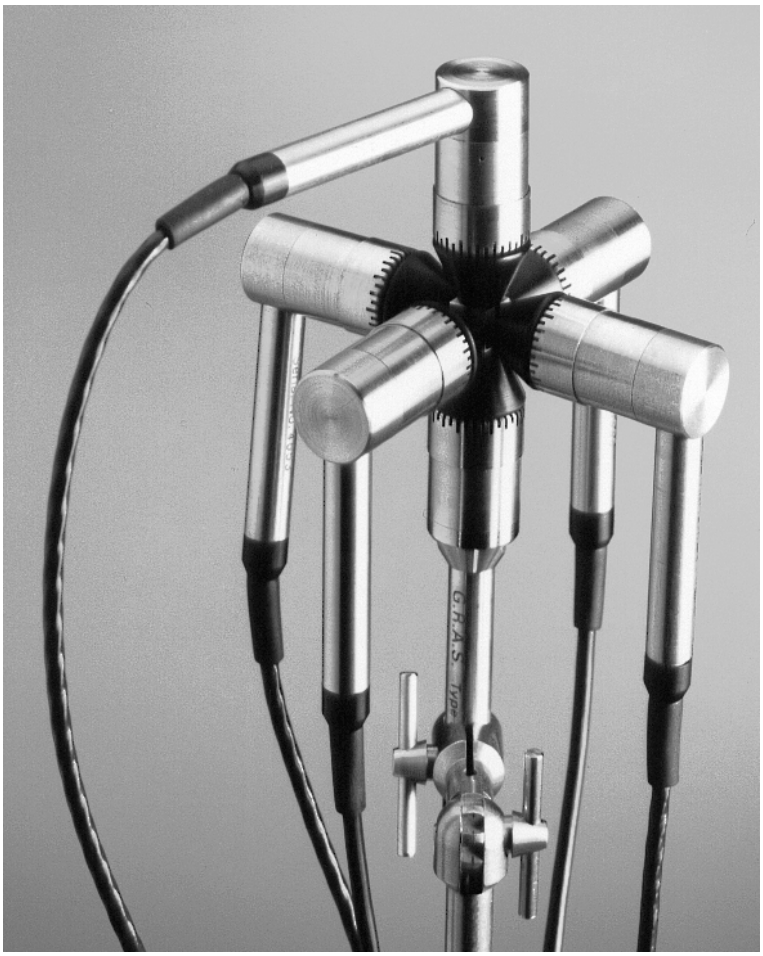

Figure 4-6: Realisation of the three-dimensional 0.5 inch p-p probe that consists on three matched pairs of pressure microphones (G.R.A.S.).

Therefore a new three-dimensional sound intensity probe based on microflown was constructed, see Figure 4-7 (Druyvesteyn et al., 1999). Although this sensor was still quite bulky, compares with the p-p probes it was quite affordable since less acoustical sensors were involved, and thus less signals (resulting in less front-end channels), and simpler computations (only cross-spectra between three p-u pairs) could be used. The first experiments were quite successful and showed that three-dimensional sound intensity probes were feasible especially if they were to be fitted in a single small housing.

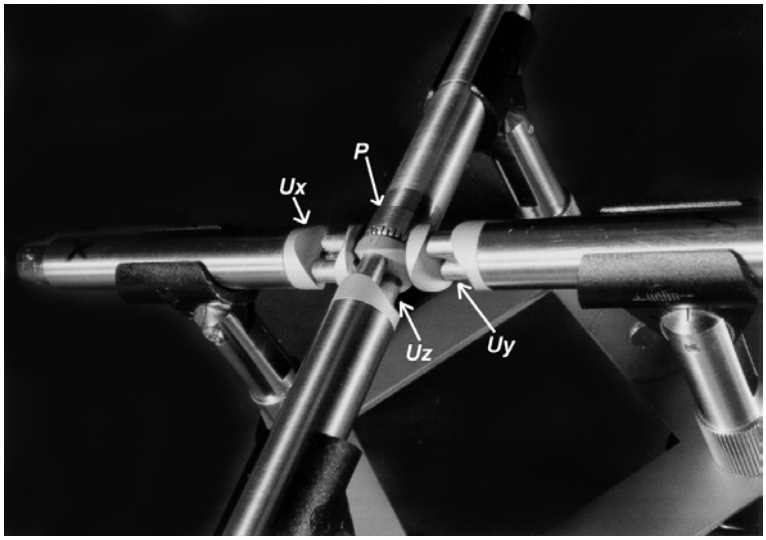

Figure 4-7: Realisation of the three-dimensional probe that consists on three 0.5 inch microflowns and a half-inch sound pressure microphone.

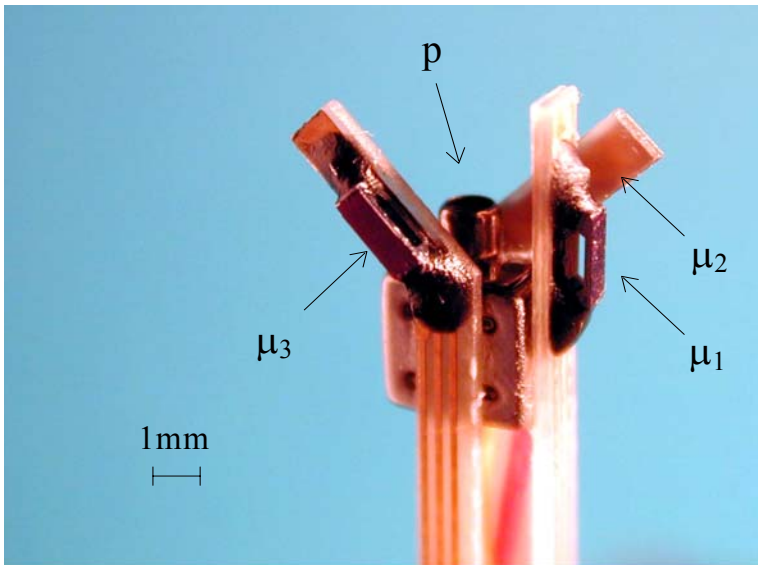

Figure 4-8: A three-dimensional pressure and particle velocity sensor (microflown Technologies) In the middle we see the pressure sensor, and around that the so-called microflowns.

After the one-dimensional 0.5 inch p-u probe had been created, the design of a three-dimensional p-u probe was started, as is shown in Figure 4-8.

In the three-dimensional sensor, the microflowns are positioned around a small microphone so that all three particle velocities and the pressure are measured at almost the same position, and are positioned orthogonally to each other. Two microflown sensors are positioned at 45° with reference to the centre axis of the probe so that they are produced in the same manner and measure the sound field in the same manner. An another advantage is that the probe can be positioned in a standing wave tube (shown in Figure 2-1) so that each microflown measures in the

same direction as the one-dimensional sound field without problems. The major advantage however is its size.

4.4 Calibration

The calibration of acoustic sensors is difficult because of the acoustic environment is not known and a reference particle velocity sensor is not available. Several calibration techniques can be used, each with its limitations. These calibration techniques include: (1) A standing-wave tube, (2) An anechoic environment, (3) A reverberant environment. The different calibration techniques are described in Chapter 2.

Although care was taken in order to position the three particle velocity sensors in the three-dimensional p-u probe perpendicular with reference to each other, this was not always the case. In Chapter 2, section 2.3.5, a three-dimensional calibration technique is described, which also retrieves the directions for each microflown.

4.5 Software

Software was created for use with the one-dimensional p-u sound intensity probe that is presented in section 4.3.1. With use of this software, a good quality sound card can be used in order to obtain the different acoustical measurements. The software and measurements performed using the one-dimensional p-u probe combined with a professional sound card, was presented at the 110th AES conference (Raangs et al., 2001a) and later in the journal of the Audio Engineering Society (Raangs et al., 2003). The measurements were compared with a commercially available p-p probe plus high quality analyser and were in good agreement, see section 4.6.1.

The software is written in MATLAB™ around a graphical user interface, and is distributed freely by its authors. MATLAB is widely used and is an intuitive program language so that users are able to modify the software according to their needs. The program however requires a functional version of MATLAB as well as the data-acquisition toolbox in MATLAB. The program is capable of working in three different modes. The instantaneous mode is very useful in examining the acoustical situation whereas the other modes are intended for writing the (audio) input to a wave file (*.wav) and for processing the data off-line from a wave file.

In the instantaneous mode it is possible to compute and show various windows containing:

- The autospectra of the pressure and particle velocities
- The coherence between the two signals
- The intensity (active, reactive, and the phase)
- The sound energy
- The active and reactive intensity divided by the energy (indicating a net power transport velocity and reflection)
- The specific acoustic impedance (magnitude, real and imaginary parts).

All axes can be chosen as linear or logarithmic scales, and the vertical axis is by default in dB. Frequency spectra can be displayed in terms of frequency (per Hz) and in one-third-octave bands. Calculated spectra can be saved to the workspace, or as MATLAB.mat files, and as ASCII files for further processing.

In the instantaneous mode it is not convenient to use large frames because of computing time and power, resulting in a small frequency resolution. The default size of the frame is set at 2048. For higher resolution, it is advisable to save the signals into wave files (*.wav) so that they can be processed off-line with higher frequency resolution. It should be noted that a good frequency resolution is necessary if one wants to use the advantage of low-frequency measurements, which is possible due to the physics of the p-u probe. The frame size for the fast Fourier transform can be altered according to the required frequency resolution and computation time (default 16834). By default, a Hanning window is used in order to increase in the spectral resolution.

It is possible to record measurements using external hardware such as analogue-to-digital converters connected to digital soundcards, CD recorders, or DAT recorders. This is also very convenient since most of these are quite mobile as measuring becomes rather easy and post-processing can be automated with the use of the available software.

4.5.1 Graphical User Interface

The program “puppy.m” is written in MATLAB™. A screen dump is shown in Figure 4-9. Although Figure 4-9 might be quite confusing and inconvenient due to

the number of windows, the program starts only with the control window visible. Depending on the application, other windows are made visible or invisible by selecting them in the control window. The required window is then maximized for convenient displaying.

The program can be used for data acquisition and calculations on signals obtained with use of a standard soundcard or from a wave file using a pressure (left channel) and particle velocity signal (right channel). The pressure spectra, particle velocity, intensity, energy and acoustical impedance spectra are calculated both in frequency per NFFT (NFFT is the number of FFT points) points and per ⅓-octave bands (see data in the output files).

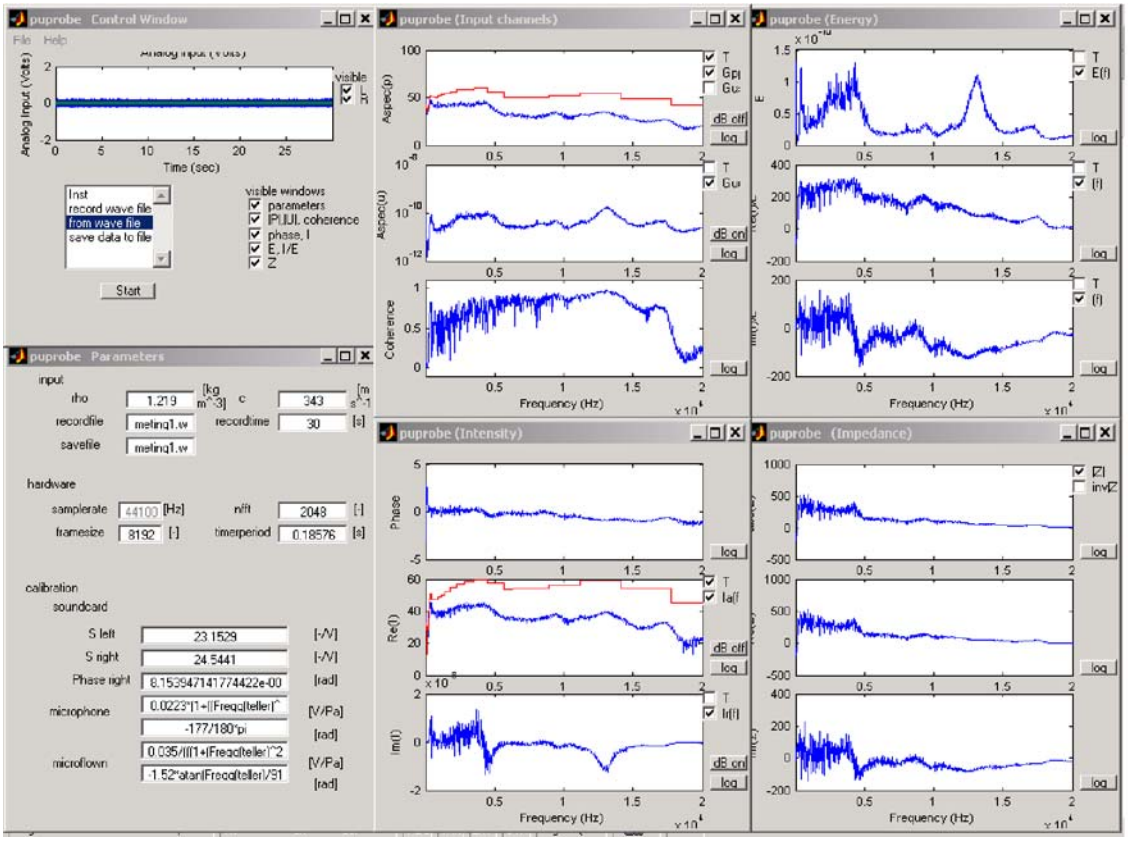

Figure 4-9: Screen dump of the whole program. Left-top shows the Control Window. Left-below shows the parameter window. The other windows contain the calculated spectra.

The cross-correlation is defined as energy per sample per NFFT point so the sum equals the total power of the time signal. The NFFT cannot be set from larger to lower values in this version.

This software requires a standard Windows sound card. The program starts with six windows from which only the Control Window is visible; all other windows can be made visible using the check boxes in the Control Window. Individual

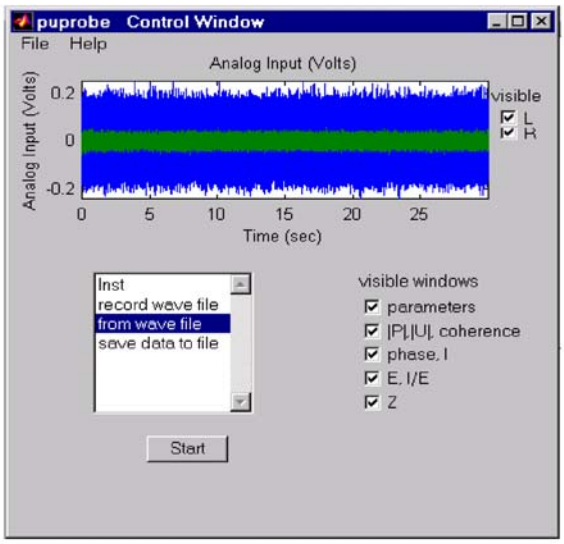

Figure 4-10: Screen dump of the control window.

Windows of the program should not be closed because the program uses the windows for plotting the calculated data. The program closes all windows if the Control Window is closed (File → Close puppy).

4.5.1.1 Control Window

In the "Control Window" (see Figure 4-10) we can choose different modes:

Instantaneously (using the PC soundcard). The advantage is that the measurements and calculations are shown instantaneously the resolution is not very good because we cannot use large number of points for our FFT because of computational time and memory. The frame size (see Parameter Window) is the size of data used per calculation. The NFFT is the numbers used for our Fourier Transform used.

Record Wave File: Data from the wave file is recorded into a wave file named in record file (Parameter Window) with length set in record time (Parameter Window)

From Wave File: Data from a wave file (record file in Parameter Window) is used for calculations and is plotted in the Windows. We can choose the time set in record time (Parameter Window) to select the first seconds required. The size of Fourier Transform can be set in the NFFT window where we have to change the frame size if the NFFT should be larger than the set frame size.

Save Data to File: Data will be saved in a .txt and a mat file with names: "'date time'_par.txt" (the parameters), "'date time'_data.txt" and "date time.mat". The Start/Stop toggle is used for starting measurements/calculations. Each time this

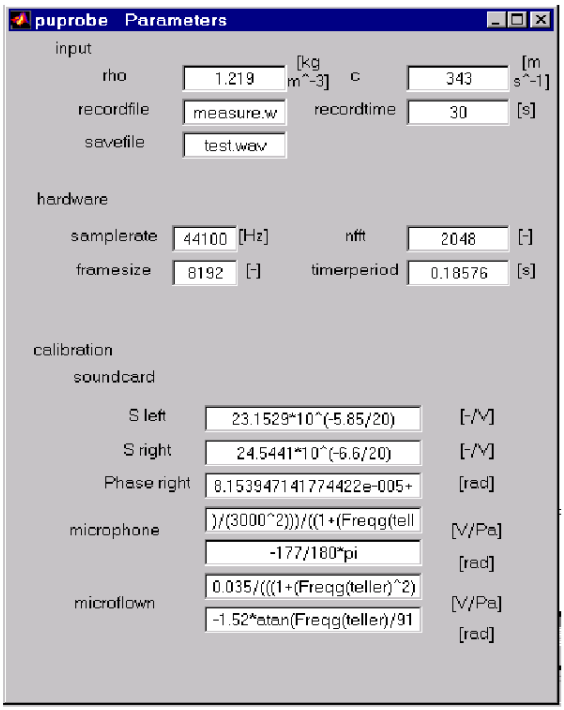

Figure 4-11: Screen dump of the Parameter Window.

toggle is pushed, the program is updated using the settings as shown in the "Parameter Window".

4.5.1.2 Parameter Window

The second window is the so-called "Parameter Window" as shown in Figure 4-11, and Figure 4-9(left, below). This window is needed to enter all parameters used in the program. This window contains three sections: input parameters, hardware, and calibration settings.

Input:

"rho" (density ρ_0) and "c" (speed of sound c) are used for calculating the particle velocity, intensity, energy spectra because the sensitivity of the microflown is given in volt per equivalent pascal (1 Pa* = 1 m s^{-1} divided by the numerical value of $\rho_0 c$). The "record file" is the filename from which the data is calculated. "Record time" is the time for recording and also the part of the signal used if calculations are performed using a wave file. "Save file" is the filename in which a measurement can be recorded.

Hardware:

"Sample rate" is set to 44.1 kHz; other sample rates are not implemented in the measurement and calculations yet. The "NFFT" is the size of the used Fast Fourier

Transform. Standard a Hanning window is used. The NFFT cannot be set from larger to lower values in this version. “Frame size” is the number of sample used in Instantaneous mode for the calculations. The “timer period” is the time set between the Instantaneous measurements if calculations are possible within this time.

Calibration:

“S_{left}” is the sensitivity of the left channel of the soundcard as data read into MATLAB as compared to the signal in volt at the input. “S_{right}” is identical as “S_{left}” but now applied on the right channel. “Phase right” is the phase of the right channel versus the left channel in radials.

“microphone”:

The upper window is the sensitivity of the microphone in volt per pascals a model can be inserted where Freqg(teller) represents the frequency in Hz. The lower window is the phase of the microphone in radials as compared with a reference. A model can be inserted (see microphone sensitivity).

“microflown”

The upper window is the sensitivity of the microflown in volt per equivalent pascal “rho” and “c” are used to convert this to m s^{-1} a model can be inserted (see microphone sensitivity) the lower window is the phase of the microphone in radials as compared with a reference. A model can be inserted by using MATLAB code (see microphone sensitivity)

For calibrating the hardware set “rho”, “c”, and all sensitivities to “1” and the phases to “0”. The calculated spectra and ⅓-octave bands and phase can be used to determine the Sensitivities and the phase of the sound card. The sum overall ⅓-octave bands will for example represent the measured power between 0 and 20 kHz which can be compared with the input signals in V^2. By using the same input signal on both inputs, the measured phase can be used for correction further measurements. By using the correct hardware settings, we can use this program for calibrating the microphone and microflown using an acoustical known environment and a reference microphone.

4.5.1.3 Other Windows

The calculated spectra are shown in the other windows. The single sided cross-spectra are plotted in power per NFFT points. The frequency axis can be toggled from linear and logarithmic scales. The checkbox "T" stands for terts; and if checked, the power is also given per sample in ⅓-octave bands.

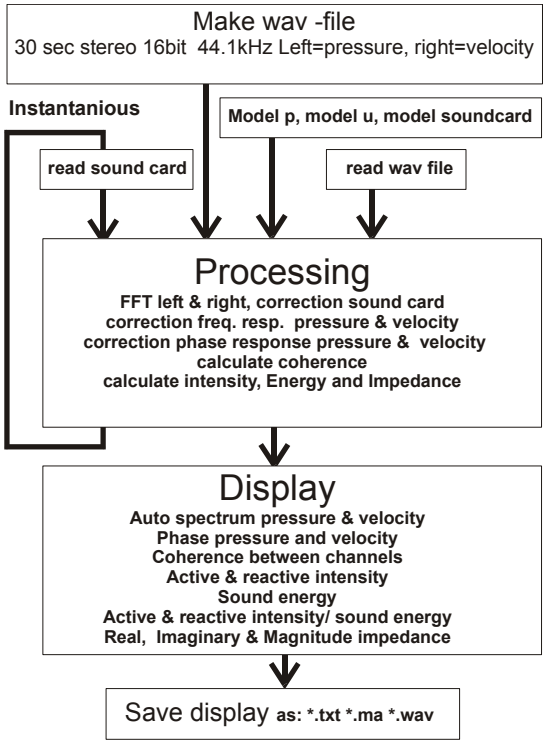

Figure 4-12: Schematic representation of software.

The third window contains the spectra of the input channels (Pressure autospectrum, particle velocity auto-spectrum and the coherence between the pressure and particle velocity signals). In this window the auto-spectra and the cross-spectrum of the input channels are plotted. Aspec P (pressure): with G_{pp} as the auto-spectrum of the pressure. The cross-spectrum of the microflown signal in equivalent pascal (Pa*) can also made visible. The coherence between the pressure and particle velocity signals. The coherence is calculated as

$$\gamma_{12}^2 = \frac{|G_{12}|^2}{\sqrt{G_{11}G_{22}}} \tag{4.10}$$

with G_{12} as Power Spectrum.

In the fourth window, the sound intensity is plotted. The three plots contain the phase of the sound intensity, the active part, and the reactive part of the complex sound intensity.

The fifth and the sixth window contain the energy density spectra and the specific acoustical impedance.

4.5.2 Data Processing

Data processing is performed on the raw data according to the flowchart given in Figure 4-12 and Figure 4-13. A short overview of the signal processing methods

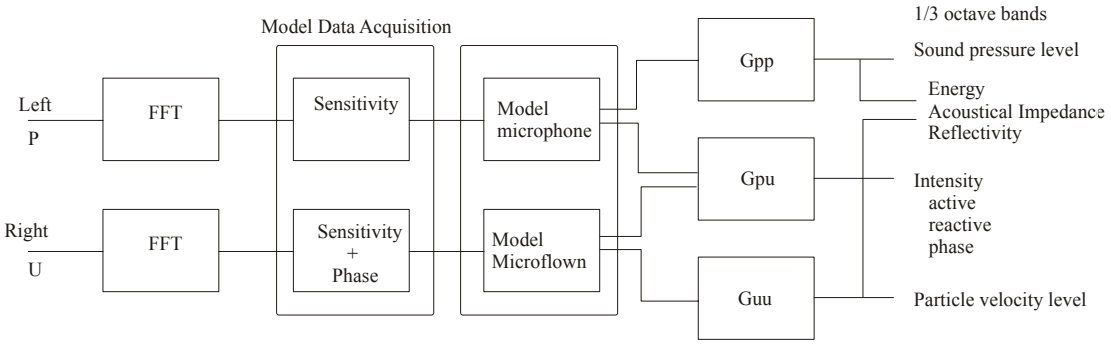

Figure 4-13: Schematic representation of the data processing.

applied is given in Chapter 3, a more thorough description is given in (Bendat and Piersol, 2002;Oppenheim et al., 1989) and others.

The left-hand signal contains data from the pressure sensor, whereas the right-hand signal contains the data from the particle velocity sensor. First, the signals are converted to the frequency domain because in this domain it is much easier to correct for the sensitivities and phases in the signals than it would be in the time domain. Second, the data are converted from arbitrary units to volt by means of the calibration of the soundcard (or external analogue-to-digital converter)–amplifier combination. Note also that the phase shift due to the soundcard is implemented here so that the signals, now expressed in volt, are in the right phase with reference to each other. If the signals are given in volt, the program converts them to the pressure and particle velocity signals using the calibration of the sensitivities and phases of the acoustical probes. The signals are converted to pascal for the pressure signal, and to meter per second for the particle velocity signal using values for ρ_0 and c, which can be altered in the parameter settings (default 1.219 kg m^{-3} and 343 m s^{-1}). From the pressure and particle velocity signals the various auto- and cross-spectra are calculated (G_{pp}, G_{uu}, G_{pu}).

Integrating over the frequency spectra we can calculate the intensity over the frequency spans,

$$I\left(f_1, f_2\right) = \int_{f_1}^{f_2} G_{\mathrm{pu}}\left(f\right) df \tag{4.11}$$

The program calculates the intensity spectrum both in the frequency domain and in one-third-octave bands.

The acoustic energy density, also known as sound energy density, is defined as the sum of the kinetic and potential energy densities at a point in an acoustic field and is defined as (Fahy, 1995)

$$E(t) = \frac{p^2(t)}{2\rho_0 c^2} + \tfrac{1}{2}\rho_0 u^2(t) \tag{4.12}$$

Using the cross-spectra calculated earlier, the time-averaged acoustic energy density can be calculated as

$$E = \frac{G_{\mathrm{pp}}}{2\rho_0 c^2} + \tfrac{1}{2}\rho_0 G_{\mathrm{uu}} \tag{4.13}$$

The specific acoustic impedance is defined as the ratio between pressure and particle velocity,

$$Z(\omega) = \frac{P(\omega)}{U(\omega)}. \tag{4.14}$$

From the computed cross-correlations we can derive the specific acoustic impedance, which the program computes as

$$Z(\omega) = \frac{P(\omega)}{U(\omega)} = \frac{G_{\mathrm{up}}}{G_{\mathrm{uu}}} \tag{4.15}$$

4.5.3 Calibration Data Acquisition Hardware

Calibration is likely to be the most essential part of this measurement technique because the results differ greatly depending on the calibration. Several parts in the system should be calibrated in order to be able to measure accurately. We should calibrate the pressure and particle velocity sensors and the analogue-to-digital converter in the soundcard or an external analogue-to-digital converter. It is also possible to introduce a preamplifier so that we use the resolution of the analogue-to-digital converter more efficiently.

The analogue-to-digital converter can easily be calibrated using a known signal because we can assume the soundcard used to be almost perfectly linear in the frequency domain. A preferably white noise signal can be connected to the inputs with known power. With little data acquisition and processing, the sensitivity and a phase difference between the channels can be calculated and implemented in the software. Also a sinusoidal signal can be used, although this will only yield the

calibration for a single frequency. We should note that the gain and panning of the input should not be altered on the personal computer since the gain and panning will be applied on the acquired signals. If a preamplifier is used, it also should not be adjusted after calibration. The preamplifier can be calibrated using the same method used for the soundcard. Note that depending on the quality of the soundcard respectively, the analogue-to-digital converter, the phase between two channels can be extremely large, for example, up to 140 degrees at 20 kHz for a standard PC soundcard, or only 2.5 degrees for an external analogue-to-digital converter.

4.6 Measurements

In this section measurements of sound intensity are shown using a 0.5 inch p-u sound intensity probe (section 4.6.1), and a three-dimensional p-u probe (section 4.6.2). The measurements as shown in section 4.6.1 are obtained with use of the software as described in section 4.5 using a professional 20 bits sound card. The results are also described in references (Raangs et al., 2001a;Raangs et al., 2003). The usage of the three-dimensional p-u probe as shown in section 4.6.2 can be found in reference (Raangs et al., 2002)

4.6.1 Intensity Measurements using a 0.5 inch p-u sound intensity probe.

Intensity measurements are performed in a reverberant room using a p-p probe and the p-u probe described. The p-p probe is a Brüel & Kjær intensity probe, type 2260 Investigator, using two 0.5 inch microphones (type 4181). Measurements were made twice, using spacers of 50 mm (type UC 5270) and 12 mm (type UC 5269) so that we could measure up to one-third-octave centre frequencies of 1.25 kHz and 5 kHz, respectively. The intensities in the one-third-octave frequency bands are calculated using the Investigator B&K 2260.

The signals of the p-u probe were measured using a personal computer combined with a digital soundcard and an external analogue-to-digital converter as well as a preamplifier set at +40 dB for both channels. A white noise of 5.1 mV_{rms} was applied in order to calibrate the data acquisition hardware. The wave file created was read into MATLAB and the power was calculated so that we were able to determine the signal in volt for our calculations. Using the software described in

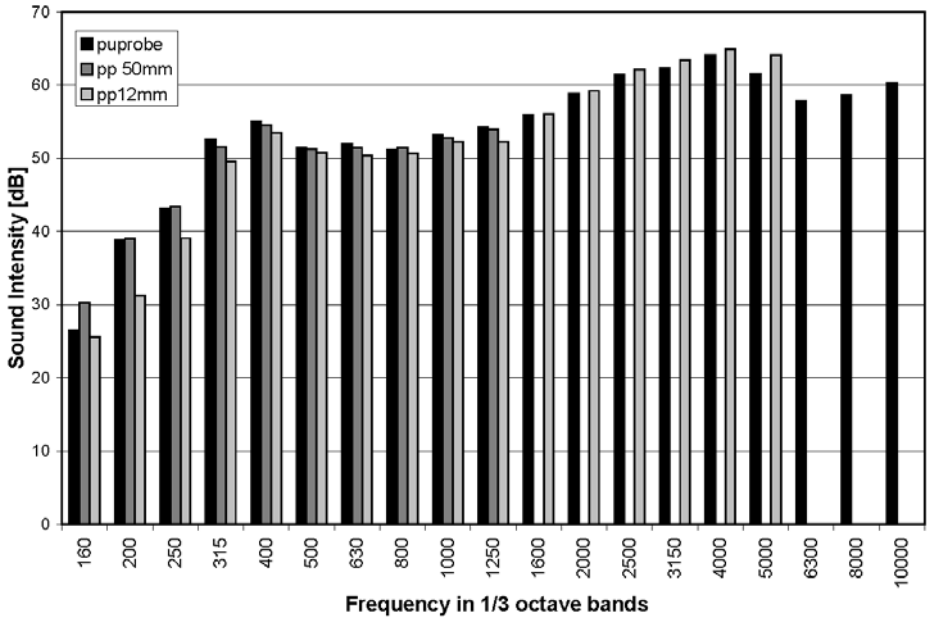

Figure 4-14: Measured sound intensity using a loudspeaker as sound source. p-u probe (black); p-p probe 50 mm (dark gray); p-p probe 12 mm (light gray).

section 4.5, we calculated the active intensity in one-third-octave bands, the results are shown in Figure 4-14 and Figure 4-15.

First, the intensity in front of a small loudspeaker was measured using the p-p and p-u techniques. The loudspeaker was positioned in a normal room at a stand and was positioned 1 metre above the floor. The 0.5 inch p-u probe was positioned at a distance of 1 metre from the loudspeaker at the same height as the loudspeaker cone. The same white noise was fed to the loudspeaker during the recording of the pressure and particle velocities, and during the measurements using the p-p probe at the same position and orientation. Figure 4-14 shows that the intensity measured with the p-u method are in good agreement with the measurements of the p-p method in all frequency bands.

Secondly, we performed intensity measurements between two identical loudspeakers, which were the same as described before. The two loudspeakers are positioned at a height of approximately 1 metre with a distance of 2 metres between each other. The p-u and p-p probes were positioned at the same height as the loudspeaker cones and was positioned exactly between the two loudspeakers. The orientation was chosen such that the probes measured in the direction of the two loudspeakers. Two uncorrelated signals S_1 and S_2 are fed to the two loudspeakers. The power to loudspeaker 1 (S_1) was kept at a constant level, whereas the power to loudspeaker 2 (S_2) was varied. A linear relationship was

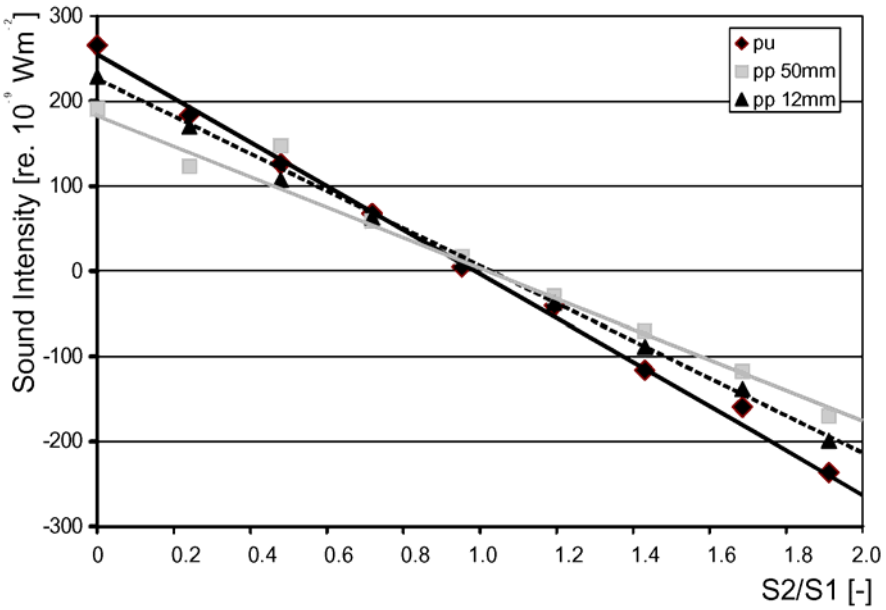

Figure 4-15: Sound intensity measurements between two identical loudspeakers at 1 kHz one-third-octave band versus ratio of electric power sent to loudspeakers. p-u probe (black diamonds); p-p probe 50 mm (gray squares); p-p probe 12 mm (black triangles).

expected between the active intensity and the ratio between the acoustic powers of both loudspeakers (Druyvesteyn and Bree de, 2000). The negative values of the sound intensity indicate that sound power is coming from the direction of loudspeaker 2, and vice versa. Out of the measurement at, for example, ⅓-octave at 1 kHz (see Figure 4-15) we can note that this is the case for both measurement techniques. We notice a small overestimation for the p-u measurement, although the deviation in the p-p measurements using 12 mm and 50 mm spacers is of the same order.

Notice that the results of the active sound intensity in between two uncorrelated sound sources, as shown in Figure 4-15, are analogue to the results of the cross-correlation between two perpendicular particle velocity probes in case of two uncorrelated sound sources positioned perpendicular as shown in Figure 3-11 (see Figure 3-10 for the experimental setup).

4.6.2 Three-dimensional Sound intensity Measurements

Because the sensitivity vectors for all three particle velocity sensors, and the miniature microphone sensitivity, and the phases are known, we are able to calculate the particle velocities and pressures and sound intensity (Raangs et al., 2002). The sound intensity can be calculated by using (Fahy, 1995):

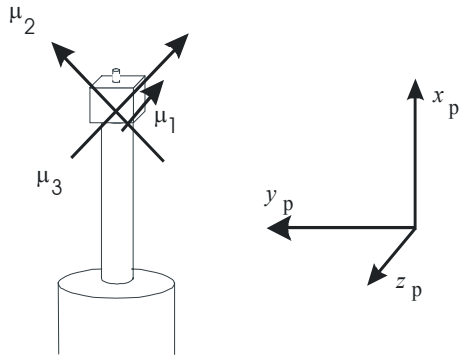

Figure 4-16: Schematically view of the three-dimensional p-u probe and the reference axis connected to the probe (see Figure 4-8).

$$
\begin{aligned}
I_1 &= \mathrm{Re}\left\{ G_{\mathrm{pu1}} \cdot S_{\mathrm{p}}^{\ -1} \cdot \left|S_1\right|^{-1} \cdot \exp\left(i \cdot \left(\varphi_{\mathrm{p}} - \varphi_{\mathrm{u1}} \right) \right) \right\} \\
I_2 &= \mathrm{Re}\left\{ G_{\mathrm{pu2}} \cdot S_{\mathrm{p}}^{\ -1} \cdot \left|\mathrm{S}_2\right|^{-1} \cdot \exp\left(i \cdot \left(\varphi_{\mathrm{p}} - \varphi_{\mathrm{u2}} \right) \right) \right\} \\
I_3 &= \mathrm{Re}\left\{ G_{\mathrm{pu3}} \cdot S_{\mathrm{p}}^{\ -1} \cdot \left|S_3\right|^{-1} \cdot \exp\left(i \cdot \left(\varphi_{\mathrm{p}} - \varphi_{\mathrm{u3}} \right) \right) \right\}
\end{aligned}
\tag{4.16}
$$

where G_{pu} is the one-sided cross-spectrum between signals of the pressure and particle velocity sensors. The cross-spectrum density is defined as $G_{\mathrm{pu}} = P^{*}U$, with * as the complex conjugate (P and U are in the frequency domain). S_{p} is the sensitivity of the microphone, $\left|S_{\mathrm{u}}\right|$, the sensitivity (magnitude) of the microflown, φ_{p} and φ_{u} the phases of respectively the microphone and microflown sensors. An extra term $\left(\rho_0 c\right)^{-1}$ is needed in equation (4.16) if the sensitivity of the particle velocity sensor is given in V/Pa* instead of V s m^{-1}.

For each microflown-pressure pair, a sound intensity can be computed using equation (4.16). In general, $\mathbf{I}_1$, $\mathbf{I}_2$ and $\mathbf{I}_3$ are not orthogonal. If the directions are known in which the microflowns do measure the particle velocity, a three-dimensional sound intensity vector can be reconstructed based on an orthogonal reference system, which is connected to the three-dimensional p-u sensor as a whole, see Figure 4-16. The relation between the sound intensity on the axis system connected to the probe and the directions in which the particle velocity is measured (see Figure 4-16 which is a copy of Figure 2-20) can be expressed as a matrix equation:

$$\mathbf{I}_{123} = \mathbf{A}\,\mathbf{I}_{xyz} = \begin{pmatrix} S_{1x}/|S_1| & S_{1y}/|S_1| & S_{1z}/|S_1| \\ S_{2x}/|S_2| & S_{2y}/|S_2| & S_{2z}/|S_2| \\ S_{3x}/|S_3| & S_{3y}/|S_3| & S_{3z}/|S_3| \end{pmatrix} \mathbf{I}_{xyz} \tag{4.17}$$

where **A** is a dimensionless directivity matrix of the three-dimensional particle velocity probe which can be retrieved using the three-dimensional calibration as shown in Chapter 2, and (Raangs et al., 2002).

By simple matrix inversion the sound intensity can be determined on our orthogonal axis system (see Figure 2-20). The sound intensity in terms of this axis system can be calculated by:

$$\mathbf{I}_{xyz} = \mathbf{A}^{-1}\,\mathbf{I}_{123} = S_{\mathrm{p}}{}^{-1}\exp\left(i\varphi_{\mathrm{p}}\right)\mathbf{A}^{-1}\begin{pmatrix} G_{\mathrm{pu}1}\left|S_1\right|^{-1}\exp\left(-i\varphi_{\mathrm{u}1}\right) \\ G_{\mathrm{pu}2}\left|S_2\right|^{-1}\exp\left(-i\varphi_{\mathrm{u}2}\right) \\ G_{\mathrm{pu}3}\left|S_3\right|^{-1}\exp\left(-i\varphi_{\mathrm{u}3}\right) \end{pmatrix} \tag{4.18}$$

where $\mathbf{I}_{xyz}$ is in this case the complex conjugate of the complex sound intensity vector. The active sound intensity is the real part of this vector.

In section 4.6.2.1 the reconstruction using equation (4.18) of the sound intensity has been checked by rotation the three-dimensional probe while keeping the sound field stable for a given three-dimensional p-u probe and sensitivity matrix belonging to it (see Chapter 2) obtained from calibration.

In section 4.6.2.3 measurements in front of a small monopole are shown before and after usage of the three-dimensional calibration using equation (4.18).

4.6.2.1 Control measurements three-dimensional p-u Probe and Calibration

With use of the three-dimensional calibration method (see Chapter 2), we can correct for the positioning of the microflowns with reference to each other and to our measurement setup itself. In order to check the results of the three-dimensional calibration method, we used a calibrated three-dimensional p-u probe, which is rotated in a sound field were it is assumed that the sound field is not changed due to the probe itself. Therefore, we should be able to reconstruct the sound field

properties (for example sound intensity), which should be independent from the rotation of the probe itself.

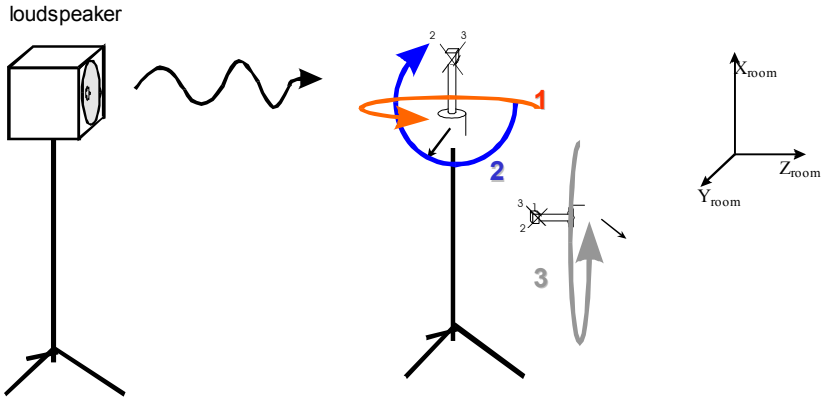

Figure 4-17: Experimental setup for the control measurements. The small numbered arrows represent the microflowns and their measuring direction.

The sound intensity vector $\mathbf{I}_{x_p y_p z_p}$ with reference to the orthogonal probes axis system can be calculated out of the cross-spectra between the several microflowns and microphone G_{pu}, and the sensitivities $S_{1,2,3}$ for the three microflowns, and the phases of the sensors φ and a dimensionless directivity matrix $\mathbf{A}$ (Raangs et al., 2002) as shown in equation (4.18). If the position and orientation of the probe is known, the sound intensity vector in the room, $\mathbf{I}_{x_{room} y_{room} z_{room}}$, can be calculated out of $\mathbf{I}_{x_{probe} y_{probe} z_{probe}}$.

Measurements are performed in a reverberating room and in a large box filled with acoustical absorbing material (see Figure 4-18). The loudspeaker and three-dimensional p-u probe were positioned at a height of approximately 1 metre. The distance between the loudspeaker and the three-dimensional p-u probe was also approximately 1 metre. The sound intensity as measured by each microflown-microphone combination can easily be calculated. Because the directions in which the microflowns are measuring are not orthogonal we have to correct for the calibrated directions in order to calculate the real sound intensity in the room due to a sound source.

Figure 4-18: A loudspeaker in our large box filled with acoustical absorbing material.

Since the sound field is not changed by rotation of the three-dimensional p-u probe, every measurement should result in the same active sound intensity (direction and amplitude), if we account for the rotation of the probe itself. Every misalignment in the probes sensitivities and directions, directionalities will result in a different active sound intensity due to the rotation.

4.6.2.2 Results of the three dimensional sound intensity reconstruction

We rotated the probe according to the picture shown (rotation 3 in Figure 4-17). During each measurement, a 1 kHz, ⅓-octave, noise was fed to the loudspeaker. The p-u probe was rotated with intervals of 30 degrees. For each angle of rotation, the cross-spectra between the three microflown and the pressure signals were measured (1 kHz, ⅓-octave band) which was converted into three sound intensities (not orthogonal) with use of equation (4.16). In Figure 4-19 the three sound intensities are shown as measured by the three microflowns combined with the pressure sensor.

The shown measurement, microflown 1 is measuring almost no sound intensity, while the other two microflowns are measuring about 0.7 times the real active sound intensity.

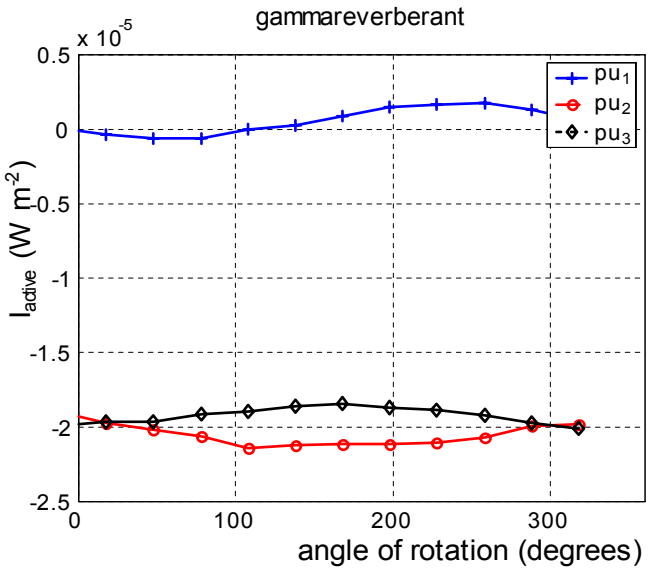

Figure 4-19: Measurements of the Sound intensity in the three microflowns directions. The active sound intensity in $Wm^{-2}*10^{-5}$.

With use of the knowledge of the directions in which the three microflowns do measure (with reference to the 3D p-u probe itself) obtained by the three-dimensional calibration technique, the three-sound intensities can be converted into a true sound intensity vector, see equation (4.18). This sound intensity is shown in Figure 4-20. The intensity axis is chosen as decibels in order to show the difference between all 12 measurements.

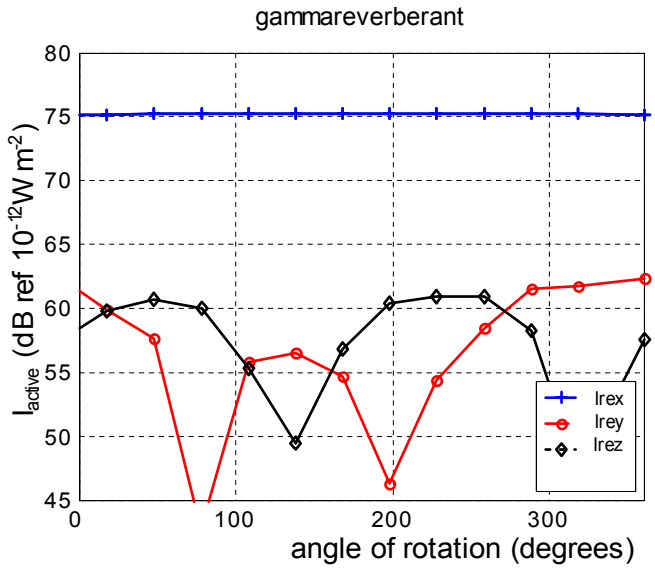

Figure 4-20: The measured active sound intensity in dB here on the orthogonal probe axes (ref $1e^{-12}$ W m^{-2}).

Since we know the relation between the probe and the room (rotation matrix), we can compute the true sound intensity vector based on our room coordinates.

The 12 measured sound intensity vectors are plotted (as arrows beginning at the origin) in Figure 4-21.

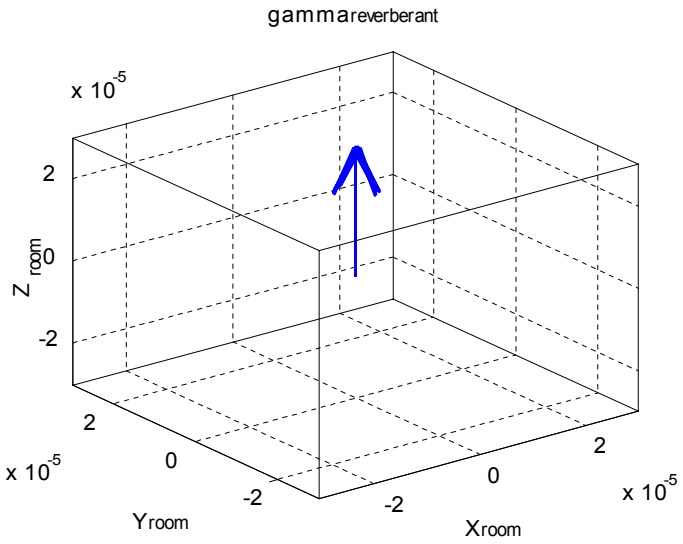

Figure 4-21: All measured sound intensities. The active sound intensity plotted as arrows (a total of 12 sound intensity are plotted.

Since the arrow almost overlap, as they should, the angle between the z-axis (room) and the actual measured sound intensity vectors, the angle of incidence, shows more detailed. In Figure 4-22 the angle of incidence for the reverberant measurements are shown. Although the experiment was setup (visually) so that the z-axis was directing from probe towards the loudspeaker, the bias error of 1 degree in Figure 4-22 is therefore within the error due to the visual alignment.

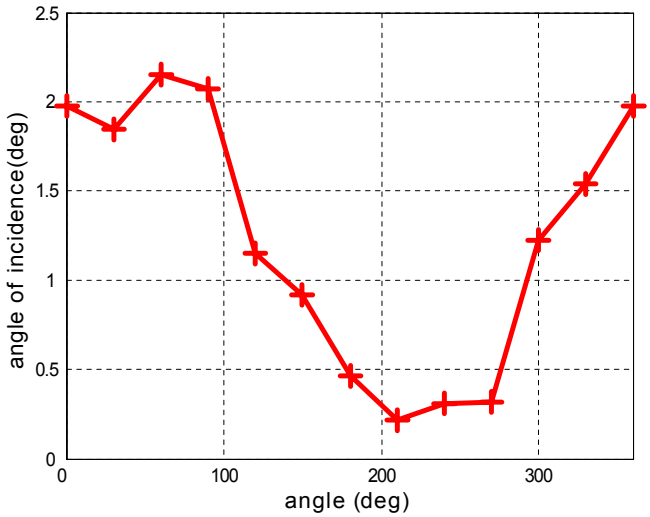

Figure 4-22: The angle of incidence (based on room coordinates) as a function of the rotation of the three-dimensional p-u probe.

In Figure 4-21 and Figure 4-22 it is shown that all active sound intensities are directing in the same direction (± 0.5 degrees, see Figure 4-22) and are of the same amplitude (± 0.02 dB). The same is true for the other rotations.

Overall, for all measurements including the measurements of rotations 1 and 2 (each 30 degrees rotation, see Figure 4-17) the variance in the angle of incidence is 0.7 degrees reverberant, and 3 degrees reverberant (not shown), and in the amplitude 0.2 dB anechoic (see Figure 4-19, right), 0.3 dB reverberant.

4.6.2.3 Results Monopole

In this section, some results of a planar scan in front of a monopole in a baffle is shown. In this experiment, the three-dimensional probe has been applied very close to the sound source, and at a frequency of 400 Hz such that the sound field is mainly reactive ($l/\lambda \approx 1/40$). It is therefore expected that other sound intensity probes, based on the p-p technique, are not likely to be able to measure the sound intensity at these positions in this sound field.

In this section we also show that we can correct for misalignments in the three microflown directions in the near field. Since the method of converting the three sound intensities (of the microflowns) in to a single sound intensity vector is already discussed in sections 4.6.2.1 and 4.6.2.2, only the results are shown in this section.

The experimental setup is shown in Figure 4-23. A midrange 10 cm loudspeaker was mounted at the rear of the baffle. A hole (3 mm radius) in the baffle was used

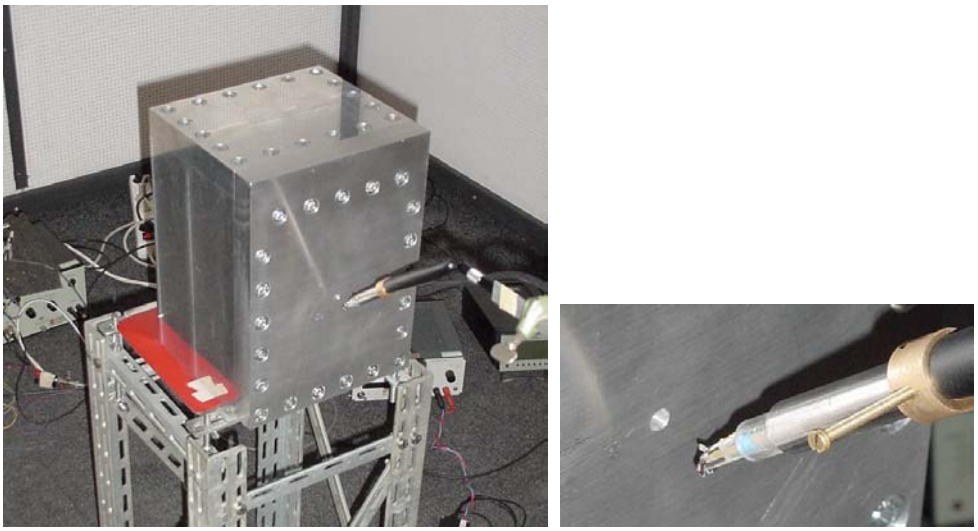

Figure 4-23: left: Measurement setup. Shown is the aluminium box with the hole. Right: close up of the volume source and the three-dimensional p-u probe.

as the monopole source, see Figure 4-23.

The sound field was measured over an area using a Dantech two-dimensional-traverse system. Pressure and particle velocities are measured using a three-dimensional p-u probe. The signals were amplified by a battery fed amplifier (LM348N) and then measured by a DSPT Siglab analyzer. The three-dimensional p-u probe was calibrated using the three-dimensional calibration method as is described in Chapter 2).

Measurements are performed on a grid (-0.1 to +0.1 m, dx=dy=0.02 m) parallel to the surface at a distance of 0.02 m. In the figures (Figure 4-24 to Figure 4-27) the result is shown for the frequency band of 400 Hz ± 10 Hz.

Figure 4-24 shows the measured three-dimensional sound intensity. In case of Figure 4-24 the three-dimensional calibration has not been applied yet, only the amplitudes of the sensitivities of the pressure and particle velocity sensors are applied. Figure 4-24 (right plot) clearly shows that the sound field is not correctly measured since not all arrows seem to correspond with only a single source.

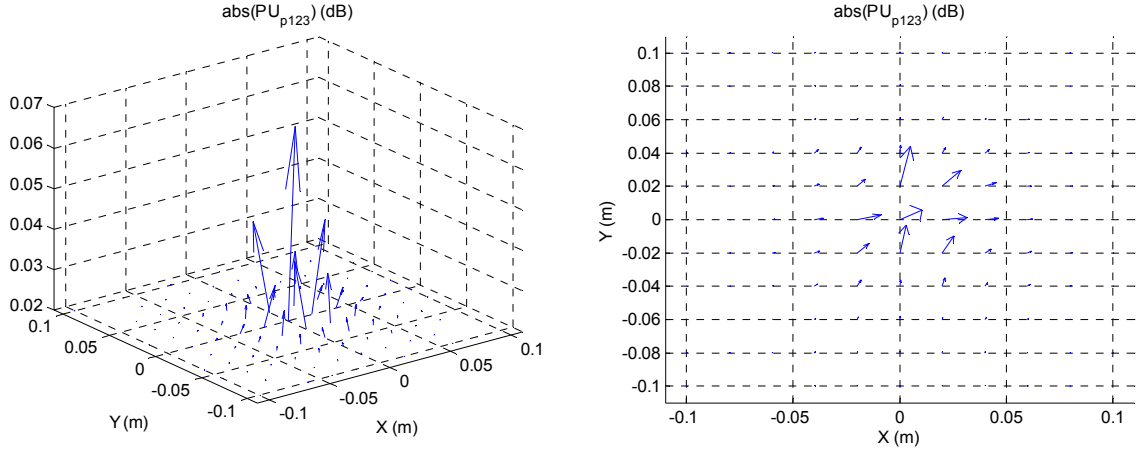

Figure 4-24: Measured absolute sound intensity (at 400 Hz) using the three microflown orientations. (no three-dimensional calibration used). Left: three-dimensional view, right: two-dimensional view.

Figure 4-25 shows the result after the three-dimensional calibration had been applied. In Figure 4-25 the measurement is however plotted based on the axis system which is connected to the sensor itself, rather than the sound field. Since the sensor is moving, and rotated, the sound intensities measured by the probe are not helpful for visualising the sound field, but since the rotation of the probe is known, we can account for its orientation.

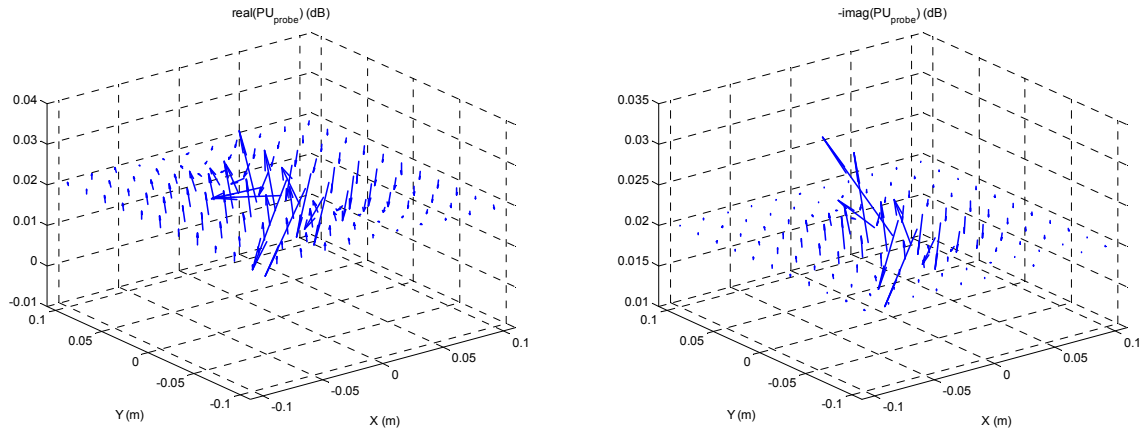

Figure 4-25: Measured Sound intensity (left: real part, right, imaginary part) as measured on the measurement grid based on the probe's axis system (see Figure 4-16).

In Figure 4-26 the results of Figure 4-25 are based on the sound field again. Figure 4-26 clearly shows that the sound intensity originates from a single (volume) sound source.

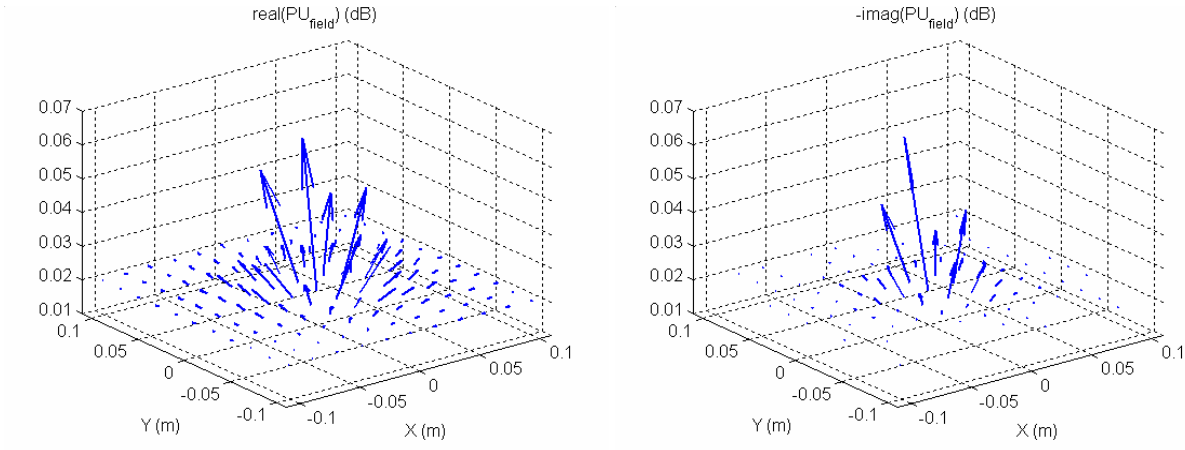

Figure 4-26: Measured Sound intensity (left: real part, right, imaginary part) as measured on the measurement grid based on the axis system as used in the measurement.

In Figure 4-27 the imaginary part of the cross-spectrum between pressure and particle velocity has been shown since the sound field is mainly reactive. It should be noticed that this is minus one times the reactive sound intensity as defined by Fahy (Fahy, 1995). The imaginary part clearly points towards the volume source.

The figures clearly show that the three-dimensional calibration is applicable and enhances the measurement results for three-dimensional particle velocity and sound intensity measurements. Comparing Figure 4-24, the three microflown directions, with Figure 4-27 corrected for the alignment of the three microflowns, it can be seen that the results have been improved using the three-dimensional calibration. In Figure 4-27 the sound intensities clearly indicate a single source,

whereas in Figure 4-24 the sound intensity behaves more randomly and do not clearly correspond to a single sound source.

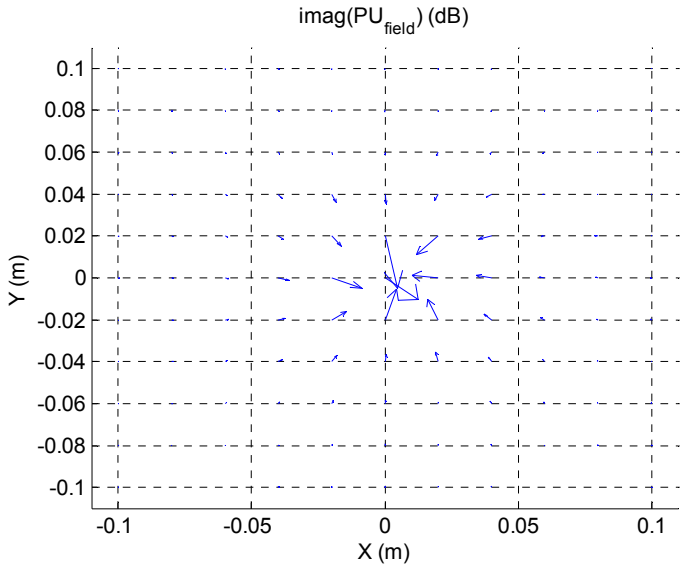

Figure 4-27: The imaginary part of the cross-spectrum between pressure and particle velocity.(two-dimensional view).

4.7 Sound Intensity out of cross-correlated microflowns

In Chapter 3, we showed that in a reverberant sound field the distinction could be made between the direct and the reverberant sound field using two microflowns. Since in the far field, the relation between direct particle velocity and active sound intensity is straightforward, namely $p_{\mathrm{dir}}^2/(\rho_0 c)$ and $u_{\mathrm{dir}}^2(\rho_0 c)$, or $p_{\mathrm{dir}}u_{\mathrm{dir}}$, this comparison was performed in section 3.4 in order to show that the computed direct particle velocity agree with expectations.

For completeness of this chapter, sound intensity, this method and the results obtained, and compared with the three-dimensional p-u technique are shortly discussed. For a complete overview of the method applied see Chapter 3 and (Raangs et al., 2001b;Raangs et al., 2002).

In case that the microflown pairs are not positioned perpendicular with reference to each other we have to solve the set of equations:

$$\begin{aligned} G_{u_1u_1} &= u_{\mathrm{dir}}^2\cos^2\alpha + \tfrac{1}{3}u_{\mathrm{rev}}^2 \\ G_{u_2u_2} &= u_{\mathrm{dir}}^2\cos^2(\alpha-\varphi) + \tfrac{1}{3}u_{\mathrm{rev}}^2 \\ G_{u_1u_2} &= u_{\mathrm{dir}}^2\cos\alpha\cos(\alpha-\varphi) + \tfrac{1}{3}u_{\mathrm{rev}}^2\cos\varphi \end{aligned} \qquad (4.19)$$

where φ is the angle between the microflowns. This set of equations can be solved for the free-field and diffuse particle velocity, and the angle of incidence. With use of our calibrated three-dimensional p-u probe (see section 2.3.5 for calibration), or two single microflowns, we can measure both the sound intensity using the p-u method, and using the cross-correlation method out of only the microflown signals for the far-field (see Chapter 3). The agreement between the two sound intensity measurements is remarkable good as can be seen in Figure 4-28, which is a copy of Figure 3-15.

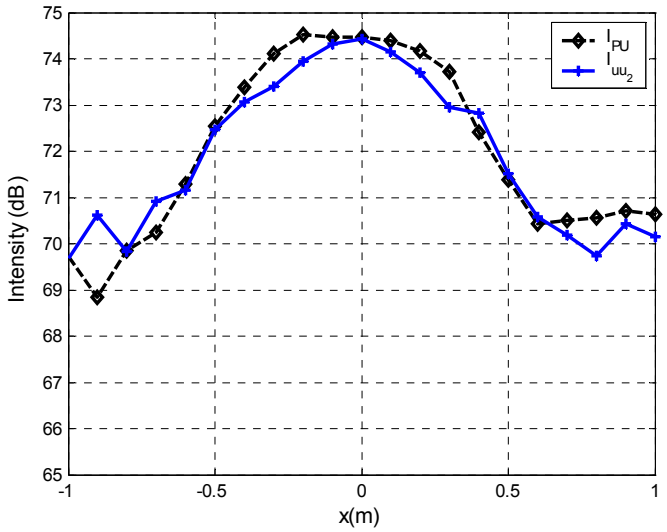

Figure 4-28: Sound intensity (active part) measurement (1 kHz ⅓-octave band) using the u-u method (using two microflown signals, see section 3.4.2.3) (+ marks) and the p-u method (diamonds).

The cross-correlation method using perpendicular microflowns delivers the reverberant, c.q. diffuse sound field, and an angle of incidence (± 180 degrees) and delivers therefore much more information about the sound field than a microphone or p-p type intensity measurement.

4.8 Signal-to-Noise Ratios of the p-p and p-u Methods

The self-noise of two separate microphones is not correlated. In the case of the p-p method, the imaginary part of the cross-spectrum is taken to get the active intensity; in the case of the p-u method, the real part of the cross-spectrum is used to obtain this figure. In either case the cross-spectrum is used, and two non-correlating sources (the self-noise of the microphones) will result theoretically in a zero output. Practical measurements have been performed for the p-u probe (Figure 4-29), and the p-p probe used (Figure 4-30). Both probes were placed in a

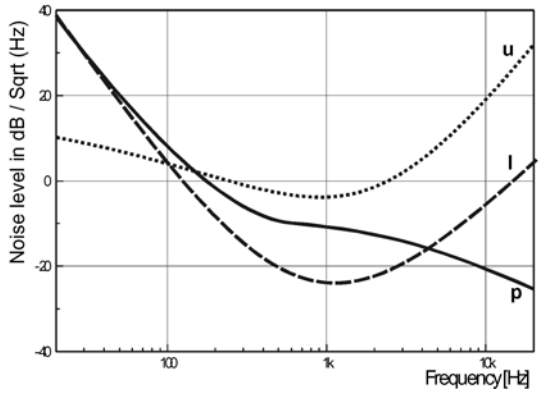

Figure 4-29: Measured noise levels of ½-in p-u probe. Noise levels of sound pressure microphone (──) in dB SPL (re 20e-6 Pa)/Hz^{½} , microflown (···) in dB SVL (re 20nm/s)/Hz^{½} , and sound intensity signal (─ ─) in dB SIL (re 1pW)/Hz^{½}.

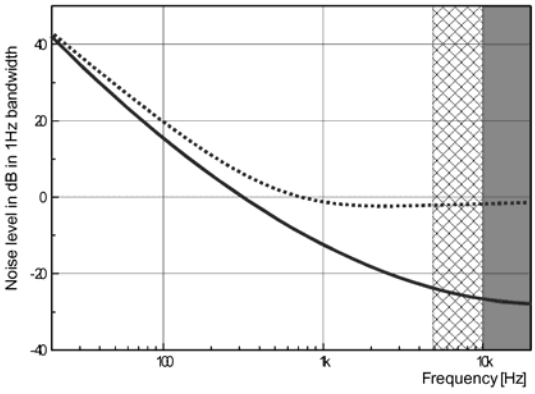

Figure 4-30: Measured noise levels of ½-in p-p probe. Noise levels of sound pressure microphone (···) in dB SPL (re 20e-6 Pa)/Hz^{½} , sound intensity signal (──) in dB SIL (re 20nm/s)/Hz^{½}. From frequencies above 5 kHz ¼-in microphones should be used so that self-noise of intensity determination as displayed here will no longer be valid. For frequencies above 10 kHz no intensity measurement can be performed.

completely silent environment and the intensity output was measured. Note that the measurement shown in Figure 4-29 is of an earlier version microflown (Raangs et al., 2001a) and does not reflect the current state and performance of modern microflowns. For more recent measurements see section 2.8, and (Microflown Technologies, 2004).

4.9 Discussion and Conclusions

Sound intensity can be measured using different techniques using as the p-p and p-u probes. This chapter dealt mainly with the latter p-u method whereas the differences are shortly described. Since the methods are such different, the given comparison is far from complete but clearly both techniques have their own advantages and disadvantages.

In the far field, sound intensity can be measured using the p-u probe and a conventional soundcard since in this situation errors due to phase mismatch are not very critical. In this sound field, the pressure and particle of interest are mainly in phase so that the sound intensity can simply be obtained out of the cross-spectra between the two sensor (p and u), as shown for the measurements performed.

The main advantage of the p-u probe versus the p-p probe is the fact that measurements over the whole frequency range can be made at the same setting, without changing the probe itself. The main disadvantage is the calibration of the p-u probe. Because the two signals measure two different acoustical properties, it is not possible to use the same method for both sensors unless the sound field is known well.

The combination of p-u probe and software creates an affordable and easy-to-use intensity-measuring device. Other acoustical parameters, such as reactive intensity, phase of sound field, energy density, and specific acoustic impedance, are being calculated without extra effort because they are also obtained from the auto- and cross-spectra of the pressure and particle velocity signals.

Other main advantages are the small size which can be obtained since the microflown particle velocity sensor is very small. Especially a three-dimensional sound intensity probe based on the microflown technique is much smaller than commercially available three-dimensional p-p probes. The three-dimensional p-u probe can therefore be used very close to the surfaces of products of interest. The smaller size will also induce less influence on the sound field itself since it is less of an acoustical obstacle. Although the three small particle velocity sensors are not always positioned perfectly orthogonal, with use of a three-dimensional calibration we can account for that. For many applications this will however not be required. It is furthermore expected that modern fabrication techniques will enhance the acoustical alignment of commercial microflown based sound intensity probes.

Chapter 5
Mapping of the Sound Field in different types of sound fields

5.1 Introduction

This chapter describes the various measurement methods and applications of mapping the sound field using the microflown in different types of sound fields.

With “mapping of the sound field” is meant the procedure of carefully catching properties in the sound field with the purpose of computing properties of the sound sources.

The chapter is divided in different sections depending on the type of sound fields. The types of sound fields can be separated into: Far Field and Near field type of sound fields. A special class of near field is know as the very near field (Bree de et al., 2004;Bree de et al., 2005). Hydrodynamic near field (Fahy, 2001) might have a close resemblance to the very near field such as described in section 5.8. Readers more familiar with the first term can read hydrodynamic near field for very near field in this thesis.

The far field is defined as the region sufficiently far from a specified source so that the sound pressure decreases as $1/r$ with distance, r, measured from the centre of the source, and for which the instantaneous particle velocity approaches $1/\rho_0 c$ times the sound pressure.

In the far field the relation between pressure and particle velocity is known as well in amplitude as well as in phase, taken the acoustical impedance of the medium is known. The far field is therefore very convenient for use in (1) calibrating the particle velocity sensor against a reference pressure microphone as well as for (2) comparing the measurements performed using a particle velocity sensor with a reference microphone.

The main difference between the microflown as particle velocity sensor and a pressure microphone in the far field is its directivity. The microflown has a typical figure of eight directivity pattern, whereas most pressure microphones are omnidirectional.

In the near field the $1/r$ law does not apply. In this part of the sound field the sound level varies from point-to-point because of the radiation pattern of the source.

The very near field is defined as the sound field at a position much closer to the source than the size of the source itself (Bree de et al., 2004). At these short distances from the sound source, it can be shown that in the very near field the normal surface velocity is almost equal to the particle velocity, which is frequency independent and almost independent of distance. The sound pressure however is suppressed and almost independent of place. The relationship between the normal surface velocity and the pressure in the very near field is frequency dependent (Bree de et al., 2004).

5.2 General introduction Near field

The near field is defined as the region surrounding a finite source, radiating at a given frequency, under free-field conditions, within which far-field conditions do not apply (Morfey, 2001). This is the region of space within a fraction of a wavelength away from a sound source. According to this definition, the outer boundary of the near field region varies inversely with frequency. Basically this is the region where the sound pressure does not obey the $1/r$ law and the particle velocity is not in phase with the sound pressure. Important dimensions are distance *r*, the size of the source (radius a or typical length L) and the wavelength λ (or combinations such as r/λ and a/λ), see for example Beissner (Beissner, 1982).

Measurements are made in the near field of the source surface, or less than a wavelength away, to capture the localized information about the sources. The localized information contains what are called evanescent waves, allowing NAH to have subwavelength source resolution (Dumbacher et al., 1998). In the near field the diffraction pattern differs substantially from that observed at a large distance. Therefore, the near field will contain more information on the vibrating surface than the far field. In the far field only radiating components can be measured, while near the surface also locally existing distortions in the sound field can be measured. These locally non-radiating sound waves are known as evanescent waves.

The sound field should be measured with a high accuracy. In principle it is not of importance whether p or u is measured, since if $p(x,y,z)$ is known, also $u(x,y,z)$ is known, by means of the force- and continuity equations. In literature often pressure-measurements are reported. In this thesis several examples are worked out where it is better to determine u instead of p, or to determine the product of p^*u or $u_i^*u_j$ or $u_i^*u_i$.

The main quantity for choosing p, u, p^*u or $u_i^*u_j$ is the S/N ratio. In fact there are a number of relevant quantities: S_p, S_u, N_p, N_u, S_{pu}, N_{pu} and so on, or the self-noise, as introduced in Chapter 1, which determine what is the best (S_p = signal pressure, N refers to noise, S_{pu} = signal of product $p^*.u$). In Chapter 3 an example was worked out, where the noise of a cross-spectrum was lower than the noise of the autospectrum.

In Figure 5-1 and Figure 5-2 (copies of Figure 2-57 and Figure 2-58) the self-noise is plotted as a function of frequency for the sensors we have used. The figure shows that at low frequencies (in Figure 5-1 at 700 Hz for the 0.5 inch p-u probe and, in Figure 5-2 at roughly 500 Hz for the three-dimensional p-u probe) the self-noise of the u-sensor is lower than the self-noise of the p-sensor. The self-noise in Figure 5-1 and Figure 5-2 of the microflowns are given in dB PVL (ref. 50 nm/s) in 1 Hz bandwidth; the self-noise of the microphone is given in dB SPL (ref. 20 μPa) in 1 Hz bandwidth. Of course this (crossing) frequency will depend on the specific characteristics of the sensors, but it is an empirical rule that the self-noise of the microflown is at low frequencies lower than the self-noise of the p-sensor, so there will always be such a “crossing” frequency. For frequencies where the self-noise of the u-sensor is much higher than that of the p-sensor the advantages to use a u-sensor no longer hold.

As was shown earlier (Chapter 3) the noise in the cross-correlation spectrum can be much lower than the noise in the p- or u-sensor. In some situations therefore the cross-spectrum gives the best signal to noise ratio.

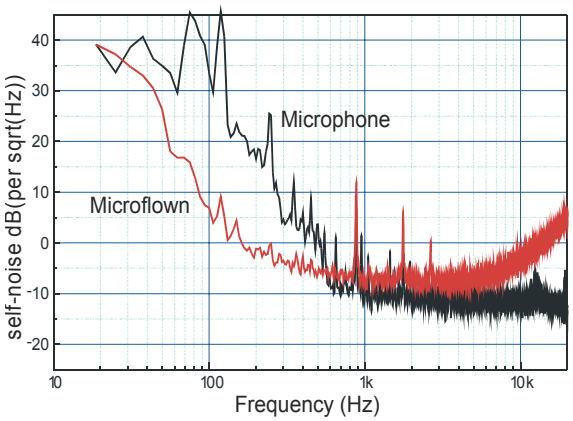

Figure 5-1: Self-noise of the 0.5 inch p-u probe signals given in sound level per (Hz)^{½}.

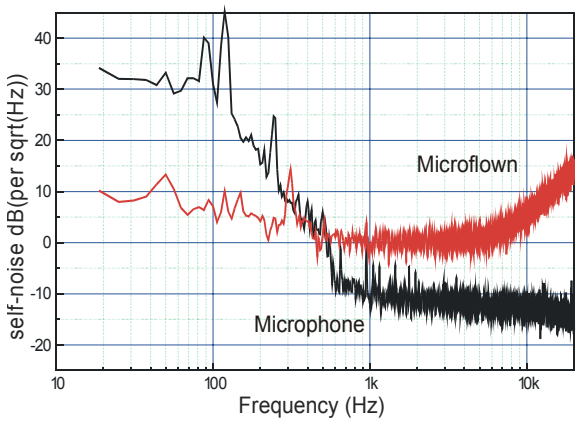

Figure 5-2: Self-noise of a modern three-dimensional p-u probe signals given in sound level per (Hz)^{½}.

Table 5-1 shows results of a simple experiment where the excitation is decreased in two steps of 36 dB (0 dB → -36 → -72 dB). The sound source was a hole in a baffle; the excitation is done by a loudspeaker behind the baffle. The coordinate system is taken such that $z = 0$ coincides with the plane of the baffle with dimensions of 0.22 x 0.30 m^2. The p- and u-sensor were positioned near the hole at a (z-) distance of 0.025 m.

CoolEdit® has been used to acquire the signals and for filtering the signals over the frequency range of 380 Hz - 420 Hz using a 16th order band pass filter. The auto- and cross-correlations are calculated in the time-domain over a time sequence of 25 seconds.

Ideally, the signals will be attenuated with the same amount as the original signal sent to the sound source. If the pressure and particle velocity signals are below a certain level, noise in the measurement (self-noise and acoustical noise) will cause the auto- (and cross-correlations) to reach a lower limit. Table 5-1 shows the order in which noise limits the level for which the sensor still yields results above the noise floor. This order equals:

$$U_i U_j > P U_i \geq U_i > P \tag{5.1}$$

meaning that the cross-correlation (or cross-spectrum) between two particle velocity components contains less noise than the cross-correlation between pressure and the particle velocity. The autocorrelations are worse since uncorrelated noise is not removed. The autocorrelation of the particle velocity contains less noise than for the pressure in the given situation.

Table 5-1: Measured Auto- and Cross-Correlations of pressure, and particle velocity for three different levels using 25 second of data using a microflown USP probe at 0.025 m distance from a monopole sound source (see Figure 5-4) for two different sound levels with reference to another measurement (0 dB).

excitation / signal	Attenuation (dB)	
	-36 dB	**-72 dB**
$\mathbf{U_x}$	-33.5	-37.8
$\mathbf{U_y}$	-35.6	-44.3
$\mathbf{U_z}$	-35.6	-48.9
P	-29.0	-30.3
$\mathbf{PU_x}$	-35.4	-46.0
$\mathbf{PU_y}$	-36.0	-44.2
$\mathbf{PU_z}$	-36.0	-44.2
$\mathbf{U_xU_y}$	-35.9	-48.2
$\mathbf{U_xU_z}$	-35.9	-51.3
$\mathbf{U_yU_z}$	-35.6	-60.6

The results given in Table 5-1 are just an example from several experiments, which were done. It is not a general rule that the particle velocity measurements give better results than the measurements of the pressure. In the next five sections experimental results are discussed, which show that in some situations p, or u, or $p^* u$ has the preference.

To illustrate the various experimental results a number of model calculations have been performed. In this model a sound source is taken as a point source, radiating spherical waves with $p = (A/r)\exp(-ikr)$ and $u_r = (1/\rho_0 c)\ (A/r)\ (1+1/(ikr))\ \exp(-ikr)$, with r the distance to the source. The total pressure and particle velocity are obtained by a simple summation of the pressure and particle velocity of the separate (point) sources. As a signal, $s(t)$, white noise is taken in a ⅓-octave band with centre frequency f_c and sample frequency f_s = 6000 Hz during about 1 sec. The noise at each scanning point and for each sensor is modelled as an independent white noise signal (⅓-octave band, f_c, f_s and 1 sec.). Possible phase differences because of a difference in travelling time $\Delta t = (r_1 - r_2)/c$ are ignored. The purpose of these calculations is not to explain the experimental results in detail, nor to explain that the experiments do confirm the calculations. These

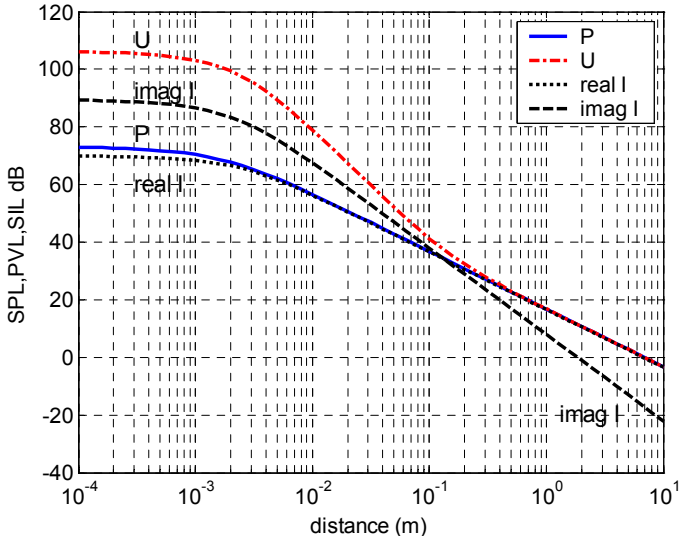

Figure 5-3: Example pressure and particle velocity and intensity versus distance, here for disc of radius 0.003 m in an infinite baffle at 400 Hz at the axis (Beissner, 1982).

calculations serve only as an illustration to the experimental results and to show the importance of the signal to noise ratio.

5.3 Velocity.(ρc) > pressure, kr <1

5.3.1 A single monopole

Consider as an example a simple point source, which emits spherical waves, then the relation between particle velocity and pressure can be written as: $u\rho_0 c = p\left(1+1/\mathrm{i}kr\right)$, thus for $kr<1$: $u\rho_0 c > p$. If the self-noise (see Chapter 1) of both sensors are about equal, a measurement of u is preferred. This near field effect is shown in Figure 5-3. In Figure 5-3 the calculated pressure (SPL(dB)), particle velocity (PVL(dB)), and sound intensity I (SIL(dB)) are plotted against the distance for a small piston in a baffle radiating at 400 Hz. The figure clearly shows that in the near field ($r_\mathrm{n} << 0.2$ m at 400 Hz), the particle velocity (times $\rho_0 c$) is larger than the pressure. In Figure 5-3 it is also shown that the particle velocity in Pa*, thus times $\rho_0 c$, equals the pressure, in Pa, in the far field ($r_\mathrm{n} >> 0.2$ m at 400 Hz). Furthermore we can notice that the sound intensity is mainly imaginary in the near field and (mainly) active in the far field.

In the experiment a measurement scan was performed at 40 mm over an area of 0.15 x 0.15 m^2 using a Dantec Dynamics three-dimensional traverse system as shown in Figure 5-10. As a sound source a monopole has been used. A

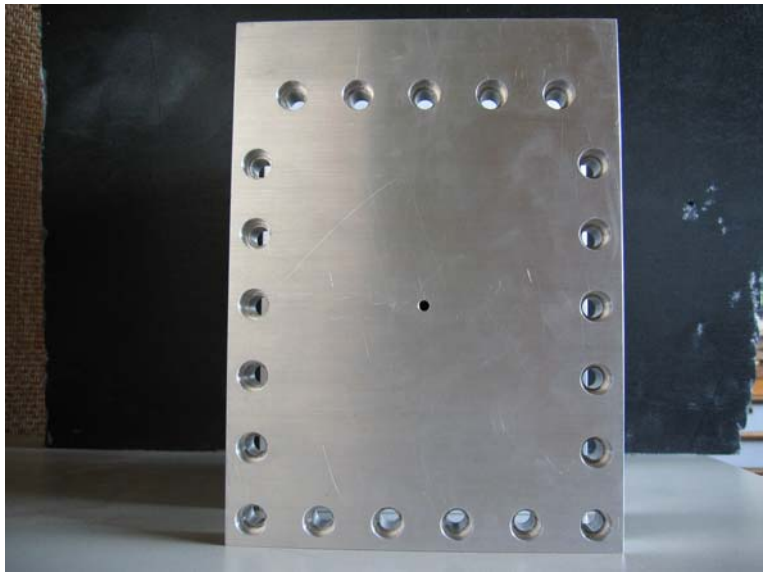

Figure 5-4: Photograph of the source used. The source consists of an aluminium box (thickness 30 mm). A hole (radius 3 mm) is driven by a midrange loudspeaker.

loudspeaker was positioned at the back of the baffle. The hole (radius 3 mm) in the baffle in front of the loudspeaker was then used as a monopole source. Sound radiation by the baffle and from the rear end of the baffle is reduced since the front plate was made of aluminium with 30 mm thickness, and mounted in an aluminium box of 30 mm thickness. White noise was fed to the loudspeaker whereas a high-pass filter was applied to reject electrical power at low frequencies. Two measurements scans were taken for two different power levels fed to the loudspeaker, with 15 dB differences between the two levels.

Measurements are performed using prototype of the so-called Ultimate Sound Probe (USP) supplied by Microflown Technologies BV, see Figure 5-5. The

Figure 5-5: The used three-dimensional p-u probe.

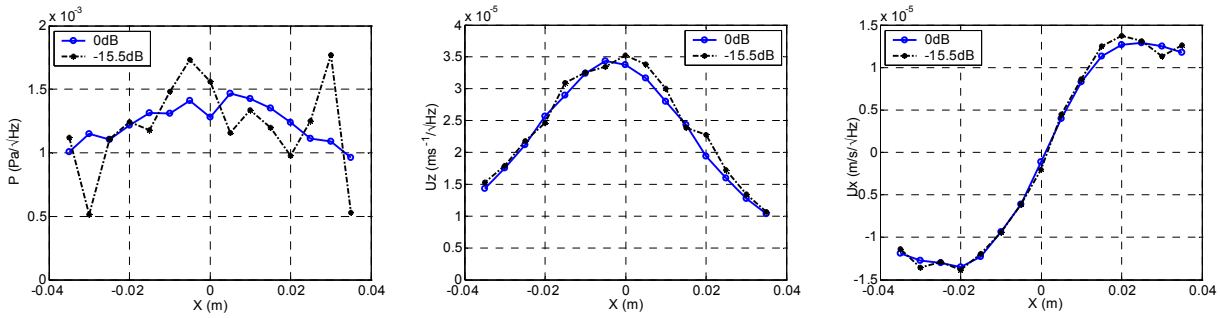

Figure 5-6: Measurement scan along the *x*-axis for the pressure (left), particle velocity in the *z*-direction (middle) and *x*-direction (right) for two different sound levels at 140 Hz for a monopole sound source. For convenient comparison of the different levels, the measured values are corrected for the attenuation.

electronics of the USP probes was powered using a 24.0 volt DC from a Microflown transformer (Westminster Type: A7-1261-1533). An amplifier (25 dB) was used to amplify the signals of the p- and u-sensors before being measured by the DSPT Siglab signal analyser.

Figure 5-6 show some experimental results (p, u_z and u_x scans) for two excitation levels of a scan along the horizontal axis at 40 mm from the baffle over a frequency band of 140 Hz ±10 Hz. The same orientation is used as described in section 5.3.2, see Figure 5-8. The measured values are corrected for the attenuation. Figure 5-6 clearly shows that the pressure p the points do not show a smooth curve along the *x*-axis, while for u_z (and u_x) the points do show a smooth curve at the same sound levels at this frequency.

To illustrate these experimental results some model calculations have been done. If we add noise to the noise free simulation (in time domain), it can be shown that this has more effect in the pressure than particle velocity.

At the different scan positions a time signal has been constructed.

$$p(t,f) = \frac{a(t)e^{-ikr}}{r} + n_i(t) \tag{5.2}$$

$$\rho_0 c\, u_z(t,f) = \frac{a(t)z}{r^2} e^{-ikr}\left(1 + \frac{1}{ikr}\right) + n_i(t) \tag{5.3}$$

$$\rho_0 c\, u_x(t,f) = \frac{a(t)x}{r^2} e^{-ikr}\left(1 + \frac{1}{ikr}\right) + n_i(t) \tag{5.4}$$

with $a(t)$ and $n_i(t)$ (different) white noise signals in a ⅓-octave band with centre frequency of $f_c = kc/2\pi$. At each scanning point and for each sensor (p, u_x, and

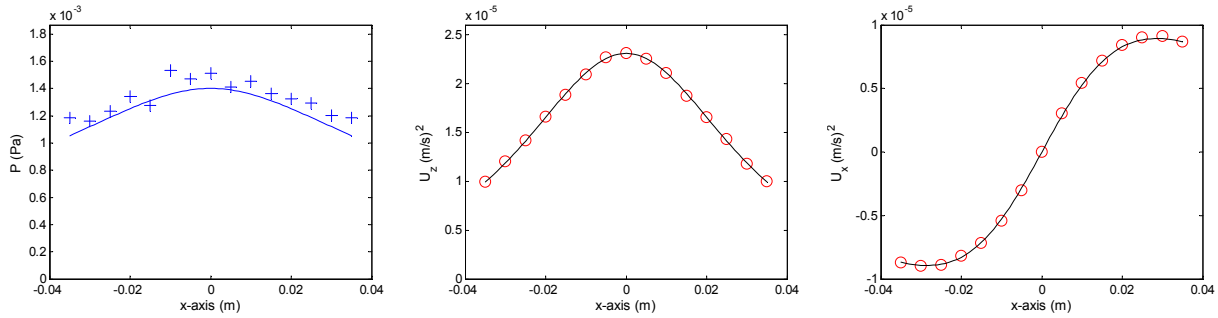

Figure 5-7: Simulated results in time domain for a centre frequency of 200 Hz. Left: Pressure *p*, middle: u_z, Right: same noise added to the u_x. $SNR_{art} = 3$ (see equations(5.2), (5.3), and (5.4)).

u_z) a different white noise signal $n_i(t)$ is taken, with $n_i(t) = C\,a(t+\Delta t)$, where C is a constant for the various sensors, and Δt is chosen random for each sensor and position. The time Δt is chosen sufficiently large to insure that there is no correlation between the different noise signals. The autospectrum of the different noise signals $n_i(t)$ are related to the autospectrum of $a(t)$ via an artificial signal to noise ratio $(S/N)_{art.}$ of the pressure at a point just above the source, where $r = r_0 = z$:

$$(S/N)_{art.} = \frac{1}{r_0}\frac{\sqrt{\overline{a^2(t)}}}{\sqrt{\overline{n_i^2(t)}}} \tag{5.5}$$

At a position just above the sound source it is the pressure as caused by the signal $a(t)$ divided by the noise $n_i(t)$. Of course the *S*/*N* ratio of the pressure further away of the source is lower than the "artificial" *S*/*N*. However, it does not mean that the *S*/*N* ratio of a component of the particle velocity, just above the sound source is equal to $(S/N)_{art.}$. The artificial *S*/*N* is in fact a measure of the ratio of the excitation of the source and the noise of the sensor.

For each position i we used independent white noise with the same stochastical properties. For simplicity, $\rho_0 c$ can be taken as 400 Pa s m^{-1}. Notice that the time signal is only correct for the given frequency, and a small frequency band around the centre frequency. For example, a ⅓-octave filter fourth order Chebyshev might be used before calculating the autospectrum using the Welch method. In Figure 5-7 some results of the model calculations are shown.

Notice that although the artificial signal to noise ratio is equal for pressure *p* and u_x and u_z (particle velocity in the *x*- and z-direction), the results of the particle velocity are visually less noisy. The $(SNR)_{art.}$ is 3 (~9.5dB) in Figure 5-7. The

mean SNR in the simulation are however, 9.1 dB for the pressure, and 24.0 dB for the particle velocity in the *z*-direction and 15.8 dB in the *x*-direction.

5.3.2 Three small monopoles coherently driven

Measurements are performed using three small sources (see Figure 5-8) in a baffle as sound source. The measurements are performed at a close-range of several millimetres. As acoustical sensors a small miniature microphone (Microtronics 8001) and two microflowns were positioned as close as possible to each other as shown in Figure 5-9. The acoustical probes are connected on a long beam connected to a three-dimensional traverse system (Dantec Dynamics) as shown in Figure 5-10. Measurements are performed on a grid of 60 x 26 points with 3 mm distance between the measurement points on the grid. The centre of the acoustical source was about $y = 3.9$ mm (vertical) and $x = 0$ mm.

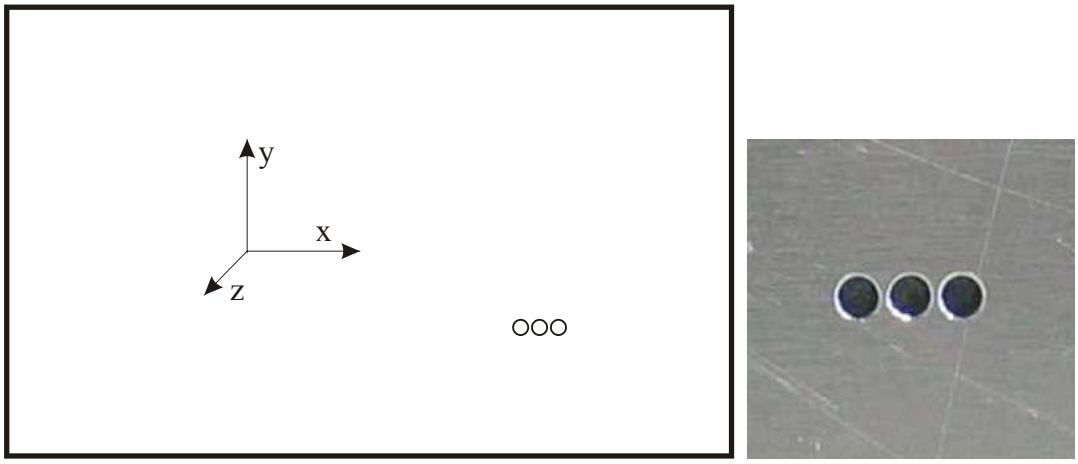

Figure 5-8: Left: Systematic view of the three sound sources used. The holes have a radius of 1 mm and there is 2.5 mm between the centres of the neighbouring holes. Right: Photograph of the three small sound sources.

A (periodic) chirp signal was sent to the loudspeaker. Each measurement was triggered on the signal. Note however that although the chirp signal yields good results using the microphone, a chirp is not a signal expected from a noisy source. The chirp signal does contain all frequency components, and is capable of delivering much power in each frequency; the maximum pressures and particle velocities can be high, especially compared with other stationary random signals.

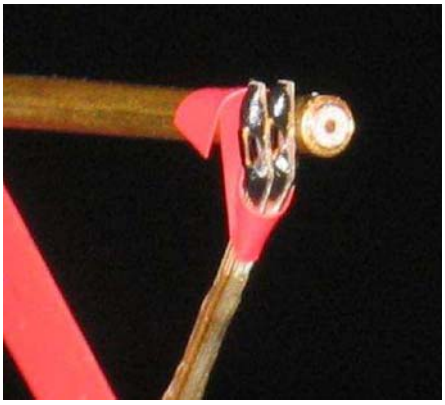

Figure 5-9: Pressure microphone (Microtronics 8001) and the two particle velocities sensors used. The three sensors are positioned as close as possible to each other.

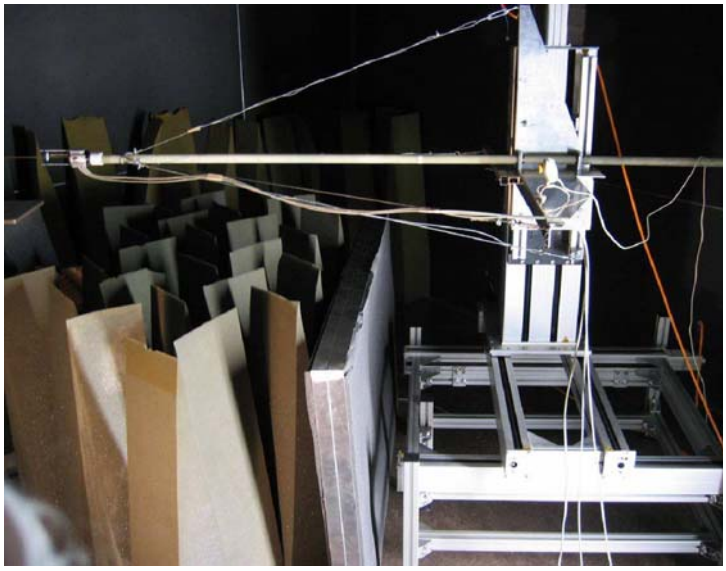

Figure 5-10: Traverse system used positioned in a semi-anechoic room (courtesy Philips Applied Technologies (formerly CFT)).

Figure 5-11, Figure 5-12, Figure 5-13, and Figure 5-14 show some experimental results for p^2 and u^2 for centre frequencies of 87.5 Hz, 180 Hz, 6870 Hz, and 9681 Hz. In the figures, the measured levels are shown for the pressure and the two particle velocity sensors.

For low frequencies, the graphs for u^2 are much better as can be seen in Figure 5-11 and Figure 5-12. For higher frequencies, the pressure measurements are better as is shown in Figure 5-13 and Figure 5-14.

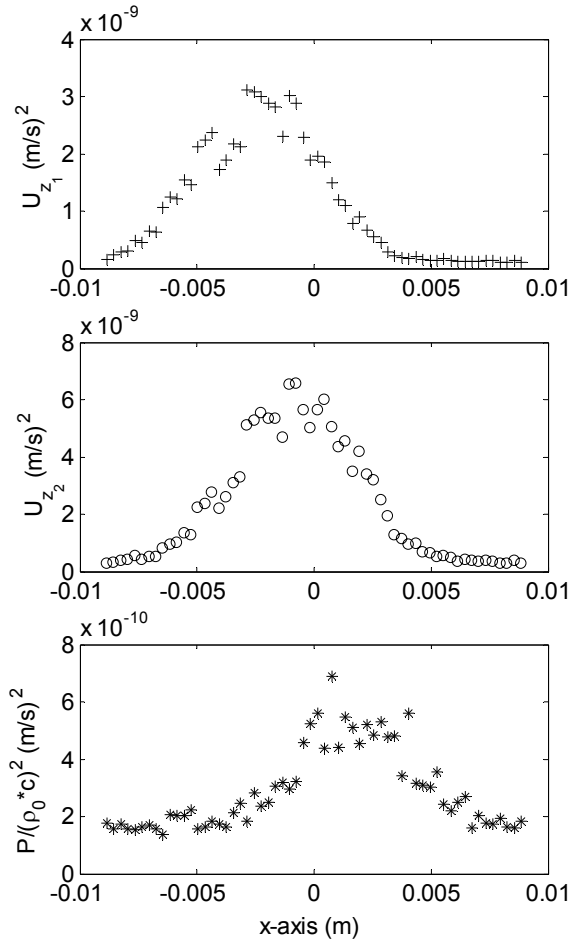

Figure 5-11: 87.5 Hz ±31 Hz, 2mm distance, y = 3.9 mm.

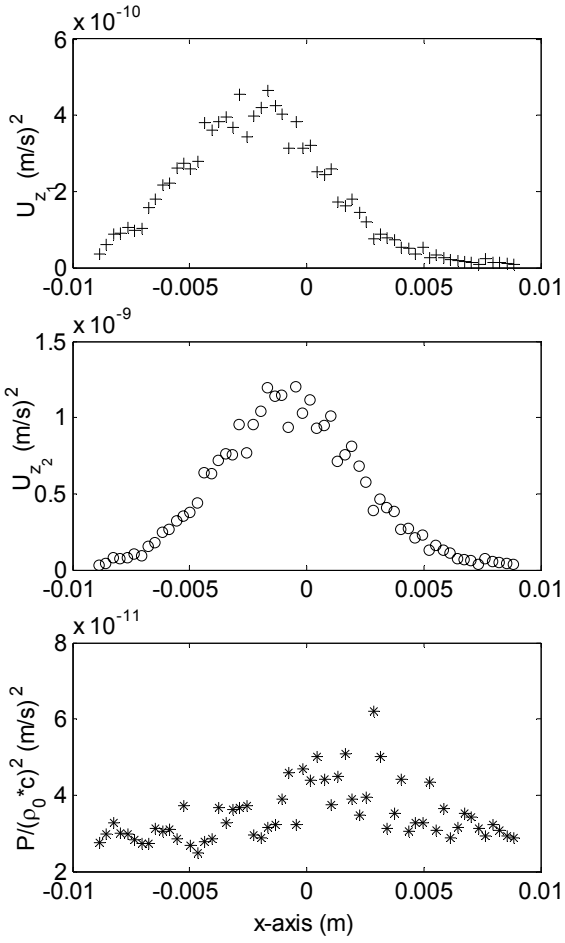

Figure 5-12: Frequency 180Hz ±62Hz, distance 2 mm, at y = 6.3 mm.

In Figure 5-15 a simulation of the measurement is shown for a centre frequency of 200 Hz with bandwidth of 40 Hz. In the simulation, the relation between source and sound field was computed for the centre frequency using the Rayleigh integral (Fahy, 2001;Williams, 1999). Using the calculated relationship (for the centre frequency) and a time signal, which consists of band filtered white noise, a time signal was constructed for the pressure and particle velocity. Band filtered white noise was added for each "measurement" simulating noise in the measurement. In Figure 5-15 20 dB more noise was added in the particle velocity than in the pressure (divided by 415).

In Figure 5-15, also the cross-correlation out of two noise particle velocity simulations are shown. Although the simulation clearly shows that the cross-

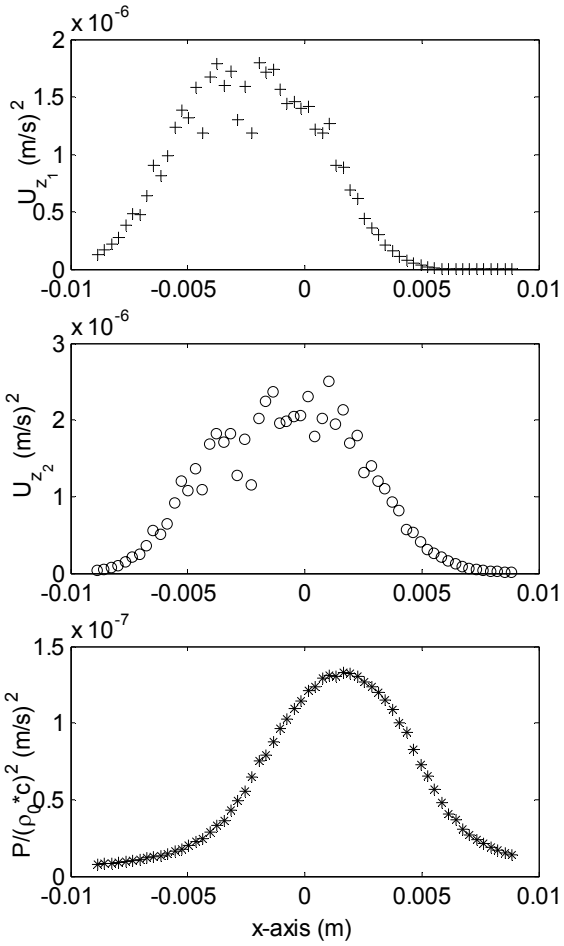

Figure 5-13: 6870 Hz ±625 Hz, 2 mm distance, y = 3.9 mm.

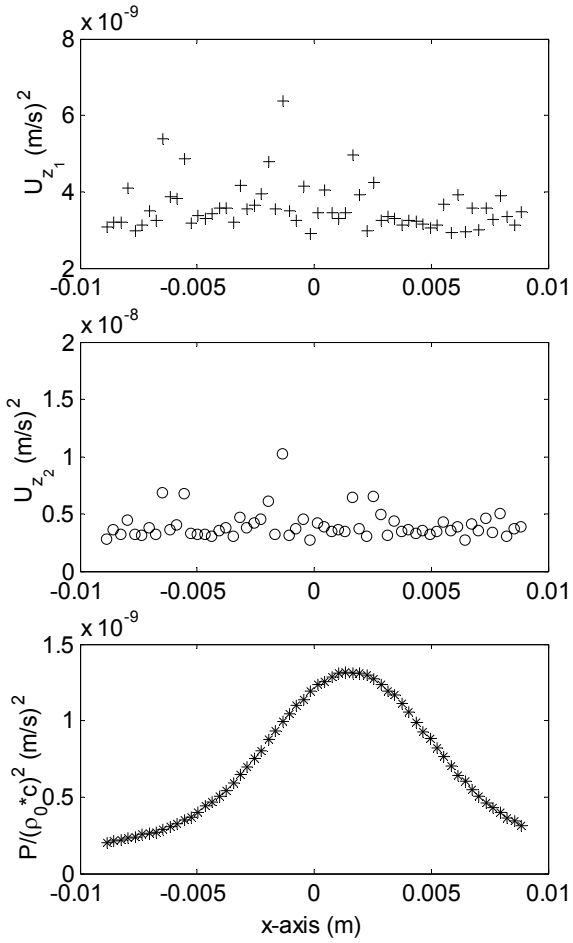

Figure 5-14: 9681 Hz ±312Hz, 3 mm distance, y = 3.9 mm.

correlations are less noisy, this effect could not be shown in the true measurements shown in Figure 5-12.

The simulated squared pressure in Figure 5-15 clearly shows why the source is not visible in the pressure measurements shown in Figure 5-12 at the given frequency. The measured pressure signals are approximately 20 dB's higher then the simulated (maximum) pressures at these positions. Note however that the noise levels, as shown in Figure 5-12, are explained by a (self)noise level which was approximately 2.5 dB lower than that for the particle velocity sensors.

The noise in the simulated pressure, as shown in Figure 5-15, is about 10 dB (ref 2.10^{-5} Pa/$\sqrt{\text{Hz}}$). Note however that Figure 5-15 is scaled so that it can be compared with Figure 5-12 so that the comparable noise would be 10 dB less due to the difference in bandwidth.

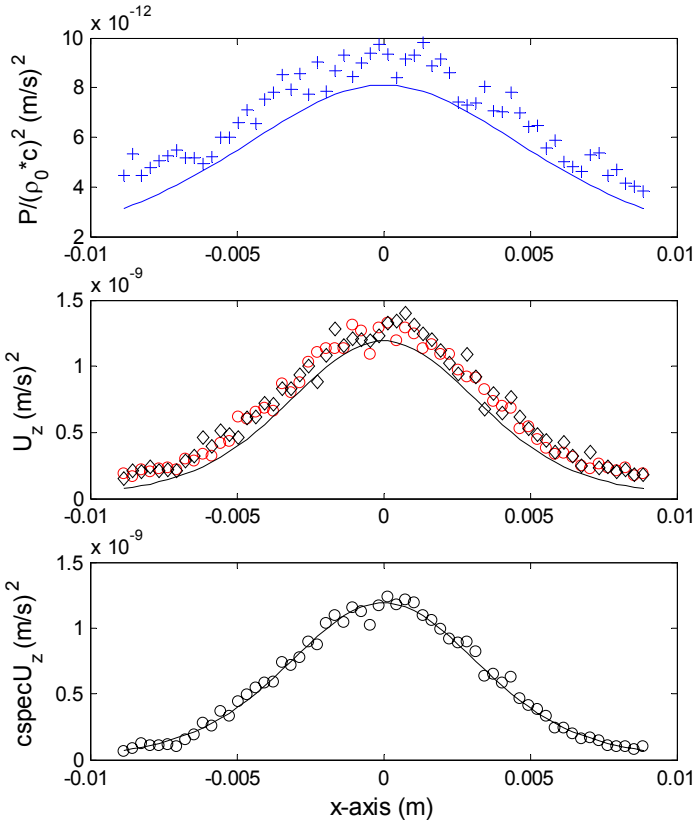

Figure 5-15: Simulation of the measured (squared) pressure divided by the specific impedance (above), particle velocity in the *z*-direction (middle), and cross-correlation of two measurements of u_z, at 200Hz ± 20Hz along *x*, for *z* = 2 mm and *y* = 6.3 mm. In the example 20 dB more noise was added to the particle velocity "measurement" than to the pressure "measurement". The lines represent the solutions without added noise.

5.4 Source configuration

The source configuration and/or the different excitation can result in a high value of the $\rho_0 c\, u/p$ ratio or in other situations to a low value of $\rho_0 c\, u/p$. Consider as an example two point sources at a short distance from each other. If they are excited by the same signal the ratio $\rho_0 c\, u_{\|}/p$ ($u_{\|}$ is the in-plane particle velocity) will be smaller than one at a position between the two sources, since there $u_{\|} \approx 0$. If on the other hand the two sources are excited by signals with reversed polarity i.e. a positive signal $s(t)$ to one source and a negative signal, $-s(t)$, to the other source, the ratio $p/\left(u_{\|}\rho_0 c\right)$ at a position between the sources will be quite small ($p \approx 0$ at that position). A number of experiments have been performed with a configuration of four sources with centres located at (x_1,y_1,z_1) = (0,-0.020,0) and (x_2,y_2,z_2) = (0,0.020,0), (x_3,y_3,z_3) = (0.019,0.005,0) (x_4,y_4,z_4) = (0.019,-0.005,0). The sources were holes with a diameter of about 3 mm in a thick plate (30 mm);

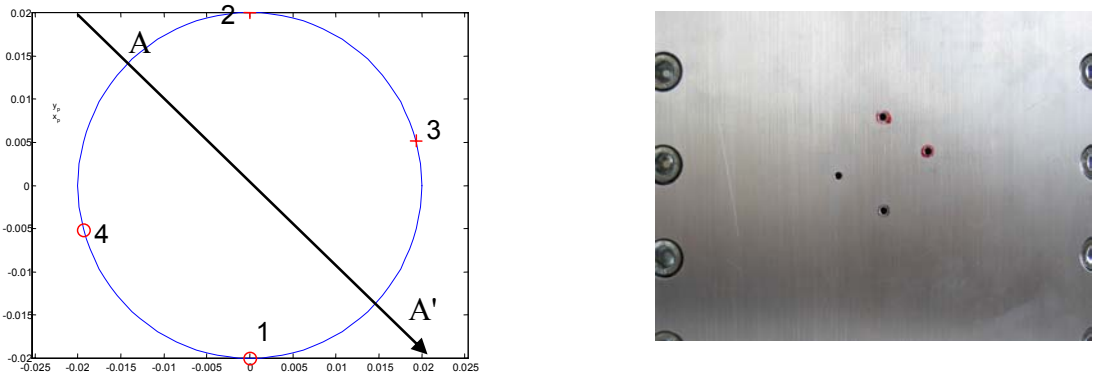

Figure 5-16: Positions of the sound sources as in measurements. The sources 1 and 4, and 2 and 3 are drive separately and can be used in or out of phase. Right a photograph is shown of the four volume source. The red marker shows the two sound sources that are in-phase.

see Figure 5-16 and the same orientation as in section 5.3.2 , see Figure 5-8, has been used.

A two-dimensional scan in a plane parallel with the source surface at a distance of 0.002 m visualizes the dipole-source configuration, as sketched in Figure 5-16. In this experiment, white noise was fed to the four sound sources. The four sound sources are grouped into two pairs, 1 and 4, and 2 and 3 (see Figure 5-16). The sound sources in a pair are in-phase, whereas the two pairs are out of phase with each other. In Figure 5-17, left, the experimental results of such a scan with a sensor measuring the u_z component of the particle velocity, is shown. On the right of Figure 5-17 calculated results with a simple model of point sources is shown using the Rayleigh integral. Since u_z (and p) are low along the line AA' it is interesting to compare the one-dimensional scans for p, u_z and $u_{||}$ along this line

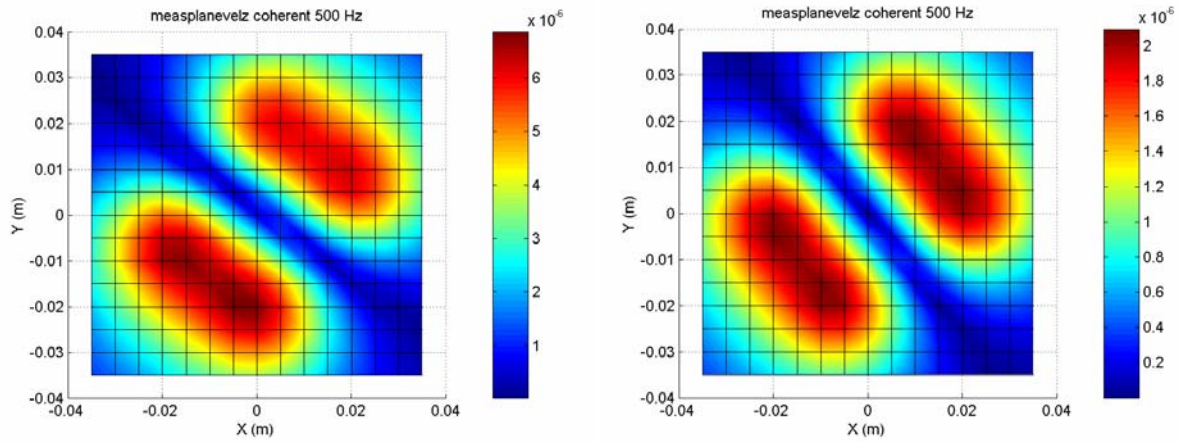

Figure 5-17: Measured (left) and simulated (right) particle velocity in the *z*-direction for the four sound sources (two coherent dipoles).

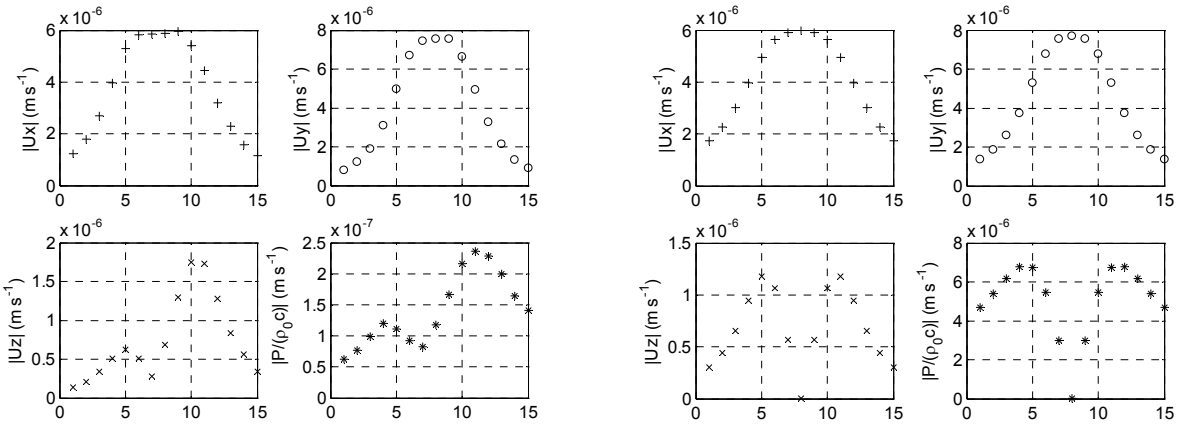

Figure 5-18: Results of a measurement (left) scan along A-A' (see Figure 5-16) for the dipole configuration for 1900 Hz. A simulation is shown (right).

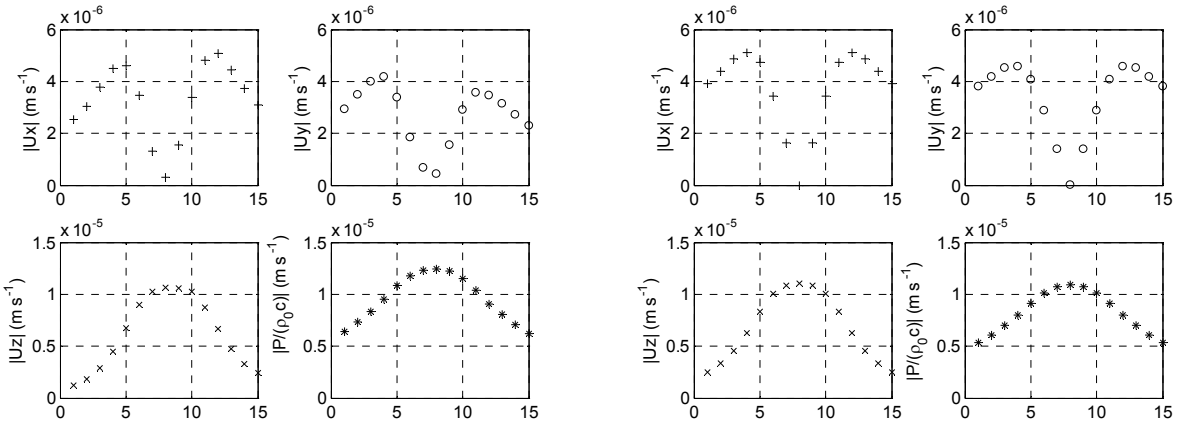

Figure 5-19: Results of a measurement scan along A-A' (see Figure 5-16) for the monopole configuration for 1900 Hz. A simulation shows the expected curves (right).

($u_{\parallel}$ is the modulus of the in-plane particle velocity $u_{\parallel} = \sqrt{u_x^2 + u_y^2}$.

In Figure 5-18 the measurements at positions between the dipoles are shown (scan-direction A-A' as shown in Figure 5-16). Position 1 represents (x,y) = (-3.5,+3.5) cm and position 15 represents position (x,y) = (+3.5,-3.5) cm. In Figure 5-19 the results of the same positions but now for the in-phase configuration are shown.

It can be seen from Figure 5-18 that in case of the dipole, the particle velocity in the y-direction (u_y) is the best measure of the sound field at these positions.

In case of the four monopoles (see Figure 5-19) the pressure and the particle velocities in the z-directions are good measures since they are large and contain less noise in this situation.

The curves in Figure 5-18 clearly show that for this source configuration better results are obtained using a u-sensor in plane, instead of a p-sensor. It should be mentioned that this effect is not caused by near field effects, where $u \gg p/\rho_0 c$ (see section 5.3) or by a better self-noise value, since these effects do not play a major role at a frequency of 1900 Hz.

Figure 5-18 clearly shows that a dipole configuration is a convincing example where the scanning of the sound field with a u-sensor works much better than using a p- sensor.

5.5 Structure of particle velocity

Irrespective of the S/N ratio's the scans of the particle velocities are often more structured than the scans of the sound pressure. This can lead to advantages for the reconstruction of the velocities at the source plane (Visser, 2003). Consider two sound sources at a distance from each other about equal to the scanning distance. The sound fields of the two sources will then overlap and the separate sources are difficult to recognize in the experimental observed scans. However, the scans of the particle velocity in the *z*-direction (direction perpendicular to the surface of the sources) have more structure than the scans of the sound pressure. Figure 5-20 and Figure 5-21 show experimental results for a configuration of two sound sources separated from each other at a distance of 0.04 m; the sources were holes with a diameter of 0.03 m in a thick plate. The excitation signals of the two sources were two, uncorrelated noise signals in a ⅓-octave band with centre frequency of 125 Hz. The Figure 5-20 and Figure 5-21 are copies of the Figure 5-30 and Figure 5-31 of section 5.7.3 (Druyvesteyn and Raangs, 2005b).

Plotted are the scans of the u_z component and the pressure for the case of two incoherent sources. The sound sources are positioned at x = 20 mm and x = 60 mm. The *p*-scan (see Figure 5-20) does not show two maximum values, thus the presence of two sources does not follow directly from this scan; the u_z scan (see Figure 5-21) clearly shows there are at least two sources.

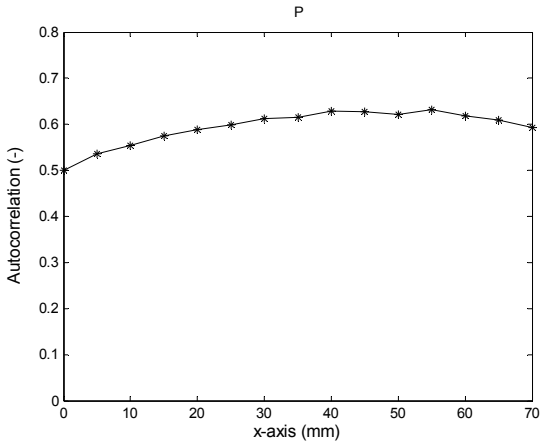

Figure 5-20: Normalized autospectra of the sound pressure p as a function of the scanning coordinate x for two uncorrelated sound sources. The x-scan was taken at $y \approx 0.5$ cm.

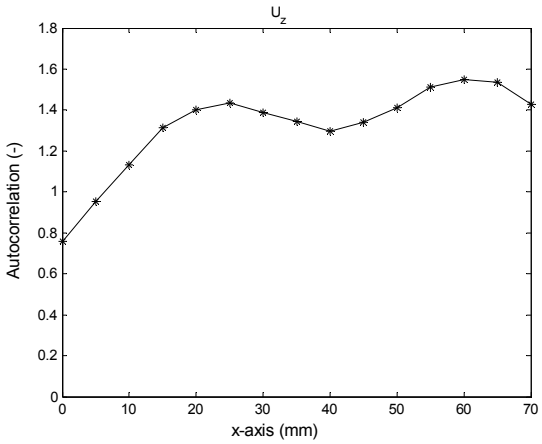

Figure 5-21: Normalized autospectra of the particle velocity component u_z as a function of the scanning coordinate x for two uncorrelated sound sources. The x-scan was taken at $y \approx 0.5$ cm.

This sharper structure of u_z, with respect to the structure of p, becomes clearer when the scanning distance to the source (z-direction) becomes small. Because there are not many experiments that show this difference in the behaviour between the particle velocity and pressure clearly, results of simulations are added. Examples of calculations with a simple model of two point sources at a distance of 0.01 m excited by the same signal (centre frequency at 200 Hz) are shown in Figure 5-22 and Figure 5-23. At for example a distance of 5 mm in Figure 5-22 it is clearly shown that the two sources are more obvious in the particle velocity u_z than in the pressure p. Figure 5-23 shows that the sound intensity ($p^* u_z$) behaves in between.

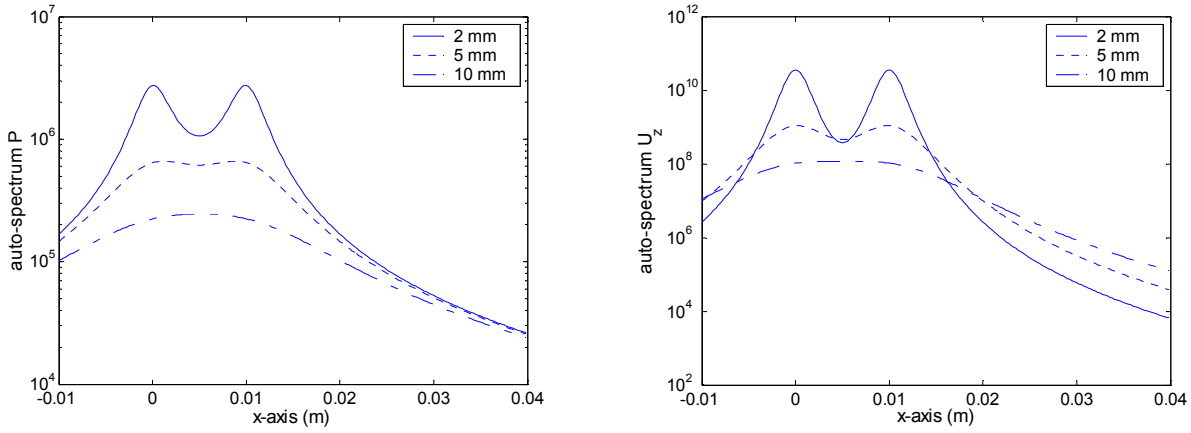

Figure 5-22: Pressure (left) and particle velocity u_z (right) calculated along a line at distances of 2 mm, 5 mm, and 10 mm distance from the source plane.

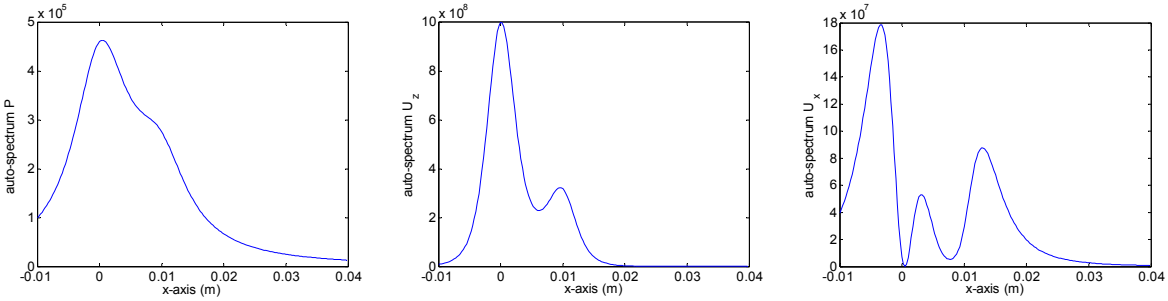

Figure 5-24: simulation of a scan in front of two sound source positioned at x =0 and x = 0.01 m at a distance of z-scan = 0.005 m). Source2 (at x = 0.01 m) is weakened by a factor half with reference to source 1 (at x = 0 m).

The particle velocity in the x-direction (in the direction of the scan) is shown in Figure 5-23 (left). The figure clearly shows a minima between the two sound sources (at x = 5 mm in Figure 5-23). At very close range the particle velocity in front of the two sound sources show a minimum (at x equals zero and plus 10 mm in Figure 5-23).

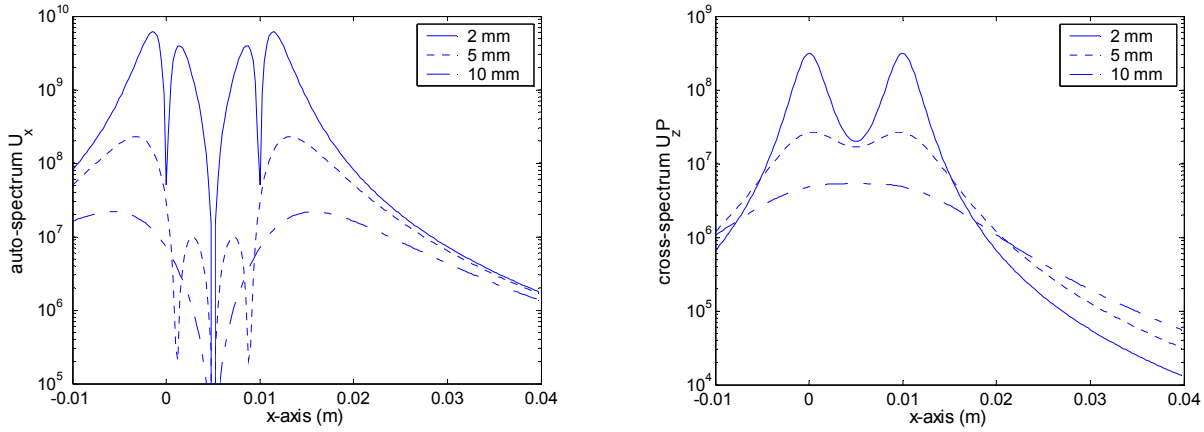

Figure 5-23: Particle velocity in the direction of the scan u_x (left) and the cross-correlation between pressure and particle velocity u_z (right) calculated along a line at distances of 2 mm, 5 mm, and 10 mm distance from the source plane.

In Figure 5-24 the pressure p and particle velocity u_z (out of plane), u_x (in plane) curves are shown for a scanning distance of 0.005 m and an excitation of one point source by a signal which is half the excitation of the other point source. This difference is seen in the curve of u_z, but hardly in the pressure p-curve.

In some of the examples discussed above the separation of different sound sources could hardly been seen in the pressure scans, in contradiction to the particle velocity scans. In the particle velocity scans, a clear separation of the individual sound sources could be recognized whereas these most details are lost in the pressure scans.

5.6 Weak sources

Consider a situation where $p \approx u\rho_0 c$, combined with an equal noise level, but that, due to the low excitation of the sources the S/N ratio's of p and u are so low that scanning with a p- or u- sensor does not give good results. In Chapter 3 lowering the noise level by taking the cross-correlation was discussed. This concept can now be applied to this situation.

In Figure 5-25 the autospectra of p and u and the cross-spectra of pu are plotted

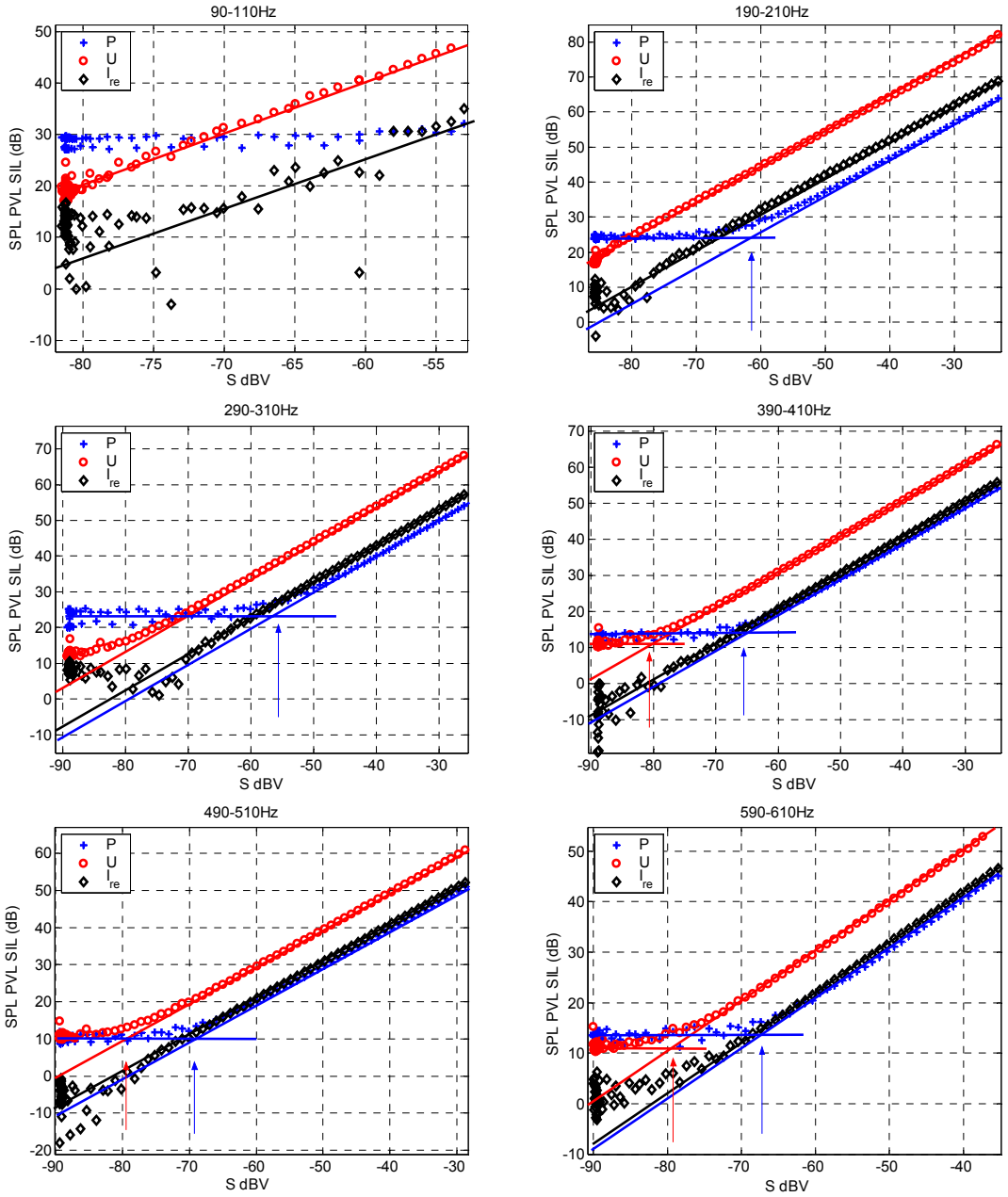

Figure 5-25: Pressure (blue + marks), Particle velocity (red circles), and the active sound intensity I_{active} (black diamonds) as function of sound source level measured at 5 cm in front of a small sound source (radius 3mm). The different figures represent different frequencies.

as a function of the excitation of the sources. Figure 5-25 clearly shows that the product of $p.u$ (or $u_i.u_j$ or $u_i.u_i$ see Table 5-1) still give reasonable results at low excitations, where the autospectrum of p or u are already independent of the excitation and about equal to the noise. Results displayed in Figure 5-25 are measured at a distance of 0.05 m in front of a monopole source in a baffle whereas the results in Table 5-1 are obtained at 0.025 m. It should be mentioned that inverse acoustics based on the cross-spectra is more difficult than inverse acoustics using the autospectra, but it appears to be possible (Roozen et al., 2002;Roozen and Scholte, 2003).

The experimental set up is shown in Figure 5-26. As a sound source a hole in a baffle was used, which was driven by a loudspeaker at the rear. Filtered random noise is sent to the monopole and simultaneously the inputs are recorded on the hard disk in volt using the Data Acquisition Toolbox in MATLAB with 20 bits resolution as shown in Figure 5-26.

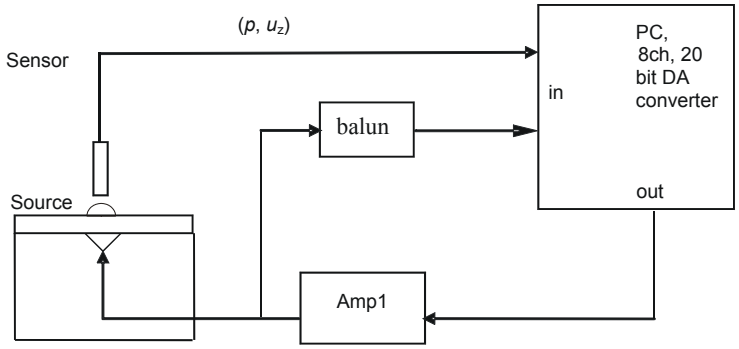

Figure 5-26: Measuring schematic Left: sound source and the half inch p-u sensor, right: the PC based data-acquisition system.

The logged data is then corrected for the sensors (absolute sensitivity and phase) so the data is in pressure and particle velocity. Furthermore, the data should be filtered using the same 24 dB/oct. filter or a much steeper filter. A steeper filter is designed to filter out the unwanted frequency components.

Figure 5-25 also shows that the microphone (Knowles type FG3329) fitted in the microflown USP probe has a larger self-noise in this measurement situation for the lower frequencies (< 400 Hz). Furthermore, the particle velocity measurement benefits from the fact that particle velocity times the numerical value of the specific impedance ($\rho_0 c$) are much larger than pressure. In case of 100 Hz, for example, the microflown can measure a small sound source which radiates 25 dB less power than the pressure microphone. For the frequencies of 200 Hz, 300 Hz,

400 Hz, 500 Hz, and 600 Hz, this was respectively: > 22 dB, ~30 dB, ~15 dB, ~10 dB, and 12 dB.

For frequencies above 400 Hz, the noise in the pressure measurement is less than or equal to the noise in the microflown sensor, but for the intermediate frequencies (400 – 1000 Hz) the microflown measurement still benefits from the fact that particle velocity times the acoustic impedance is still higher in the situation shown.

In Table 5-1 also the cross-correlations $u_i^*.u_j$ are considered. In that experiment these cross-correlations gave the best result.

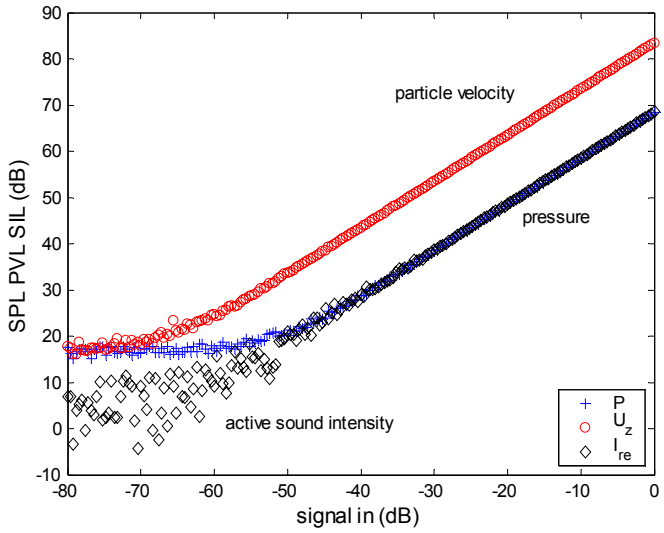

Figure 5-27: Simulation of the Pressure (+) and the particle velocity in the *z*-direction (o) in front of a small piston (radius 1 mm) at 5 cm distance for a centre frequency of 200 Hz.

In Figure 5-27 results from model calculations with one source is shown. The noise level of the p- and u-sensor are kept constant and equal, while the amplitude signal used as input for the driven piston was decreased.

In the simulation, a filtered white noise signal (200 Hz ± 20 Hz) was used which simulates the sound source. The relations between pressure, particle velocity, and source, calculated at the same frequency using the Rayleigh integral (Beissner, 1982;Fahy, 2001;Williams, 1999), was used to simulate the "measured" pressure and particle velocities. For each "measurement", a signal of 1 second with sample frequency of 6 kHz was used. In Figure 5-27 noise was added to the "measured" pressure and particle velocities. For each "measurement", the same signal was used whereas the added noise was randomized by taking a different section out of

a signal. For simplicity, the self-noise in the pressure and particle velocity measurement, in Pa and m s^{-1} (times 415), are equal in the given simulation.

Figure 5-27 shows that for a small source (radius 1 mm) at 200 Hz, a particle velocity sensor can be used to measure sound source which are 15 dB weaker at a distance of 5 cm than a pressure sensor with comparable self-noise and in case particle velocity is measured in the optimal direction.

Furthermore, the simulation again shows that for this experimental setup, the active sound intensity value (L_I (dB)) almost equals the pressure values (L_p (dB)). Also, it is shown that the noise in the active sound intensity is somewhat lower since the cross-correlation between two noise signals is used although the improvement is limited due to the small bandwidth and short time sequences used see also Chapter 3.

5.7 Incoherent Sources

In this section recent experiments are presented about scanning the sound field when incoherent sound sources are present. It is an example where using a u-sensor, instead of a p-sensor more relevant information about the sound field is obtained. These results will be presented at the Forum Acusticum conference in august 2005 in Budapest (Druyvesteyn and Raangs, 2005b) and are described in the journal of Acta Acustica United with Acustica (Druyvesteyn and Raangs, 2005a). The submitted journal paper is copied in this section.

5.7.1 Introduction.

In near field acoustic holography (NAH) (Maynard et al., 1985;Veronesi and Maynard, 1987;Williams, 1999) the sound field is measured near the vibrating object. A special form is the planar acoustical holography, PNAH, the scan is done in a plane near the object. Measurement of the sound pressure (Williams et al., 2000) as well as the particle velocity have been published (Roozen et al., 2002;Roozen and Scholte, 2003). In the case of correlated sound sources one reference sensor can be used. When the sound sources are not correlated the technique with one reference signal does not work; the number of reference signals should be at least equal to the number of uncorrelated sources. Suppose there are two uncorrelated sound sources A and B. When the distance between A and B is relative large the reference signal for source A is taken in the neighbourhood of A, and vice versa for B. However, when near source A the contribution of source B to the total sound field is considerably this method will not work. A number of papers have been published (Ginn and Hald, 1989;Hallman and Bolton, 1992;Kim et al., 2004;Kwon and

Bolton, 1998;Nam and Kim, 2001;Tomlinson, 1999) discussing the problem of multi-, incoherent, sound sources in acoustical holography; as sensors pressure microphones were used. In this study we used a three-dimensional particle velocity sensor (Raangs et al., 2002), with which the three components (x, y, z) of the particle velocity vector can be measured. Since the particle velocity is a vector, and not a scalar like the sound pressure p, the particle velocity from source A has a well-defined direction, $u_{\|A}$. As a consequence, in a direction perpendicular to this direction $u_{\|A}$, the particle velocity from source A vanishes and only a contribution from source B is measured. Similarly there is a direction where the particle velocity component from source B vanishes and only the contribution from source A is measured. Define these two directions as $u_{\perp A}$ and $u_{\perp B}$. In order to find these two directions use is made from the property that the cross-correlation between the particle velocities in the directions $u_{\perp A}$ and $u_{\perp B}$ vanishes, since source A and B are uncorrelated and the measured signal in the direction of $u_{\perp A}$ contains only the signal from source B, and vice versa the signal in the direction of $u_{\perp B}$ only the signal from source A. The *x*-*y* distribution of e.g. the pressure, caused by source A, $p_A(x, y)$, can then be found from the cross-correlation between $p(x, y)$ and $u_{\perp B}$; the contribution of $p_B(x, y)$ in this cross-correlation with $u_{\perp B}$, vanishes since $u_{\perp B}$ does not contain the B-signal. Also the phase distribution can be determined from the (complex) cross-correlation of $p(x, y)$ and $u_{\perp B}$. In a similar way the pressure distribution caused by source B can be found from the cross-correlation of $p(x, y)$ and $u_{\perp A}$. Knowing the pressure distribution of $p_A(x, y)$ and $p_B(x, y)$ the known procedure (Maynard et al., 1985;Veronesi and Maynard, 1987;Williams, 1999) for obtaining the vibration structure of the source can be used.

5.7.2 Experiments.

The experimental set up consists of a plate with dimensions $30 \times 22 \times 3$ cm^3, with near the centre of the plate two holes with a diameter of about 0.3 cm, separated from each other by about 4 cm; the holes are denoted as A and B. Two loudspeakers were clamped at the back of the plate, at the positions of the two holes A and B. Low frequency noise in a ⅓-octave band with centre frequency of 125 Hz was used as excitation; the cross-correlation between the two noise signals averaged over a time of 0.1 seconds and normalized to the square root of the auto-spectra was about 0.04 (autospectrum = p_{rms}^2). The measuring probe consists of three microflowns, oriented in perpendicular directions (Raangs et al., 2002) and a small (pressure) microphone. A *x*,*y* scan at a distance $z = 2$ cm from the plate (*z*-direction perpendicular to the plate) was done in 16×16 points, with steps of 0.5 cm; the scanned area was thus 8×8 cm^2. From a rough interpretation of the measured data of p and u_z it was concluded that the source A was in the region $x \approx 2$ cm, $y \approx 3.5$ cm and source B in the region $x \approx 6$ cm and $y \approx 3.5$ cm (the scanned area is in the centre of the plate and in the first quadrant of the *x*-*y* coordinate system, with the lower corner at $x = y = 0$). The region $x \approx 4$ cm and $0.5 < y < 5.5$ cm was taken to detect the direction of $u_{\perp A}$ and $u_{\perp B}$.

5.7.3 Experimental results.

From the measured in plane particle velocity components directions of $u_{\perp A}$ and $u_{\perp B}$ have been deduced. The procedure we used is probably not the best, or in terms of computer time, the most optimum, procedure; it is straightforward algebra and is of almost no interest from a point of view of acoustics. It is therefore reproduced in the appendix. Take in a point (x_1, y_1), with x_1 = 4 cm and y_1 = 1.5 cm, the solution for $u_{\perp B}$ is $u(\alpha_2)$ with α_2 = 130.9. The sound pressure and particle velocity in the perpendicular direction (u_z) from source A can then be found from the cross-correlation of $p(x,y)$ (or u_z) and $u(\alpha_2)$. For a scan in the *x*-direction almost above the two sources ($y \approx 3.5$ cm) the results are shown in Figure 5-28. The points denoted as (*) represent the (auto-spectra)$^{1/2}$ of $p(x,y)$, divided by the value of the (autospectrum)$^{1/2}$ of $p(x_1,y_1)$. The points denoted as (+) are from the cross-correlation CC $p(x,y)\cdot u(\alpha_2)$, normalized to the product of the (auto-spectra)$^{1/2}$ of $p(x_1,y_1)$ and $u(\alpha_2)$.

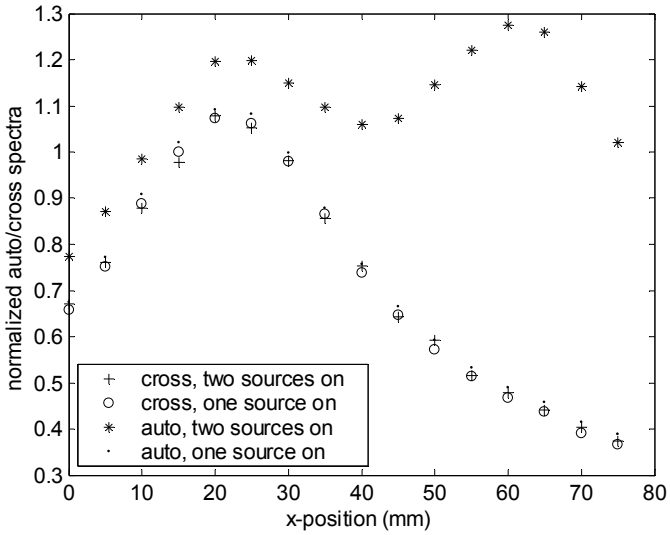

Figure 5-28: Normalized cross-correlations and (auto-spectra)$^{1/2}$ of the sound pressure p as a function of the scanning coordinate *x*. The points denoted as (*) and (+) refer to the experiment with two sources on; the points denoted as (o) and (.) to the experiment with one source on. The *x*-scan was taken at $y \approx 3.5$ cm.

The points denoted as (o) and (.) relate to a second experiment where only source A was excited by noise (source B was switched off). The points denoted as (o) are from the CC $p(x,y)\cdot u(\alpha_2)$ normalized to the product of the (auto-spectra)$^{1/2}$ of $p(x_1,y_1)$ and $u(\alpha_2)$; the values for $u(\alpha_2)$ are of course taken from the experiments with two sources on.

The normalization is done in order to make a comparison between the autospectrum of $p(x,y)$ with dimension (Pa)^2 and a cross-correlation of CC $p\cdot u$ with dimension Pa m s^{-1} possible, and to eliminate the differences in sensitivities of the p-sensor and the u-sensors.

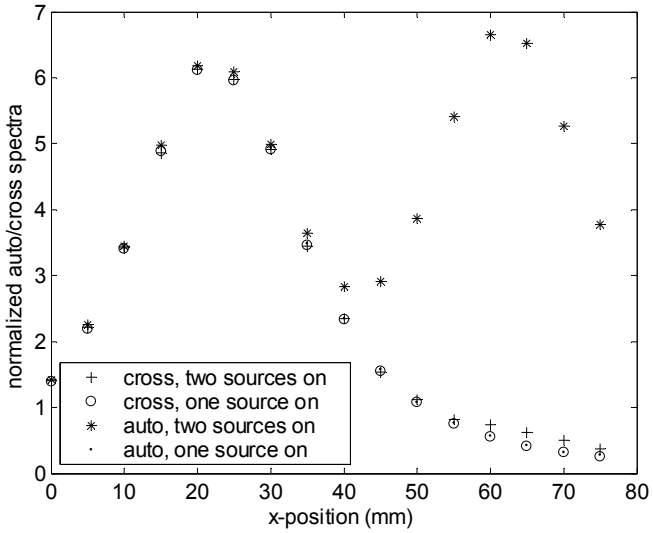

Figure 5-29: Normalized cross-correlations and (auto-spectra)^{½} of the particle velocity component u_z as a function of the scanning coordinate x. The points denoted as (*) and (+) refer to the experiment with two sources on; the points denoted as (o) and (.) to the experiment with one source on. The x-scan was taken at $y \approx 3.5$ cm.

Figure 5-29 show similar results for u_z (the points *, + , o and . refer to the same situations as in Figure 5-28; the normalization is similar, except that $p(x_1, y_1)$ is replaced by $u_z(x_1, y_1)$). Figure 5-30 and Figure 5-31 show the results for a x-scan at about $y \approx 0.5$ cm, thus 2 cm from the sources; Figure 5-30 represents results of the sound pressure p, Figure 5-31of the particle velocity component u_z. Comparing Figure 5-28 and Figure 5-29 with each other (and Figure 5-30and Figure 5-31) yields the result that the particle velocity in the z-direction is more structured and more concentrated near the source than the sound pressure. This makes that measurements of this component of the

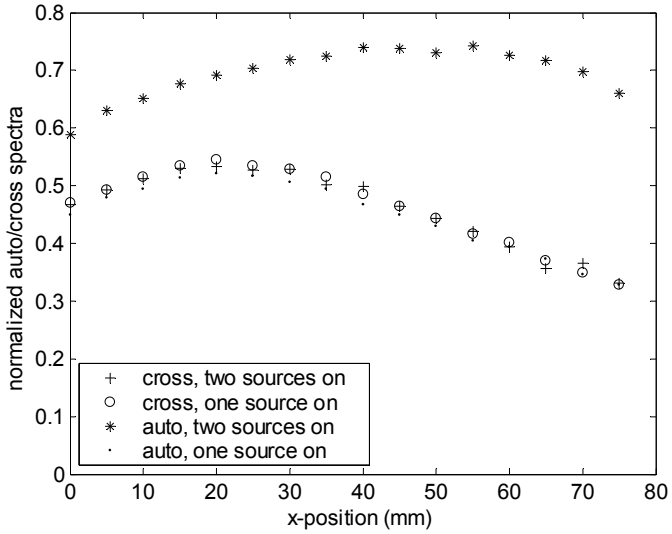

Figure 5-30: Normalized cross-correlations and (auto-spectra)^{½} of the sound pressure p as a function of the scanning coordinate x. The points denoted as (*) and (+) refer to the experiment with two sources on; the points denoted as (o) and (.) to the experiment with one source on. The x-scan was taken at $y \approx 0.5$ cm.

particle velocity should give more accurate results in NAH, than the measurements of the sound pressure (Visser, 2003).

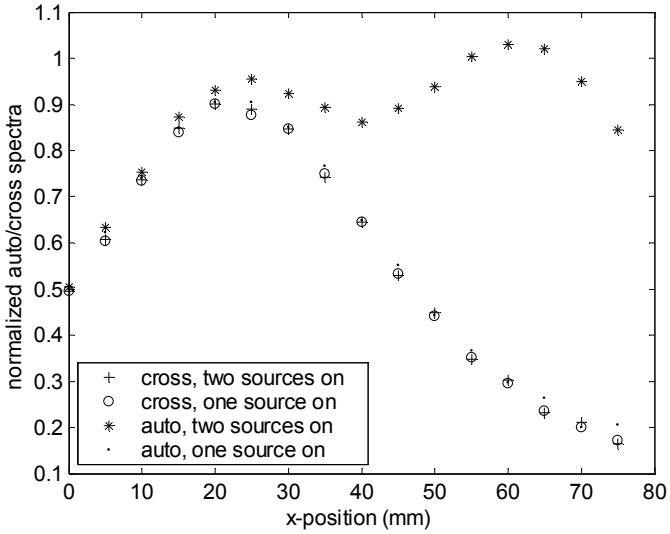

Figure 5-31: Normalized cross-correlations and (auto-spectra)^{½} of the particle velocity component u_z as a function of the scanning coordinate x. The points denoted as (*) and (+) refer to the experiment with two sources on; the points denoted as (o) and (.) to the experiment with one source on. The x-scan was taken at $y \approx 0.5$ cm.

5.7.4 Conclusions.

It has been shown that in an experiment with two sound sources, excited by two incoherent signals, the contribution to the total pressure (or particle velocity) of the two signals can be separated. As reference signal for NAH the in-plane particle velocity in a direction perpendicular to the particle velocity from one source can be used. For the two sources, these two directions were found from the vanishing of the cross-correlation between these two particle velocities directions. These results can also be applied to the situation with two or more sources excited by two incoherent signals, say $s_1(t)$ and $s_2(t)$, or excited by a combination of $s_1(t)$ and $s_2(t)$. At a point (x_1, y_1) the particle velocity belonging to the signal $s_1(t)$ has a well defined direction. In a perpendicular direction the contribution from $s_1(t)$ thus vanishes, and only a contribution of $s_2(t)$ remains. These two directions $\alpha_{1\,1}$ and α_2 can be found from the vanishing value of their cross-correlation: CC $u(\alpha_1) \cdot u(\alpha_2) = 0$. A similar reasoning can be applied for the signal $s_2(t)$.

When one expects that not two incoherent signals, but only one is present, the above described method can be used as a check for this.

Using the three components of the particle velocity vector it should be possible to separate three incoherent sources. When even more than three incoherent sources are present an extension/combination of this letter with the papers referred as (Ginn and Hald, 1989;Hallman and Bolton, 1992;Kim et al., 2004;Kwon and Bolton, 1998;Nam and Kim, 2001;Tomlinson, 1999) seems to be a good opportunity to separate the different sources.

5.7.5 Acknowledgement.

The authors wish to thank L. Alink for carrying out the measurements, as part of his study for M.Sc. at the University of Twente and the Dutch Technology Foundation STW for financial support.

5.7.6 Appendix, Finding $u_{\perp A}$ and $u_{\perp B}$.

The $u_{\perp A}$ and $u_{\perp B}$ measured signals have the property that the cross-correlation vanishes, since the signals are uncorrelated. Denote the cross-correlation between two in-plane velocity components $u(\alpha_i)$ and $u(\alpha_j)$ as CC $u(\alpha_i)\cdot u(\alpha_j)$. Define α_1 as the direction corresponding to the direction of $u_{\perp A}$, and α_2 to the direction of $u_{\perp B}$. Then in a point (x_1, y_1): CC $u(\alpha_1)\cdot u(\alpha_2) = 0$. However, in that point (x_1, y_1) there will be many directions where CC $u(\alpha_i)\cdot u(\alpha_j) = 0$, and α_1 and α_2 are therefore not unique solutions. In the cross-correlation $u(\alpha_i)\cdot u(\alpha_j)$, the contribution of u_A or u_B in the direction α_i can be positive or negative and vice versa for α_j. In the cross-correlation thus positive and negative terms occurs, which can cancel each other. Consider now two points (x_1, y_1) and (x_2, y_2), where in the (x_2, y_2) point the directions β_1 and β_2 correspond to the directions of $u_{\perp A}$ and $u_{\perp B}$. Then considering points A and B separately there are no unique solutions for $u_{\perp A}$ and $u_{\perp B}$, but combining the two points there are two extra equations, being that the two cross-correlations CC $u(\alpha_1)\cdot u(\beta_2)$ and CC $u(\alpha_2)\cdot u(\beta_1)$ will also vanish. Thus there are then four equations CC $u(\beta_i)\cdot u(\alpha_j) = 0$ with four unknown variables α_1, α_2, β_1 and β_2, which results in most cases in unique solutions. There are even two extra equations: CC $u(\alpha_1)\cdot u(\beta_1) = 1$ and CC $u(\alpha_2)\cdot u(\beta_2) = 1$ (the cross-correlations should be normalized with the auto-spectra of $u(\alpha_i)$ and $u(\beta_j)$). When taking two coordinate points (x_1, y_1) and (x_2, y_2) it is not self-evident that the found solutions indeed correspond to $u_{\perp A}$ and $u_{\perp B}$, there can be an unwanted (unknown) correlation between the particle velocities in these points. Therefore as extra check more points (five in our study) have been considered and all the cross-correlations have been calculated. These five points have been taken in the region $x \approx 4$ cm and $0.5 < y < 5.5$ cm. The solutions for the angles are given in Table 5-2. The 45 normalized cross-correlations have been calculated for the obtained 10 solutions for which it was assumed that they correspond to $u_{\perp A}$ and $u_{\perp B}$. Table 5-3 shows that indeed the 25 CC $u_{\perp A}\cdot u_{\perp B}$ are quite small and the 20 CC $u_{\perp A}\cdot u_{\perp A}$ or CC $u_{\perp B}\cdot u_{\perp B}$ are close to one; the 10 CC $u_{\perp A}\cdot u_{\perp A}$ for the same direction are by definition equal to 1. The results in Table 5-3 confirm that these directions are indeed the directions of $u_{\perp A}$ and $u_{\perp B}$.

Table 5-2: Results for the angles (see text).

y-coordinate, cm	Angle1, degrees	Angle2, degrees
1.0	$\beta_1 = 45$	$\beta_2 = 138.6$
1.5	$\alpha_1 = 50.6$	$\alpha_2 = 130.9$
2.0	$\gamma_1 = 57.9$	$\gamma_2 = 122.6$
2.5	$\delta_1 = 66.5$	$\delta_2 = 111.5$
5.5	$\zeta_1 = 300.5$	$\zeta_2 = 236$

Table 5-3: (<0.001 means that the value is between -0.001 and 0.001).

	$U(\beta_1)$	$U(\beta_2)$	$U(\alpha_1)$	$U(\alpha_2)$	$U(\gamma_1)$	$U(\gamma_2)$	$U(\delta_1)$	$U(\delta_2)$	$U(\zeta_1)$	$U(\zeta_2)$
$U(\beta_1)$	1	<0.001	0.998	<0.001	0.997	-0.007	0.997	-0.004	0.998	-0.004
$U(\beta_2)$	<0.001	1	<0.001	0.997	0.006	0.998	-0.001	0.997	0.004	0.9992
$U(\alpha_1)$	0.998	<0.001	1	<0.001	0.9993	-0.007	0.9995	-0.003	0.996	-0.006
$U(\alpha_2)$	<0.001	0.997	<0.001	1	0.006	0.9997	<0.001	0.9998	<0.001	0.996
$U(\gamma_1)$	0.997	0.006	0.9993	0.006	1	<0.001	0.9994	0.003	0.995	<0.001
$U(\gamma_2)$	-0.007	0.998	-0.007	0.9997	<0.001	1	-0.007	0.9997	-0.005	0.996
$U(\delta_1)$	0.997	-0.001	0.9995	<0.001	0.9994	-0.007	1	-0.003	0.994	-0.007
$U(\delta_2)$	-0.004	0.997	-0.003	0.9998	0.003	0.9997	-0.003	1	-0.003	0.995
$U(\zeta_1)$	0.998	0.004	0.996	<0.001	0.995	-0.005	0.994	-0.003	1	<0.001
$U(\zeta_2)$	-0.004	0.9992	-0.006	0.996	<0.001	0.996	-0.007	0.995	<0.001	1

End of paper.

5.8 Very near field

5.8.1 Introduction Very Near Field

The concept of "Very Near field, VNF" was introduced by H.E. de Bree. The idea is that in a region, very near to the sound source, the particle velocity in a direction perpendicular to the surface of the source is equal to the normal velocity of the vibrating structure. Thus by using a microflown sensor, positioned near the source the vibration amplitude of the source can be determined. Until now for contactless measurements a relative (complicated and) expensive laser vibrometer is used for measuring the vibration amplitude of the structure.

In this section, experiments are reported using a microflown sensor near the vibrating structure. These experiments are presented at the Eleventh International Congress on Sound and Vibration (Bree de et al., 2004). Although my contributions to this paper are limited to the experiments, the full paper is copied (see section 5.8.2) in order to put the experiments in the right context. The idea was later extended and presented at the Noise & Vibration Conference 2005 (Bree de et al., 2005).

In this introduction to these papers two simple cases, for which analytical expressions have been published, are worked out: a spherical balloon and a flat piston in an infinite baffle.

5.8.1.1 Spherical Source

The model is a spherical symmetrical balloon, which radiates spherical waves; the radius of the balloon is taken as $r = a$. The source is considered to be centred at the origin and to have complete spherical symmetry insofar as the excitation of sound is considered. For $r > a$ the solutions of the wave equation can be written as:

$$p = \frac{A}{r}\exp\left(-ikr\right) \tag{5.6}$$

, and

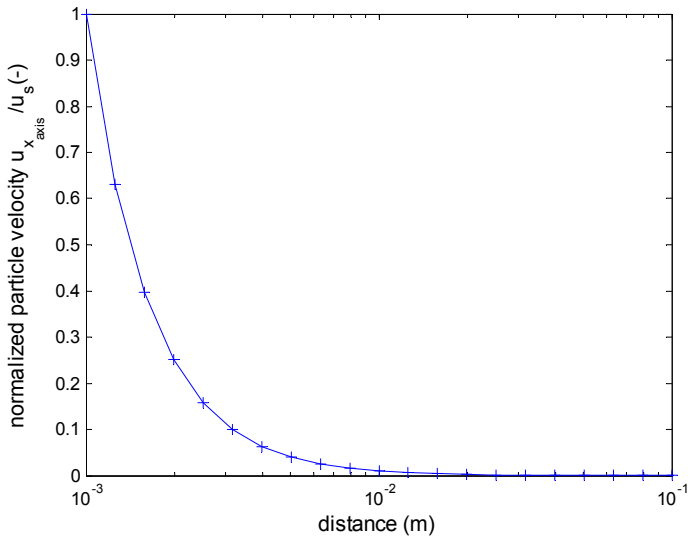

Figure 5-32: Normalized particle velocity versus distance for a small spherical sound source (radius 1 mm, frequency 343 Hz).

$$u_{x_{axis}} = \frac{1}{\rho_0 c}\frac{A}{r}\left(1+\frac{1}{ikr}\right)\exp(-ikr) \tag{5.7}$$

For $r = a$ the particle velocity $u_{x_{axis}}(r=a) = u_n$, the latter being the normal velocity of the balloon. In Figure 5-32 the value of the modulus of the complex $u_{x_{axis}}(r)$, equation (5.7), normalized to u_n, as a function of the distance r, for the case that a = 0.001m, is shown.

In case equation (5.7) is plotted using the distance from the surface instead of the distance from the centre as in Figure 5-32, this Figure 5-32 turns into Figure 5-33.

Figure 5-33(left) shows the same scales as used in Figure 5-32. In Figure 5-33(right) a double log scale has been applied. In the Figure 5-33(right) the behaviour is more obvious, a $1/r$ dependency in the far field, $1/r^2$ in the near field, and a linear dependency in the so-called hydrodynamic near field towards the surface.

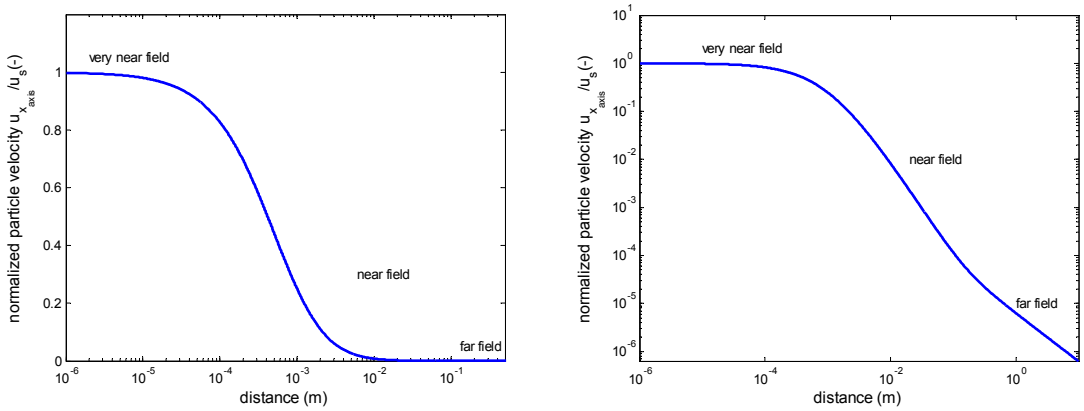

Figure 5-33: Normalized particle velocity versus distance from the surface for a small spherical sound source (radius 1 mm, frequency 343 Hz). Left: lin-log scale, right: log-log scale.

In Figure 5-34: the modulus of the complex $u_{xaxis}(x)$ is plotted as a function of the distance from the surface for four radii of the balloon: a = 1 m, 0.1 m, 0.01 m and 0.001 m.

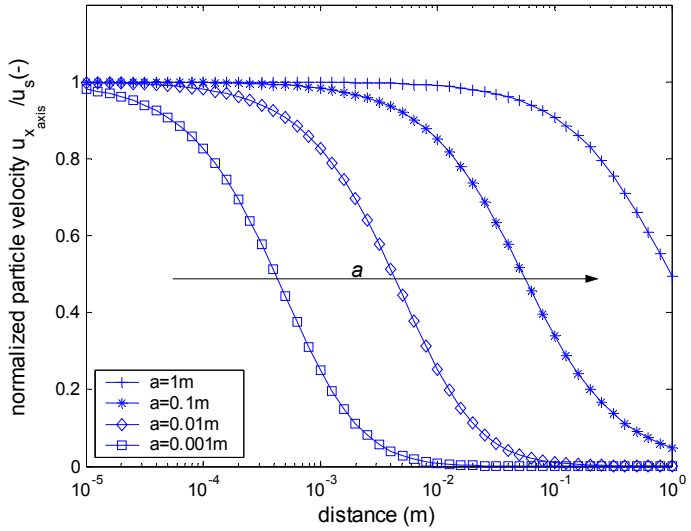

Figure 5-34: Normalized particle velocity versus distance for different radii for a spherical source at frequency 343 Hz.

5.8.1.2 Piston in infinite baffle.

Beissner (Beissner, 1982) has derived expressions for the sound field on the axis of a piston with radius $r = a$, positioned in an infinite baffle:

$$\begin{aligned} p &= \rho_0 c u_n e^{i(-kx)}\left(1 - e^{-2i\gamma}\right) \\ u &= u_n e^{i(-kx)}\left(1 - \beta e^{-2i\gamma}\right) \end{aligned} \tag{5.8}$$

with:

$$k = \frac{2\pi f}{c_0},\ \beta = \frac{x}{\sqrt{x^2 + a^2}},\ \text{and}\ \gamma = \frac{k}{2}\left(\sqrt{x^2 + a^2} - x\right) \tag{5.9}$$

where u_n is the normal velocity of the piston, x the distance from the piston.

In Figure 5-35 the modulus of the complex u_r is plotted as a function of the distance to the piston for $a = 1$ m, 0.1 m, 0.01 m and 0.001 m and a frequency 343 Hz; $\left|u_{x_{axis}}\right|$ is normalized with respect to u_n. This figure shows that indeed for a distance $x < a/10$ the particle velocity becomes about equal to the normal velocity of the piston. Therefore, it seems interesting to write equation (5.8) for the case that $x << a$. Simple algebra gives as a result:

$$u_{x_{axis}} \cdot u_{x_{axis}}{}^{*} = 1 - \left(\frac{2x}{a}\right)\cos(ka) \tag{5.10}$$

with $u_{x_{axis}}{}^{*}$ is the complex conjugate of $u_{x_{axis}}$.

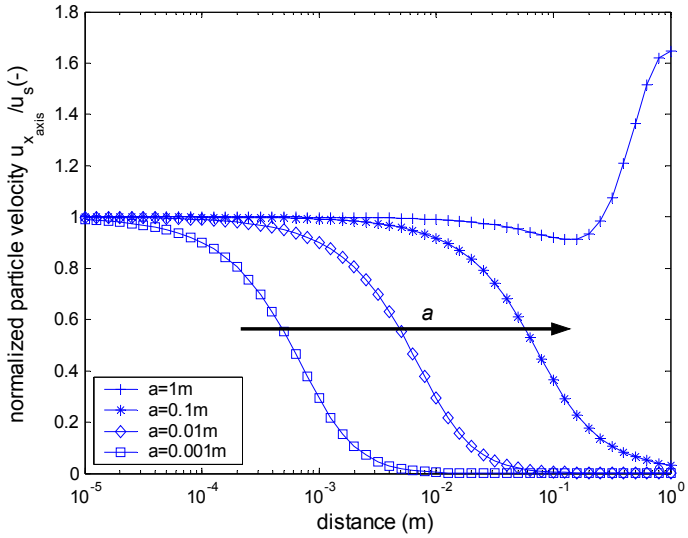

Figure 5-35: Normalized particle velocity versus distance for different radii.

In Figure 5-36 the modulus of the complex $u_{x_{axis}}$, as calculated from equation (5.8), is plotted as a function of the distance x, for three frequencies, $f = 343$, $343*1.25 = 429$ Hz, $343*1.5 = 514.5$ Hz, and $343*2 = 686$; $f = 343$ Hz and $a = 1$ corresponds to $ka = 2\pi$. For $x << a$ equation (5.10) can be recognized in Figure 5-36.

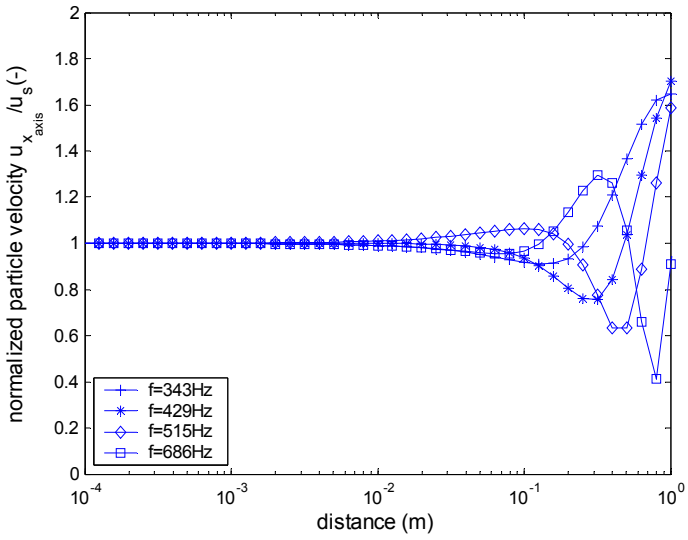

Figure 5-36: Normalized particle velocity versus distance for different frequencies.

5.8.1.3 Conclusion

Figure 5-34 and Figure 5-35 show that in a region where the distance to the surface of the source is smaller than about $a/10$ (a = radius balloon or radius piston) the particle velocity is about equal to the value at the surface of the source. So when

the radius of the source is not to small, e.g. >= 0.01 m, the method to measure with a microflown in this region the particle velocity, is a simple method to obtain the normal velocity of the vibrating structure. When, however, the radius becomes quite small, e.g. =< 0.001 m the VNF region becomes to small to position there a particle velocity sensor. For a real point source therefore, with $a \to 0$, the region becomes also infinitesimally small and the VNF-method does not work.

The experiments using a piston with a = 0.095 m and r = 0.007 m can be found in section 5.8.2.5 of paper (Bree de et al., 2004).

5.8.2 Conference paper St Petersburg 2004

In this section the full content of our conference paper "The Very Near field; Theory, simulations and measurements of sound pressure and particle velocity" is given, which was written by Bree de,H.E., Svetovoy,V.B., Raangs, and Visser,R (Bree de et al., 2004). The formatting of equation numbers and references has been changed in order to comply with the rest of the thesis.

5.8.2.1 Abstract

In acoustics concepts like the "far field" and "near field" are well-known. The sound field at a position much closer to the source than its typical size is introduced in this paper as the "very near field". The boundary conditions are specified and verifying measurements are demonstrated. It is shown that in the very near field the particle velocity is frequency independent and almost independent of the distance to the source whereas the sound pressure is suppressed, frequency dependent and almost independent of position.

5.8.2.2 Introduction

In acoustics the properties of far field and near field are well-known. In this paper the sound field very close to a source is described. We call this field the "very near field". Hydrodynamic near field and geometric near field might have a close resemblance to the very near field such as described in this paper.

Sensors to measure sound pressure are known, for the measurement particle velocity, a novel sensor is used, the so-called microflown (Bree de et al., 1995;Bree de et al., 1996b). It is a very small sensor that measures the particle velocity directly and broad banded.

Particle velocity is a vector that can be measured in three directions. In this paper only the sound pressure and normal particle velocity are analysed, in further research the lateral velocity will be investigated.

5.8.2.3 Theory

In any sound field the sound pressure p and particle velocity u are related by the specific acoustic impedance Z. In the far field this impedance is given by:

$$Z = \frac{p}{u} = \rho_0 c \tag{5.11}$$

Here ρ is the density and c is the speed of sound in the medium. The sound pressure and particle velocity are in phase and the sound pressure level (SPL) and particle velocity level (PVL) equal:

$$\mathrm{SPL} \equiv 20Log\frac{p}{20\mu\mathrm{Pa}} = 20Log\frac{u\rho_0 c}{20\mu\mathrm{Pa}} \approx 20Log\frac{u}{50\mathrm{nm/s}} \equiv \mathrm{PVL} \tag{5.12}$$

In the near field the particle velocity level is elevated compared to the sound pressure level and a phase shift between sound pressure and particle velocity is observed. For example a point source has an acoustic impedance of:

$$Z = \frac{p}{u} = \rho_0 c\frac{\mathrm{i}kr}{1+\mathrm{i}kr} \tag{5.13}$$

with k the wave number defined by: $k = 2\pi f/c$ and r the distance to the source, f the frequency and $\mathrm{i}=\sqrt{-1}$. As can be seen for reducing r, when the factor kr becomes smaller that unity, the acoustic impedance drops and a phase shift occur. The PVL is elevated compared to the SPL:

$$\mathrm{PVL} \equiv 20Log\frac{u}{50\mathrm{nm/s}} = 20Log\frac{p}{20\mu\mathrm{Pa}}\sqrt{(1+\frac{1}{k^2r^2})} = \mathrm{SPL} + 10Log(1+\frac{1}{k^2r^2}) \tag{5.14}$$

More in general, the near field can be defined as $kr < 1$; so $r < c/2\pi f$. If r is chosen infinite small, equation (5.14) predicts that the particle velocity level should be infinite and this can of course not be true. If the source is not a (infinite small) point source, and the distance to the source becomes very small compared to the size of the sound source, a region can be introduced that is called the very near field. In the very near field sound pressure and particle velocity are not very dependent on the distance to the source any more.

5.8.2.4 The Very Near field

In this paragraph theory is presented that predicts the region of the very near field and how sound pressure and particle velocity behaves in this region. A sound wave of frequency f can be described by the acoustic potential $\varphi(r)$ obeying the Helmholtz equation:

$$\Delta\varphi + k^2\varphi = 0 \tag{5.15}$$

Here Δ is the laplace operator, $k = 2\pi/\lambda = 2\pi f/c$ is the wave number, λ is the wavelength. To describe the sound field from some source, which is a vibrating surface, this equation should be solved with the boundary conditions:

$$\begin{aligned} &\frac{\partial \varphi}{\partial n} = u_{\mathrm{n}} \text{ on the surface,} \\ &\varphi \propto \frac{\exp\left(\mathrm{i}k_0 r\right)}{r} \text{ at infinity } r \to \infty, \end{aligned} \tag{5.16}$$

where $\partial/\partial n$ is the derivative normal to the surface, u_{n} is the normal component of the velocity, in general, a function of the point on the vibrating surface. The observable acoustic values, sound pressure p and particle velocity u, are connected with the potential in the following way:

$$u = grad\,\varphi\ ,\ p = -\mathrm{i}\omega\rho_0\varphi \tag{5.17}$$

where ρ_0 is the density of the background medium (air).

Suppose that the vibrating surface can be considered as flat on some lateral length scale L. One can choose the x-y plane on the surface then the z-direction will coincide with the normal to the surface. In the direct vicinity of the surface the potential can be expanded in the power series in z:

$$\varphi\left(x,y,z\right) \approx \varphi_0\left(x,y\right) + \varphi_1\left(x,y\right)z + \frac{1}{2}\varphi_2\left(x,y\right)z^2 + O\left(z^3\right) \tag{5.18}$$

The functions $\varphi_{0,1,2}$ are connected with the velocities on the surface. From the boundary condition it follows that:

$$\varphi_1\left(x,y\right) = u_{\mathrm{z}}(x,y,0) \equiv u_{\mathrm{z}}^{\mathrm{S}} \tag{5.19}$$

It means that measured particle very close the surface coincides with the surface velocity where the superscript S shows that the velocity should be taken on the surface (this is verified by measurement, see below). Connection of the velocity and potential gives us the relations:

$$\frac{\partial \varphi_0}{\partial x} = u_{\mathrm{x}}^{\mathrm{S}}\ ,\quad \frac{\partial \varphi_0}{\partial y} = u_{\mathrm{y}}^{\mathrm{S}} \tag{5.20}$$

A comment should be made concerning these relations. The right hand sides are the velocity components taken directly on the surface. For any viscous fluid they should be zero. However, in most cases acoustic fields can be described with the ideal fluid equations. It means that the boundary layer where the velocity changes from zero to some finite value should be very thin. It is exactly the case because the thickness of boundary layer δ for the lateral velocity components is estimated as $\delta \sim \sqrt{\nu/\pi f}$, where ν is the fluid viscosity. For air and frequency f = 100 Hz this thickness is just of about of 50 μm. We have to consider the components $u_{\mathrm{x,y}}{}^{\mathrm{S}}$ as taken on the outer side of the boundary layer. Finally, taking the second derivative with z from equation (5.18), one finds:

$$\varphi_2(x,y)=\left(\frac{\partial u_z}{\partial z}\right)^S \tag{5.21}$$

Therefore, the expansion equation (5.18) can be written as:

$$\varphi(x,y,z)\approx\varphi_0+u_z^S z+\frac{1}{2}\left(\frac{\partial u_z}{\partial z}\right)^S z^2 \tag{5.22}$$

where φ_0 is also completely defined by the velocities by equation (5.20).

Let us insert now the potential equation (5.22) in the Helmholtz equation and take the limit $z\to 0$. We will find:

$$\left(\frac{\partial^2}{\partial x^2}+\frac{\partial^2}{\partial y^2}\right)\varphi_0+k^2\varphi_0+\left(\frac{\partial u_z}{\partial z}\right)^S=0. \tag{5.23}$$

Suppose that the surface vibration can be described by some spatial wavelength *L*. It means that the surface vibrations can be represented by a harmonic in space function like $\sin(2\pi x/L)$ and similar for *y*-direction. The first two terms in equation (5.23) then can be estimated as:

$$\left(\frac{\partial^2}{\partial x^2}+\frac{\partial^2}{\partial y^2}\right)\varphi_0\sim\left(\frac{2\pi}{L}\right)^2\varphi_0,\quad k^2\varphi_0=\left(\frac{2\pi}{\lambda}\right)^2\varphi_0 \tag{5.24}$$

Typical situation in acoustic is that the vibrating body radiates the sound waves with the wavelength:

$$\lambda\gg L \tag{5.25}$$

Then, according to (5.24), the second term in equation (5.15) is small in comparison with the first one and in the vicinity of the body the Helmholtz equation (5.15) is reduced to the Laplace equation:

$$\Delta\varphi=0 \tag{5.26}$$

Equation (5.26) is the equation of uncompressible fluid that means that in this approximation the pressure level (dB) is negligible compared to the velocity level. The normal velocity in this range coincides with velocity of the vibrating surface.

Physically it means that nearby the surface the fluid can be considered as uncompressible and for this reason the sound pressure level (dB) is small compared to the particle velocity level. The latter has to be clearly explained. The sound waves are the compression-decompression waves and if equation (5.26) would be exact there would be no sound pressure at all. In reality these equations are approximate and the pressure still finite but it is suppressed. To find this suppression factor we have to estimate the value of φ_0. It can be done using the equation (5.20). As was explained above the derivative $\partial\varphi_0/\partial x\sim(2\pi/L)\varphi_0$ and similar for the derivative with respect to *y*. Nearby the surface all the velocity components are of the order of some vibration velocity u_0, which is defined by the vibration amplitude and frequency. One can use any suitable definition for

u_0, for example, it can be defined as a maximal particle velocity u_z measured nearby the surface. Then from equation (5.20) one gets the estimate:

$$\varphi_0 \sim \frac{L}{2\pi} u_0 \tag{5.27}$$

The pressure is connected with the potential as $p = -2\pi i f \rho_0 \varphi$ and in the limit $z \to 0$ one finds the following estimate for the pressure:

$$p \sim -\mathrm{i}\rho c u_0 \frac{L}{\lambda} \tag{5.28}$$

It shows that the pressure is suppressed in comparison with the particle velocity by the factor L/λ (the ratio of the spatial wavelength L of the source and the wavelength) and the phase between the particle velocity and sound pressure is shifted 90 degrees.

Equation (5.26) is true if the normal distance $r_n = z$ to the vibrating surface is small in comparison with the size L and that the wavelength λ is larger than the vibrating surface L.

$$r_n << \frac{L}{2\pi} << \frac{\lambda}{2\pi} = \frac{c}{2\pi f} \tag{5.29}$$

The condition equation (5.29) can be named by the condition of the very near field. In this range the normal component of the velocity coincides with that for the vibrating surface but there are no restrictions on the lateral components of the velocity, which can be distributed in some way along the surface. In the table below the properties summarized.

Region	condition	***u*** [m/s]	p [Pa]	Phase [deg]
Very near field	$r_n << \frac{L}{2\pi} << \frac{\lambda}{2\pi}$	$u(r_n) \approx$ constant $u(f)$ = constant	$p(r_n) \approx$ constant $p(f) \sim f$	80-90
Near field	$\frac{L}{2\pi} << r_n << \frac{\lambda}{2\pi}$	$u(r_n) \sim r^{-2}$	$p(r_n) \sim r^{-1}$	80-10
far field	$r_n >> \frac{\lambda}{2\pi}$	$u(r_n) \sim r^{-1}$	$p(r_n) \sim r^{-1}$	0-10

Where r_n is the normal distance to the source, L is the typical size of the source and λ is the wavelength of the sound wave.

5.8.2.5 Simulation and measurement

A 19 cm circular aluminium plate was glued on a bass loudspeaker so that a piston was realized. The sound field (sound pressure and particle velocity) in front of this piston is simulated and measured as a function of the distance at several frequencies.

A half inch p-u probe (Io microflown element) of Microflown Technologies was used to measure the sound pressure and the particle velocity.

Figure 5-37: Measurement setup: a loudspeaker with an aluminium plate glued on and the p-u probe on a traverse robot.

The levels of sound pressure and particle velocity field for a plane circular piston in an infinite baffle along the axial distance are given by (Beissner, 1982):

$$
\begin{aligned}
p &= \rho_0 c u_n e^{\mathrm{i}(\omega t - kr)} \left(1 - e^{-2\mathrm{i}\frac{k}{2}\left(\sqrt{r^2+L^2}-r\right)} \right) \\
u &= u_n e^{\mathrm{i}(\omega t - kr)} \left(1 - \frac{r}{\sqrt{r^2+L^2}} e^{-2\mathrm{i}\frac{k}{2}\left(\sqrt{r^2+L^2}-r\right)} \right)
\end{aligned}
\tag{5.30}
$$

As can be seen in Figure 5-37, at several frequencies the sound field is almost flat in the very near field; at a distance smaller than $L/2\lambda$. In the near field ($L/2\lambda < r < c/2\pi f$) the particle velocity has an elevated level compared to the sound pressure. The frequency dependent distance $r < c/2\pi f$, the distance where the sound field convert from the near field in to the far field is clearly noticeable. In the far field the sound pressure level and particle velocity level are of the same magnitude.

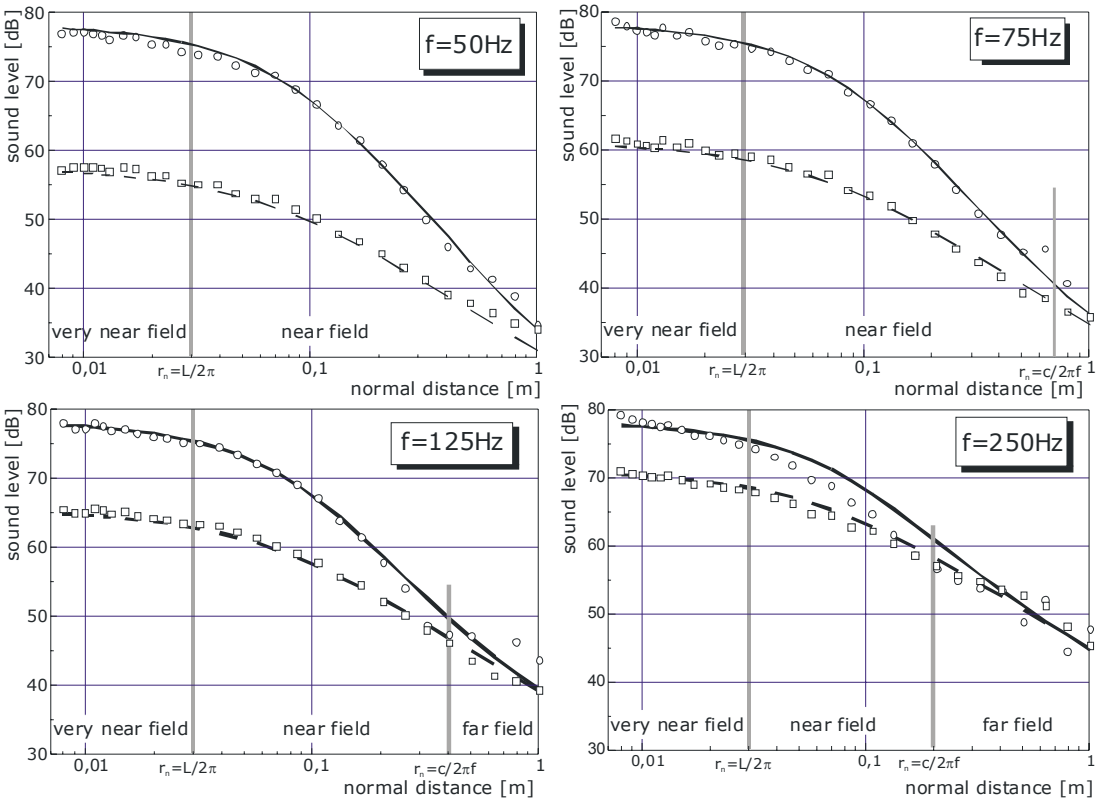

Figure 5-38: Simulated particle velocity level (black line), simulated sound pressure level (dashed line), measured particle velocity (dots) and measured sound pressure (squares) as function of normal distance to the source at different frequencies.

5.8.2.6 Laser vibrometer versus microflown sensor at r_n=7 mm

The particle velocity level of the sound field at 7 mm in front of the disk is compared with the surface velocity. The acoustic particle velocity level was measured with a microflown and the surface velocity level was measured with a laser vibrometer (Polytec OFV505 sensitivity 25 mm/s/V).

As can be seen in Figure 5-39 (left), the surface velocity measured by the laser vibrometer and the particle velocity of the sound field measured at 7 mm in front of the plate measured with a microflown sensor coincide. The deviation at 50 Hz, 75 Hz, 125 Hz and 250 Hz is determined respectively 0.5 dB, 0 dB, 0.5 dB and -1.4 dB.

The noise, the signal that was measured when the plate was not excited (and the setup was placed on a stable underground), of both measurement techniques is comparable, see Figure 5-39 (right). The self-noise of the laser vibrometer is about 10 dB higher than the self-noise of the microflown sensor. So the microflown sensor performs 10 dB (about 3 times) better. The noise level is measured in 1 Hz bandwidth and given in dB with a reference level of 50 nm/s (0 dB equals 50 nm/s) which is the pressure equivalent of the threshold of hearing at 1 kHz.

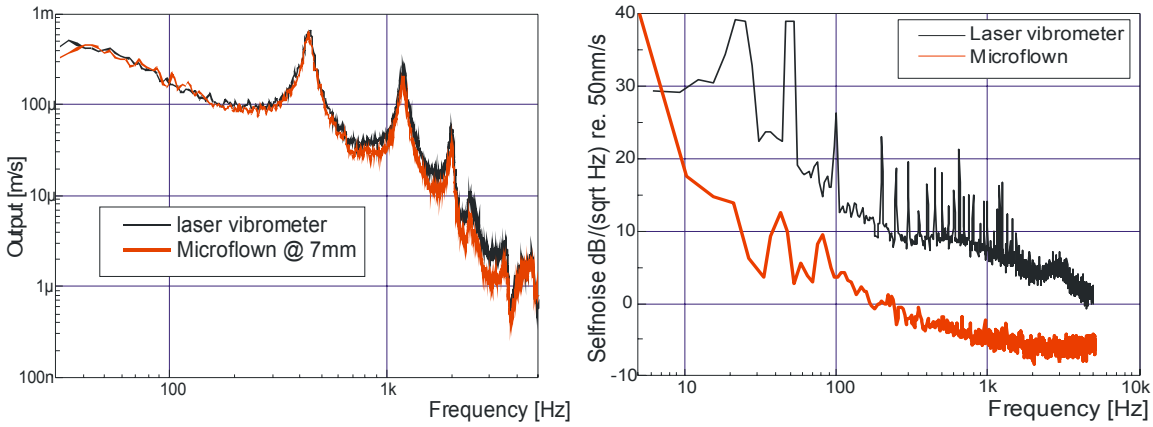

Figure 5-39Left: measured particle velocity at 7 mm distance from the plate and the surface velocity measured with a laser vibrometer. Right: Measured self-noise of a microflown sensor and the laser vibrometer 7 mm from the non-excited aluminium plate.

5.8.2.7 Conclusion

It has been shown with a 19cm in diameter vibrating piston that close to a vibrating object the Microflown can be used to measure the normal structural vibrations of that object. Measurements have to be in the very near field. Conditions of the very near field are: the measurement distance should be closer than the structural size of the object divided by 2π and the wavelength of the sound should be larger than the structural size of the object.

End of paper (Bree de et al., 2004)

Additionally, a simulation of a sound field in front of a 19 cm piston is shown in Figure 2-53 and Figure 2-54 ,using equations (5.8) and (5.9) (Beissner, 1982). Figure 2-53 shows the particle velocity field, Figure 2-54 shows the sound pressure field. Zero dB in the right plots means that the measured particle velocity, or the pressure divided by $\rho_0 c$, coincides with the surface velocity. For convenience, the very near field region as defined in (Bree de et al., 2004;Bree de et al., 2005) is illustrated in Figure 2-53(right) and Figure 2-54(right). As can be seen in Figure 2-53: in the very near field c.q. hydrodynamic near field the particle velocity is almost constant for variations in position and frequency variations and the pressure is frequency dependent (Figure 2-54).

5.9 Conclusions

Most publications on acoustical holography deal with the measurement of the sound pressure for scanning the sound field. In this section it is shown that in a number of cases the measurement of the particle velocity, or product of pressure and particle velocity, or product of two components of the particle velocity give

better results. An example where the use of a u-sensor has the advantage above a p-sensor is when the sensor is near a low frequency source ($kr < 1$ section 5.3). Also for a dipole-source configuration the measurement of the in-plane particle velocity gives better results in terms of S/N ratio, than a measurement of the sound pressure (section 5.4). When the sound sources are quite weak and the signal is of the same order as the sensor noise, the cross-correlation of $p.u^*$ or $u_i.u_j^*$ can still give good results (section 5.6). When incoherent sound sources are present the measurement of the particle velocity vector give the opportunity to separate the different incoherent signals. This technique is much simpler than the methods described in literature (Ginn and Hald, 1989;Hallman and Bolton, 1992;Kim et al., 2004;Kwon and Bolton, 1998;Nam and Kim, 2001).

In very near field situations, i.e. very close to the vibrating surface, the measurement of the particle velocity gives direct information about the vibration of the source surface. This technique is much simpler than the laser vibrometer. It has been shown (with a 19 cm in diameter vibrating piston) that close to a vibrating object the microflown can be used to measure the normal structural vibrations of that object. This experimental result also demonstrates that the microflown is definitely a u-sensor, since with a quite independent technique (laser vibrometer) exactly the same frequency response is measured (Figure 5-39 Left). Conditions of the very near field are: the measurement distance should be closer than the structural size of the object divided by 2π and the wavelength of the sound should be larger than the structural size of the object.

Chapter 6
Summary and Conclusions

In this thesis, the theoretical and practical aspects of acoustical particle velocity and especially measurements of acoustical particle velocity using a micro-machined particle velocity sensor, the microflown, are discussed.

The interesting field of acoustics was and is mainly based on sound pressure, and sound pressure measurements. Acoustical sensors were mainly pressure microphones. Other types of microphones such as pressure gradient microphones, or combinations of pressure gradient microphones and pressure microphones, do exist but their use is mainly limited for music and speech recordings. Due to the finite size of the diaphragm of the pressure microphones used, corrections have to be made, depending on their size, and the sound field in which it is designed for. In this thesis, we discuss a sound particle velocity sensor, the microflown, which is, by design, and due to its limited size, only sensitive for acoustical particle velocity.

Since a measurement in general is only as good as the calibration of the sensor used we started by investigating the applicable methods of calibrating this new acoustic sensor. There was, however, no reference particle velocity is available, and therefore we have chosen to use well calibrated pressure microphones as a reference. We investigated several possibilities for acoustical environment such as the anechoic room, the standing wave tube, the reverberant room. Out of these methods, we found that the standing wave tube was the most practical solution and this method has been treated more thoroughly in this thesis, and the method has been optimized in the process of doing so.

Since acoustical particle velocity could not be measured well, particle velocity was never investigated as thoroughly as sound pressure. In order to show that the microflown actually does measure particle velocity, and not pressure, we compared the measurements using the microflown with measurements using an optical technique, laser doppler anemometry (LDA). This photon correlation technique is only sensitive for the velocity of the small particles in the acoustical sound field, and this particle velocity could be used to calibrate the microflowns absolute sensitivity for various frequencies. Since the obtained sensitivity equals the sensitivity we derived using the standing wave tube, which was already

compared successfully with anechoic calibration techniques; we could definitely show that the microflown is only sensitive for particle velocity.

The microflown is a very small particle velocity sensor. Due to its small size, three microflowns can be positioned around a small pressure microphone while still being a small acoustical obstacle as compared with half-inch microphones. Since we were interested in the accuracy of the alignment of the three-particle velocity probes, and we had to calibrate two microflowns that we positioned at an angle of 45 degrees on this probe, we realised a three-dimensional calibration technique based on many measurements in the standing wave tube. The obtained directions are used and were shown to improve the results of the free field measurements using the cross-correlation technique as is discussed in section 3.4.2.

The electrical noise in microflown particle velocity sensors is treated in several parts of this thesis. Although it can be discussed if it is possible to compare noise levels, and how one should compare equivalent noise levels of the microflown with other types of acoustical sensors such as pressure microphones. In this thesis, we have chosen to compare the equivalent noise taken a sound field consisting out of plane waves. The noise levels can be compared using their levels (using the accompanying reference levels). The particle velocity can be converted into a equivalent pressure using the characteristic specific acoustic impedance of air.

The earlier prototypes showed more noise for this far field situation as compared with sound pressure. In this thesis, we describe a method to reduce the noise level of the particle velocity sensor. This method is based on the utilisation of cross-correlation spectra instead of auto-correlation spectra of two of these sensors. For a large averaging time we could decrease the noise levels up to 30 decibels. By applying an acoustical signal in this situation, we could show that the signal to noise ratio in a measurement was increased with the same amount. The same effect occurs for two different acoustical sensors such as a pressure microphone and particle velocity sensor used to measure sound intensity.

The directivity characteristics of the microflown particle velocity make very interesting acoustical measurements feasible. Due to the directivity, a sound source is measured differently depending of the direction. By applying two of these particle velocity sensors, the angle of incidence can be found using the auto- and

the cross-correlations of the two signals. More interestingly is the situation in a perfect diffuse sound field since in this sound field, sound waves coming from all directions can be considered to be uncorrelated. This results in the fact that the impact of the diffuse sound in such a measurement can be computed separately from the direct sound. In section 3.4 of this thesis, we use this effect in order to find the sound source in a two-dimensional case. In this thesis, we therefore show that free field measurements can be performed in a reverberating room. The results were compared with another free-field measurement technique, namely sound intensity measurement.

In Chapter 4 we discuss the usage of the microflown in sound intensity measurements. We show that the microflown, complemented with a pressure sensor measuring at the same position, results in a small and affordable sound intensity probe. We show that measurements performed using a professional sound card for data acquisition, and easy to program computations result in good measurements of the sound intensity. The results are compared and were found to be in good agreement with results obtained by a commercially available sound intensity probe based on two closely matched pressure microphones. The presented program also returned energy density, acoustical impedance, phase, and etcetera. Although these acoustical parameters are not compared with other measurement techniques, the program showed that this could be easily computed out of the already measured auto- and cross-spectra of the pressure and particle velocity sensor signals.

The three-dimensional p-u probe can be used for measuring three-dimensional sound intensity. We showed that the three-dimensional calibration can be applied in case the three particle velocity sensors do not build an orthogonal basis by themselves out of the measuring directions.

In the far field, the difference between pressure and particle velocity is mainly limited by and caused the difference in the directivity. Nearer to the sound source, in the near field, the sound field starts to behave differently. Closer to the sound source, in general, a phase difference occurs between the pressure and the particle velocity, and in general, the particle velocity increases faster with decreasing distance than the pressure increases for the same change in distance. This near field effect increases in generally for decreasing frequency and distance, or with other words, the near field is, in general, larger for lower frequencies. In Chapter 5,

numerical and experimental data are presented which supports this idea for several different sound sources. For low frequencies, in many situations, the performance of the microflown excels the performance of small pressure microphones, in case of small structural sound sources at close range of the sound source at the same measurement positions. Even if the self-noise of the microflown is higher, taken a free field comparison, the signal to noise ratio can be and will be in many measurements be higher than that in the pressure measurements. Combined with the fact that structural information is attained over a further range in the particle velocity field, as compared with the pressure field, results in the fact that particle velocity is an interesting acoustical sensor in case close range measurements are possible.

Most publications on acoustical holography deal with the measurement of the sound pressure for scanning the sound field. In this thesis it is shown that in a number of cases the measurement of the particle velocity, or product of pressure and particle velocity, or product of two components of the particle velocity give better results. When the sound sources are quite weak and the signal is of the same order as the sensor noise, the cross-correlations between pressure and particle velocity sensors, or between two particle velocity sensors, can still give good results. In case there are multiple incoherent sound sources present, the measurement of the particle velocity vector give the opportunity to separate the different incoherent signals. This technique is much simpler than the methods described in literature (Ginn and Hald, 1989;Hallman and Bolton, 1992;Kim et al., 2004;Kwon and Bolton, 1998;Nam and Kim, 2001).

A special sound field has been identified as the very near field (VNF). This is the range where the sound source becomes large in relation to the distance. In this very near field the particle velocity becomes almost equal to the surface velocity of the vibrating structure. This is a very interesting sound field, and occurs for example in case panels resonate at low frequencies. We have showed that the difference between the measured particle velocity and the structural velocity is quite small and predictable. The conclusion is supported by numerical and experimental data for a flat disc in a baffle and numerically for a small pulsating balloon. In general, it is therefore expected that particle velocity data will be of higher quality, and will be interesting to use as input for inverse techniques based on measurement in the near field.

Appendix A
List of Symbols

Symbol		Units
$\mathbf{A}$	dimensionless directivity matrix	-
a	radius	m
c	Sound speed in air	m s^{-1}
c_1	velocity of propagation of extensional waves in an infinite thin plate	m s^{-1}
C	complex acoustic intensity of a harmonic sound field	W m^{-2}
CPSD	cross-power spectral density	
d, D	diameter	m
E	energy density	J m^{-3}
$E[\ ]$	estimate of	
f	frequency	Hz
$G_{xx}(f)$	single sided autospectral density function	
$G_{xy}(f)$	single sided cross-spectral density function	
$H_{xy}(f)$	frequency response function	
h	thickness	m
$\mathbf{I}$	mean intensity vector	Wm^{-2}
I	active part of the sound intensity	Wm^{-2}
I_r	radial component of active part of the sound intensity	Wm^{-2}
i	complex number equivalent to $\sqrt{-1}$	-
$\mathbf{J}$	reactive part of the sound intensity vector	Wm^{-2}
J_0	Bessel function of zeroth order	-
k	wave number	m^{-1}

LFS	low frequency sensitivity	V s m^{-1}
$L_{\sim}$	symbol for level	decibel
L_p	sound pressure level	dB (ref 2 10^{-5} Pa)
L_v	particle velocity level	dB (ref 5 10^{-8} m s^{-1})
L_I	Sound Intensity Level	dB (ref 1 10^{-12} W/m^2)
λ	wave length	m
N	time integrated intensity	J m^{-2}
N	Number of points per record, number of averages	-
NFFT	length of the discrete Fourier transforms	-
$p(t)$	instantaneous sound pressure	Pa
p	equivalent continuous sound pressure level	Pa
p_{dir}	pressure due to direct sound field	Pa
p_{rev}	pressure due to diffuse sound field	Pa
$\tilde{p}(t)$	complex sound pressure in time domain	Pa
pSD	pressure spectrum density	$Pa^2/\sqrt{Hz}$
PSD	power spectrum density	
PVL	particle velocity level	dB (ref 5 10^{-8} m s^{-1})
rms	root mean square	
RMSE	root mean square error	
R	electrical resistance	Ω
$R_{xx}(\tau)$	Auto-correlation function	V^2
$R_{xy}(\tau)$	Cross-correlation function	V^2
s	shear wave number	-
SIL	sound intensity level	dB (ref 1 10^{-12} W/m^2)
SPL	sound pressure level	dB (ref 2 10^{-5} Pa)
SWR	standing wave ratio	-

S	sensitivity	
S_t	Stokes number	-
$S_{xx}(f)$	Autospectral density function (double sided)	V^2 Hz^{-1}
$S_{xy}(f)$	Cross-Autospectral density function (double sided)	V^2 Hz^{-1}
t	Time variable	s
T	Record length	s
T_c	characteristic time scale	s
u	acoustic particle velocity	m s^{-1}
$\vec{u}$	acoustic particle velocity vector	m s^{-1}
$\tilde{u}(t)$	complex acoustical particle velocity	m s^{-1}
u_x	Acoustic particle velocity in direction x	m s^{-1}
u_{dir}	particle velocity due to direct sound field	m s^{-1}
u_{rev}	particle velocity due to diffuse sound field	m s^{-1}
u_m	acoustic particle velocity amplitude (equation 2.43)	m s^{-1}
V	electrical voltage	V
$x(t)$, $y(t)$	Time history records	
$X(f)$	Fourier transform of $x(t)$	
Z_s	specific acoustic impedance	Pa s m^{-1}
α , β	angle of rotation	rad or deg
ε	Normalised error	
φ	phase angle	rad or degrees
$\gamma_{xy}^2(f)$	Ordinary coherence function	-
γ	specific heat ratio	-
Γ	viscothermal wave propagation coefficient	-

μ	dynamic viscosity	Pa s
μ	symbol for microflown	
θ , φ	phase angle	rad or deg
ρ_0	density of air	kg m^{-3}
σ	Standard deviation	
σ^2	Variance	
σ	square root of the Prandtl number (in equation (2.10))	-
ω	radian frequency	rad s^{-1}

Appendix B
Two microflowns in a diffuse sound field

Consider two microflowns positioned in an ideal three-dimensional diffuse sound field. The ideal diffuse sound field can be simulated by many (uncorrelated) sound sources uniformly distributed over a sphere. Take the root mean square value of the particle velocity of the waves from a solid angle $d\Omega$ equal to u_{m}, then the total effective particle velocity in a point of the field is:

$$u_{\mathrm{rev}}^2 = \int u_{\mathrm{m}}^2 d\Omega = 4\pi u_{\mathrm{m}}^2 \tag{B.1}$$

For the calculating the cross spectrum from the two u-sensors we must integrate all contributions of all sources over $d\Omega$; $d\Omega = \sin(\phi) d\theta d\phi$; ϕ over 0 - π and θ over 0 - 2π.

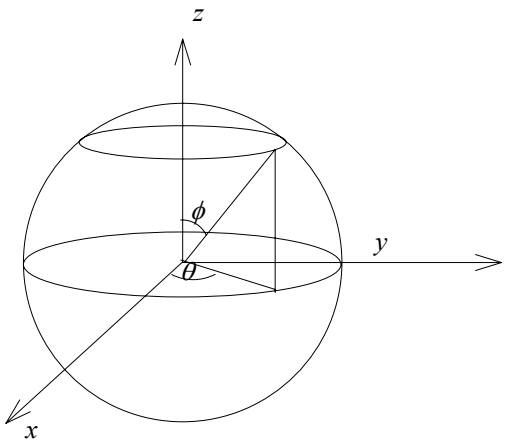

Consider two microflowns placed in this sound field. The two microflowns are positioned at the same position, at the centre, but are measuring the particle velocity in different directions:

$$\vec{\mu}_1 = \left[\mu_{1x}, \mu_{1y}, \mu_{1z} \right] \tag{B.2}$$

$$\vec{\mu}_2 = \left[\mu_{2x}, \mu_{2y}, \mu_{2z} \right] \tag{B.3}$$

For each angle (θ, ϕ) the microflown measures a signal depending on the angles and the direction of the microflown $\vec{\mu}$ since the microflown only measures the particle velocity component in direction $\vec{\mu}$. For each angle, the microflown measures a signal $S(t)$:

$$S(t) = \vec{\mu} \cdot \vec{u}_{\mathrm{m}}(\theta, \phi, t) \tag{B.4}$$

Using $x = r\cos\theta\sin\phi$, $y = r\sin\theta\sin\phi$, and $z = r\cos\phi$, equation (B.4) and (B.2) turns into:

$$\begin{aligned} S(\theta,\phi,t) &= -\left[\mu_x,\mu_y,\mu_z\right]\cdot\left[\cos\theta\sin\phi,\sin\theta\sin\phi,\cos\phi\right]u_{\mathrm{m}}(\theta,\phi,t) \\ &= -\left(\mu_x\cos\theta\sin\phi+\mu_y\sin\theta\sin\phi+\mu_z\cos\phi\right)u_{\mathrm{m}}(\theta,\phi,t) \end{aligned} \tag{B.5}$$

For two microflowns, the cross correlation (for $\tau = 0$) for each direction equals thus:

$$R_{12}(\theta,\phi,\tau=0) = \int S_1(\theta,\phi,t)S_2(\theta,\phi,t)\,dt \tag{B.6}$$

combining (B.5) and (B.6) results in:

$$\begin{aligned} R_{12}(\theta,\phi,\tau=0) = \int\Big(&\left(\mu_{1x}\cos\theta\sin\phi+\mu_{1y}\sin\theta\sin\phi+\mu_{1z}\cos\phi\right)u_{\mathrm{m}}(\theta,\phi,t)\Big) \\ &\Big(\left(\mu_{2x}\cos\theta\sin\phi+\mu_{2y}\sin\theta\sin\phi+\mu_{2z}\cos\phi\right)u_{\mathrm{m}}(\theta,\phi,t)\Big)\,dt \end{aligned} \tag{B.7}$$

Thus, integrating over all angles in a diffuse sound, most cross-terms in equation (B.7) will result in a zero value using $\int_0^{2\pi}\cos\theta\sin\theta d\theta = 0$, $\int_0^{2\pi}\cos\theta d\theta = 0$ and so forth.

$$R_{12}(0) = \int_0^{\pi}\sin\phi d\phi\int_0^{2\pi}d\theta\left\{\mu_{1x}\mu_{2x}\left(\sin^2\phi\cos^2\theta\right)+\mu_{1y}\mu_{2y}\left(\sin^2\phi\sin^2\theta\right)+\mu_{1z}\mu_{2z}\left(\cos^2\phi\right)\right\}u_{\mathrm{m}}^2(\theta,\phi,t) \tag{B.8}$$

and using $\int_0^{2\pi}\cos^2\theta d\theta = \pi$, $\int_0^{\pi}\sin^3\phi d\phi = 4/3$ and $\int_0^{\pi}\sin\phi\cos^2\phi d\phi = 2/3$ this turns into:

$$\begin{aligned} R_{12}(0) &= \frac{4}{3}\left(\vec{\mu}_1.\vec{\mu}_2\right)\int_0^{\pi}\sin\phi d\phi\int_0^{2\pi}d\theta\left(u_{\mathrm{m}}^2(\theta,\phi,t)\right) \\ &= \frac{4\pi}{3}u_{\mathrm{m}}^2\left(\vec{\mu}_1.\vec{\mu}_2\right) \\ &= \frac{1}{3}u^2{}_{\mathrm{rev}}\left(\vec{\mu}_1.\vec{\mu}_2\right) \end{aligned} \tag{B.9}$$

Combined with equation (B.1) this results into:

$$R_{12}(0) = \frac{1}{3}u^2{}_{\mathrm{rev}}\left(\vec{\mu}_1.\vec{\mu}_2\right) \tag{B.10}$$

Instead of writing out all the components of the arbitrary vectors $\vec{\mu}_1$ and $\vec{\mu}_2$ a faster derivation of equation (B.10) is possible. Since the integration should be

performed over all mirror sources equally distributed over the sphere the result of the integration is independent of any rotation of the *x*,*y*,*z* coordinate system. Rotate then the coordinate system such that $\vec{\mu}_1$ = [0,0,1] and $\vec{\mu}_2$ = [0,sin(ϕ_μ),cos(ϕ_μ)]. The angle between $\vec{\mu}_1$ and $\vec{\mu}_2$ is ϕ_μ and the inner product $\vec{\mu}_1.\vec{\mu}_2$ is equal to cos(ϕ_μ). The integral equation for the contribution of the reverberant field to the cross-spectrum becomes:

$$\begin{aligned} R_{12}(0) &= u^2{}_{\mathrm{m}} \int_0^{\pi} \sin\phi d\phi \int_0^{2\pi} d\theta (\cos\phi)\left(\sin\phi_\mu \sin\phi \sin\theta + \cos\phi_\mu \cos\phi\right) \\ &= 2\pi u^2{}_{\mathrm{m}} \int_0^{\pi} \sin\phi \cos^2\phi \cos\phi_\mu d\phi = \frac{4\pi}{3} u^2{}_{\mathrm{m}} \cos\phi_\mu = \frac{1}{3} u^2{}_{\mathrm{rev}} (\vec{\mu}_1.\vec{\mu}_2) \end{aligned} \tag{B.11}$$

Appendix C
Calculation of the Specific Acoustic Impedance of Air

The acoustic impedance is defined as the ratio between the pressure and particle velocity; $Z = P/U$ which can be defined for a medium as being : $Z = P/U = 1/(\rho_0 c)$. The density and speed of sound are calculated using the atmospheric pressure, temperature, and relative humidity. The density of air is calculated using equations found in Davis (Davis, 1992):

$$\rho_0 = \frac{PM_a}{ZRT}\left(1 - \mathrm{X}_\upsilon\left(1 - \frac{M_\upsilon}{M_a}\right)\right) \tag{C.1}$$

where P is the atmospheric pressure, T is the thermodynamic temperature, X_υ is the molar fraction of water vapour, M_a is the molar mass of dry air, M_υ is the molar mass of water vapour, R is the molar gas constant and Z is the compressibility factor for moist air. Equation (C.1) is also known as the CIPM-81/91 formula. The molar mass of dry air is assumed constant. The mole fraction of water vapour is calculated out of the pressure and the relative humidity (Giacomo, 1982). The uncertainty in the calculation of the density is 0.025% (MacGillivray, 2002).

The speed of sound is calculated using equations found in Cramer (Cramer, 1993). An overview is given in MacGillivray (MacGillivray, 2002):

$$c^2 = \gamma\frac{RT}{M}\left(1 + \frac{2PB}{RT}\right) \tag{C.2}$$

where γ is the specific heat ratio, M is the molar mass of air (mixed with water vapour), P is the atmospheric pressure, and B is the second virial coefficient of state (Cramer, 1993). The accuracy is the calculation of the speed of sound is 0.5% (MacGillivray, 2002).

In Figure Appendix C-6-1 the change in the inverse acoustic impedance is shown as function of change in pressure, humidity, and temperature around atmospheric conditions of 20.5° C, 1005 hPa, and 34% RH. In Figure Appendix C-6-1 it is seen that the inverse acoustic impedance is most sensitive for change in pressure. An accuracy of 1 percent in the pressure measurement for example results in an error of 1 percent in the inverse acoustical impedance. The change

due to temperature is less than 0.04% (due to 0.2°C), and due to relative humidity is less than 0.002 (due to 1% change in RH).

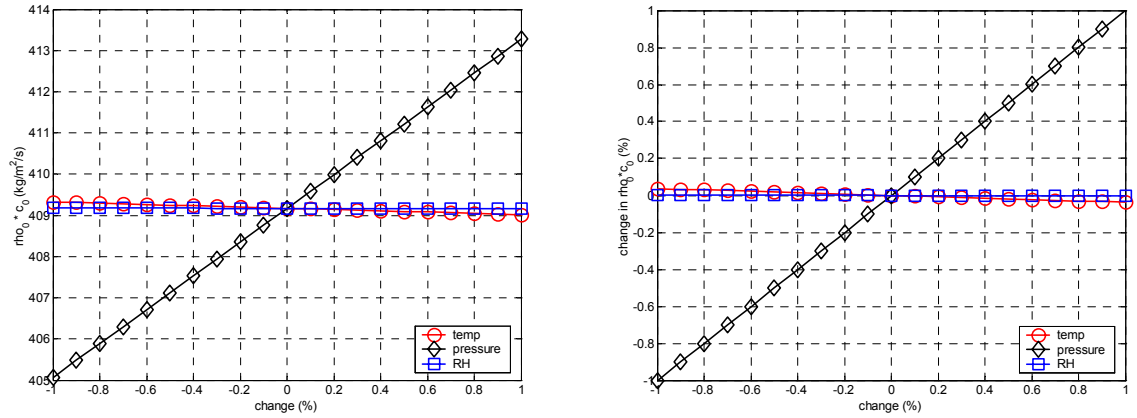

Figure Appendix C-6-1: The inverse acoustic impedance as a function of change in temperature (o), atmospheric pressure (diamonds), and relative humidity (blue squares). Left: absolute values, Right: change in percentage.

We should notice that although the inverse acoustical impedance is not as sensitive for errors in temperature and humidity measurements, the temperature and humidity needs to be recorded since they can vary much for different situations and accommodations. For example; a change in temperature of 4 degrees Celsius results also in 1% change in acoustical impedance.

In Table Appendix C-1 the resolution of our weather station is given and its result on the calculation of the acoustical impedance. In the worst case the total error due to the measurement of the air quality sums up to 0.75% in the acoustical impedance which is equivalent with 0.06 dB.

Table Appendix C-1: The resolution of our barometer (Oregon Scientific BA888) and its result on the accuracy of the acoustical impedance calculation.

parameter	resolution	accuracy	resulting error due to resolution	resulting error due to accuracy
Temperature	+/- 0.5 °C	+/-1 °C	+/- 0.09%	+/- 0.18%
pressure	+/- 1 hPa	+/- 5 hPa (Oregon Scientific, 2003a)	-/+ 0.10%	-/+ 0.50%
relative humidity	+/- 1%	+/- 5%(Oregon Scientific, 2003b)	+/- 0.05%	+/- 0.03%

References

Acoustics & Vibration Technologies. Meauring Microphone. http://www.avt-sa.com/education/Measuring%20Microphones%20-%20BA721615.pdf . 2005.
Ref Type: Internet Communication

Beissner,K, 1982, On the plane-wave approximation of acoustic intensity: Journal of the Acoustical Society of America, v. 71.

Bendat,JS, A G Piersol, 1986, Random Data: Analysis and Measurement Procedures, Wiley.

Bendat,JS, A G Piersol, 2002, Engineering Applications of Correlation and Spectral Analysis, John Wiley & Sons, Inc..

Beranek,LL, 1954, Acoustics, New York, McGraw-Hill.

Bjor,OH. 1367-1370. 1997. Budapest. Internoise 97.
Ref Type: Conference Proceeding

Bolt,R, A A Petrauskas, 1943, An acoustic impedance meter for rapid field measurements: Journal of the Acoustical Society of America, v. 15.

Brandt,O, H Freund, E Heidemann, 1937, Schwebstoffe in Schallfeld: Zeits.Phys., v. 104, p. 511-533.

Bree de,HE. The Microflown. 1997. University of Twente, Enschede, The Netherlands.
Ref Type: Thesis/Dissertation

Bree de,HE, 2001, The Microflown; Report 1996 - 2001.

Bree de,HE, 2003a, An overview of Microflown Technologies: Acta Acustica, v. 89, p. 163-172.

Bree de,HE, 2003b, The Microflown, an acoustic particle velocity sensor: Australian Acoustics, v. 31, p. 91-94.

Bree de,HE, 2005, The Microflown 2005, To be published.

Bree de,HE, M T Korthorst, P J Leussink, H V Jansen, M C Elwenspoek. A method to measure apparent acoustic pressure, Flow gradient and acoustic intensity using two micro machined flow

microphones. 1996a. Leuven, Belgium. Eurosensors X, Leuven. 1996a.
Ref Type: Conference Proceeding

Bree de,HE, T S J Lammerink, M C Elwenspoek, J H J Fluitman. Fluid flow measuring device as a microphone and system comprising such a microphone. Bree de, H. E. 08/765,597[PCT/NL95/00220]. 1995. Enschede, the Netherlands.
Ref Type: Patent

Bree de,HE, P J Leussink, M T Korthorst, H V Jansen, T S J Lammerink, M C Elwenspoek, 1996b, The micro-flown: a novel device for measuring acoustic flows: Sensors and Actuators A-Physical, v. 54, p. 552-557.

Bree de,HE, V B Svetovoy, R Raangs, R Visser. The Very Near Field; Theory, simulations and measurements of sound pressure and particle velocity. 2004. St. Petersburg, Russia. The Eleventh International Congress on Sound and Vibration. 5-7-2004.
Ref Type: Conference Proceeding

Bree de,HE, V B Svetovoy, R Raangs, R Visser. The Very Near Field II: An introduction to Very Near Field Holography. 2005. Noise & Vibration Conference and Exhibition,May 16-19, 2005,Grand Traverse Resort,Traverse City, MI. 16-5-2005.
Ref Type: Conference Proceeding

Brüel&Kjær. Measuring Microphones. http://www.bksv.com/lectures/BA721615.pdf BA 7216-15. 2005.
Ref Type: Internet Communication

Cheng,YS, W E Bechtold, C C Yu, I F Hung, 1995, Incense smoke: Characterization and dynamics in indoor environments: Aerosol Science and Technology, v. 23, p. 271-281.

Cramer,O, 1993, The variation of the specific heat ratio and the speed of sound in air with temperature, pressure, humidity, and CO2 concentration: Journal of the Acoustical Society of America, v. 93, p. 2510-2516.

Cullen,JS, C Greated, D M Campbell, 1999, LDA measurement of sound: amplitude modulation of laser Doppler signals: Measurement Science and Technology, v. 10, p. 812-823.

Davis,RS, 1992, Equation for the determination of the density of moist air: Metrologia, v. 29, p. 67-70.

Dring,RP, 1982, Sizing Criteria for laser Doppler anemometry particles: Journal of Fluids Engineering, v. 104, p. 15-17.

Druyvesteyn,WF, H E Bree de, 1998, Intensity measurements in various rooms: A new intensity probe: The Journal Of The Acoustical Society Of America, v. 103, p. 3074.

Druyvesteyn,WF, H E Bree de, 2000, A Novel Sound Intensity Probe; Comparison with the Pair of Pressure Microphones Intensity Probe: Journal of the Audio Engineering Society, v. 48, p. 49-56.

Druyvesteyn,WF, H E Bree de, M C Elwenspoek. A new acoustic measurement probe, the microflown. 21[3], 139-149. 1999. London, U.K. Proc. IOA.
Ref Type: Conference Proceeding

Druyvesteyn,WF, R Raangs, 2005a, Acoustic holography with incoherent sources: Acta Acustica United with Acustica, v. 91, p. 932-935.

Druyvesteyn,WF, R Raangs. Scanning the sound field from uncorrelated sources. 2005b. Budapest, Hungary. Forum Acusticum 2005. 2-8-1929b.
Ref Type: Conference Proceeding

Dumbacher,SM, D L Brown, J R Blough, R W Bono. Practical Aspects of Making NAH Measurements. 99NV-174. 1998. The Modal Shop, Inc.
Ref Type: Report

Durrani,TS, C A Greated, 1977, Laser systems in flow measurements, New York, Plenum Press.

Dutta,P, P M Horn, 1981, Low-frequency fluctuations in solids: 1 / f noise: Review of Modern Physics, v. 53, p. 497-516.

Eerden,FJMvd, H E Bree de, H Tijdeman, 1998, Experiments with a new acoustic particle velocity sensor in an impedance tube: Sensors and Actuators A-Physical, v. 69, p. 126-133.

Fahy,FJ, 1977, Measurement of acoustic intensity using the cross-spectral density of two microphone signals: The Journal Of The Acoustical Society Of America, v. 62, p. 1057-1059.

Fahy,FJ, 1995, Sound Intensity, London UK, E&FN Spon.

Fahy,FJ, 1997, International standards for the determination of sound power levels of sources using sound intensity measurement: An exposition: Applied Acoustics, v. 50, p. 97-109.

Fahy,FJ, 2001, Foundations of Engineering Acoustics, Academic Press.

Finke,HO, 1991a, Particle Velocity, in O Madelung, J Bortfeldt, B Kramer, O Madelung, J Bortfeldt, and B Kramer (eds), Units and Fundamental Constants in Physics and Chemistry; Subvolume a: Units in Physics and Chemistry: New York Berlin Heidelberg, Springer Verlag, p. 2-347-2-341.

Finke,HO, 1991b, Sound, in O Madelung, J Bortfeldt, and B Kramer (eds), Units and Fundamental Constants in Physics and Chemistry; Subvolume a: Units in Physics and Chemistry: New York Berlin Heidelberg, Springer Verlag, p. 2-330-2-347.

Gameiro da Silva,MC, 2002, Measurements of comfort in vehicles: Measurement Science and Technology, v. 13, p. R41-R60.

Giacomo,P, 1982, Equation for the determination of the density of moist air: Metrologia, v. 18, p. 33-40.

Ginn,KB, J Hald. STSF-Practical instrumentation and application Digital Filter Analysis: Real-rime and non Real-time performance. Brüel & Kjær Technical Review 2. 1989.
Ref Type: Magazine Article

Grinstein,G, T Hwa, H J Jensen, 1992, 1/f noise in dissipative transport: Phys.Rev.Lett.B, v. 45, p. 559-562.

Hallman,D, J S Bolton. Multi reference nearfield acoustical holography. 1165-1170. 1992. Proc. Inter-Noise 92.
Ref Type: Conference Proceeding

Hann,D, C A Greated, 1993, Acoustic measurements in flows using photon correlation spectroscopy: Measurement Science and Technology, v. 5, p. 157-164.

Hernández-Ramírez,I. Multilevel Multi-Integration Algorithm for Acoustics. 2005. University of Twente.
Ref Type: Thesis/Dissertation

Honschoten,JWv. Modelling and optimisation of the Microflown. 2004.
Ref Type: Thesis/Dissertation

Honschoten,JWv. package gain of a half inch microflown. 2005.
Ref Type: Personal Communication

Honschoten,JWv, H E Bree de, F J M v d Eerden, G J M Krijnen. The influence of viscothermal effects on calibration measurements in a tube. 2000. Los Angeles, U.S.A. 109th AES Convention. 22-9-2000.
Ref Type: Conference Proceeding

Honschoten,JWv, W F Druyvesteyn, H Kuipers, R Raangs, G J M Krijnen, 2004, Noise reduction in acoustic measurements with a particle velocity sensor by means of a cross-correlation technique: Acta Acustica United with Acustica, v. 90, p. 349-355.

Honschoten,JWv, W F Druyvesteyn, R Raangs, G J M Krijnen, M C Elwenspoek. Selfnoise reduction in acoustic measurements with a Particle velocity sensor by means of a cross-correlation technique. 2002a. Sevilla. Forum Acusticum, The 3rd EAA European Congress on Acoustics. 16-9-2002a.
Ref Type: Conference Proceeding

Honschoten,JWv, G J M Krijnen, V B Svetovoy, H E Bree de, M C Elwenspoek. Optimisation of a two wire thermal sensor for flow and sound measurement. 523-526. 2001. Interlaken. MEMS. 2001.
Ref Type: Conference Proceeding

Honschoten,JWv, V B Svetovoy, T S J Lammerink, G J M Krijnen, M C Elwenspoek. Determination of the sensitivity behaviour of an acoustic and thermal flow sensor by electronic characterisation. 2002b. Orlando, Florida, U.S.A. IEEE Sensors 2002. 12-6-2002b.
Ref Type: Conference Proceeding

International Electrotechnical Commission. Measurement microphones, part2 : Primary method for the pressure calibration of laboratory standard microphones by the reciprocity method. IEC 61094-2. 1992. International Electrotechnical Commission.
Ref Type: Report

Jacobsen,F, 1991, A simple and effective correction for phase mismatch in intensity probes: Applied Acoustics, v. 33, p. 165-180.

Jacobsen,F, H E Bree de. A comparison of p-p and p-u sound intensity probes. 2004. St. Petersburg, Russia. The Eleventh International Congress on Sound and Vibration (ICSV11). 5-7-2004.
Ref Type: Conference Proceeding

Jacobsen,F, H E Bree de, 2005a, A comparison of two different sound intensity measurement principles: Journal of the Acoustical Society of America, v. 118, p. 1510-1517.

Jacobsen,F, H E Bree de. Measurement of sound intensity: p-u probes versus p-p probes. 2005b. Saint Raphaël, France. NOVEM 2005. 18-4-2005b.
Ref Type: Conference Proceeding

Kim,YJ, J S Bolton, H S Kwon, 2004, Partial sound field decomposition in multireference near-field acoustical holography by using optimally located virtual references: Journal of the Acoustical Society of America, v. 115, p. 1641-1652.

Kinsler,LE, A R Frey, A B Coppens, J V Sanders, 2000, Fundamentals of Acoustics, New York, John Wiley & Sons, Inc..

Korn,GA, T M Korn, 2000, Mathematical Handbook for Scientists and Engineers: Definitions, Theorems, and Formulas for Reference and Review, Dover Publications, Incorporated.

König,W, 1891, Ann.Phys.(Leipzig), v. 43, p. 43.

Kuttruff,H, 1979, Room Acoustics, Essex, England, Applied Science Publishers LTD..

Kwon,H-S, J S Bolton. Partial field decomposition in nearfield acoustical holography by the use of singular value decomposition and partial coherence procedures. 649-654. 1998. Ypsilanti, USA. Proc. Noise-Con 98.
Ref Type: Conference Proceeding

Lagarias,JC, J A Reeds, M H Wright, P E Wright, 1998, Convergence Properties of the Nelder-Mead Simplex Method in Low Dimensions: SIAM Journal of Optimization, v. 9, p. 112-147.

Liu,SH, 1977, Theory of 1/f noise in metal films and whiskers: Physical Review B, v. 16, p. 4218-4223.

MacGillivray,TJ. The application of laser anemometry in acoustic measurement standards. 2002. The University of Edinburgh.
Ref Type: Thesis/Dissertation

MacGillivray,TJ, D M Campbell, C A Greated, R Barham, 2003, The Development of a Microphone Calibration Technique Using Photon Correlation Spectroscopy: Acustica, v. 89, p. 369-376.

Maynard,JD, E G Williams, Y Lee, 1985, Nearfield acoustic holography: I. Theory of generalized holography and development of NAH: Journal of the Acoustical Society of America, v. 78, p. 1395-1413.

Microflown Technologies. www.microflown.com . 2004.
Ref Type: Internet Communication

Morfey,CL, 2001, Dictionary of Acoustics, London, Academic Press.

Nam,KU, Y H Kim, 2001, Visualization of multiple incoherent sources by the backward prediction of near-field acoustic holography: Journal of the Acoustical Society of America, v. 109, p. 1808-1816.

Nelder,JA, R Mead, 1965, A simplex method for function minimization: Computer Journal, v. 7, p. 308-313.

Olson,HF. System responsive to the energy flow of sound waves. [1.892,644]. 1932. 29-5-1931.
Ref Type: Patent

Oppenheim,AV, R W Schafer, J R Buck, 1989, Discrete-time signal processing, Upper Saddle River, NJ, Prentice-Hall International.

Oregon Scientific. The tolerance of the barometer. 2003a.
Ref Type: Internet Communication

Oregon Scientific. The tolerance of the relative humidity reading. 2003b.
Ref Type: Internet Communication

Papoulis,A, 1991, Probability, Random Variables and Stochastic Processes, McGraw-Hill Companies.

Pathria,RK, 1986, Statistical Mechanics, University of Waterloo, Canada.

Pierce,AD, 1989, Acoustics, An introduction to its Physical Principles and Applications, New York, Acoustical Socity of America.

Powell,JH, J H T Roberts, 1922, On the Frequency of Vibration of Circular Diaphragms: Proc.Phys.Soc.London, v. 35, p. 170-182.

Press,WH, S A Teukolsky, W T Vetterling, B P Flannery, 1992, Numerical Recipes in C, Cambridge Univ..

Raangs,R, W F Druyvesteyn, H E Bree de. A low cost intensity probe. 2001a. Amsterdam, The Netherlands, Audio Engineering Society. AES 110th Convention. 5-12-2001a.
Ref Type: Conference Proceeding

Raangs,R, W F Druyvesteyn, H E Bree de. A novel two-dimensional sound particle velocity probe for source localization and free field measurements in a diffuse field. Boone, M. M. 1919. 2001b. The Hague, The Netherlands, Nederlands Akoestisch Genootschap (NAG) . Internoise 2001. Boone, M. M. 27-8-2001b.
Ref Type: Conference Proceeding

Raangs,R, W F Druyvesteyn, H E Bree de. Sound Source Localization Using Sound Intensity Measured by a Three-Dimensional PU-Probe. 1-10. 2002. Munich, Germany, Audio Engineering Society. AES 112th Convention. 10-5-2002.
Ref Type: Conference Proceeding

Raangs,R, W F Druyvesteyn, H E Bree de, 2003, A low cost intensity probe: Journal of the Audio Engineering Society, v. 51, p. 344-357.

Raangs,R, Schlicke.T, R Barham, 2005, Calibration of a micro-machined particle velocity microphone in a standing wave tube using a LDA photon correlation technique: Measurement Science and Technology, v. 16, p. 1099-1108.

Rienstra,SW, A Hirschberg. An introduction in acoustics. IWDE Report 92-06, version 1/06/92, February 1992. 2002.
Ref Type: Report

Rondeau,J-F, A Duval, G Deshayes, M Lassalas, H E Bree de, S Chaigne. Vehicle Acoustic Synthesis Method: improving acquisition time by using p-u probes. 2005. Noise & Vibration Conference and Exhibition,May 16-19, 2005,Grand Traverse Resort,Traverse City, MI. 16-5-2005.
Ref Type: Conference Proceeding

Roozen,NB, W Potze, E C Mulkens. Nearfield acoustic holography using cross-spectra. 2002. Orlando, FL, U.S.A. ICSV9 2002. 8-7-2002.
Ref Type: Conference Proceeding

Roozen,NB, R Scholte. On the direct propagation of sound intensity using cross-spectral NAH. 2003. Stockholm, Sweden. Tenth International Congress on Sound and Vibration. 7-7-2003.
Ref Type: Conference Proceeding

Schoeps. Principal Characteristics of the Different Microphone Types. 2005.
Ref Type: Internet Communication

Schultz,TJ. Acoustic Wattmeter. [2,836,656]. 1958. 31-10-1955.
Ref Type: Patent

Scofield,JH, J V Manteste, W W Webb, 1985, 1/f noise of metals, A case for extrinsic origin: Physical Review B, v. 32, p. 736-742.

Semenova,T, S F Wu, 2004, The Helmholtz equation least-squares method and Rayleigh hypothesis in near-field acoustical holography: Journal of the Acoustical Society of America, v. 115, p. 1632-1640.

Sharpe,JP, C A Greated, 1987, The measurement of periodic acoustic fields using photon correlation spectroscopy: Journal of Applied Physics D: Applied Physics, v. 20, p. 418-423.

Stanzial,D, N Prodi, G Schiffrer, 1996, Reactive acoustic intensity for general fields and energy polarization: Journal of the Acoustical Society of America, v. 99, p. 1868-1875.

Svetovoy,VB, I A Winter, 2000, Model of the Microflown microphone: Sensors and Actuators A-Physical, v. 86, p. 171-181.

Taylor,KJ, 1976, Absolute measurement of acoustic particle velocity: Journal of the Acoustical Society of America, v. 69, p. 691-694.

Taylor,KJ, 1981, Absolute calibration of microphones by a laser-Doppler technique: Journal of the Acoustical Society of America, v. 70, p. 939-945.

Tijdeman,H, 1975, On the propagation of sound waves in cylindrical tubes: Journal of Sound and Vibration, v. 39, p. 1-33.

Tijs,E. Creating a calibration setup for the Microflown. 2004. Saxion Hogeschool Enschede.
Ref Type: Thesis/Dissertation

Tomlinson,MA, 1999, Partial source discrimination in near field acoustic holography: Applied Acoustics, v. 57, p. 243-261.

Veronesi,WA, J D Maynard, 1987, Nearfield Acoustic Holography (NAH) II. Holographic reconstruction algorihmis and computer implementation: Journal of the Acoustical Society of America, v. 81, p. 1307.

Visser,R. Acoustic Source Localization based on Pressure and Particle Velocity Measurements. 2003. Inter-Noise 2003 Congres, Jeju, Korea, from August 25 to 28, 2003. Korea. 25-8-2003.
Ref Type: Conference Proceeding

Visser,R. A boundary element approach to acoustic radiation and source identification. 2004. University of Twente.
Ref Type: Thesis/Dissertation

Weikert,O. Realization of a diffuse sound field with a PC-based sound card solution. 2002. Hamburg, Germany. Proc. of the 5th Int. Conference on Digital Audio Effects (DAFx-02). 26-9-2002.
Ref Type: Conference Proceeding

Welch,PD, 1967, The Use of Fast Fourier Transform for the Estimation of Power Spectra: A Method Based on Time Averaging Over Short, Modified Periodograms: IEEE Trans.Audio Electroacoust., v. AU-15, p. 70-73.

West,W, 1949, The Accuracy of Measurements by Rayleigh Disc: Proc.Phys.Soc.B, v. 62, p. 437-444.

Williams,EG, 1999, Fourier Acoustics : Sound Radiation and Near field Acoustical Holography, Academic Press.

Williams,EG, B H Houston, P C Herdic, S T Raveendra, B Gardner, 2000, Interior near-field acoustical holography in flight: Journal of the Acoustical Society of America, v. 108, p. 1451-1463.

Wolff,O, R Sottek. Binaural Panel Noise Contribution Analysis - An Alternative to the Conventional Window Method. 2004. Strasbourg, France. CFA DAGA.
Ref Type: Conference Proceeding

Wolff,O, R Sottek. Application of a New Window Technique for Panel Noise Contribution Analyses. 2005. Noise & Vibration Conference and Exhibition,May 16-19, 2005,Grand Traverse Resort,Traverse City, MI. 16-5-2005.
Ref Type: Conference Proceeding

Wong,GSK, 1995, Comments on "The variation of the specific heat ratio and the speed of sound in air with temperature, pressure, humidity, and CO2 concentration": Journal of the Acoustical Society of America, v. 97, p. 3177-3179.

Wong,GSK, T F W Embleton, 1994, AIP Handbook of condenser microphones: Theory, calibration, and measurements, NY, AIP Press.

Wood,AB, 1935, A correction to the theory of the rayleigh disc as applied to the measurement of sound-intensity in water: Proc.Phys.Soc., v. 47, p. 779-793.

Ziel,Avd, 1954, Noise in Measurements, New York, Prentice Hall.

Zyl,BGv, F Anderson, 1975, Evaluation of the intensity method of sound power determination: The Journal Of The Acoustical Society Of America, v. 57, p. 682-686.

List of Publications

1. Raangs,R, Schlicke.T, R Barham, 2005, Calibration of a micro-machined particle velocity microphone in a standing wave tube using a LDA photon correlation technique: Measurement Science and Technology, v. 16, p. 1099-1108.
2. Raangs,R, W F Druyvesteyn, H E Bree de, 2003, A low cost intensity probe: Journal of the Audio Engineering Society, v. 51, p. 344-357.
3. Raangs,R, W F Druyvesteyn, H E Bree de. Sound Source Localization Using Sound Intensity Measured by a Three-Dimensional PU-Probe. 1-10. 2002. Munich, Germany, Audio Engineering Society. AES 112th Convention. 5-10-2002.
4. Raangs,R, W F Druyvesteyn, H E Bree de. A novel two-dimensional sound particle velocity probe for source localization and free field measurements in a diffuse field. Boone, R. 1919. 2001. The Hague, The Netherlands, Nederlands Akoestisch Genootschap (NAG) . Internoise 2001. Boone, R. 8-27-2001.
5. Raangs,R, W F Druyvesteyn, H E Bree de. A low cost intensity probe. 2001. Amsterdam, The Netherlands, Audio Engineering Society. AES 110th Convention. 12-5-2001.
6. Raangs,R, G Bakker, A P v Loon, P M Biesheuvel, C Huiskens, G H d Rooij, C Dirksen, H Verweij. A new osmotic tensiometer with an aqueous polymer retained by a ceramic membrane. 183. 1999. Salt Lake City, USA., American Society of Agronomy, Crop Science Society of America, Soil Science Society of America. proceedings of the Agronomy meetings (American Society of Agronomy, Crop Science Society of America,Soil Science Society of America).
7. Raangs,R, A P Loon, C Dirksen, P M Biesheuvel, R A Feddes. Design of an osmotic tensiometer. 1999. Den Hague, The Netherlands, European Geophysical Society.
8. Druyvesteyn,WF, R Raangs, 2005, Acoustic holography with incoherent sources: Acta Acustica United with Acustica, v. 91, p. 932-935.
9. Bree de,HE, V B Svetovoy, R Visser, R Raangs. The Very Near field; Theory, simulations and measurements of sound pressure and particle velocity. 2004. St. Petersburg, Russia. The Eleventh International Congress on Sound and Vibration. 7-5-2004.
10. Bree de,HE, R Raangs, W F Druyvesteyn. Sound intensity measurements with the Microflown sensor. 2004. Prague, Czech Republic, Organized by the Czech Acoustical

Society and the International Institute of Noise Control Engineering. Internoise 2004. 8-22-2004.

11. Honschoten,JWv, W F Druyvesteyn, H Kuipers, R Raangs, G J M Krijnen, 2004, Noise reduction in acoustic measurements with a particle velocity sensor by means of a cross-correlation technique: Acta Acustica United with Acustica, v. 90, p. 349-355.
12. Honschoten,JWv, W F Druyvesteyn, R Raangs, G J M Krijnen, M C Elwenspoek. Selfnoise reduction in acoustic measurements with a Particle velocity sensor by means of a cross-correlation technique. 2002. Sevilla. Forum Acusticum, The 3rd EAA European Congress on Acoustics. 9-16-2002.
13. Druyvesteyn,WF, H E Bree de, R Raangs. Free field measurements in a reverberant room using the microflown sensors. 2001. Rome, Italy.
14. Biesheuvel,PM, A P Loon, R Raangs, H Verweij, C Dirksen, 2000, A Prototype osmotic tensiometer with polymeric gel grains: European Journal of Soil Science, v. 51, p. 355-364.
15. Biesheuvel,PM, R Raangs, H Verweij, 1999, Response of the osmotic tensiometer to varying temperatures: modeling and experimental validation: Soil Science Society of America Journal, v. 63, p. 1571-1579.
16. Bijnen,FGC, H Zuckermann, R Raangs, E Mateman, J Reuss, D H Parker, F J M Harren, 1995, Trace gas emission monitoring from fruit and insects by laser photoacoustic techniques: Romanian J.Biophys, v. 5, p. 371-383.
17. Bijnen,FGC, J v Dongen, R Raangs, F J M Harren, D H Parker, J Reuss. Thermoacoustic amplification of photoacoustic signal, a step for improving photoacoustic detection limits. 1994. Najaarsvergadering 1994 van de sectie atoomfysica en quantumelektronica van de Nederlandse Natuurkunde Vereniging (NNV).

Dankwoord

Aan al het goede komt een einde. Met dit proefschrift wordt daarom een hele leuke periode afgesloten die ik bij de leerstoel Signalen en Systemen heb gehad.

Als eerste wil ik echter mijn familie bedanken. Zonder hun steun en hulp was het afronden van dit proefschrift onmogelijk geweest. In het bijzonder wil ik Sandra, Dennis, Nienke en mijn ouders bedanken.

Graag wil ik mijn promotor Erik Druyvesteyn bedanken voor zijn hulp en gedegen enthousiaste begeleiding die hij mij gegeven heeft om tot het afronden van dit proefschrift te komen. Daarnaast wil ik iedereen van de leerstoel Signalen en Systemen bedanken voor de prettige samenwerking en hulp. Met name wil ik bedanken; Kees Slump voor zijn begeleiding en net de juiste woorden als het wat tegenzat, Anneke van Essen voor alle hulp, Henny Kuipers voor zijn hulp op het gebied van akoestische metingen en elektronica, Geert Jan Laanstra omdat hij altijd weer mijn computer aan de praat kreeg, en Johan Wesselink. Ook mijn kamergenoten, Mark Schrijver, Joost Kauffman, Marnix Heskamp, en studenten Rick Scholte, Edwin Mulkens, Geertjan Schrijen, Laurens Alink en Erik Dobbelsteijn, wil ik bedanken voor de leuke tijd en de vele diverse discussies.

Natuurlijk was dit onderzoek niet mogelijk zonder microflowns. In het bijzonder wil ik daarom Hans-Elias de Bree bedanken. Het was een enorm genoegen om met je samen te mogen werken. Het gehele microflown team, in het bijzonder, Peter van der Stap, Phillip Ekkels, en Martijn van der Schaaf. En ook wil ik Alex Koers van Microflown Technologies hierbij bedanken voor zijn hulp. Doekle Yntema wil ik speciaal nog bedanken voor het vervaardigen en het modificeren van de vele verschillende microflowns die we gebruikt hebben.

Van de Universiteit in Edinburgh wil ik Ted Schlicke bedanken voor de prettige samenwerking. Het uitvoeren van de metingen in Edinburgh en het daarna schrijven van het artikel was voor mij een zeer leerzame ervaring.

Tijd is vaak een schaars goed. Vooral als je de illusie hebt dat je de resultaten binnen een redelijke termijn in boekvorm op papier kunt krijgen. Ik wil daarom TalkingHome bedanken, en in het bijzonder Felix Smits en Jan Teeling, voor hun steun en inzet, en in het bijzonder voor het mogelijk maken van de laatste eindsprint. Ook wil ik mijn collega's van TalkingHome, Barry van der Veen en

Erik Stegeman, en bijna collega Inge Siemerink bedanken voor de leuke momenten en gesprekken.

Het onderzoek valt binnen het STW project ‘Efficiënte akoestische reken- en meettechnieken’ dat volledig door de technologiestichting STW gefinancierd werd. De twee medepromovendi binnen dit project, René Visser, Isias Hernández Ramírez, wil ik bedanken voor de prettige samenwerking. Daarnaast wil ik de gehele gebruikerscommissie van dit project bedanken voor de prettige samenwerking en discussie. In het bijzonder wil ik Leo Korstanje en Henk Tijdeman bedanken voor de begeleiding van het project, Bert Roozen voor het gebruik van de faciliteiten bij Philips en Jos van Heck voor de opbouwende kritiek.

Bert Wolbert wil ik bedanken voor zijn hulp met verschillende microfoons en metingen met de p-p probe, en Philippus Feenstra voor de hulp met de laser vibrometer metingen, Linda Jonker en Marije Florijn voor hun hulp tijdens de LOB2 modulen, en Giulio Pispola voor de leuke discussies over de microflown.

Tot slot bedank ik vrienden en familie die me altijd gesteund en aangemoedigd hebben.

Bedankt,

Ron

Lochem, 2005